Epoxy-graphite Resistive Composites: Formulation, Characterization and Applications

THÈSE N^{O} 5346 (2012)

PRÉSENTÉE LE 20 AVRIL 2012

À LA FACULTÉ DES SCIENCES ET TECHNIQUES DE L'INGÉNIEUR
LABORATOIRE DE PRODUCTION MICROTECHNIQUE 2
PROGRAMME DOCTORAL EN SYSTÈMES DE PRODUCTION ET ROBOTIQUE

ÉCOLE POLYTECHNIQUE FÉDÉRALE DE LAUSANNE

POUR L'OBTENTION DU GRADE DE DOCTEUR ÈS SCIENCES

PAR

Nathalie SERRA

acceptée sur proposition du jury:

Prof. H. Bleuler, président du jury
Prof. P. Ryser, Dr T. Maeder, directeurs de thèse
Prof. D. Damjanovic, rapporteur
Dr E. Grivei, rapporteur
Prof. M. Negri, rapporteur

ÉCOLE POLYTECHNIQUE
FÉDÉRALE DE LAUSANNE
Suisse
2012

Abstract

In this thesis, we proposed to study polymer-based thick-film resistors (TFRs) made of graphite particles dispersed in an epoxy matrix. Three main axes were investigated:

- formulation of the composites,
- characterization with the determination of electrical, mechanical and thermo-mechanical properties of the material,
- potential applications.

Special care was first given to the formulation of the composite formed by an epoxy matrix in which graphite particles are dispersed, providing conductivity to the material. As application temperatures of a polymer is limited by its glass transition T_g we used two epoxies: a standard T_g one (ca. 90°C) and a high T_g one (ca. 200°C). Particle size and shape effects were also investigated: synthetic graphite (ellipsoidal shape) and expanded graphite (worm-like shape) were taken as fillers. For comparative purposes, carbon black was also tested. For TFRs to be deposited by the standard process of screen-printing, viscosity of the paste must be controlled. Therefore, we performed a study on solvents and we proposed an appropriate set adapted to epoxies. Functionalization of the particle surface through an oxidation process was studied. The aim was to create reactive groups, which could further react with the polar group of the epoxy and provide a better adhesion.

The main part concerned the characterization of these materials, which helps to understand their behavior. Electrical properties were first determined for our composites. We showed that particle size has little effect on the resistivity, whereas a specific surface area and a high structure of the filler give significantly lower resistivity values at low volume fractions. As our composites should form percolative systems, we fit the results using the theoretical conductivity formula. However, the values determined were incoherent, thus, we think that the conductivity in our composites is driven by the so-called " debris model", i.e. the overall conductivity depends on the small debris dispersed in the matrix. This was confirmed by the microscopic analysis of our composites. The piezoresistivity study showed that larger particles tend to give smaller gauge factors, which is linked to the aspect ratio of the particles. In these

experiments, temperature and substrate effects highlighted the importance of the T_g regarding stability of the properties. Dynamic Mechanical Analysis (DMA) was then performed on our materials. As expected, the higher the volume fraction, the higher the storage modulus. Larger particles and expanded graphite gave the same tendency, due to the fact that, overall, "less" resin was present in the composite. A better adhesion between epoxy matrix and functionalized particles was also demonstrated: oxidation led to a higher storage modulus. In parallel to DMA, thermal expansion of the composites was determined with an optical dilatometer. A one-time shrinkage was observed in the standard epoxy, which highlighted a "cycling effect" of the epoxy. The shrinkage was found to decrease with the filler volume fraction, and was not observed with expanded graphite, these two parameters diminishing the amount of resin in the composite. On the contrary, the high T_g epoxy did not show this effect. We proposed that this is linked to its two-step polymerization process. The values of T_g were determined from DMA and dilatometry and were additionally compared to the values obtained with Differential Scanning Calorimetry (DSC). Same tendencies were found for all methods, proving the consistency between our results.

Finally, these composites were used in different applications. Firstly, combined with sacrificial layers, they allowed the fabrication of microstructures such as microchannels, or cantilevers. Appropriate formulations based on sublimable polyols were developed, the high advantage being the fabrication of fine structures, by avoiding capillary forces linked with evaporation of the liquid phase. However, strong interactions between the sacrificial layers and the epoxy occurred. Over-layers based on ethylcellulose and silicone loaded with synthetic graphite were therefore formulated. The high potential of the process was demonstrated. Secondly, composite material formulations for the development of a testing set-up for the oil industry were investigated. The aim is to recreate a dummy and yet representative rock to help in the quality control of tools that measure the resistivity. The use of composites based on polymer and carbon-based filler presents several advantages: large range of available resistivities, ease of the process and transportable set-up. Comparative tests between TFRs and bulk objects were made. Differences in resistivity appeared and were found to come from the affinity of the epoxy with water, the amount of water trapped inside a bulk object being higher and more difficult to evaporate because of the thickness. Therefore, in order to manufacture more massive objects than thick-films, a longer polymerization time should be envisaged to allow the diffusion of water molecules from the material.

KEYWORDS: thick-film resistor, epoxy-graphite composite, screen-printing process, resistivity, piezoresistivity, DMA, dilatometry, organic sacrificial layers

Résumé

Dans cette thèse, nous nous sommes attachés à l'étude de résistances polymères en couche épaisse (TFRs), fabriquées à partir de particules de graphite dispersées dans une matrice époxy. La recherche s'est orientée autour de trois axes:

- la formulation des composites,
- la caractérisation avec la détermination des propriétés électriques, mécaniques et thermomécaniques du matériau,
- les applications potentielles.

Un soin particulier fut d'abord accordé à la formulation du composite, formé d'une matrice époxy et de particules conductrices en graphite. L'utilisation d'un polymère nous contraint à des applications ayant des températures inférieures à la celle de la transition vitreuse T_g. Nous avons choisi deux époxys avec deux T_g différents: un standard ($\approx 90°C$) et l'autre élevé ($\approx 200°C$). Les effets de taille et de forme de particules ont été examinés: du graphite synthétique (ellipse) et du graphite expansé (feuillet) constituent nos charges. Le noir de carbone a également été testé à des fins comparatives. Comme le dépôt de nos TFRs se fait via la sérigraphie, il est donc nécessaire de contrôler la viscosité de la pâte. Une étude sur les solvants nous a permis d'obtenir un assortiment adapté aux époxys. Enfin, grâce à un procédé d'oxydation, nous avons étudié la fonctionnalisation de la surface des particules. La création de groupes capables de réagir avec les groupes polaires de l'époxy pourrait donner une meilleure adhésion particule/matrice.

La partie principale concernait la caractérisation de ces matériaux, qui est primordiale pour comprendre leur comportement. Leurs propriétés électriques ont d'abord été déterminées. Ainsi, la taille de particules a peu d'effet sur la résistivité, alors qu'une grande surface spécifique doublée d'une haute structure donnent des valeurs significativement plus basses pour de plus basses concentrations. Nos matériaux formant des systèmes percolatifs, nous avons essayé d'appliquer la formule théorique de conductivité. Malgré une régression en apparence correcte, les valeurs ainsi déterminées étaient incohérentes. Par conséquent, nous pensons que la conductivité de nos composites suit le "modèle des débris", i.e. elle dépend des débris provenant des particules et dispersés

dans la matrice. Cela a été vérifié par l'observation microscopique de nos matériaux. L'étude de la piézorésistivité a montré que les grandes particules tendent à donner des facteurs de jauge plus petits, ce qui est lié au rapport d'aspect. Dans ces expériences, les effets de température et de substrats ont permis de souligner l'importance du T_g sur la stabilité des propriétés. L'Analyse Mécanique Dynamique (DMA) de nos matériaux a mis en évidence qu'une plus grande concentration de charges conduit à un plus grand module élastique (E) du composite. Les plus grandes particules ainsi que le graphite expansé produisent le même effet, ce qui peut s'expliquer par le fait qu'il y a moins de matrice dans le composite. Nous avons également observé une meilleure adhésion matrice/particules oxydées, E étant plus élevé. En parallèle, l'étude de la dilatation de ces matériaux a montré que l'époxy avec le T_g standard rétrécit lorsque qu'elle est aux alentours de son T_g. Ce rétrécissement est seulement observable lors du premier cycle, mettant en évidence un cyclage de l'époxy. Il devient plus faible avec la concentration et n'a pas été observé avec le graphite expansé, ces deux paramètres diminuant la quantité de résine dans le composite. Au contraire, l'époxy ayant un haut T_g ne présente pas cet effet, ce qui pourrait venir de son mode de polymérisation en deux étapes. Les valeurs de T_g calculées à partir des données de DMA et dilatométrie ont été comparées à celles obtenues par DSC et sont cohérentes entre elles.

Enfin, ces composites ont été utilisés pour des applications diverses. Des microstructures (microcanaux, cantilevers) ont d'abord été fabriquées par combinaison avec des couches sacrificielles, formulés à partir de polyols sublimables. Ces systèmes présentent l'avantage de permettre l'obtention de structures nettes (pas de forces capillaires liées à l'évaporation de la phase liquide). Cependant, comme l'époxy tend à réagir avec les polyols, des surcouches en éthylcellulose et silicone (chargées en graphite) ont été formulées. Nous avons donc prouvé le potentiel de ce procédé. Dans un deuxième temps, en vue de la fabrication d'un dispositif de test pour l'industrie pétrolière, différentes formulations de composites ont été examinées. Le but est de récréer une roche artificielle avec une résistivité définie, permettant de tester la qualité des outils mesurant la résistivité dans le puits. L'utilisation de composites polymères/charges carbone présente plusieurs avantages: large domaine de résistivité, facilité du procédé... Des tests comparatifs entre des TFRs et des objets massifs ont été effectués. Nous avons pu observer des différences que nous avons attribuées principalement à l'affinité de l'époxy pour l'eau, la quantité d'eau emprisonnée dans un objet massif étant plus importante et plus difficile à évacuer du fait de l'épaisseur. Ainsi, pour fabriquer des objets plus épais, un temps de polymérisation plus long doit être envisagé pour permettre aux molécules d'eau contenues dans le composite de diffuser.

Mots-clés: résistance couche épaisse, composite époxy-graphite, sérigraphie, résistivité, piézorésistivité, DMA, dilatométrie, couches sacrificielles organiques

Remerciements

Même si au final, seul mon nom apparait sur le document, je n'oublie pas que derrière se trouvent plein de gens sans qui cette thèse n'aurait pas été possible.

Je tiens tout d'abord à remercier le Professeur Peter Ryser qui a eu la gentillesse de m'accueillir au sein de son laboratoire. Il m'a accordé une grande liberté dans mon travail tout en laissant la porte ouverte, au cas où. Un énorme merci à mon co-directeur de thèse le Dr Thomas Maeder. Ses 1000 idées à la minute, son très large savoir et sa disponibilité ont largement contribué à faire de cette thèse ce qu'elle est. J'ai beaucoup apprécié nos discussions scientifiques et la recherche au laboratoire, même si je sais que ma formation de chimiste nous a parfois mis en désaccord sur les questions de sécurité et de manipulation de produits ;). Ces deux personnes ont relu et corrigé ma thèse, l'agrémentant de commentaires et remarques qui ont grandement amélioré sa qualité. Ils m'ont également accordé le privilège de pouvoir rédiger en partie à New York. J'ai plus qu'apprécié la confiance qu'ils ont eu en moi et j'espère avoir été à la hauteur de leurs attentes. A ce propos, j'aimerais également remercier le Prof. Weinstein du Weil Cornell Medical College de m'avoir intégré ponctuellement dans son laboratoire, simplifiant ainsi les longues (et fastidieuses) démarches administratives et me permettant d'avoir une place confortable à la bibliothèque de l'institut. J'en profite aussi pour faire un clin d'œil à la « bande des New Yorkais » : merci d'avoir égayé de sorties, restos et apéros cette période de rédaction pas toujours facile !

Je tiens également à exprimer ma gratitude aux membres du jury, le Professeur Martin Negri, le Dr Eusebiu Grivei et le Dr Dragan Damjanovic ainsi qu'au président du jury le Professeur Hannes Bleuler pour leur relecture, le temps qu'ils m'ont consacré et leurs remarques pertinentes lors de mon examen.

Une thèse, ça n'est pas rien, et quand la pression devient trop forte c'est important d'avoir des gens autour de soi sur qui compter. En tant que petite parisienne fraichement débarquée, je ne savais pas trop à quoi m'attendre et je me suis retrouvée dans un laboratoire plus que sympathique, où l'année est ponctuée d'apéros, de soupers de Noël, de sorties, de raclettes sauvages et bien d'autres choses! Merci donc à tout le LPM et plus particulièrement à Karine de perpétuer les traditions et gérer la bande de gamins que nous formons, à Momo d'enrichir mon vocabulaire d'expressions de « djeun's » pire cools,

à l'équipe avec qui j'ai passé une bonne partie de mon temps: Christophe, Lucas, Bibi, Showtime, Giuseppe et tous les autres qui ambiancent sec. Un gros merci à ma super collègue de bureau Caro pour nos discussions, les confs et surtout nos ragots ! Je n'oublie pas les anciens avec qui je passe encore pas mal de temps : Zoltan et sa chatoyance, Yannick, Gianluca et les physiciens Simon (futur MdM mais déjà champion de la grillade) et Antoine. Je suis bien contente de vous connaître ! Merci aussi au Dr Cath et future Dr Sandra pour nos discussions de filles, les activités communes (hein Mme la Queen ;)) et les coups de gueule partagés qui font qu'on se sent moins seule.

Ma thèse a aussi été ponctuée de virées parisiennes et de voyages tous plus géniaux les uns que les autres et que je dois à ma super bande de chimistes! On se voit moins qu'avant, mais je sais que je peux compter sur vous et c'est important. Vous l'avez une fois de plus montré ! Un grand merci donc à Nadia, Fiona, Benjy, Caro, Grand Fred, Guitou, Titou et plus particulièrement à ma petite Virginie pour sa présence et son écoute et à Kevin de me suivre dans mes délires. Je me réjouis à fond de nos futurs voyages les jeunes!

Un tout grand merci à la belle-famille qui m'a accueillie à bras ouverts : Stephan, Silke, Brigitte, Arash, Ruedi et plus particulièrement Rita pour sa gentillesse et sa présence, surtout pendant cette dernière année.

Merci également à mes parents de m'avoir toujours poussée et soutenue toutes ces années, même si cela impliquait que je m'éloigne de plus en plus. Un gros merci à ma sœur Aurélie et son caractère mordant et mon petit frère Romain qui n'est plus si petit.

Enfin, je tiens à remercier mon physicien préféré Niki pour son soutien inconditionnel et sa patience (surtout dans cette dernière ligne droite) et pour tous nos moments passés et à venir ensemble. Il a également eu la gentillesse de relire ma thèse, y apportant la touche de physique qui manquait à une chimiste ☺. Merci mille fois d'être toi, de me faire rire et je me répète, mais sans toi, ça aurait été plus que dur !

Contents

List of Figures

List of main abbreviations and symbols

Abbreviations

CTE	Coefficient of Thermal Expansion
DMA	Dynamic Mechanical Analysis
DMHD	2,5-dimethly-2,5-hexanediol
DSC	Differential Scanning Calorimetry
EG	Expanded Graphite
GF	Gauge factor
$\mathbf{GF_L}$	Longitudinal gauge factor
$\mathbf{GF_T}$	Transverse gauge factor
NPG	Neopentyl glycol
PCB	Printed Circuit Board
TCR	Temperature Coefficient of Resistance
TFR	Thick-Film Resistor
$\mathbf{T_g}$	Glass transition temperature
TME	Trimethylolethane
TMP	Trimethylolpropane
XPS	X-ray Photoelectron Spectroscopy

Symbols

σ	Conductivity
E''	Loss modulus
ν	Poisson's ratio
ρ	Resistivity
E'	Storage modulus
ε	Strain
ϕ	Volume fraction
E	Young's modulus

Chapter 1

Introduction

1.1 Conductive composites

Nowadays, composites seem to surround us and are present in various fields such as sports, construction, textiles... Some brands even using the term "composite" as a selling point. So, are they "super" materials? The answer is yes! But, let us first come back to some basic notions: what is a composite?

A composite is defined as the assembly of *at least* two non-miscible materials, leading to a new material, whose properties are different from the separate components. Depending on the filler (particles, fibers in various materials) and matrix (polymer, metal, glass, ceramic) types, the resulting properties can touch several domains, which is the reason why they find increasing use in our modern world. People are usually familiar with composites as materials with high mechanical properties, such as fiber-reinforced materials, which can be found in many sports articles (for instance skis or tennis racket). However, they can also be designed to tune the electrical properties of an insulating matrix, i.e. confer conductive or resistive properties to an otherwise insulating material. In this part we will more specifically deal with polymer matrix, as this is the subject of this project.

Having a conductive polymer-based composite can be of great interest for anti-static purposes, where a low, but non-zero conductivity is needed, or, on the opposite, in electromagnetic interference shielding, where a high filler loading is desired for efficient shielding (with or without additional magnetic losses). As the amount and type of fillers can be chosen, the composites can be formulated with a desired and adjustable conductivity, which is why those materials are also widely used in electronics. Finally, the choice of appropriate polymers (such as polyurethanes, epoxies, acrylates etc.) allows their use in biomedical applications where biocompatibility is needed [1, 2]. Due to the various types of fillers available, several options must therefore be considered.

The filler geometry (i.e. fiber or particle) will not be detailed in this discussion, the focus will be on the nature of the material. From this point of view, we will first expose why conductive polymer-based composites are needed despite the fact that conductive polymers (so without any filler) already exist, then we will deal with the different possibilities available to obtain a conductive polymer-based composite.

We first propose to have a look at intrinsically conducting polymers (ICPs), which are not composites but deserve a few lines here in order to fully understand the need to design conductive composites in polymer. ICPs are organic polymers that conduct electricity. They are highly conjugated polymers (i.e. they alternate single and multiple bonds), whose conductivity comes from doping by oxidation (removal of electrons) or reduction (addition of electrons) [3,4]. ICPs can also be "self-doped": in this case, "the counterions are covalently bonds to the polymer backbone, charge injected in the π-electron system is compensated by proton ejection" [5]. In the neutral state (i.e. undoped), the electron density is not the same between all atoms due to the Peierls instability, which makes them basically behave as semiconductors [4]. Typical conductive polymers are polyacetylene, polyaniline (PANI, the first to be synthesized) or polypyrrole. Their range of applications is wide: corrosion protection (coating of a metal with a PANI barrier, the problem being that it is pH-dependent: depending on the pH the predominant salt form will change, hence the properties), sensors, LED, batteries, solar cells [3]... However, even if research groups have recently proved synthesis of soluble conducting polymers [6], they generally show poor long-term stability and low solubility in organic solvents and water, which leads to a difficult processability. Therefore, due to their synthesis, the costs are high, preventing large-scale development, hence the need of conductive polymer-based composites based on more common insulating polymers and conductive fillers.

Such composites can be manufactured with fillers of different nature. The first possibility would be to use oxides as fillers. Dispersed in an insulating matrix, they will form percolative materials (i.e. conduction mechanisms are governed by the percolation theory). For instance, ruthenium oxide (RuO_2) is extensively used together with a glass matrix to prepare thick-film resistors for ceramic circuits or sensors, or simply as surface-mount components soldered on standard printed-circuit boards (PCBs) [7–9]. These composites show well-defined electrical properties and stability as well as interesting piezoresistive response, making them readily suitable for applications in high-reliability industrial sensors. They are more commonly used with a glass matrix but can of course be used in polymers as well [10]. However, the use of oxides in this very matrix is more related to optical properties than electrical ones [11]. In theory, any oxides could potentially be used, nevertheless a thermodynamically unstable oxide will be less protected in an organic matrix. Indeed, due to higher diffusion than in a glassy matrix, an oxidation (corrosion) layer can form on the surface, hence impairment of the conductivity. This is the case

for instance for Ni, Cu, Fe, Fe_3O_4 etc. On the opposite, if stable and highly conductive oxides are taken (such as RuO_2) the costs become really high.

Another possibility is to use metallic particles [12] or metallic coatings on particles, such as glass or polymeric particles. The coating option presents the advantage to give a lighter filler than the bulk metal, which can be desired in some applications. Silver is often used as a coating material due to its high conductivity, moreover, its oxide exhibits conductivity as well. The resulting composites show interesting electrical properties. For instance Krupa et al. [13] demonstrated the manufacturing of composites formed by polyamide-6 particles coated with silver in a high-density polyethylene matrix. The main problem lies in the coating process. Even if it will induce less cost than the pure metal, the metallic deposition requires high adhesion between the particles and the metal, which is not always the case, resulting in a potential unreliable coating. It also requires a chemical process to metallize the particles, such as electrolytic co-deposition or electro-less deposition [14, 15]. The problem of such systems lies in the stability of the layer (corrosion or electromigration in harsh environments). To avoid that, gold and platinum can be used, but these fillers are very expensive.

Finally, the most common option is by far the use of carbon-based materials as filler, which will be the subject of this thesis. More general information about these composites can be found in Section 2.1. Alternatively, pigments Minatec© from Merck can be used in order to obtain anti-static colored surfaces, but present less conductivity. The percolative materials formed by polymers and carbon-based compounds allow the formulation of composites with a large and controllable range of conductivity at low cost and will be studied throughout the following chapters.

1.2 Thesis overview

As explained before, this project deals with carbon-based polymer composites and more specifically epoxy-graphite composites (silicon-graphite systems were also partly studied). In the next chapter, we will first review the above-mentioned composites and what they are composed of. The different filler types will be detailed and compared, i.e. carbon black, carbon nanotubes, graphene and graphite, followed by the influence of the matrix types, which can be either a thermoplastic or thermosetting resin. One of the main uses of these composites is the fabrication of thick-film resistors (TFRs). We will therefore present the thick-film technology and distinguish the “classic” mineral paste case from the “exotic” one that we are interested in: the organic paste case. The electrical and mechanical properties will then be investigated. Indeed these composites are known to form conductive percolative networks: the conductive mechanisms will be studied as well as the piezoresistive effect. As far as the mechanical properties are concerned, it seems quite obvious that

the filler shape has a tremendous effect on the resulting properties. This will be explained in the last section as well as the possibility to functionalize the graphite surface (i.e. adding reactive groups) through an oxidation process.

Chapter 3 will be dedicated to the formulation and the structure of our composites. In the first part, we will show how to make a screen-printable thick-film paste, which has some requirements concerning viscosity. This is the reason why tuning of the paste through solvents and additives is of high importance in order to obtain desired properties. The filler can also be functionalized as seen in Chapter 2. The oxidation process and the determination of the degree of oxidation by X-ray Photoelectron Spectroscopy (XPS) can also be found here. When making composites, one may wonder how the particles interact with the matrix, therefore, the structure of the composites were examined with an optical microscope. Finally, the thermal properties were studied, thanks to Differential Scanning Calorimetry (DSC) measurements and allowed the determination of the glass transition temperature T_g.

The chapter 4 will be fully dedicated to the functional characterization of the composites. Electrical properties such as resistivity and piezoresistivity will be first reviewed and compared depending on the volume fraction, filler type, particle size and shape and substrate type. Following this, mechanical properties of the composites will be presented. Measurements will be performed with a Dynamic Mechanical Analyses (DMA), allowing determination of T_g and the complex Young's modulus. T_g will also be determined by dilatometric analysis. To validate our experiments, the relationship and coherence between the resistive, piezoresistive and thermomechanical properties determined by different methods will be discussed at the end.

Chapter 5 will deal with sacrificial layers. These layers are sublimable and allow the fabrication of microchannels or cantilevers. Their formulation will be first described and studied as they meet several requirements: viscosity (i.e. they must be screen-printable), drying (they must dry properly at moderate temperatures) and absence of deleterious chemical reactions with the resistive upper layer. The micromechanical and microfluidic devices obtained by this novel process will be characterized.

In the chapter 6, we will take interest in the possible applications of our epoxy-graphite composites. In this context, the study of bulk resistive composites will be endeavored.

Finally, the last chapter will be of course dedicated to the conclusions of this work, i.e. how we were able to formulate, characterize the electrical, mechanical and thermo-mechanical properties of these systems and use them in some applications. Open and remaining questions will also be discussed in this part.

Chapter 2

Carbon-based polymer composites: properties and use in thick-film technology

In the previous chapter, we have discussed the importance and omnipresence of conductive composite materials in our modern world. The following part will deal more specifically with carbon-based polymer composites, their properties and their use in thick-film technology, which is the object of this thesis.

2.1 Carbon-based polymer composites: an overview

2.1.1 One chemical compound, many possibilities

Carbon can be found in many different allotropic forms, sizes and shapes. From common carbon black to carbon nanotubes or graphene, these fillers will confer different properties to the resulting composites. This is why it is of high importance to define these fillers well, as they are often confused. This is the purpose of the following paragraphs. Diamond will not be treated here as it is electrically insulating.

2.1.1.1 Carbon black

Carbon black is formed of colloidal particles, coming from the incomplete combustion or thermal decomposition of gaseous or liquid hydrocarbons under controlled conditions [16]. Its internal structure is rather complex and supposedly formed by mixed hybridization sp^2 and sp^3 [17], with the presence of some impurities such as oxygen or sulphur coming from respectively the process and the feedstock [18]. It cannot be considered as truly amorphous as it presents

some degree of order in the basal plane [19, 20]. Two main industrial processes allow the fabrication of this material:

- furnace black, the most common process, uses heavy aromatic oils which are put in a closed reactor. The feedstock is introduced in a hot gas stream where it will vaporize and pyrolize in the vapor phase, forming thereby microscopic carbon particles.
- thermal black uses natural gas (methane) or heavy aromatic oils. This feedstock is put in a pair of furnaces that alternates between preheating and carbon black production every 5 minutes. Carbon black comes from the decomposition of the natural gas in a hot refractory lined furnace.

Depending on the process, low/high surface area carbon black can be obtained, low surface area carbon black presenting chain-like structure comparable to acetylene black, i.e. a carbon black formed by an exothermic decomposition of acetylene, [21]. The specific surface area of a material is a property determined by measuring the total surface per unit of mass, solid or bulk volume and it is of high importance for adsorption, heterogeneous catalysis, and reactions on surfaces. This measurement gives the "real" surface of a material. Another interesting characteristic of carbon black is its structure. This feature is different from the specific surface area. High structure carbon black presents a high number of primary particles per aggregate, while low structure carbon black exhibits only a weak aggregation [22].

This material looks like black powder or pellets, with particle sizes ranging from 10 to 100 µm [23]. Systems based on carbon black/polymer can be easily found in traditional as well as emerging applications such as low-current conductors in electronics (interconnects, keyboards...), electromagnetic interference (EMI) shielding, anti-static composites and coatings, foams, electrodes for fuel cells, supercapacitors, carbon resistors and potentiometers [24–29]. However, despite its low percolation threshold, one of the drawbacks of carbon black is its low intrinsic conductivity, which limits the conductivity of the resulting composites at high filler loads. Moreover, carbon black remains a less well-defined material than graphite.

Finally, carbon black must be distinguished from the so-called "glassy carbon" which is a non-graphitizing carbon with *a priori* a 100% sp^2 structure [30]. Glassy carbon is mainly used for fabrication of chemical electrodes.

2.1.1.2 Carbon nanotube

Carbon nanotubes (CNTs) are allotropes of carbon with a cylindrical nanostructure (Fig. 2.1). They are separated in two categories: Single-Wall NanoTubes (SWNTs) and Multi-Wall NanoTubes (MWNTs). SWNTs are a one-atom thick-layer of graphite wrapped into a cylinder, whereas MWNTs are multiple rolled layers of graphite (concentric tubes).

Carbon nanotubes can be produced by:

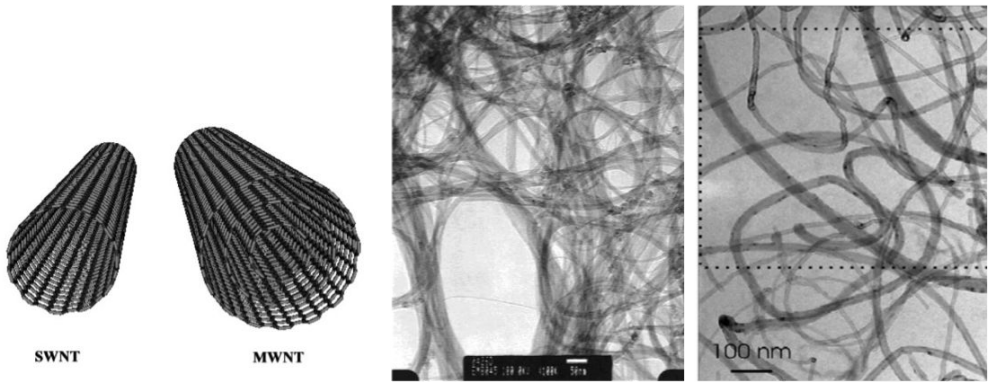

(a) (b) (c)

Figure 2.1: Molecular structure of carbon nanotubes (a), TEM images of respectively a SWNT (b) from [31] and a MWNT (c) from [32]

- arc discharge: the carbon contained in the negative electrode will sublime due to high discharge temperatures [33].
- laser ablation: a pulsed laser vaporizes a graphite target in a high-temperature reactor. At the same time, an inert gas is brought into the chamber, leading to formation of carbon nanotubes on the cooler reactor surfaces, while the carbon condenses [34, 35].
- chemical vapor deposition process: a substrate with a layer of metal catalyst particles is heated to 700°C. Two gases are brought into the reactor to initialize the growth of the nanotubes: a process gas such as ammonia, nitrogen or hydrogen, and a carbon-containing gas such as methane, ethanol, acetylene or ethylene. Nanotubes will grow at the site of the metal catalyst, the diameter will be therefore linked to the size of these particles [36].

Members of the fullerene family, their particular structure gives carbon nanotubes extraordinary properties, such as a very high tensile strength and Young's modulus, which makes them particularly suitable for matrix reinforcement. They also demonstrate good intrinsic conductivity, hence their increasing use in nanotechnology applications as well as material science, such as transparent, electrically conductive films for touch screens and flexible displays [37, 38]. Conductivity depends on the CNTs type, SWNT showing higher conductivity values than MWNT. The particular high aspect ratio of carbon nanotubes confers to the resulting composite to present a very low percolation threshold [39]. However, also due to their shape, the maximum experimentally achievable conductivity is not really high. Indeed, as the excluded volume is very large, the amount of CNTs that it is possible to incorporate to the matrix is limited (i.e. maximum volume fraction is low). For practical purposes, only

MWNTs are used to make resistive composites: they are cheaper and always conductive (the SWNTs presenting a random conductivity, which depends on chirality).

Public opinion attributes the discovery of carbon nanotubes to Sumio Iijima in 1991 [40]. However, in 2006, Monthioux et al. [41] highlighted the fact that this was not the first time carbon nanotubes were found in literature. Once more, distinction must be done between SWNTs and MWNTs. Indeed, if the first ones were unquestionably discovered simultaneously by Iijima et al. from NEC and Bethune et al. from IBM in 1993 [42, 43], existence of MWNTs were already reported in 1952 by Radushkevich et al. in the Journal of Physical Chemistry of Russia [44]. This was followed by several publications from various authors such as Hillert and Lange in 1958 or Baker in the seventies [45, 46]. The impact of the "rediscovery" of Iijima in 1991 can be attributed to the cold war, which limited scientific communications between Russia and the western countries, but also to the lack of interest of fundamental physicists. Indeed, nanotubes have been widely studied by materials scientists and chemists, as they wanted to prevent their formation in coal and steel industry processing.

2.1.1.3 Graphene

The latest member of the family, graphene is, as well, an allotrope of carbon. Its structure of a one-atom-thick planar sheet of sp^2-bonded carbon atoms densely packed in a honeycomb crystal lattice, gives this uncommon 2D material astonishing properties [47, 48]. Graphene is the basic structure leading to the formation of all the graphitic forms we know: fullerene when it is wrapped, nanotube when rolled and graphite when stacked (Fig. 2.2).

Various methods allow the fabrication of graphene, the two most well-known are:

- mechanical exfoliation of graphite: adhesive tape is used repeatedly on graphite crystals to obtain increasingly thinner pieces. It was the method used first by A. Geim from the University of Manchester in 2004 (Nobel Prize in Physics in 2010 with K. Novoselov) [49]
- epitaxial growth on silicon carbide (SiC): SiC is heated to temperatures above 1100°C in vacuum to produce a graphene layer by evaporation of silicon. Dimensions of this epitaxial graphene will depend on the size of the wafer [50]

So, what makes graphene such a remarkable material? First, it presents extraordinary electronic transport properties, as it shows high electron mobility at room temperature and it is a zero-gap semiconductor [49]. Regarding mechanical properties, with a Young's modulus of ≈ 1 TPa [51], graphene is today the stiffest material ever measured, which is why researchers are eager to find new and exciting applications for graphene, such as in sensors [52–54],

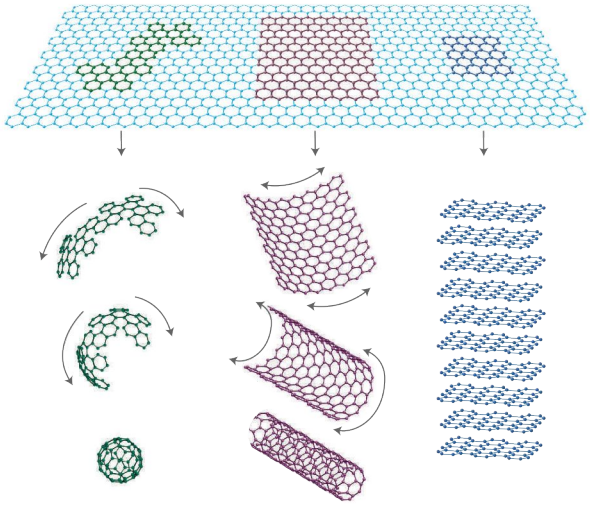

Figure 2.2: Graphene structure leading to fullerene (left, wrapped), nanotube (middle, rolled) and graphite (right, stacked) [47]

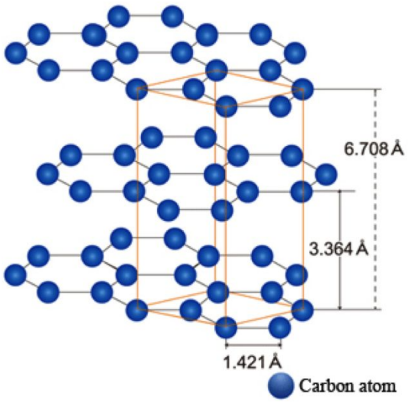

Figure 2.3: Structure of graphite

transistors [55,56], solar cells [57,58] or biodevices [59,60]. However, concerning its application as a filler in a polymer matrix, this material must be incorporated and distributed homogeneously inside the matrix, which is quite complex (manufacturing process...).

2.1.1.4 Graphite

Graphite is the most stable form of carbon under standard conditions (more stable than diamond). Its structure is layered and planar, each layer being arranged in a hexagonal lattice (Fig. 2.3). When speaking about graphite, one should distinguish natural from synthetic graphite.

Natural graphite is found all around the world, where it is mined by both open pit and underground methods. It comes from the transformation of organic matter deposits, which have undergone very high pressures and temperatures over millions of years. Due to its high-temperature stability in inert atmosphere and chemical inertness, natural graphite is a perfect candidate for refractory applications in O_2-free environments. Another possible application is as a lubricant at very high or very low temperatures [61, 62]. Natural graphite presents a lower degree of purity than the synthetic variant, which makes it less suitable for some industrial applications, where contamination is a concern (modern battery cells, electric arc furnaces...).

Two types of synthetic graphites can be found: primary synthetic graphite, which is graphite synthesized specifically for the desired application and secondary graphite, which is a by-product of the manufacturing of electrodes. Primary synthetic graphite is produced from selected carbon precursors (petroleum, coal-tar based cokes...) that are submitted to heat treatment at high temperatures (above 2500°C) under exclusion of oxygen. During this heat treatment, the amorphous material is purified and transformed into crystalline carbon [63]. Graphite presents several advantages such as a much higher electrical and thermal conductivity than carbon black. However, it shows also a strong anisotropy and tends to have a high percolation threshold in polymers. Nevertheless, graphite is used in wide ranges of applications such as sensors and fuel cells and its composites are extensively studied [64–70].

Recently, new forms of graphite were developed, such as expanded graphite (EG). Expanded graphite consists in natural graphite that undergoes a chemical treatment: it is first converted into "Graphite Intercalation Compound" (GIC) after an oxidation in a mix of sulphuric and nitric acid. Then, this compound is put in a furnace above 600°C and expanded graphite is obtained after a rapid expansion and exfoliation of GIC, resulting in very thin flakes (<100 nm) [71]. The particular worm-like shape of this material, compared to standard graphite and its ellipsoidal particles, will give different properties, in particular due to the higher aspect ratio (Fig. 2.4). The corresponding composites present very interesting properties such as higher conductivity at a lower volume fraction or low thermal conductivity [72–76]. EG appears as a good compromise between graphite and graphene.

2.1.2 Short comparisons of the different fillers

The previous paragraph proving the wide diversity of carbon-based fillers, we intend now to make a brief comparison of their main properties, toxicity and costs. We first propose a summary of the basic properties of the materials (see Table 2.1). Young's modulus values were not available for carbon black. Graphite and carbon black are quite comparable in terms of electrical resistivity values, however, graphite shows higher thermal conductivity. Graphene is clearly extraordinary in many domains and carbon nanotubes are between

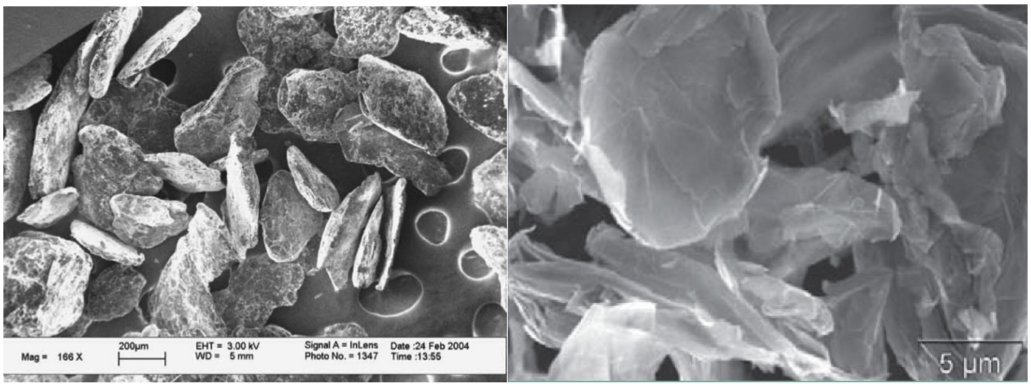

(a) (b)

Figure 2.4: SEM images of standard graphite from [71] (a) and expanded graphite from [77] (b)

these two groups, with general properties closer to graphene but with a different morphology.

Table 2.1: Main properties of carbon black, carbon nanotube, graphene and graphite

Filler types	Size range	Young's modulus [GPa]	Thermal conductivity [$W.m^{-1}.K^{-1}$]	Electrical resistivity [Ω.m]	Morphology
Carbon black	10-100 µm	NA	0.2-0.3 [78]	$3{,}5.10^{-5}$ [79]	$\approx$ particles: 3D
CNTs	nm	$\approx$ 1'000 [80]	3'200 (MWNT) 3'500 (SWNT) [81, 82]	10^{-5} (MWNT) 10^{-6} (SWNT) [83]	needles: 1D
Graphene	nm	1'000 [51]	$\approx$ 5'000 [84]	10^{-8} [85]	flakes: 2D
Graphite	2-200 µm	600 (in-plane) 10.5 (out-of-plane) [86]	160 [87]	10^{-6} [87]	EG: 2D ellipsoid: 3D

Regarding toxicity, a rapid look at the Material Safety Data Sheets (MSDS) of these fillers shows that they are basically separated in two: carbon black and graphitic material (i.e. graphite, carbon nanotube and graphene). Table 2.2 summarizes the properties. However, we have to keep in mind that, even if it is not clearly mentioned on the MSDS, graphene and carbon nanotube are in nanosize in at least one dimension, which means that they can potentially

pass and travel in the body more easily, but also have special interactions with the biosystem different from the corresponding fine particle (i.e. graphite in this case). Therefore, using these materials will require more specific handling regarding safety equipment, especially when they are not in a matrix, as we do not really know the consequences on health yet. Moreover, as far as carbon nanotubes are concerned, their shape is closely related to that of asbestos fibers, a material of very high concern during the last decades due to its consequences on human health, i.e. lung cancers. Poland et al. [88] have exposed the mesothelial lining of the body cavity of mice to long MWNTs and highlighted the fact that, as for asbestos, it causes inflammations and lesions (known as granulomas). Even if it is impossible to know at the present time the biopersistence of carbon nanotubes inside the body, caution is *de rigueur* regarding these new materials, as they don't behave as graphite. This is the reason why intensive studies are performed to quantify their possible impact on health [89–91].

Table 2.2: Toxicity information

Filler types	Skin irritation	Eye irritation	Respiratory track irritation	Carcinogenic
Carbon black	no	no	mild	possibly to humans
Graphite / graphene	yes	yes	slightly hazardous	NA
CNTs	yes	yes	slightly hazardous	close to asbestos fibers in shape → lung cancer?

Finally, from an industrial point of view, it can be interesting to have an idea of the costs of these fillers. The data are presented in Table 2.3. No data were available concerning synthetic graphite production: few firms producing it, the results are confidential. As expected, we can see that as graphene is a quite new material, it is therefore really expensive and there is nowadays no simple way to produce it on a mass-production scale. Differences in the SWNTs production and MWNTs come respectively from purity and diameter sizes. However, one has to keep in mind that if a very interesting industrial application is found with graphene for instance, a process will probably be found as well, allowing mass production at a lower cost.

Table 2.3: Production and costs (from US Geological Survey and www.lecarbone.com, 2011)

Filler types	World production in 2009 [tons]	Average cost [$/kg]
Carbon black	7'000'000	1-5
SWNT	<1000	25'000-80'000
MWNT		6'000-20'000
Graphene	no mass production	≈ 50'000
Natural graphite	1'090'000	≈ 2
Synthetic graphite	NA	6-20

With all this information collected in the literature, from the point of view of properties only, graphene or at least carbon nanotubes would appear as good candidates for composite formulation and sensors manufacturing. However, their prices remain, at the moment, too high for any industrial applications and their shape limits the processability. Carbon black presents properties similar to graphite and is widely used in the industry. However, it is a not so well-defined material compared to graphite, making it not so suitable for a study. Consequently, graphite meets all the requirements for potential industrial applications and is the best compromise between properties, prices and toxicity. Another good compromise is the use of expanded graphite, as this material presents a shape close to graphene, but at a lower price and with more interesting electrical properties.

2.1.3 Influence of the matrix

When talking about composites, two parts have to be taken into consideration: filler and matrix. Whereas the previous section intended to compare carbon-based fillers, this section will be dedicated to the matrix. Matrices can be of various kinds: glass, ceramic, metal or polymer, leading obviously to different properties and application ranges. As this thesis only deals with polymer-based composites, we will only discuss this type.

Two types of polymers are used as matrix:

- thermosetting polymer: a prepolymer (in a soft solid or viscous liquid state) that polymerizes *irreversibly* into an infusible, insoluble polymer network by curing, such as epoxies or phenolics
- thermoplastic polymer: a polymer that *reversibly* turns to a liquid when heated and freezes into a glassy (i.e. amorphous) or semi-crystalline state when cooled, such as polyethylene (low and high-density), polypropylene, polystyrene, polyamides or acrylics.

Compared to ceramics and metals, polymers exhibit high thermal expansion and poor thermal stability. However, by using proper fillers and additives, these

drawbacks can be mitigated. Usually, thermosets are thermally more stable than thermoplastics due to the strong 3D network chemical bonds (cross-links). Their curing process can be done by heat, chemical reaction or irradiation and induces a cross-linking process that will in principle form a single enormous molecule with a higher molecular weight. Thermosets may be (and usually are) formulated to be initially liquid, so do not intrinsically need solvents to be deposited. Thermoplastics are high-molecular-weight polymers, whose chains can associate through weak bonds (Van der Waals forces) or hydrogen bonds. These bonds are thermally labile, which allows the polymer to become liquid again upon reheating. Thermoplastics require dissolution/dispersion in a suitable solvent for screen-printing. Here, thermal treatment usually merely consists in drying, i.e. evaporation of the solvent. Regarding storage, thermosets have a limited storage pot-life due to their reactive nature, which means that they are often prepared by mixing two parts and used almost immediately, whereas thermoplastics can be prepared and stored for extended periods, their properties not degrading (for instance, some pastes used in our laboratory are perfectly functional after over 10 years!). Polycomponent thermosets (typically epoxies) present also a storage shelf-life, which is much longer than the pot-life as the component are not mixed yet; the shelf-life depends on the degradation/alteration of each component. Alternatively single-component epoxies also exist, but often entail a compromise between shelf-life, curing temperature and storage temperature.

An important characteristic of polymers is the *glass transition temperature* T_g, which corresponds to the moment where the amorphous phase of the material presents a transition between a hard glassy state and a rubbery one. It is more a range than a strict temperature and often defines one end of the operating range of the polymer: for strength and stiff amorphous materials, it is the upper limit, whereas for elastomers and semi-crystalline materials, it corresponds to the lower operating temperature, below which the material will become hard and brittle. For instance, most epoxies and amorphous plastics (such as PMMA, polystyrene, polycarbonate) are useful at temperatures below T_{g} , whereas silicones, which present a very low T_{g} (ca. -40°C), are usually used above this temperature. T_g can be decreased by the use of a plasticizer (a small molecule "dissolved" in the polymer and not chemically bonded with it) [92] or a flexibilizer (with the same effect but chemically bonded to the polymer).

Depending on the polymer matrix, the intrinsic properties are different, hence differences in the resulting composites. For instance, Kuilla et al. [93] have listed the conductivity of graphite composites in various polymer matrices (epoxy, PMMA, HDPE, polycarbonate...) and showed that, depending on the matrix, the materials exhibited different values.

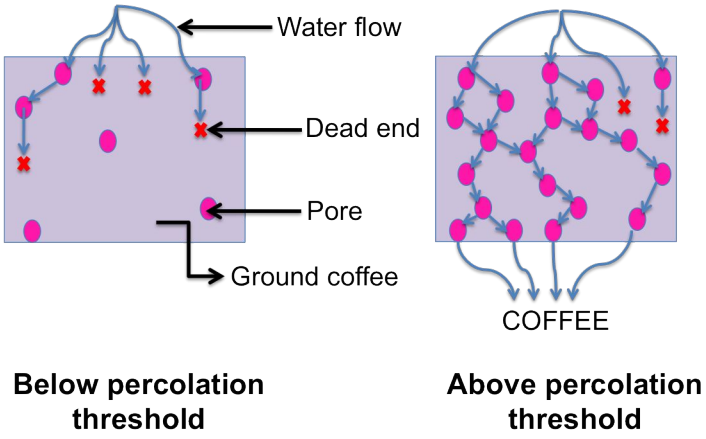

Figure 2.5: Schematic explanation of coffee percolation

2.2 Electrical properties

We have briefly exposed in Section 2.1 the conductive properties of carbon-based composites. We will now look into the conduction mechanisms that govern the behavior of these materials. However, despite the fact that the theory is rather simple, when put in practice, it becomes a lot more complex due to external phenomena and small interactions. More extensive investigations and modeling work on the subject can be found in the theses of Ambrosetti and Johner [94, 95] who studied the conduction mechanisms in such composites.

2.2.1 Percolation theory

The dispersion of a conductive carbon-based component into a polymer matrix is known to form a percolative composite system, which means that in order to obtain conductivity, a minimum amount of conductive particles, called *the percolation threshold*, will be needed, below which the composite is an insulator. A simple application of representing it in daily-life is a coffee maker: a certain number of pores are necessary for the water to flow through the ground coffee and extract flavor and taste, which gives a nice beverage at the end. If not, the liquid is blocked and nothing comes out (Fig. 2.5).

The composites we are studying are called random resistive networks. According to the classical theory firstly developed by Kirkpatrick [96], they are often found to follow a power law of the form:

$$\sigma \propto \sigma_0 \left(\phi - \phi_c\right)^t \tag{2.1}$$

where σ represents the bulk conductivity of the composite, ϕ the volume fraction and ϕ_c the percolation threshold.

The percolation threshold, as well as the proportionality constant σ_0, depends on microscopic details (microstructure and mean intergrain junction conduction), whereas the transport critical exponent t is supposed to be independent of the material. In the literature [97], it was determined that $t = t_0 \approx 2$ in three-dimensional lattices. However, Vionnet-Menot et al. exposed more recently that the universality of t is limited: in almost 50% of the values reported, the exponent t was different from t_0, most of the time above this "ideal" value [8]. Several models were developed to explain the origin of this non-universality. One of them is the tunneling-percolation model (or inverted random void model) which was proposed by Balberg [98]. Conducting spheres are dispersed in insulating medium and current flows between these particles by a tunneling process. The idea of Balberg is that the critical exponent t depends on a microscopic variable (the mean-tunneling distance a) that can be modified by a suitable external perturbation. This model can be applied to systems in which intergrain tunneling is the main transport mechanism, which is our case. However, various parameters influence electrical conductivity such as the shape, the particle surfaces or the size. Ambrosetti et al. [99] have therefore developed a new model by taking into account all these features to explain tunneling-percolation in nanocomposites. They demonstrated that conductivity depends on the interparticle tunneling. Indeed classical theory supposed that there is a cutoff in the interparticle conductivity, i.e. particles are either connected or disconnected, which is odd as it is a continuum phenomenon. By using the critical path approximation, they found that conductivity can be described by the following equation:

$$\sigma \backsimeq \sigma_0 \exp\left(-\frac{2\delta_c\left(\phi,\, a,\, b\right)}{\xi}\right) \tag{2.2}$$

where ξ is the characteristic tunneling length and a/b defines the aspect ratio of the particle, σ, σ_0 and ϕ having already been defined previously. δ_c represents the "geometrical" critical distance, it corresponds to the minimum value between two connected particles.

2.2.2 Piezoresistivity

Additionally to the conductivity, it is of high interest to know the piezoresistive behavior. Indeed, as our composites form percolative systems, their resistance will be strongly influenced by a mechanical strain. Piezoresistivity has been found to be a more sensitive tool to study tunneling percolation [95] and is also of important practical use in sensor applications [100].

2.2.2.1 General theory

Piezoresistivity is defined as the change of resistance due to deformation by an applied strain ϵ. It appears therefore as another useful way to study tunneling

percolation inside a thick-film resistor. An important parameter to describe the piezoresistivity response is the gauge factor GF defined as:

$$GF = \frac{dR}{R\varepsilon} \quad with\ \varepsilon = \frac{dL}{L} \tag{2.3}$$

This equation is valid in an isothermal case: otherwise, we have $\varepsilon = dL/L - \alpha_R \Delta T$, with a_R the coefficient of thermal expansion of the resistor. This particular case will be discussed later in Part 4.4.1. The following theoretical explanations come mostly from Ref. [101]. If we take a parallelepiped resistor with L_x, L_y and L_z as dimensions, and we then apply a stress onto it, it can deform in x, y and z directions. ρ being the resistivity, the resistance R can be expressed as:

$$R = \rho \frac{L_x}{L_y L_z} \tag{2.4}$$

We have therefore:

$$\frac{dR}{R} = \frac{d\rho}{\rho} + \frac{dL_x}{L_x} - \frac{dL_y}{L_y} - \frac{dL_z}{L_z} = \frac{d\rho}{\rho} + \varepsilon_x - \varepsilon_y - \varepsilon_z \tag{2.5}$$

By combining Eq. 2.3 and 2.5, we can express the gauge factor as:

$$GF = \frac{d\rho}{\rho\varepsilon} + \frac{\varepsilon_x}{\varepsilon} - \frac{\varepsilon_y}{\varepsilon} - \frac{\varepsilon_z}{\varepsilon} \tag{2.6}$$

If we assume shear stress to have no significant effect[1], the resistivity depends on ε_x, ε_y and ε_z and we can write:

$$\frac{d\rho}{\rho} = \frac{\partial\rho}{\rho\varepsilon_x}\varepsilon_x + \frac{\partial\rho}{\rho\varepsilon_y}\varepsilon_y + \frac{\partial\rho}{\rho\varepsilon_z}\varepsilon_z \tag{2.7}$$

We can thus define the longitudinal piezoresistive factor Γ_L and the transverse piezoresistive factor Γ_T:

$$\Gamma_L = \frac{d\rho}{\rho\varepsilon_x} \tag{2.8}$$

$$\Gamma_T = \frac{d\rho}{\rho\varepsilon_y} = \frac{d\rho}{\rho\varepsilon_z} \tag{2.9}$$

Using Eq. 2.7, 2.8 and 2.9 in Eq. 2.6, we obtain the general formula for the gauge factor:

$$GF = (\Gamma_L + 1)\frac{\varepsilon_x}{\varepsilon} + (\Gamma_T - 1)\frac{\varepsilon_y + \varepsilon_z}{\varepsilon} \tag{2.10}$$

[1] This assumption is often made for percolative disordered materials, but it is not generally true; especially single-crystalline semiconductors, such as silicon, have very strong shear piezoresistive effect.

If we now consider the isotropic piezoresistive factor, i.e. the resistivity change upon an isotropic strain $\varepsilon = \varepsilon_x + \varepsilon_y + \varepsilon_z$. The strains being small, it is possible to write:

$$\Gamma = \frac{d\rho}{\rho\varepsilon_x} + \frac{d\rho}{\rho\varepsilon_y} + \frac{d\rho}{\rho\varepsilon_z} \tag{2.11}$$

There are only two possibilities: either the deformation is parallel to the current or transversal. By using Eq. 2.8 and 2.9 we obtain the following equation, which is useful in the common case where the experimental set-up does not apply an isotropic strain:

$$\Gamma = \Gamma_L + 2\Gamma_T \tag{2.12}$$

Experimentally, we measure the gauge factors (coming from the conductance variation) and not the piezoresistive factors, therefore, the strains in the resistive composite have to be known in order to extract Γ_L and Γ_T. Piezoresistivity in thick-film resistors was demonstrated to strongly depend on the nature of the conductive grains, the microstructure and the sheet resistivity of the paste [102, 103]. Typical values of GFs for thick-film resistors are comprised between 2 and 35 at room temperature [104].

2.2.2.2 Application to the case of a cantilever in bending

Gauge factors will be measured using cantilever beams (see Part 4.1.4). Such a beam is clamped at one end and a weight is then applied on its free tip. On the surface, four resistors forming a Wheatstone bridge allow to obtain the corresponding electrical signal response, which is recorded, leading, after calculation, to both gauge factors. The longitudinal gauge factor $\mathrm{GF_L}$ is the case where the current flows along the length of the beam (i.e. the current is parallel to the applied strain) and the transverse gauge factor $\mathrm{GF_T}$ where the current flows along the width of the beam (i.e. current perpendicular to the applied strain). While the force is applied, the beam will deform (Fig. 2.6). A tensile stress appears at the surface of the beam and strains are transferred to the resistor as well. The strains along the x, y and z axis are therefore approximately [105]:

- $\varepsilon_x = \varepsilon$
- $\varepsilon_y = -\nu\varepsilon$
- $\varepsilon_z = -\nu'\varepsilon$

where ϵ is the applied strain, ν is the Poisson's ratio of the substrate and ν' the "effective" Poisson's ratio of the resistor. From [106], we can define the "effective" Poisson's ratio as:

$$\nu' = \nu_R \frac{1-\nu_S}{1-\nu_R} \tag{2.13}$$

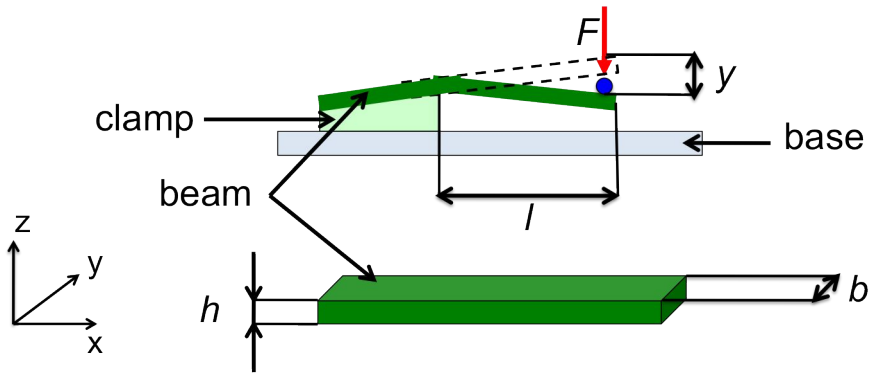

Figure 2.6: Beam clamped at one end and with a force applied at the other (sectional view) and side view of the beam

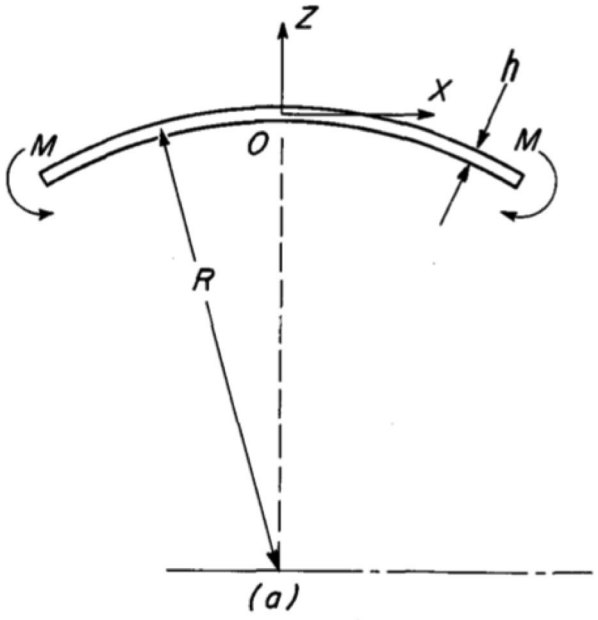

Figure 2.7: Radius of curvature on a bending plate, M being the moment (from [108])

with ν_R the Poisson's ratio of the resistor. This "effective" Poisson's ratio is most of the time close to the Poisson's ratio of the resistor.

In some cases, ε_y can be considered as equal to 0. This is not applicable here. Indeed, to do so, the ratio $b^2/(Rh)$ must be more than 1.6 with R the radius of curvature (see Fig. 2.7), b the width and h the thickness [107]. Considering the dimensions of the beam we have, R should be less than 25.6 mm (with $b = 5.08$ mm and $h = 0.63$ mm in our case): this condition is not true.

In the following part, indexes i, j and k assume the axis x, y and z with cyclic permutations. The piezoresistive gauge factors can be defined as [105]:

$$GF_{ij} = \frac{dR_i}{\varepsilon_j R} \tag{2.14}$$

where R is the resistance and R_i is the resistance when a strain ϵ_j is applied.

By expressing the cantilever strains into Eq. 2.10 and using Eq. 2.14, we directly obtain the longitudinal gauge factor GF_Ldefined as:

$$GF_L = GF_{xx} = (1 + \Gamma_L) + (1 - \Gamma_T)(\nu + \nu') \tag{2.15}$$

Likewise, the transverse gauge GF_T is obtained:

$$GF_T = GF_{yx} = GF_{zx} = -(1 + \Gamma_L)\nu - (1 - \Gamma_T)(1 - \nu') \tag{2.16}$$

2.2.3 Temperature coefficient of resistance

In thick-film resistors (and as in other materials), the resistance value changes with temperature. The temperature coefficient of resistance (TCR) is used to quantify this effect and is defined as:

$$TCR = \frac{R - R_{ref}}{R_{ref}(T - T_{ref})} \tag{2.17}$$

where R is the resistance of the conductor at temperature T, R_{ref} the resistance of the conductor at reference temperature T_{ref} (usually around room temperature, conventionally 25°C).

This value can be either positive, which means that the resistance will increase with an increase in temperature (case of pure metals for instance) or negative, meaning that the resistance decreases with an increase in temperature (such as semiconductor materials: silicon, germanium...). TCR is often quite non-linear and subject to transitions in the materials, such as glass transition or melting in the matrix, or solid-solid transitions in the filler. For instance, a glass/metal oxide system is a temperature sensitive product. At low temperatures, the TCR being negative (predominance of semi-conducting properties in the glassy matrix) and becomes positive but non linear (usually, just below room temperature) [109, 110].

This non-linearity is particularly true in the case of conductive polymer composites as drastic changes occur around the glass transition temperature. The matrix dilates, creating rearrangement inside the composite, hence dramatic changes for the TCR value. Therefore, when speaking about TCR in this case, it is of high importance to give the temperature range and the glass transition temperature.

2.3 Mechanical properties

A composite is defined as the assembly of two non-miscible materials, leading to the formation of a new one, which gives the resulting materials properties that its components alone cannot have. Historically, they were used for their improved mechanical properties. It has been reported that in ancient times, men already made composites by mixing mud and straw to obtain "bricks" for building purposes. The discovery of new types of fillers such as carbon fibers or nanotubes has increased their use in leading edge technologies, allowing the fabrication of light and strong materials. The following sections intend to sum up how a composite works, to demonstrate the importance of the filler shape and finally, to highlight another way of improving the filler through surface functionalization.

2.3.1 Influence of filler shape

Let us first take a composite that can be found in nature and is used since the mists of time for construction purposes: wood. Wood is made of cellulose fibers embedded in a lignin matrix. This particular composition gives a material with a high tensile strength when the stress is applied parallel to the grain. However, it exhibits a poor compressive and tensile strength across the grain [111]. Another common composite we encounter in our daily-life is concrete. Mainly composed of aggregates such as gravel or crushed rocks (typically limestone or granite) linked with cement, it presents a high compressive strength (typically 20-40 MPa) but a low tensile strength, which may be however improved by adding another strengthening phase, most commonly steel rebar (resulting in reinforced concrete).

These two simple examples demonstrate the importance of the filler shape but also the inner arrangement of the filler in the matrix. This can also affect the isotropic/anisotropic character of the studied property. We will therefore distinguish two cases: fiber and particle.

Fiber-reinforced composites are divided into two main categories: short and long fiber materials. Continuous fiber-reinforced (i.e long fibers) composites define laminated structures, whereas short fiber-reinforced materials usually present randomly dispersed fibers (Fig. 2.8). Glass, aramid or carbon are types of fibers widely used as matrix reinforcement, due to their interesting intrinsic properties, which are summarized in Table 2.4[2]. Therefore, if the fibers are all oriented in the same way, intuitively, the resulting composite will have a high unidirectional tensile strength. Such composites are particularly useful to fabricate masts, fishing pole, rackets or rigging. Another possibility is to orient fibers at a predefined angle (for instance 90°), which give multidirectional reinforcement: this is the case of bulletproof vest where the fibers are woven, guaranteeing a high strength. Finally, randomly oriented fibers should confer

[2]E-glass stands for electrical-glass and S-glass for stiffness-glass.

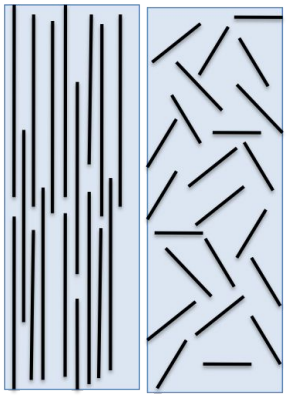

(a) (b)

Figure 2.8: Fiber composite: continuous fiber-reinforced material (a), randomly oriented short fiber-reinforced material (b)

the composite isotropic resistance. However, this must be moderated, as the way of shaping the composites will likely orient the fibers. For instance, if the composite is injected, this will tend to align the fibers parallel to material flow. This will be of course less effective than a composite with oriented fibers.

Table 2.4: Main properties of typical fibers (supplier data, www.carbonfibertubeshop.com, 2011)

Fiber types	Young's modulus [GPa]	Density [g/cm^3]	Tensile strength [MPa]	Tensile strength of the epoxy composite [MPa]
Carbon	228	≈ 2	4'000	1'900
Aramid	124	≈ 1.5	2'760	1'310
E-Glass	72	≈ 2.5	3'450	1'770
S-Glass	86	≈ 2.5	4'590	2'360

Particle-reinforced composites exhibit nominally isotropic properties due to their dispersion in the matrix. Depending on the size of the particles, they are divided in two subgroups: large-particle and dispersion-strengthened composites. The first category acts by restraining the movement of the matrix. It is the case of concrete, an example we discussed previously, or tires. Dispersion-strengthened composites consist in using very hard, small particles to strengthen a matrix. The matrix carries most of the load but particles will prevent it from moving under compression. This method is most of the time used for metals and metal alloys. According to the Nondestructive Testing Resource Center, particles like oxides do not react with the matrix, leading to

a strong material even at high temperatures. Particles typically used to manufacture these composites are glass beads, Al_2O_3 or clay for instance [86, 112]. However, one has to keep in mind that a certain anisotropy is induced by most processing conditions of metal-matrix composites, which results in an anisotropy of the properties of the materials [113].

Fiber-reinforced composites are stronger materials than particle-reinforced ones because the matrix-filler strain loading is distributed all along the fibers, resulting into a more efficient load transfer to the fibers, hence a stronger material as the fibers exhibit already a high tensile strength. As the addition of particles to a matrix will not bring much difference to the resulting mechanical properties, the purpose of these composites may be to decrease the thermal expansion [114] or increase the thermal or electrical conductivity [115].

Application to carbon-based composites If we now go back to our carbon-based materials, it seems quite obvious that depending on the shape, the properties of the composites and their use will be different. Table 2.5 shows mechanical properties of the fillers.

Table 2.5: Comparison of some mechanical properties for different carbon-based fillers

Filler types	Young's modulus [GPa]	Tensile strength [MPa]
Carbon nanotube (along length)	≈ 1'000 [80]	≈ 50'000, theoretically up to 150'000 [80]
Graphene (in plane)	1'000 [51]	130'000 [51]
Graphite	600 (in-plane) 10.5 (out-of-plane) [86]	8-12 [116]

Regarding graphite, the reader has to keep in mind that it is an anisotropic material, therefore, depending on the orientation, the properties will be different [117]. No values were available for carbon black alone, however, it is commonly used has a reinforcing material for rubber in tires, which gives typical values of 20 to 30 MPa for the tensile strength [118, 119]. Carbon black can also be found in harder polymers, such as epoxies. It was for instance demonstrated that it could stiffen epoxy, increasing its Young's modulus from 2 GPa to 15 GPa. It has also the effect to shift the thermal decomposition to a higher temperature [120]. Although graphene as well as carbon nanotubes present very high tensile strength and Young's modulus, producing graphene and efficiently dispersing it into a composite remains difficult and onerous, hence no large-scale industrial applications at the moment. Nevertheless, it is possible

to obtain exfoliated graphite with a few monolayers quite easily. Intensive research is done on carbon nanotubes in order to use them instead of carbon fibers, for instance for some sports equipments (bikes, racket) or textiles (bulletproof vest). Indeed, they would be particularly suitable for applications where high strength and light composites are needed. However, in spite of the amazing mechanical properties reported by several authors about the CNTs, those values have to be taken cautiously as factors such as defects, chemical environment, concentration or temperature will affect the properties of the resulting composites [121, 122]. CNTs are also difficult to process into composites.

Graphite can be used to stiffen polymer matrices such as epoxies, polypropylene or polyethylene, but, above all, graphite has an impact on the thermal properties of the resulting composites, which is the main reason of its use as a filler [66, 75]. Graphite decreases thermal expansion, which is a desired effect for engineering applications but also increases thermal stability [86]. Higher thermal conductivity was also reported [68], which is of great use for heat spreader for instance. In this application, the anisotropic nature of graphite is used as well [123].

2.3.2 Surface functionalization through graphite oxidation

When talking about mechanical properties, one has to keep in mind the importance of the interactions between the filler and its matrix. Graphite is a quite inert material and its matrix/filler interactions are low. Compared to graphene or carbon nanotubes, it exhibits poor mechanical properties. A way of improving this weakness can be to functionalize the particle surfaces, i.e. add chemical groups on the surface. Considering the chemical structure of an epoxy, it can be really interesting to have O groups on the graphite surface (-OH, =CO, -COOH). This can be done through an oxidation process (see Fig. 2.9).

Several processes allow the oxidation of graphite: air oxidation, wet oxidation in concentrated HNO_3 or anodic oxidation [124–127]. The reactive groups will therefore be able to create bonds with the matrix, hence reinforcing the interactions. Four reactive sites were counted on the graphite surface [128]. Magne et al. highlighted the fact that graphite has two reactive sites set on unstable carbons, these sites being able to form complexes with the oxygen during the oxidation process. The two others sites are fixed on carbon belonging to the network. They will form complexes at the surface for oxidation temperature below 950°C with a maximum decomposition speed at 650°C for the first type, and for oxidation temperature above 950°C with a maximum decomposition speed at 750°C for the second type.

Yumitori et al. studied the interfacial shear strength between an epoxy matrix and a carbon fiber and showed better adhesion in the case of oxidized fibers [129, 130]. Other examples can be found in the literature [131, 132],

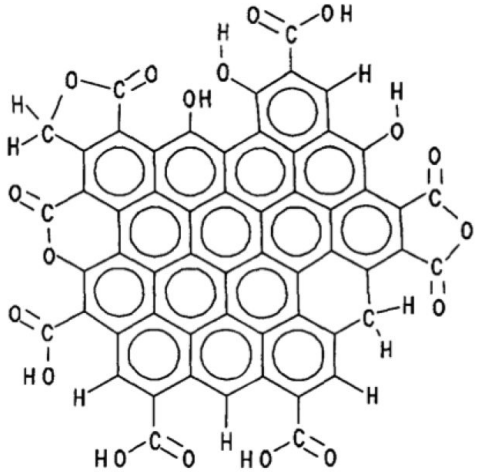

Figure 2.9: Possible structure of a partially oxidized graphite particle from [124]

however, almost nothing has been done on graphite particles, most of the studies dealing with carbon fibers, with the goal of achieving high-strength composite materials. Interfacial cohesion may also be important in our case, as it may lead to better stability of the properties, in particular mechanical ones. Therefore, studying functionalization in the case of graphite particles is of high interest as well.

2.4 Thick-film technology

Thick-film technology is one of the common techniques used to produce electronic devices such as sensors or hybrid circuits. Historically, it came from a desire to obtain a way to deposit resistors *en bloc*. As the samples used in this thesis are thick-film resistors, we will explain in the following paragraph this process.

2.4.1 Case of mineral paste

In thick-film technology, the pastes can be either mineral or organic, which induces modifications in formulation or process temperatures for instance. Traditionally, mineral pastes are used. Their process will only be briefly detailed hereafter, as this type of pastes was not used in this thesis.

2.4.1.1 The screen-printing process

First reported in the Song Dynasty in China (960-1279 BC), screen-printing was traditionally considered as a form of art. In order to use it for thick-film technology, it had to be modernized, mainly by mechanization, automation,

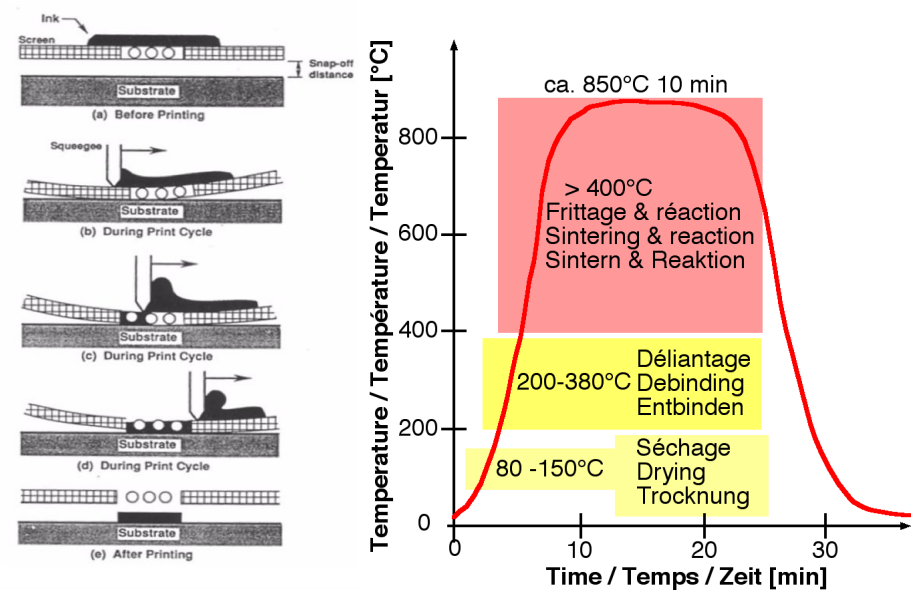

(a) (b)

Figure 2.10: Screen-printing process: deposition (a) and typical firing schedule of a thick-film paste (b) [100]

use of stiffer and more precise metal screens and more careful paste formulation. The process is rather simple: a paste is forced through a screen with a squeegee. It goes inside the holes of the screen, leaving at the end the desired pattern onto the substrate. Fig. 2.10a shows in broad outline the steps of the process.

Screens are made of stainless steel wires, a UV-sensitive emulsion is deposited onto the screen with the desired pattern. By developing, the emulsion is removed selectively, leaving the pattern on the screen, which can thereafter be reproduced on the substrate. Screen-printing allows deposition of layers with a thickness ranging from 10 to 200 µm [133], the thickness depending on the meshes of the screen, the emulsion deposited to make it, the pressure and the speed of the squeegee.

Three types of pastes are mainly used: conductive, insulating and resistive, the last kind will be more discussed in the following sections as it is the study of this thesis.

After deposition of the paste, it must be dried. This is done in two steps: a first drying in a regular oven to evaporate the solvents and a second called firing in a belt furnace where densification and reactions of the components will occur at pre-programmed steps (Fig. 2.10b).

2.4.1.2 The materials

To manufacture a device using thick-film technology, we know that three kinds of pastes can be used:

- conducting paste, which should not interact too much with the substrate, i.e. no alteration, (such as Au, Ag/Pd...) and also be solderable when required
- insulating paste, i.e. dielectric, which provide insulation from the substrate if needed (for instance when the substrate is electrically conductive) or allows multilayer circuits
- resistive paste

Let us now detail two components in particular that will need special attention when using thick-film technology:

- the resistive paste
- the substrate

A mineral resistive paste is formed of an insulating matrix, i.e. a glass powder ("frit", typically lead borosilicate) and a conductive filler phase such as ruthenium oxide. These powders are then mixed together with an organic vehicle formed by a thermoplastic binder (e.g. ethylcellulose) diluted in a solvent (e.g. terpineol). Fig. 2.11 shows the approximate proportions of the components [100, 110]. The glass powder will define the firing temperature of the paste and the conductive phase the electrical properties. As far as the vehicle is concerned, it is only a temporary constituent in the mineral paste and eventually disappears during the drying process, its purpose being purely to confer suitable rheological properties to the paste. Indeed, rheology is a very important characteristic for screen-printing process. It has been demonstrated that it requires a thixotropic paste [134] so that the paste can pass through the holes formed by the pattern on the screen with the squeegee pressure, and yet not spread excessively on the substrate and keep a well-defined shape. Fig. 2.12 shows the evolution of the viscosity undergone by a thick-film paste, throughout the printing steps. Finally, for special properties, pastes can be tuned with various additives. For instance, a paste with a desired conductivity and a certain temperature coefficient of resistance (TCR) can be needed. To adjust the values, oxides are added to the paste to move the TCR up or down. Explanations about TCR can be found in Sec. 2.2.3.

As far as the substrate is concerned, special requirements are needed such as: good electrical insulation, stability, high thermal conductivity (for power dissipation), dimensional stability at firing temperatures up to 1000°C or chemical and physical compatibility with the appropriate glaze components of conductor and resistor [110]. High alumina ceramics with alumina contents of 94-97% appear therefore as the best candidates for most applications. However,

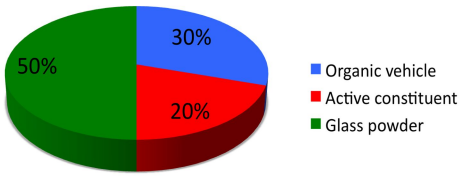

Figure 2.11: Traditional composition of a thick-film resistor paste

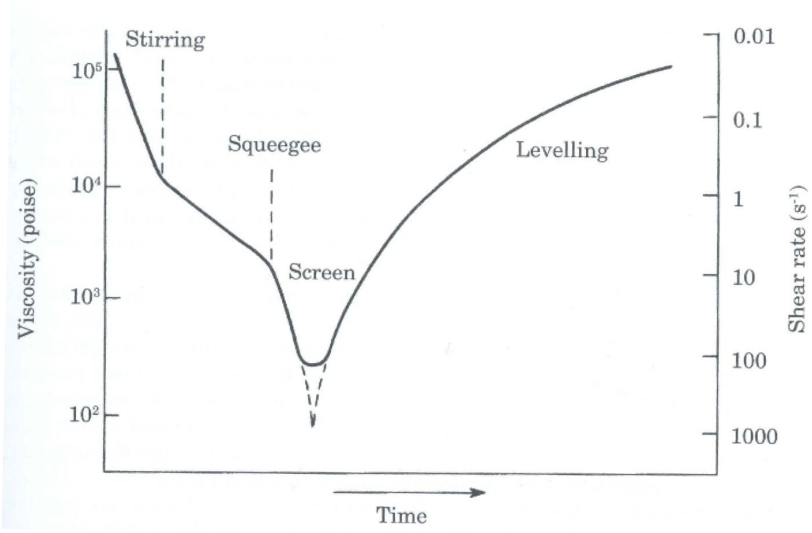

Figure 2.12: Shear rates and viscosity changes during the printing process [110]

depending on the application, other materials can be used such as aluminum, steel (for strain sensors typically [135–137]), glass or Low Temperature Co-fired Ceramic (LTCC) tapes [138, 139].

2.4.2 Case of organic paste

2.4.2.1 The materials

In the case of an organic resistive paste, there are only two basic components: an insulating phase, i.e. a polymer (epoxy, silicone, ethylcellulose for instance) and a conductive phase (graphite, carbon black...). As for a mineral paste, an organic one can also be tuned with solvents or additives in order to adjust the viscosity to a honey-like paste (i.e. correct viscosity required by the screen-printing process), as well as the final properties of the material: plasticizers, stabilizers, anti-oxidants, etc. The case of organic paste will be studied in this

thesis.

The deposition process is basically the same as for mineral pastes, albeit with a much milder heat treatment in an oven (otherwise it would destroy the paste). Two mechanisms are possible depending on the polymer type. The first case is when the polymer is already formed (thermoplastic, for instance ethylcellulose) and merely dissolved in an appropriate solvent; therefore heat is only used to dry the paste on the substrate. In the case of thermoset resins, heat is necessary to polymerize/cross-link the starting product(s), which are usually liquid initially and thus do not intrinsically require solvents. This is typically the case for epoxies, which cross-link with temperature and form a hard layer on the surface of the substrate. In most cases, this drying (resp. polymerization) process is carried out between 80°C to 150°C, but some resins may set at room temperature and others (high-temperature epoxies, polyimides...) require processing temperatures higher than 200°C. Finally, some resins may also set by reaction with the ambient air, i.e. with oxygen or moisture.

Due to the process temperatures, it becomes possible to use other materials than alumina or metallic substrates, such as printed circuit board (PCB, usually a composite of epoxy resin and glass fibers, typically FR-4) , polyethyleneterephtalate (PET) for solar cells for example [140] or polyimide, which extends the application range.

2.4.2.2 Other potential processes

The use of an organic paste involves a wider choice for the deposition process. A common one is the inkjet printing. It consists in the ejection of a certain quantity of ink (fixed) from a nozzle. The ink is stored in a chamber and by the application of an external voltage, the chamber will contract, causing a shockwave in the liquid, hence a liquid drop to be ejected from the nozzle. This low cost process can be used to produce RFID (Radio-Frequency IDentification) tags for instance and will more and more substitute the classical PCB manufacturing process in the future. The main requirement is for the ink to be liquid, with possibly nanoparticles in it. If larger particles are used, there will be a sedimentation problem due to the very low viscosity of the ink [141].

Pastes may also be deposited by an aerosol process. In this case, the ink is stored in an aerosol chamber. It is then aerosolized (for instance by vibrating the aerosol chamber). After that, a gas (N_2, He...) carries the aerosols to the deposition nozzle where the sheath gas focuses the material into lines and draws the pattern [142, 143]. Compared to inkjet-printing, this process is less restrictive. Indeed, as the ink will be aerosolized prior to deposition, it can be stored in paste form, allowing the use of larger particles.

Finally, intaglio also belongs to the family of printing techniques. A plate (typically made of copper or zinc) is etched with the desired pattern, creating therefore incisions. Ink is then applied onto the surface and pushed into them. Excess ink is removed from the plate with a tarlatan cloth, leaving ink only in

the incisions. The substrate is placed on top of the plate and run together in a rolling press. The press pushes the substrate into the plate's grooves in order to cover it with ink. This process requires obviously a very flexible substrate, as it has to be able to go inside the holes of the plate when the pressure is applied. It is also expensive due to high losses during the ink deposition on the plate. Therefore, this process is mainly used for production of stamps and bank bills.

Regarding the available processes, they all have various requirements about viscosity, particle size or types of substrate. From this point of view, screen-printing appears to be the most convenient one to allow the formulation of a wide range of composite materials.

2.5 Summary

This chapter was dedicated to polymer/carbon-based composites, their properties and their use in thick-film technology. In it, we have first detailed the two parts that form a polymer/carbon-based composite: the filler and the matrix. The filler can be of various size and shape types (carbon black, graphite, carbon nanotubes or graphene), which all have consequences on the applications but also on the costs. A polymer matrix is either a thermoplastic or a thermosetting material; in any case, a particular value, i.e. the *glass transition temperature* T_g, which defines the transition from a glassy state to a rubbery one, has to be taken into consideration due to its influence on the material properties. The second section dealt with thick-film technology and explained how the screen-printing process works and its requirements in the case of a mineral or an organic paste. Some other deposition processes (such as inkjet-printing) were also reviewed in the case of organic pastes. Finally, the electrical and mechanical properties were presented. As these materials are percolative, i.e. they are governed by percolation theory, a notion is important: the *percolation threshold*. The piezoresistive behavior was also explained. Last but not least, we have demonstrated the influence of the filler shape upon mechanical properties: not only it will have an impact on the tensile/compressive strength but also on the applications and the use of the composites. Fiber composites are mainly used in case where a stronger material is needed, whereas particulate composites are fabricated when other properties are needed, such as thermal conductivity or thermal stability. In the last part, we have drawn attention on the matrix/filler interactions and its possible tuning for instance with surface functionalization.

Regarding all these features, a specific composite materials system was selected for this work. Concerning the filler, carbon nanotubes and graphene are too expensive for industrial applications, and carbon black, despite its low percolation threshold, presents a low conductivity at high loadings. Graphite appears therefore as the best compromise between good properties (higher

electric and thermal conductivity for instance) and costs. Epoxies (thermosetting polymers) were chosen as matrices, another research group doing the characterization for thermoplastics. This materials choice induces constraints for the deposition process. Due to the particle size (i.e. micrometer range), inkjet-printing is not a good option, as there will be sedimentation of the paste. Intaglio prevents the use of alumina as substrate (too brittle) and induces too much loss of ink. Screen-printing is thus the simplest and most flexible way to deposit the paste. Electrical characterization through resistivity and piezoresistivity measurements as well as mechanical characterization will be performed on these epoxy-graphite composites. A chemical oxidation process of the graphite particles will also be investigated in order to see the influence on the mechanical properties.

In the following parts, we will explain how these composites are formulated and what are their structure and main characteristics.

Chapter 3

Formulation and structure

In the previous chapter, we have exposed the basics of carbon-based polymer composites. A short review of the filler and matrix types was done. Important properties (mechanical and electrical) were detailed. Finally, the deposition process was investigated and screen-printing was chosen. We have explained that this choice has consequences on the composite paste such as for viscosity. This part will be dedicated to the composite itself: how it can be fabricated and tuned, how the filler interacts with the matrix and its intrinsic properties.

3.1 Formulation of the composite

An organic thick-film paste is mainly composed of a polymer matrix and a filler. In this very case, the matrix is an epoxy and the filler is graphite. Depending on the materials chosen, the resulting properties of the composite will change. In the following parts we will firstly have a look at the compounds and the mixing process, then we will explain to what extent it is possible to tune a paste.

3.1.1 How to make a thick-film paste?

3.1.1.1 The components

A two-part epoxy was chosen as matrix, and will polymerize when heated to a sufficient temperature. From Part 2.1.3, we know that a particular value is important when designing a polymer composite, i.e the glass transition temperature T_g. Two different epoxies with different T_g values will therefore be used in this thesis. Their main characteristics are summarized in Table 3.1. These two epoxies present different hardener types, which will result in different chemical reactions (Fig. 3.1 and 3.2).

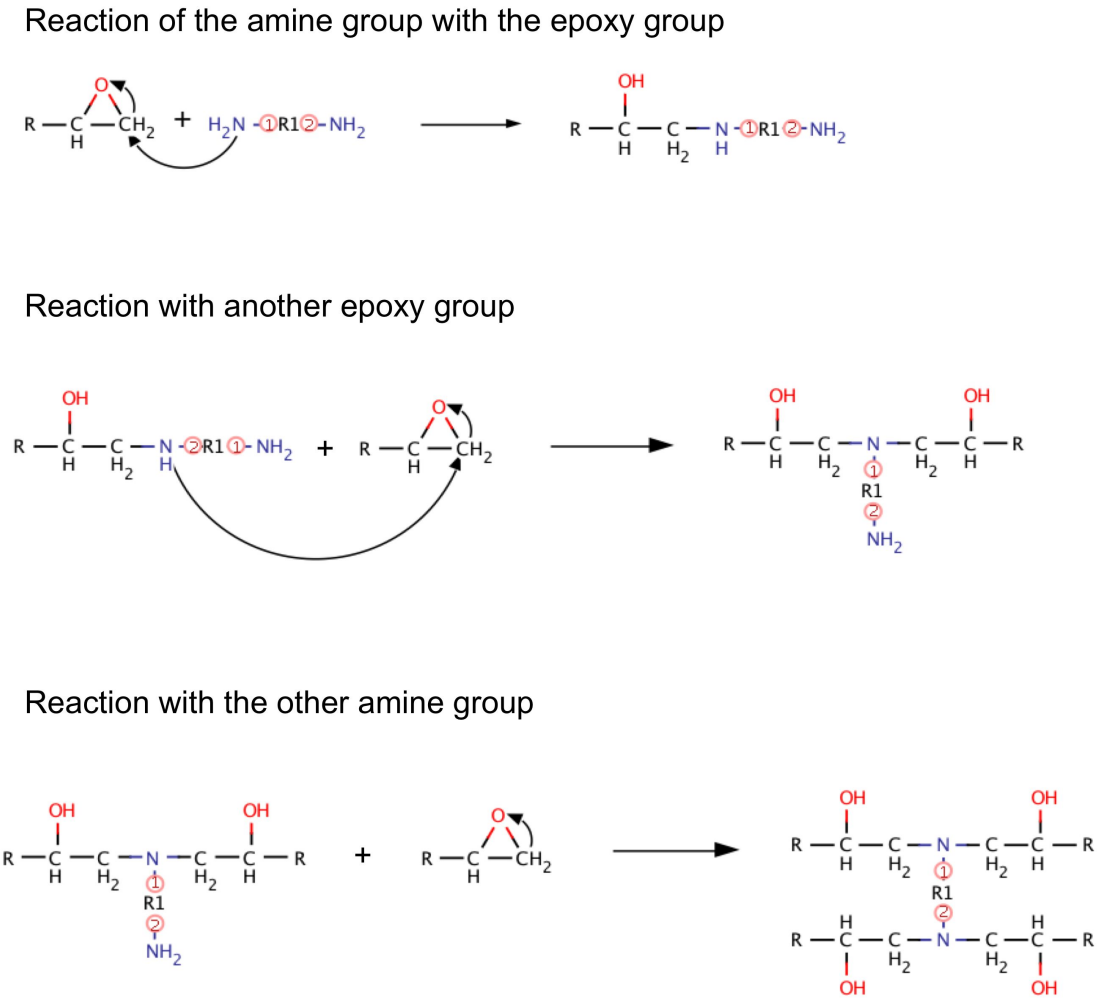

Figure 3.1: Chemical reactions of polymerization in the case of an amine hardener (Macrogalleria: http://www.pslc.ws/mactest/index.htm)

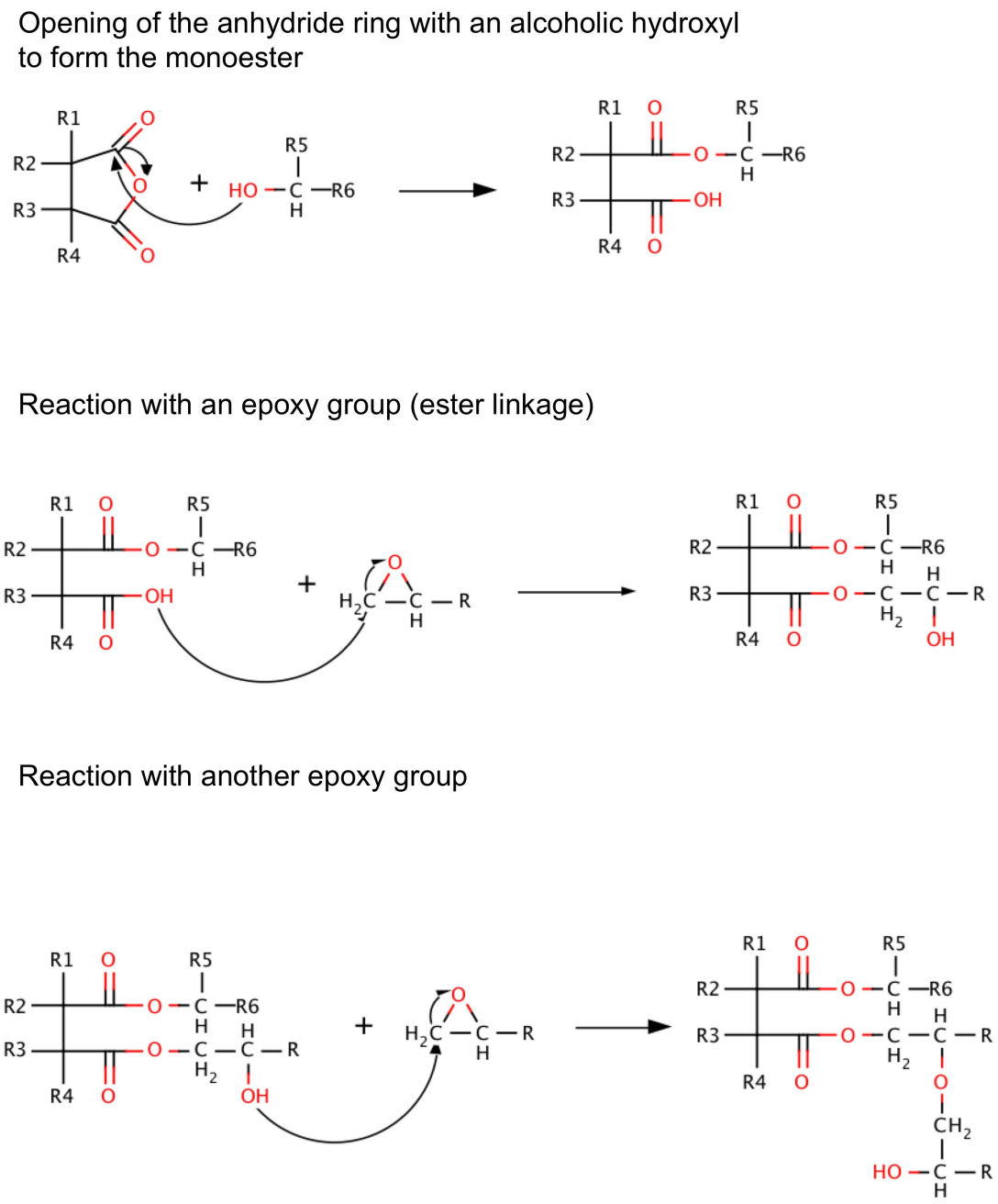

Figure 3.2: Chemical reactions of polymerization in the case of an acid anhydride hardener (www.dow.com)

Synthetic graphite Timrex from the company Timcal, Switzerland, was used as filler. Graphite is available in various sizes and shape. Ellipsoidal particles with maximal sizes ranging from 4 to 44 µm will be studied. As a comparison, composites with expanded graphite as well as with carbon black (Ensaco 250P, also from Timcal) will also be investigated. Table 3.2 presents the characteristics of the graphite and carbon black powders, the KS series corresponding to ellipsoidal graphite and BNB90 to expanded graphite. In the KS series, as far as the particle size is concerned, the nominal given value means that 90% (in mass) of the particles are smaller than 4 µm (resp. 15 and 44 µm). For BNB90, the flakes are present in different sizes in the same batch. Properties for KS44 are only given as information. Indeed as the deposited layers are around 100 µm, in order to have a 3D distribution of the particles inside the film, the thickness has to be at least 3 times the size of the particle, which would not be the case for KS44.

Table 3.1: Main properties of the epoxy resins (suppliers' data)

Commercial name	T_g [°C]	Viscosity at RT [mPa.s]	Curing schedule	Pot life [hour]	Hardener type
EpoTEK 377	≈ 95	150-300	2h@150°C	24	amine
R&G Martens Plus	≈ 200	2'300	24h@100°C + 15h@230°C	12	acid anhydride

Table 3.2: Main properties of graphite powders (supplier data)

Commercial name	Shape	Density [g/cm^3]	Particle size [µm]	Specific surface [m^2/g]
KS4	ellipse	≈ 2.2	< 4	26
KS15	ellipse	≈ 2.2	< 15	12
KS44	ellipse	≈ 2.2	< 44	9
BNB90	flake	≈ 2.2	≈ 0.05 in thickness, 90 in the plane	28.4
Ensaco 250P	powder	2	0.045 (primary particle) 0.15-0.2 (aggregate)	65

When a conductive composite is manufactured, the amount of filler appears as one of the key value, as it will determine the electrical properties. For instance, if the number of particles is below the percolation threshold, the composite will be an insulator. On the opposite, if the amount is too high,

there will be not enough polymer to fully bind the particles together, resulting in a porous composite. This value, which corresponds to the "free-volume" of the powders, can be determined by performing the oil absorption experiment. Several methods allow the determination of this value. One of them is the "spatula rub-out method", whose procedure is as follows [144]:

- approximately 75% of the amount of oil required to saturate the pigment is added to the pigment
- this is worked with a spatula into a glass plate until a mixture forms (mixture is still in a *dry powder form* at this stage)
- oil is added in decreasing quantities with mixing between each oil addition
- total mixing time is approximately 20 minutes

Two points are observed: the first one is when the pigment can be made to adhere in a solid mass (mixture still dry and crumbly at this moment) and the second one corresponds to the point where the mixture changes into a paste that sticks slightly to the spatula or tailed when the ball of paste is shaken from the spatula. Values can be then recorded as the grams of oil to wet 100g of pigments. Linseed oil can be used for this test. This method presents the advantage to be relatively easy to carry out, however, it is also subjective and the results are therefore expected to somewhat depend on the operator. Following this procedure, the oil absorption values for the graphite powders were determined and are reported in Table 3.3. As a comparison, the values provided by Timcal are also reported, differences can come from the fact that the procedure is different. For KS series, we can see that, although the results are not the same, the tendency is similar in both methods. On the other hand, the behavior of BNB90 is surprising. This can be explained by the fact that Timcal used a different method inducing the use of a centrifuge for various times (DBP, [145]), which can compress the powder. Paraffinic oil was also introduced to do their experiments, hence different acidity.

Table 3.3: Comparison of the oil absorption of the graphite powders

Name	Spatula rub-out method, point 1 [g/100g]	Spatula rub-out method point 2 [g/100g]	Timcal [g/100g]
KS4	113	130	175
KS15	108	123	165
BNB90	330	399	150
Ensaco 250P	458	531	NA

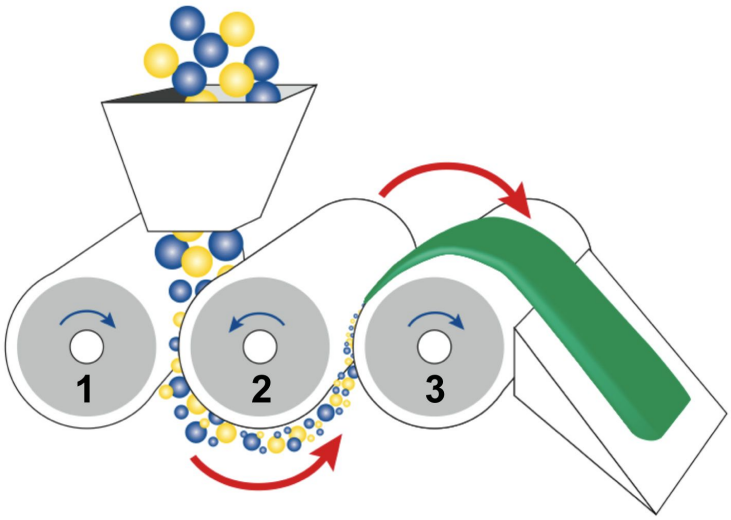

Figure 3.3: Three-roll mill principle (www.exakt.de, october 2011)

3.1.1.2 Paste processing

The paste processing is rather simple and starts by the weighting of the compounds. The two parts of the epoxy resin are first weighed in the appropriate mixing ratio (see datasheet) and then mixed together. The conductive phase (in our case the graphite) is added to the resin in order to get a certain volume fraction in the composite, with a solvent if the viscosity is too high. The whole paste is mixed together, first with a spatula and then with a three-roll mill EXAKT 50, aluminum oxide rollers, which guarantees the homogenization of the paste. This device is composed of three adjacent rolls (most of the time in alumina) that rotate at progressively higher speeds. Paste is put between the rolls 1 and 2 and mixes in this space for a certain time (typically several minutes). The space between roll 2 and 3 is narrowed and paste can be scraped of the three-roll mill thanks to a knife blade (Fig. 3.3). The three-roll mill uses shear force created by the three rolls horizontally positioned that rotate in opposite directions. It was determined that the paste has to undergo this mixing 3 times in order to have a good homogenization [100]. Finally, the viscosity of the paste is checked and additional solvents can be added to adjust it. In a more experimental and pictured point of view, the desired viscosity should be somewhat honey-like to allow a good deposition by screen-printing process. More detailed on solvents can be found in Part 3.1.2.1.

3.1.1.3 Other possibilities

Epoxy is a convenient polymer in a sense that it does not require any preprocess and can just be weighed, mixed and polymerized. For instance 5-minute

epoxy is really common in our daily life. On the other hand, thermoplastic polymers such as ethylcellulose or polycarbonate, which are solid at room temperature, will first need to be dissolved in a solvent. This is done in a beaker at moderate temperature (ca. 60°C typically, to avoid degradation of the polymer) under agitation. Dissolution is followed by a rapid cooling down while mixing with a spatula. Once the polymer is formed, it can be mixed to the conductive phase and go through the three-roll mill as well.

3.1.2 Tuning of the paste

In order to obtain special properties, it is possible to modify the paste. In the following lines, we will detail the two main cases, i.e. solvents and additives.

3.1.2.1 Solvent

Depending on the application, high conductivity can be desired, resulting in higher filler loadings. However, because of processability reasons, these higher loadings cannot always be achieved with simple resin–solid systems, requiring the addition of solvents in order for the inks to remain processable; solvents have a double effect on the composite: the dilution decreases the viscosity of the matrix, and the filler concentration in the "raw" composite ink decreases. It is even possible to exceed the maximum filler concentration, resulting in a porous material after solvent evaporation. Ideally, solvents should be miscible with the resin, but remain inert, without chemical reactions. Miscibility can be predicted from Hansen solubility parameter theory [146–148].

Concerning reactivity, epoxies are known to have reactivity towards –OH groups, which leads us to avoid alcohols as solvents. The last important point is the boiling point, which should be high enough to avoid the formation of bubbles within the coating during the heating phase. Moreover, for screen-printing, high-boiling points (in the 200-250°C range) are preferred, as they avoid premature drying of the ink. However, the boiling point should also be low enough in order for the solvent to fully evaporate during the resin curing phase. Considering all these requirements, a range of esters and ethers were therefore selected and tested as potential solvents.

Table 3.4: Properties of tested solvents. T_b = boiling temperature, $P_{150°C}$ = vapor pressure at 150°C, M = molar mass, d = density (source: www.sigmaaldrich.com, 2009)

Name	Type	CAS-n°	T_b [°C]	$P_{150°C}$ [kPa]	M [g/mol]	d [kg/m^3]	Symbol
diglyme	ether	111-96-6	162	76	134.17	943	A/B1
triglyme	ether	112-49-2	216	11	178.23	986	A/B2
tetraglyme	ether	143-24-8	275	1.8	222.28	1009	A/B3
dibutyl carbitol	ether	112-73-2	256	4.2	218.33	885	A/B4
dipropylene glycol dimethyl ether	ether	111109-77-4	175	49	162.23	903	A/B5
amyl acetate	ester	628-63-7	149	103	130.18	876	A/B6
propylene glycol diacetate	ester	623-84-7	191	30	160.17	1050	A/B7
triacetin	ester	102-76-1	258	2.3	218.20	1160	-

Table 3.4 sums up their relevant characteristics and Table 3.5 the calculated Hansen parameters of the solvents with epoxy (δ = global solubility parameter, δ_d = dispersion parameter, δ_p = polar interactions parameter and δ_h = hydrogen bonding parameter) the Hansen distance D and their water solubility [1]. This table also reports the RED number defined as D/R with R, the radius of solubility (12.7 MPa$^{1/2}$ in the case of epoxy). If RED is :

- < 1 : dissolution
- $= 1$: partial dissolution
- > 1 : no dissolution

We can notice that the resin will be either dissolved or partially dissolved in our solvents, the dipropylene glycol dimethyl ether being the less adapted.

[1] Hansen parameters come respectively: § from [149], * from [150], ** from [146], §§ from www.dow.com and + from [151], and water solubility was found from http://www.chemblink.com, www.dow.com and http://www.glymes.clariant.com/.

Table 3.5: Hansen parameters with epoxy and water affinity of the studied solvents

Name	δ [MPa$^{1/2}$]	δ_d [MPa$^{1/2}$]	δ_p [MPa$^{1/2}$]	δ_h [MPa$^{1/2}$]	D [MPa$^{1/2}$]	RED	Water solubility [g/100mL]
epoxy[§]	26.3	20.4	12	11.5	-	-	-
diglyme[*]	19.3	15.8	6.2	9.2	11.2	0.88	miscible
triglyme[*]	17.9	15.8	2.3	8.2	13.8	1.09	soluble
tetraglyme[*]	17.9	15.8	2.1	8.2	14	1.10	soluble
dibutyl carbitol[**]	17.7	16.2	2.3	6.9	13.6	1.07	0.3
dipropylene glycol dimethyl ether[*]	15.5	14.9	2.1	3.8	16.7	1.31	35
amyl acetate[*]	18.5	16.2	2.1	8.6	13.3	1.05	1
propylene glycol diacetate[§§]	18.6	15.7	3.5	9.4	12.8	1.01	8
triacetin[+]	19.4	16.5	4.5	9.1	11.1	0.87	6.4

Fig. 3.4 presents their vapor pressure vs. temperature. In the experiments, A/B0 will refer to the reference sample, i.e. without any solvent. Triacetin was not tested in this study, and is given only for comparison purposes as a high-boiling ester. In this list, the reader will notice that diglyme and triglyme are toxic solvents [152–154] and the water affinity of these glymes is rather a drawback, as they may pick up undesired moisture from the air during processing or storage. Conversely, hydrophobic solvents may help in minimizing water uptake. Therefore it is of great interest to find less problematic substitutes to these compounds. In the glycol ethers, for instance, switching from the E-series (based on ethylene glycol) to the P-series (derived from propylene glycol) tends to lower the toxicity and yields somewhat more hydrophobic compounds. Hydrophobicity is strongly increased by replacing the methyl end groups with longer (e.g. butyl) ones.

In order to see the influence of solvents upon the composites, several experiments were performed: weight measurement, resistivity and rheology. Samples were made using KS4 as a filler in EpoTEK 377 matrix. Volume fraction was 10% (A series) and 20% (B series). Then, 20% (mass) of solvent was added and mixed to the paste. The study can be found in Ref. [70]

Weight measurements Adequate solvents for epoxies must evaporate completely during the curing process of the composite (2 h at 150°C in the oven),

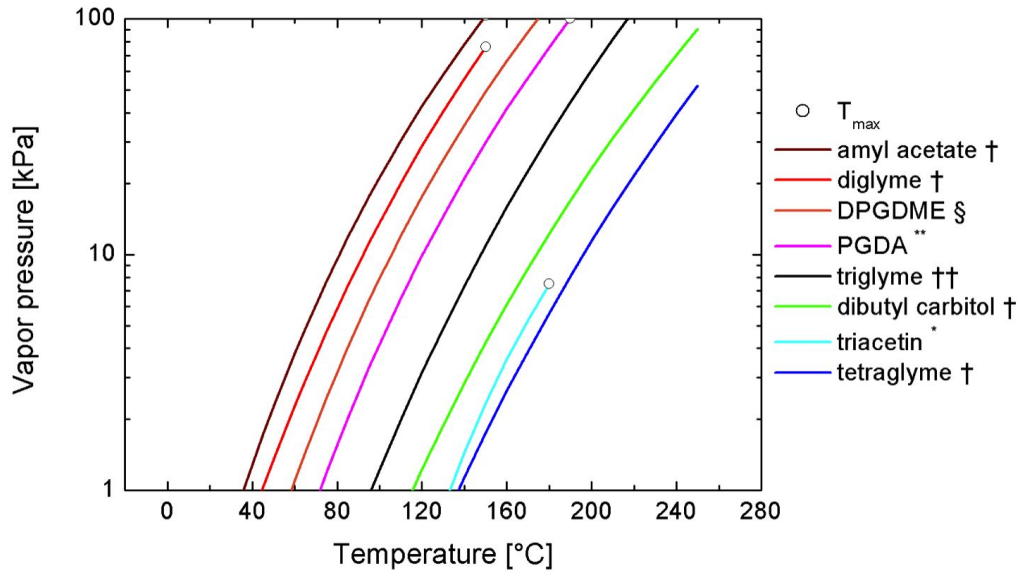

Figure 3.4: Vapor pressure vs. temperature (calculated by the Antoine equation [155, 156]). † [156]; * [155]; §dipropylene glycol dimethyl ether, approximate data from [157]; **propylene glycol diacetate, data from [158] refitted together with boiling point; ††interpolated between di- and tetraglyme and adjusted to known pressure at 162°C [159]. Tmax is the maximum validity temperature indicated for the fits in the references.

which was checked through mass loss measurements. The composite mass was measured at 30, 60 and 120 min, and the results are reported in Fig. 3.5. Several remarks can be drawn from the graphs. First, the reference sample shows a loss, probably corresponding to water evolution. As far as the A series (10% volume fraction in graphite) is concerned, we can notice that in each case, at least 80% of the total mass loss occurs in the first 30 min, not to say almost all of the loss for samples 1, 5 and 6. This result is ascribed to the high vapor pressure of the corresponding solvents (see Fig. 3.4): solvents 2 and 7, and especially 3 and 4, have low vapor pressures, and thus slower evaporation. This trend is also observed for composites loaded at 20%, where the evaporation process, however, is slowed down by the presence of a higher fraction of filler particles, which increases the tortuosity of the diffusion paths to the surface.

Influence on rheology In Part 2.4.1.2, we have exposed that a thick-film paste should present a thixotropic behavior, which corresponds to the decrease in the apparent viscosity with time under a shear stress and the subsequent recovery of viscosity when the flow is discontinued [160]. However, this recovery is only partial and a hysteresis can be observed, which can affect the reproducibility of thick-film pastes (Fig. 3.6).

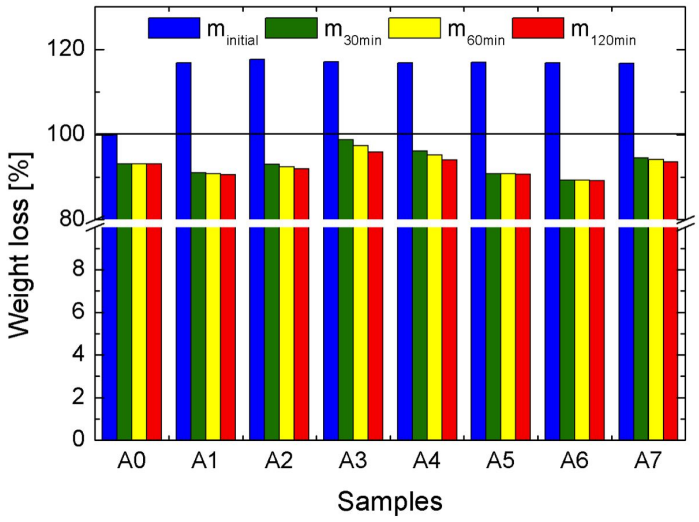

(a)

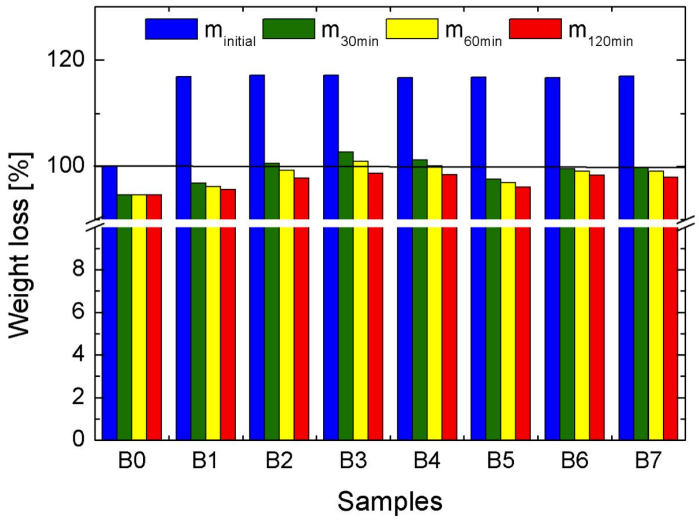

(b)

Figure 3.5: Mass loss profile of composite loaded with graphite at 10% (a) and 20% (b) volume fraction (see symbols in Table 3.4)

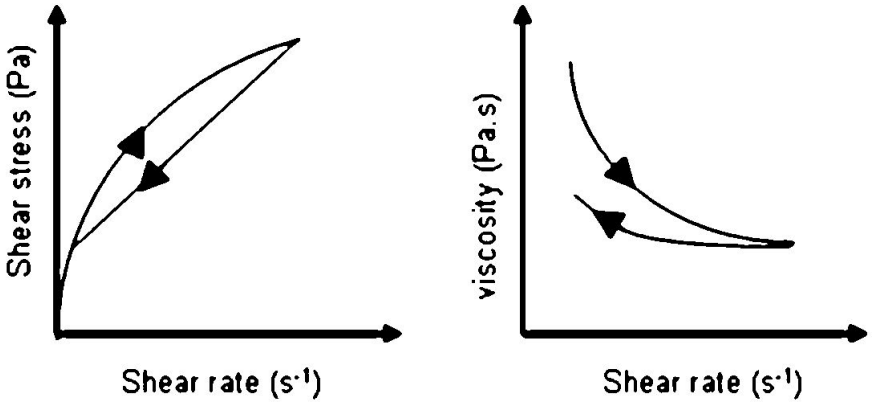

Figure 3.6: Thixotropic behavior

The dynamic viscosity was measured with a rotary viscosimeter, Rheomat RM180 from Mettler. In a first series of experiment, we determined the viscosity of composite, without any solvent, regarding particle size and volume fraction. Experiments were performed with KS4 and KS15 in EpoTEK 377 for different volume fractions. The results are reported in Fig. 3.7.

We can see that smaller particles tend to lead to higher viscosity (see Fig. 3.7a) , which can be explained by the fact that particles are less deformable with a decrease in the size, so they accommodate less with their neighbors, hence an increase in viscosity [161, 162]. If we now look at the effect of volume fraction (Fig. 3.7b), obviously, an increase leads to a higher viscosity, this is governed by the Krieger-Dougherty equation (here presented in a simplified form):

$$\eta = \eta_c \left(1 - \frac{\phi}{\phi_m}\right)^{-2}$$

where η is the viscosity of the paste, η_c the viscosity of the continuous phase, Φ is the volume fraction of the particles and Φ_m the maximum volume fraction of particles.

Let us now look at the effect of the solvents upon rheology. The same Rheomat was used to measure the dynamic viscosity of the paste formed by 10% of KS4 in the EpoTEK 377 matrix, with 20% (mass) of solvent. Fig. 3.8 presents the results. Measurements were impossible with diglyme, triglyme and dipropylene glycol dimethyl ether, the viscosity being out of the range of application of the device (too low). We can see that the viscosity has significantly decreased, which was the purpose of the use of solvents, and that the corresponding values are close, no matter the solvent.

Influence on resistivity The room-temperature resistivity of the composites formulated with solvents is given in Fig. 3.9, as a percentage of the reference

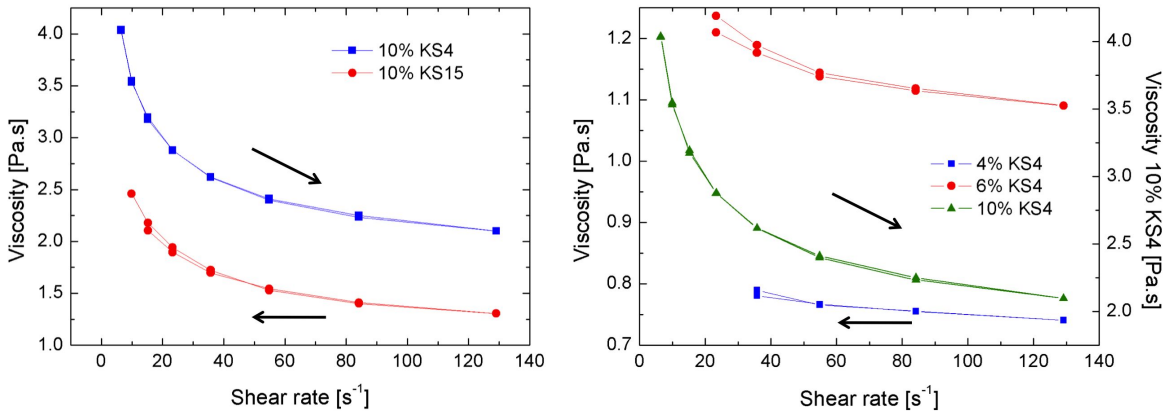

(a) (b)

Figure 3.7: Particle size (a) and volume fraction (b) effect upon viscosity measurement

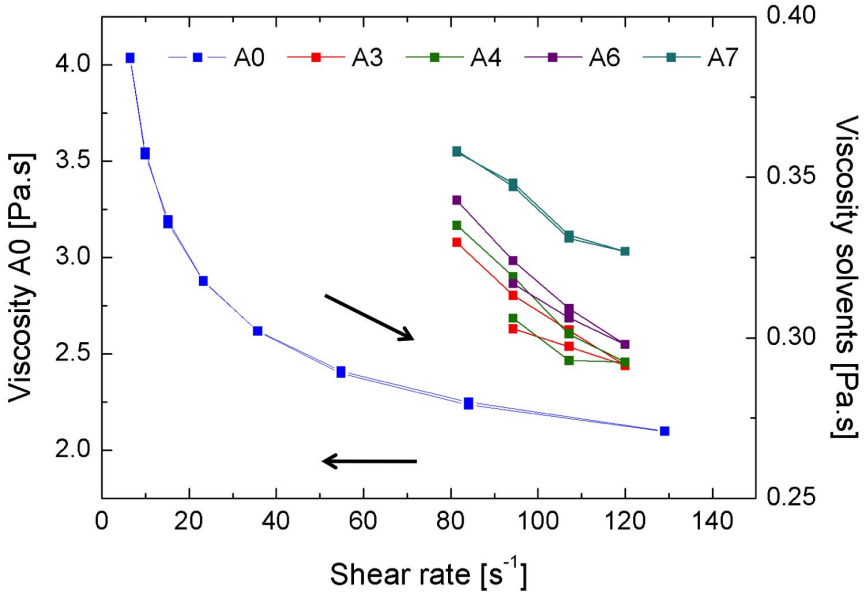

Figure 3.8: Viscosity measurement for the different solvents (see symbols in Table 3.4)

sample (without solvent). Solvents strongly decrease resistivity, which is a desired effect at high filler loadings, where maximal conductivity is wanted. We suppose the increased fluidity allowed by the solvent facilitates contact between the graphite particles, an effect also driven by the contraction of the matrix brought by the evaporation of the solvent. This effect is very marked at higher filler loadings: in this case, there are much more graphite particles, thus, with appropriate fluidity of the paste, it becomes easier to create conductive paths between particles, resulting in a higher conductivity of the final composite. It must also be noted that working with the reference (without solvent) sample becomes difficult at higher loading, as for instance at 20% volume fraction in graphite; processing of even higher loadings would only be possible through solvent addition. If we have a closer look at the values, we can see that they are quite disparate. This can be linked to the affinity for water, but also to the affinity for the epoxy. For instance, the sample diluted with dibutyl carbitol presents the lowest affinity for water among the studied solvents and a good affinity with the epoxy, leading to a very small value of resistivity. On the opposite, the dipropylene glycol dimethyl ether has a much higher affinity for water as well as the lowest affinity for the epoxy (see RED number), hence higher resistivity. Another potential explanation of the results is the solvative power, i.e the rheology of the final paste. In Fig. 3.8, we can see that the propylene glycol diacetate presents a slightly higher viscosity value. If we compare this solvent with amyl acetate, we can see that it also has a higher water solubility and that they show the same behavior regarding the affinity for epoxy. However, their resistivity values are quite different. Indeed, due to the higher solvative power of amyl acetate, water will be more able to diffuse in a less viscous paste, hence a higher conductivity. The resistivity values at 20% are closed: indeed, there are more particles inside the composite, the material is therefore less submitted to the effects induced by the matrix (water/matrix affinity).

3.1.2.2 Additives

The other possibility to tune a polymer composite is the use of additives. Two types were studied in this thesis, both commercially available for epoxy tuning: a flexibilizer and an active diluent.

Flexibilizer The flexibilizer has an impact on mechanical properties, allowing the design of a more flexible epoxy. It is directly integrated to the resin molecule during polymerization. Thanks to its long linear chain, the material will develop a high and permanent extensibility. As it becomes part of the polymer, the mixing ratio (hardener amount) must be adapted when the amount of flexibilizer is above 10%. Calculations can be done by using the epoxy value (molar mass of the resin that contains an epoxy group). Fig. 3.10

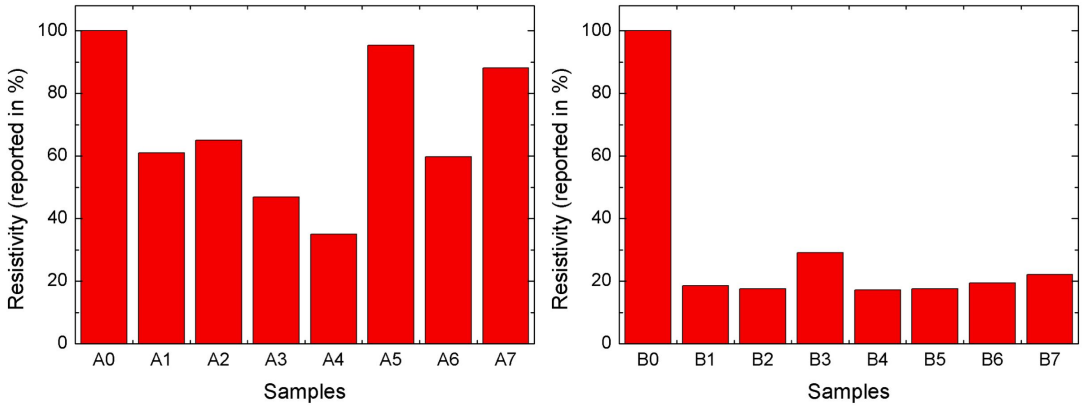

(a) (b)

Figure 3.9: Resistivity of composite loaded with graphite at 10% (a) and 20% (b) volume fraction (see symbols in Table 3.4)

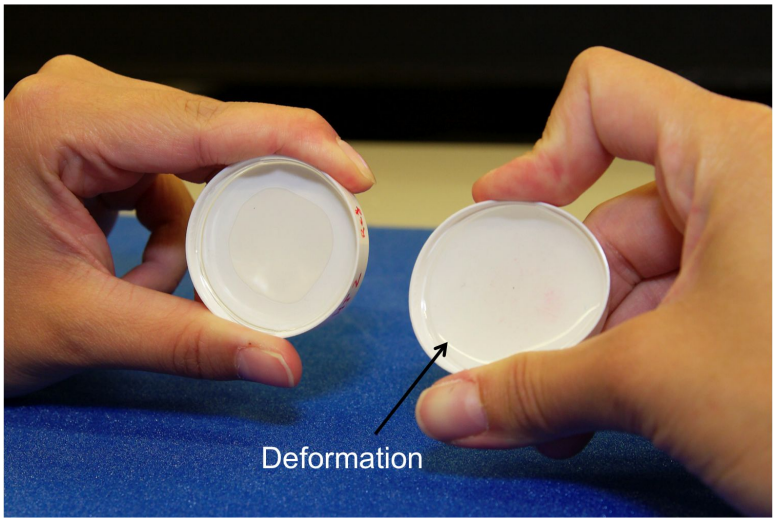

Figure 3.10: Comparison in compression between both resins: without (left) and with (right) flexibilizer

compares a pure epoxy and an epoxy tuned with 50% of flexibilizer, highlighting the new plastic nature of the material.

Active diluent This active diluent is used to decrease the viscosity of the paste. It is called "active" because, contrary to the solvents discussed previously, this diluent contains active groups that will fix to the macromolecule during polymerization. As for the flexibilizer, the mixing ratio must be adapted when the amount of additives is above 10%. However, too much active diluent can

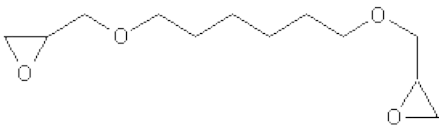

Figure 3.11: 1,6 hexanedioldiglycidylether

damage the mechanical properties as well as the chemical durability of the final product. This diluent is in fact 1,6 hexanedioldiglycidylether (Fig. 3.11). Preliminary tests showed that the action of this additive is less efficient than regular solvents, which is the reason why this additive was not used afterwards. Moreover as it can damage mechanical properties and chemical resistance of the final material, it is not recommended for paste formulation in our case. However, when making bulk products, such diluent becomes preferable to solvents. Indeed, solvents may not be able to evaporate properly on massive objects, resulting in emissions of solvent vapors later, whereas the diluent is incorporated to the matrix and is therefore stable.

3.2 Microscopic structure of the composite

In the first section above, we have extensively explained how a thick-film paste is formulated and processed. To complete the study, a microscopic approach of the composite is necessary to understand its structure. In order to see the impact of the grain shape as well as the volume fraction, it was decided to use an optical microscope, the particles having a minimum particle size of 4 µm. From this point of view, several samples with different concentrations and particle shapes were investigated. Samples containing carbon black were also manufactured, this way differences in the particle distribution inside the matrix can be observed. Finally, these samples were compared to the ones made of two commercially available carbon-based pastes.

Table 3.6 summarizes the investigated samples, whose effects will be detailed in the next parts. The solvent chosen was amyl acetate. In addition to that, samples made from two resistive commercial pastes ED7500 100 Ω and 10 kΩ (Electra Polymers) were also fabricated.

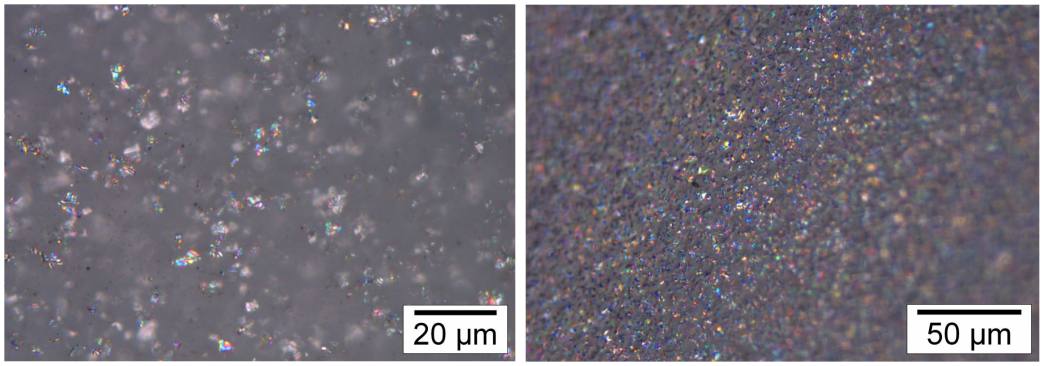

(a) (b)

Figure 3.12: Microstructures of 4%KS4 (a) and 15%KS4 (b) in EpoTEK 377

Table 3.6: Samples for microscopic study, matrix: EpoTEK 377

Volume fraction [%]	Filler type [%]	Additive
4	KS4/BNB90/Ensaco 250P	-
15	KS4	-
15	KS4	20% solvent
15	KS4	60% solvent

In the next parts, colors of the particles can be observed on the photos coming from the optical microscope. This is due to the reflection of the light on different planes of the particles.

3.2.1 Microstructures of the composites

We will first take interest in the effect of the volume fraction. Fig. 3.12 presents the microscopic structures investigated by optical microscopy of the two composites loaded with 4% KS4 and 15% KS4 in EpoTEK 377.

We can see that both samples show apparent good homogeneity, which validate our process of homogenization with a three-roll mill. The particle density obviously increases with the volume fraction. The particle size distribution has to be noticed. In the composite loaded at 4% volume fraction, smaller particles can be seen. This will probably have an impact upon resistivity, as these debris dispersed in the insulator matrix will make the theoretical model, formed by monosize conducting particles in an insulating medium, more complex.

The influence of solvent was also investigated. Amount of 20% and 60% (in mass) of amyl acetate were added to the composite EpoTEK 377 + 15%KS4

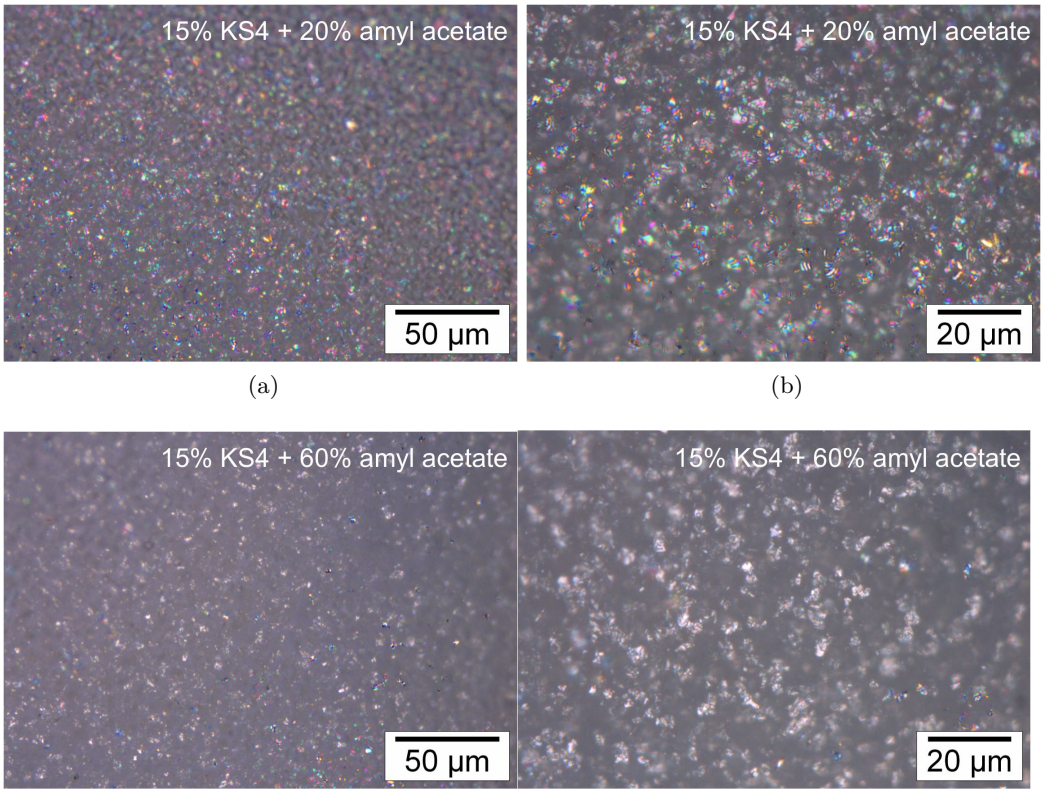

Figure 3.13: Microstructures of 15%KS4 + 20% amyl acetate zoomed 500 times (a) 15%KS4 + 20% amyl acetate zoomed 1000 times (b), 15%KS4 + 60% amyl acetate zoomed 500 times (c) and 15%KS4 + 60% amyl acetate zoomed 1000 times (d) in EpoTEK 377

and then observed. Results can be found in Fig. 3.13. We can see that the structure of EpoTEK 377 + 15% KS4 with or without 20% of solvent is quite similar (compare Fig. 3.12b and 3.13a). The microstructure of the composite with 60% of solvent is different: particles seem more spaced. We therefore propose to look more deeply on the effect. Fig. 3.13b and 3.13d show both composites zoomed 1000 times. We can see that the quantity of solvent is so important that the apparent volume seems larger, hence more spaced particles (see Fig. 3.13d).

3.2.2 Influence of the filler type

We propose now to look at the structure of different fillers. Fig. 3.14a presents the microstructure of a composite EpoTEK 377 + 4% BNB90 (the color is different due to a thin coating). The particular structure of the expanded

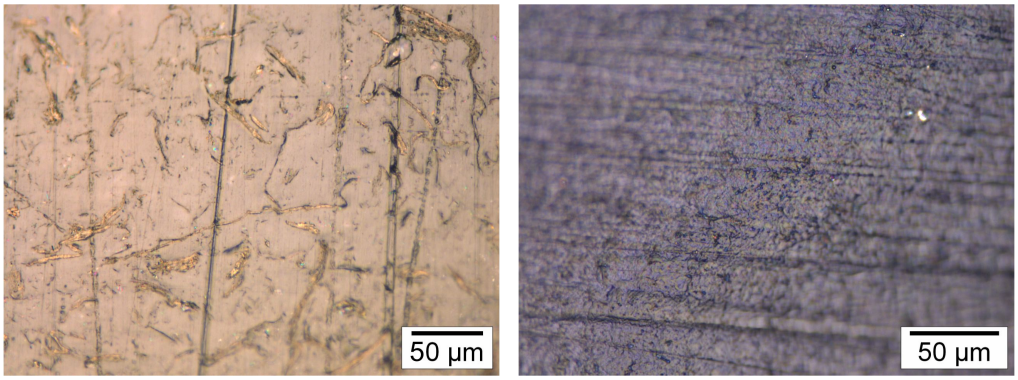

(a) (b)

Figure 3.14: Microstructures of 4% BNB90 (a) and 4% Ensaco 250 P (b) in EpoTEK 377

graphite can be observed. Small debris can also be seen, which should promote conductivity.

The microstructure of the composite with carbon black filler (Ensaco 250P) can be found in Fig. 3.14b. The structure is also quite different from the one observed with "standard" graphite (i.e. KS series): small particles, aggregates and debris can be observed. This could therefore give similar results than expanded graphite regarding conductivity.

By comparing both microstructures to the 4% KS4 one, they both seem less "empty" (ratio matrix/filler smaller), leading in theory to a better electrical conductivity.

3.2.3 Comparison with commercial resistive pastes

Finally, we propose to have a look at two commercial resistive pastes from Electra Polymers, in order to see if it is possible to determine what they are composed of. Results are reported in Fig. 3.15. Prima facie, for both pastes, the microstructure appears more complex than ours. This presupposes that additives were added to the pastes (such as stabilizer possibly), which was predictable due to the long pot life of the pastes. Small particles can be observed as well as a kind of apparent roughness. The less conductive paste (see Fig. 3.15b) shows less particles, with a small size distribution. On the opposite, ED7500 100 Ω paste (Fig. 3.15a) presents particles with different size, which may indicate the use of mixes of particles (for instance, graphite and carbon black). This provides, in theory, better conductivity with less viscosity impairment.

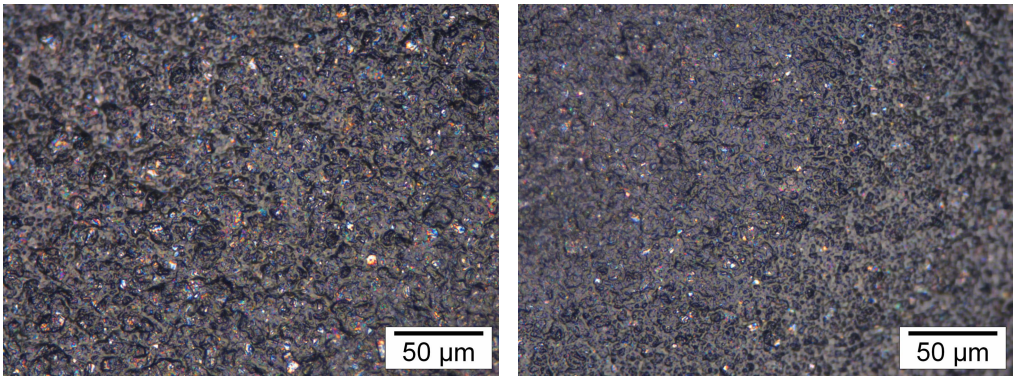

(a) (b)

Figure 3.15: Microstructures of pastes ED7500 100 Ω (a) and ED7500 10 kΩ (b)

3.3 Oxidation process

In Part 2.3.2, we have exposed that oxidation can be a way of functionalizing graphite by creating polar reactive groups -OH, -COOH and =CO on the surface. We will now explain in details how this experiment can be carried out and how the effect can be analyzed.

3.3.1 Description of the process

Oxidation can be made through different processes: anodic, air or wet oxidation. We chose to carry out the experiment with a wet process. The procedure is described in Ref. [126] and is as follows:

- Concentrated nitric acid HNO_3 (at 60% or more) is put into a balloon and heated to 118°C by reflux. This process allows the vapors of the acid to condensate and go back inside the balloon. Therefore the experiment can last for an extended period of time. Reflux is well used in chemistry, for instance for distillation.
- 1 g of graphite is then introduced into the balloon and stays for various oxidation times.
- Once the oxidation is done, the graphite is rinsed by distilled water, followed by four rinses in boiled distilled water, and then flushed again with temperate distilled water. The purpose of this operation is to eliminate the nitric acid, hot water enhancing this elimination.
- Graphite is then dried at 110°C to eliminate water residue and stored in a desiccator.

Oxidation was carried out for various times (1, 2 and 4 hours), the more it is oxidized, the more there are reactive groups on the surface in theory.

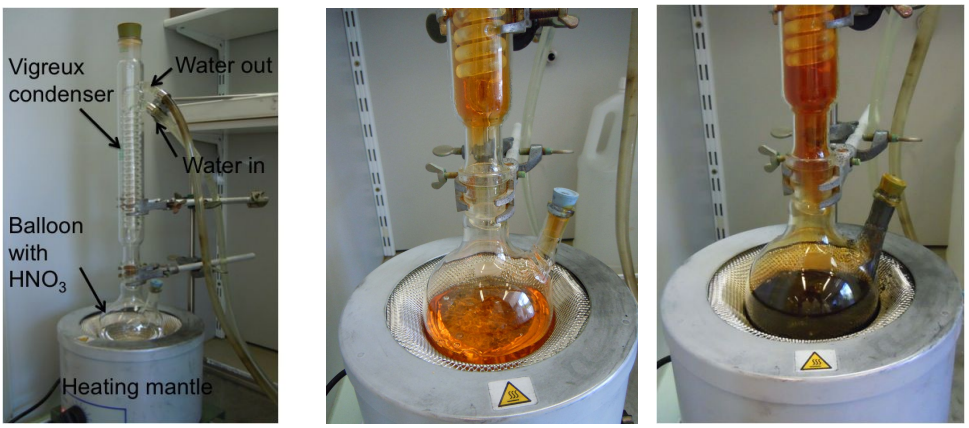

(a) (b) (c)

Figure 3.16: Reflux for oxidation experiment: introduction of HNO_3 in the balloon and heating (a), HNO_3 at 118°C and bubbling (b) and introduction of graphite for oxidation (c)

Fig. 3.16 shows the different steps of the experiment. We can notice that HNO_3 becomes orange when heated, this comes from the nitrogen dioxide (NO_2).

3.3.2 XPS analysis

Once the experiment is done, one obviously wants to characterize the oxidation degree of the powder surface. It was found in the literature that X-Ray Photoelectron Spectroscopy (XPS) is appropriate for this purpose [132, 163–166], as this technique is adapted for surface chemical analysis (elements and quantity), and will allow us to follow the oxidation of the surface. Spectra are obtained by irradiating the material with a beam of X-rays, while simultaneously measuring the kinetic energy and number of electrons that escape from the top, 1 to 10 nm of the material being analyzed. The data can therefore be processed with an appropriate software. XPS requires ultra high vacuum (UHV) conditions.

The graphs in Fig. 3.17 show XPS analysis of pure graphite, and oxidized graphite after 1, 2 and 4 hours in nitric acid for oxidation. Data are given in Intensity (CPs) vs. binding energy (eV). We can see that a peak corresponding to oxygen appears after 1 hour of oxidation. This peak becomes larger as the oxidation time is extended. One would also notice that, aside from carbon and oxygen, there is no other element (such as nitrogen that could possibly come from HNO_3). The procedure is therefore validated. Table 3.7 presents the corresponding atomic and mass concentrations. A small amount of oxygen can be observed also in the reference sample, which means that oxidation is a natural process for graphite. However, and in a sense fortunately, it is also slow, owing to the inert nature of graphite. As in Fig. 3.17, the more the

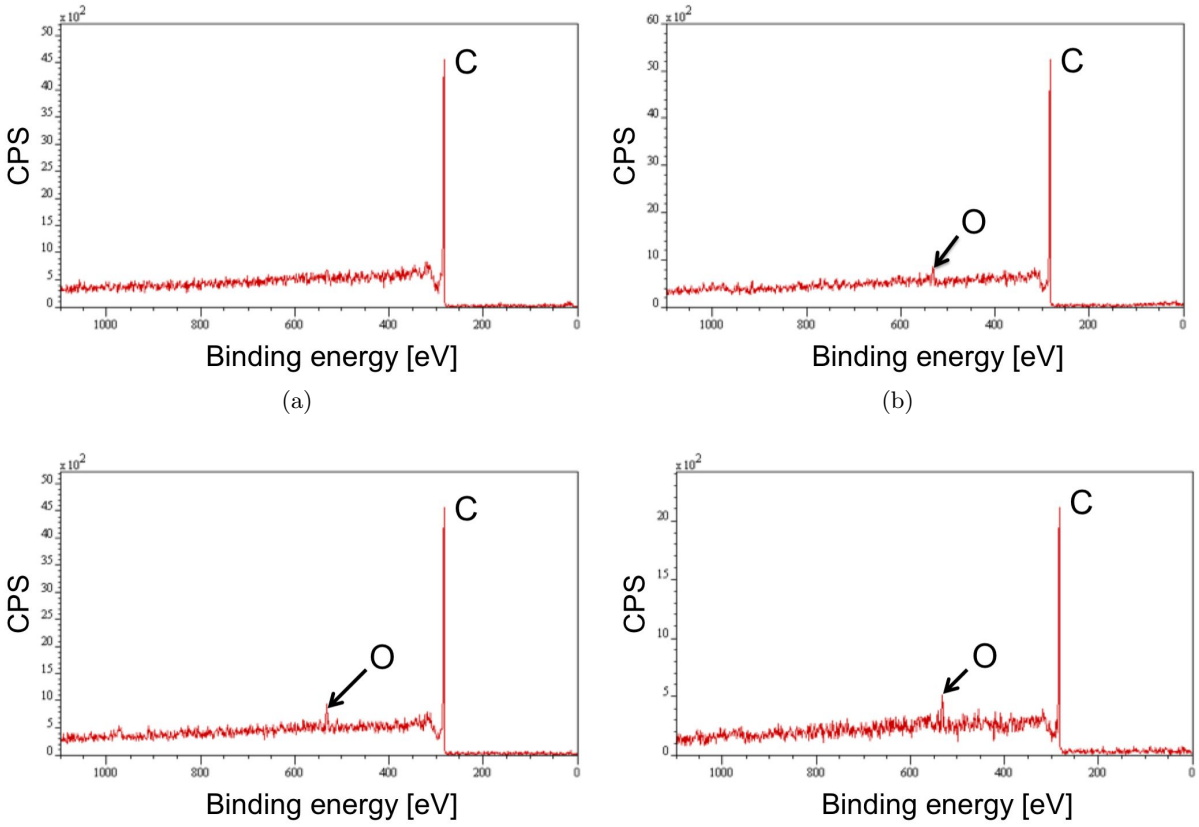

Figure 3.17: Oxidation process followed by XPS: reference measurement (a), after 1 hour (b), 2 hours (c) and 4 hours (d) oxidation

oxidation time is extended, the more we found oxygen. However, one would notice that the 4-hour sample presents a slightly smaller amount of oxygen; this could come from bad homogenization of the graphite powder during the experiment.

Table 3.7: Atomic and mass concentrations during the oxidation process

Element	Atomic concentration [%]	Mass concentration [%]
C	98.05	97.41
O	1.95	2.59

(a) reference sample

Element	Atomic concentration [%]	Mass concentration [%]
C	96.58	95.50
O	3.42	4.50

(b) 1 hour

Element	Atomic concentration [%]	Mass concentration [%]
C	95.12	93.60
O	4.88	6.40

(c) 2 hour

Element	Atomic concentration [%]	Mass concentration [%]
C	95.52	94.12
O	4.48	5.88

(d) 4 hour

3.4 Thermal properties of the composite

Thermal properties of the composite were investigated with Differential Scanning Calorimetry (DSC). After a brief review of this analytical method, analyses will be explained.

3.4.1 What is Differential Scanning Calorimetry?

DSC is a thermoanalytical technique, which consists in measuring the difference in the amount of heat flow required to increase the temperature of a sample and a reference (that presents a well-defined heat capacity over the range of temperature to be scanned) as a function of temperature. Sample and reference are both maintained at nearly the same temperature throughout the experiment. In general, the sample holder temperature increases linearly with time. The point of DSC is the detection of *phase transitions*. Indeed, when the sample undergoes a physical transformation, more (resp. less) heat will be needed in order to maintain temperature with the reference's. In the case of an endothermic reaction (such as in solid→liquid transformation), the sample absorbs a lot of heat to undergo the transition, therefore more heat will be needed to increase the temperature to follow the reference's. On the opposite, in the case of an exothermic reaction (such as crystallization), less heat will be required by the sample. DSC presents the greatest temperature accuracy, but most of the time it cannot detect weak transitions, in particular in filled materials [167]. When performing a DSC on a polymer, this type of curve (Fig. 3.18) can be obtained. Several transitions can be observed. The first one is the glass transition temperature T_g, which corresponds to an increase in the

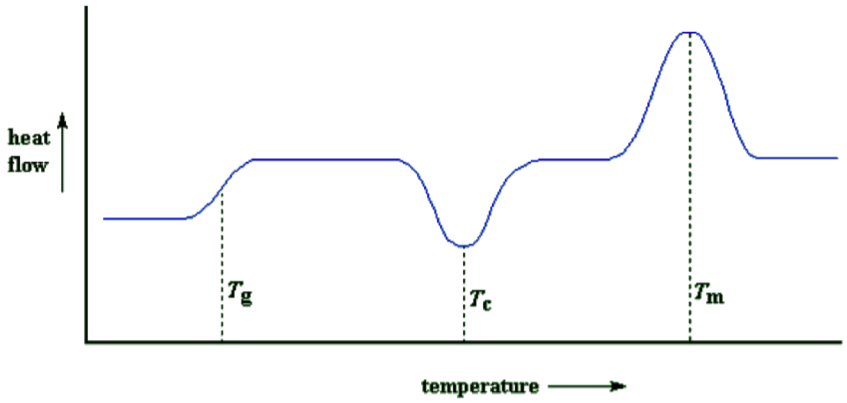

Figure 3.18: Typical DSC scan of a polymer (from Macrogalleria)

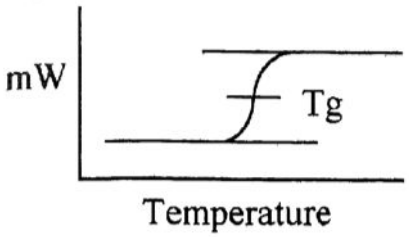

Figure 3.19: Determination of T_g on an ideally DSC curve (from Ref. [167])

heat capacity. Above T_g, the mobility increases until it reaches the temperature of crystallization T_c. This exothermic transition will not occur in all polymers as not all polymers crystallize. Finally, if we keep heating, the polymer melts at the melting temperature T_m. This time it is an endothermic transition that will occur also in crystals. Transitions are separated in two kinds: if there is latent heat, the transition is of the first order (case of crystallization and melting), whereas if there is only change in heat capacity and therefore no latent heat (case of T_g), the transition is called a second order transition.

In the case of epoxy, we will be able to see T_g, which is the reason why we are using the device. It will not crystallize nor melt, hence no first order transition. Using DSC, T_g is usually determined on the graph as the midpoint of the shift in baseline (see Fig. 3.19).

3.4.2 Application to epoxy-graphite composites: determination of the T_g

The glass transition temperature was determined for both pure epoxies, i.e. EpoTEK 377 and Martens Plus. Fig. 3.20 shows the DSC curve that was

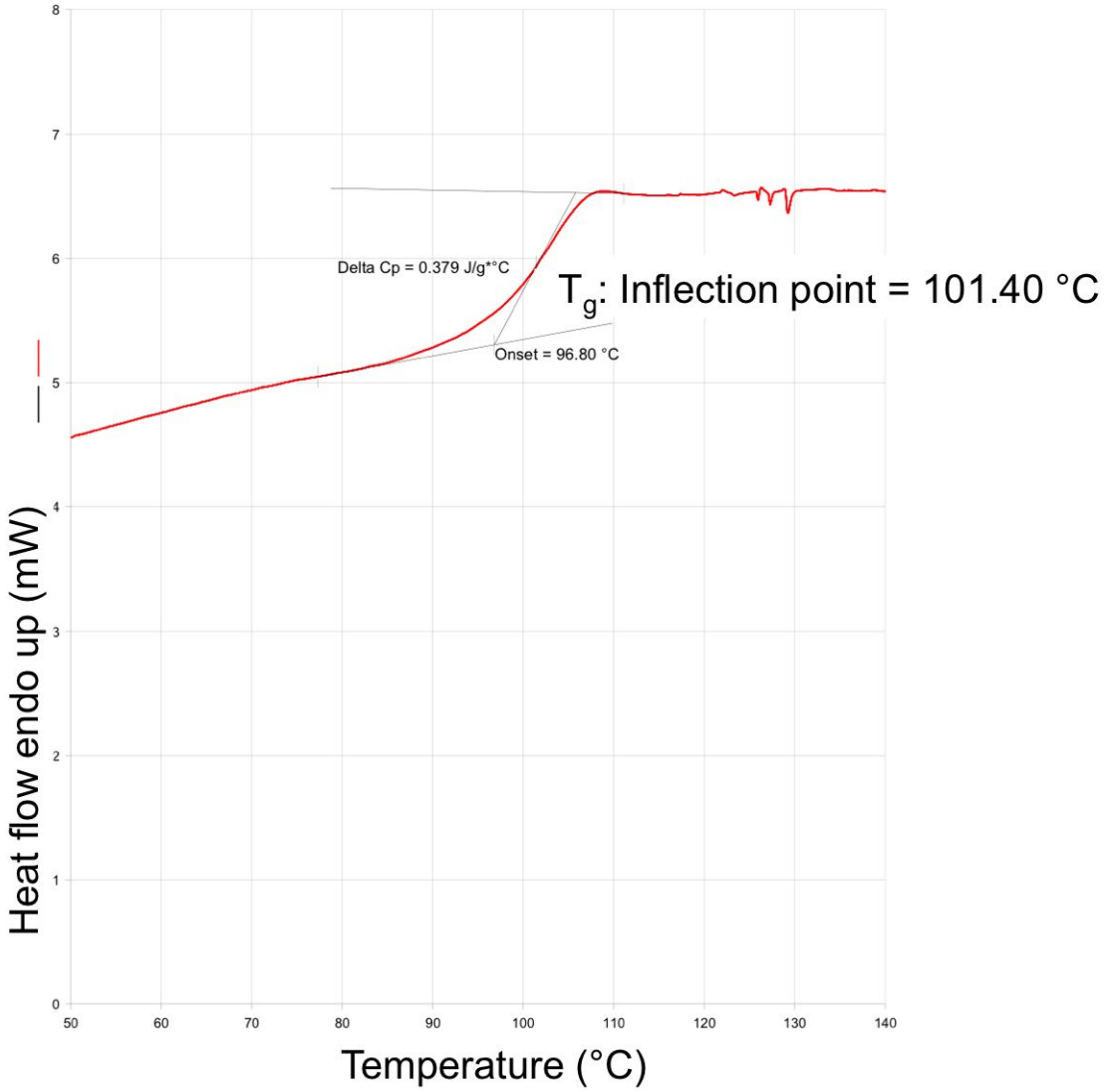

Figure 3.20: DSC curves of pure EpoTEK 377

obtained for EpoTEK 377. In order to complete the study, several samples were synthesized, so as to determine the impact of volume fraction, particle size and shape on T_g (Table 3.8). Same curing were used than the one described in Table 3.1 for each epoxy. Temperature profile was for EpoTEK 377 samples from 40°C to 140°C at 10°C/min., and for Martens Plus samples from 50°C to 300°C at 15°C/min. The results are reported in Fig. 3.21.

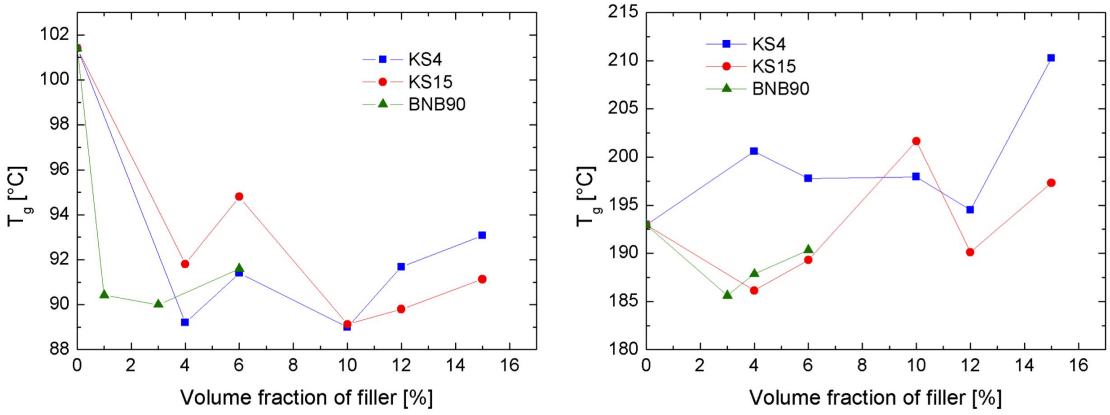

(a) (b)

Figure 3.21: Determination of T_g for EpoTEK 377 (a) and Martens Plus (b) loaded with KS4, KS15 and BNB90

Table 3.8: DSC samples

Volume fraction [%]	Filler type	Shape
4	KS4/ KS15	ellipse
6	KS4/ KS15	ellipse
10	KS4/ KS15	ellipse
12	KS4/ KS15	ellipse
15	KS4/ KS15	ellipse
1	BNB90	flake
3	BNB90	flake
4	BNB90	flake
6	BNB90	flake

(a) EpoTEK 377

Volume fraction [%]	Filler type	Shape
4	KS4/ KS15	ellipse
6	KS4/ KS15	ellipse
10	KS4/ KS15	ellipse
12	KS4/ KS15	ellipse
15	KS4/ KS15	ellipse
3	BNB90	flake
4	BNB90	flake
6	BNB90	flake

(b) Martens Plus

Several observations can be made. If we first look at the effects on EpoTEK 377, the T_g values of the loaded samples seem to be quite chaotic and oscillate between 89°C and 93°C. Considering the fact that T_g is more a

range than a strict temperature, we could say that the loading concentration has little effect upon T_g. However, the tendency is that a first addition of filler leads to a decrease in T_g (ca. 10°C) and then any more addition of filler has no real impact. If we now compare the KS4 and KS15 curves, below 10% volume fraction, samples with KS15 tend to have a higher T_g, the situation is reversed above 10%. Finally for the shape effect, the values are lower than for the other samples. As for the Martens Plus is concerned, the loading tends to slightly increase the glass transition temperature. The samples loaded with KS4 show higher T_g values. Finally, the shape effect is the same than for EpoTEK 377.

The behavior for both epoxies is therefore slightly different. This might be explained by the fact that Martens Plus has a so-called "double curing" and is stronger than EpoTEK 377 so probably more densely cross-linked. Their hardeners are also different (see Part 3.1.1.1), which induces different polymerization reactions.

3.5 Summary

In this chapter, formulation of a thick-film paste was detailed. The tuning with solvents and additives was also reviewed. It was demonstrated that solvents can be used to adapt the viscosity of the paste, the requirements being that they should be miscible with the resin, but remain inert, without chemical reactions. Miscibility of the solvents may be estimated from the Hansen parameters. Weight loss, rheology as well as conductivity measurements were performed for various components and showed that the solvents evaporate during the curing process and decrease the viscosity. These measurements also highlighted the fact that the use of solvents increases the conductivity of the corresponding composites due to a better contact between graphite particles. Tetraglyme, dibutyl carbitol, dipropylene glycol dimethyl ether, amyl acetate and propylene glycol diacetate are therefore good solvents for epoxies. We do not recommend the use of diglyme and triglyme as they are toxic.

Another tuning possibility through surface functionalization was also investigated. Oxidation of graphite particles was performed by a reflux process in concentrated nitric acid for various times, the degree of oxidation being controlled by X-ray Photoelectron Spectroscopy (XPS). The results showed increasing amount of O groups (-OH, =CO, -COOH) on the surface, which validate the procedure.

The microstructure of composites was examined through an optical microscope. Differences in the structure depending on the volume fraction and type of filler were exposed. This should have impact on the electrical conductivity of the corresponding composites. For comparative purposes, resistive commercially available pastes were also observed, revealing more complex structures (use of additives) and probably mixes of particle types.

Finally, thermal properties were studied. Differential Scanning Calorimetry

(DSC) was used to determine the glass transition temperature of both pure epoxies EpoTEK 377 and Martens Plus, as well as the one of loaded samples. In EpoTEK 377, it was shown that a first addition of filler leads to a decrease in T_g (ca. 10°C) and then any more addition of filler has no real impact. The shape effect was more defined and showed lower T_g for all the loaded samples. Martens Plus loaded samples showed an increase of T_g values with volume fraction, with higher values for the smallest particles. The shape effect was the same than for EpoTEK 377.

We have therefore explained how to make a thick-film paste and its thermal characterization. The following chapter will be fully dedicated to the functional characterization of the composites: electrical, mechanical and thermomechanical properties.

Chapter 4

Functional characterization of the composites

In the two previous chapters we have detailed what an epoxy-graphite composite is made of and have therefore reviewed the properties of its constituents: the matrix and the filler. The formulation of a thick-film paste and its special requirements (such as viscosity) were exposed as well. In this chapter, we will focus on the properties of the final composite. Electrical characterization (i.e. resistivity and piezoresistivity) will be studied first. The next section will deal with the mechanical behavior, measurements being performed with dynamic mechanical analysis, and finally we will have a look at the thermo-mechanical properties, more specifically the thermal dilatation of the material.

4.1 Electrical properties

When manufacturing a thick-film resistor, the electrical characteristics of the paste are obviously of high importance. In order to potentially use it in a sensor for instance, the resistivity as well as the piezoresistive response have to be known. These will be characterized in the following sections.

4.1.1 Sample design and manufacturing process

As it was explained before, screen-printing was chosen as deposition process. This requires specific design of the samples, which will be explained here. Extended explanations about layout design can be found in the thesis of Fournier [139]. Hyde and Altium designer are the standard softwares used to draw the patterns that will be reproduced first on a film, then on the screen and finally on the substrate. The standard substrates used in the laboratory are square of 101.6 mm wide (4 inches) made of 96% alumina from Kyocera,

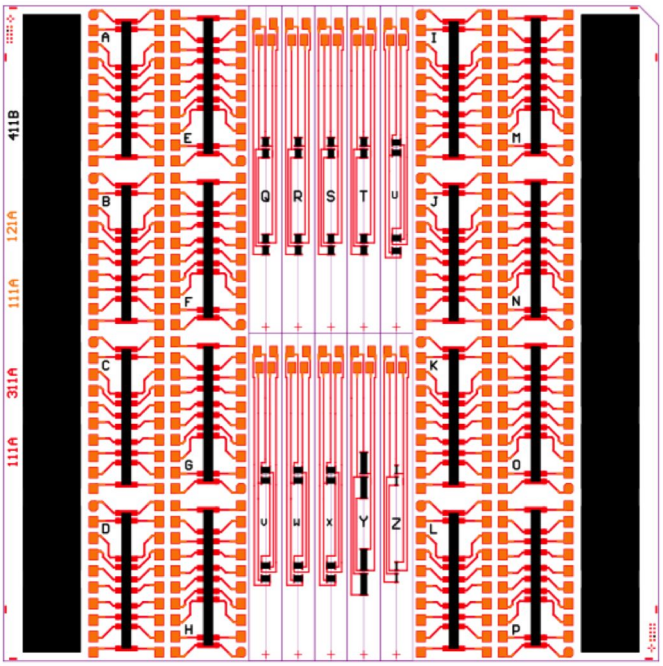

Figure 4.1: Layout design of a substrate used for resistivity and piezoresistivity measurements

Japan (A-476). A layout allowing manufacturing of resistors and beams for piezoresistive characterization was developed at the Laboratoire de Production Microtechnique and is shown in Fig. 4.1. Resistors can be seen on each side, they are 1.5 mm wide with various lengths and allow sheet resistivity as well as TCR measurements. In the central part, beams (longitudinal and transverse) with a Wheatstone bridge are manufactured, enabling the calculations of both gauge factors. On alumina substrates, the resistor terminations were made with thick-film gold ink (ESL 8837, ESL = ElectroScience Laboratories, USA) and the pads for external spring contacts with Ag:Pd 3:1 alloy ink (ESL 9635B or 9635G). Both conductor materials were screen printed, dried and fired for ca. 10 min. at 850°C in a belt furnace (in air). On organic substrates or organic insulating layers, a single epoxy-silver conductive adhesive (Épotecny E212) ink was used for both terminations and contact pads; it was hardened for 15 min in air at 150°C.

In our case, a wide range of filler concentrations was needed for a better characterization of the pastes. A low-viscosity epoxy was therefore chosen as matrix, allowing high loadings of graphite (without the use of solvent). The resulting problem is that at low loadings, the paste might be not viscous enough to stay properly on the substrate. Therefore, an alternative concept, inspired from "dam-and-fill" PCB technology, was used. A dam, made with

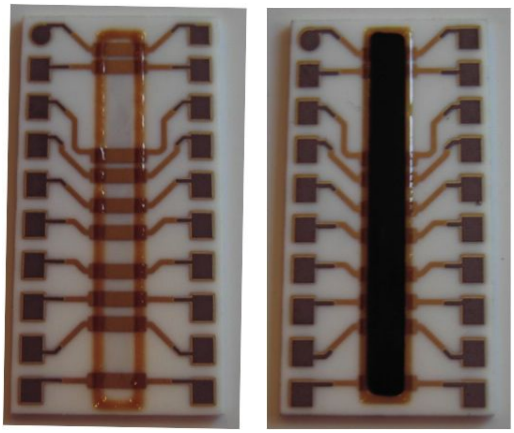

(a) (b)

Figure 4.2: Dam and fill concept: first a dam is screen-printed (a), which is then filled with the resistive paste (b)

highly viscous epoxy loaded with silica (EpoTEK 354T from Polyscience + 50% mass SiO_2), is first screen-printed on the sample, forming a cavity. This cavity is then filled with the resistor (Fig. 4.2). The same concept was applied for the fabrication of beams for piezoresistive studies. The process requires the samples to be screen-printed one by one, which appears slightly less efficient than the previous layout. However, when other substrates than alumina are used, such as aluminum for instance, the use of the whole-substrate layout on Fig. 4.1 is impractical. Indeed, no plate with divisible elements is available: resistors and beams have to be screen-printed one by one.

4.1.2 Study of the resistivity

For various volume fractions, several effects were investigated: particle size and filler type, temperature and substrate. Properties of the components were exposed in Part 3.1.1.1. Experimentally, the resistors are measured through a four-probe method. The principle is simple and widely used. Four probes are disposed on the resistor to be measured (Fig. 4.3). The current set-up using the two outer probes and the difference in potential between the two inner probes is measured [168]. As the length of the resistors is known, this allows the determination of the sheet resistance of the sample. To determine the resistivity, the thickness of the resistor needs to be measured, which was done using an optical profilometer. Typical thicknesses obtained with these thick-films are ca. 100 µm. Moreover, in order to calculate the TCR, measurements are done at 30°C, 40°C, 50°C and then back at 30°C remaining below the glass transition temperature range.

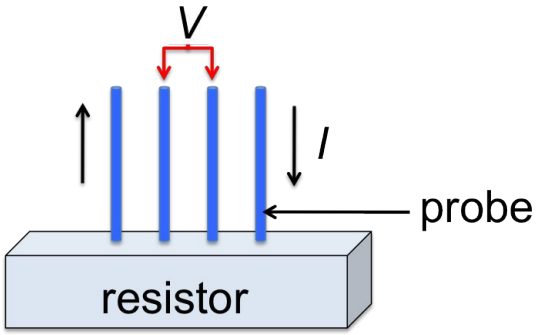

Figure 4.3: Four-probe method

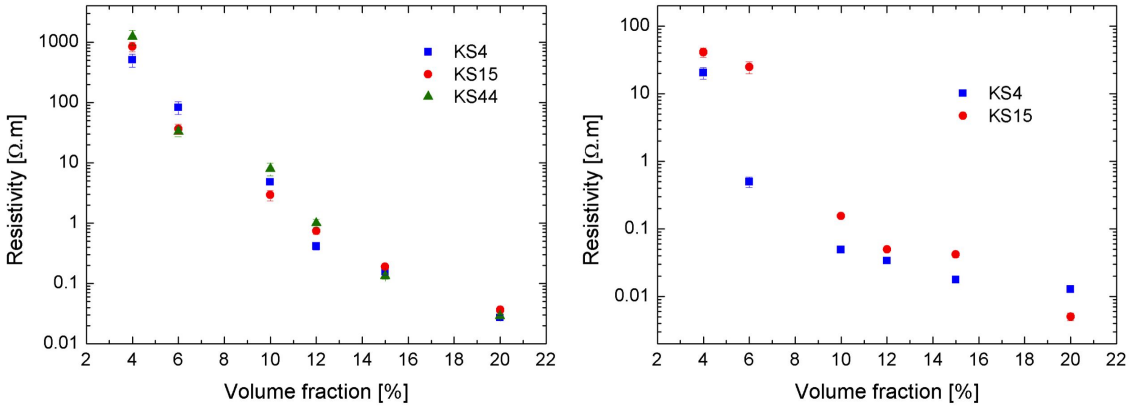

(a) (b)

Figure 4.4: Resistivity of the composites vs graphite volume fraction of KS4, KS15 and KS44 in EpoTEK 377 (a) and of KS4 and KS15 in Martens Plus (b)

4.1.2.1 Influence of the particle size

The first effect to be investigated is the particle size. KS4 and KS15 were used for experiments at various volume fractions, as they are "standard" graphite with an ellipsoidal shape. Informative results with KS44 are also presented here, but one has to keep in mind that these results have to be interpreted with caution as the particle size (ca. 44 µm) is of the same order of magnitude as the height of the thick-films (ca. 100 µm). It is therefore dubious to consider the spatial distribution of the graphite flakes as 3-dimensional and differences with measurements of the bulk properties of the same composite are to be expected. Results with EpoTEK 377 matrix are reported in Fig. 4.4a. They show that the particle size has little effect upon the resistivity. We can also notice that despite the fact that KS44 is too large to guarantee a 3D distribution in our samples, the values seem to fit with the others.

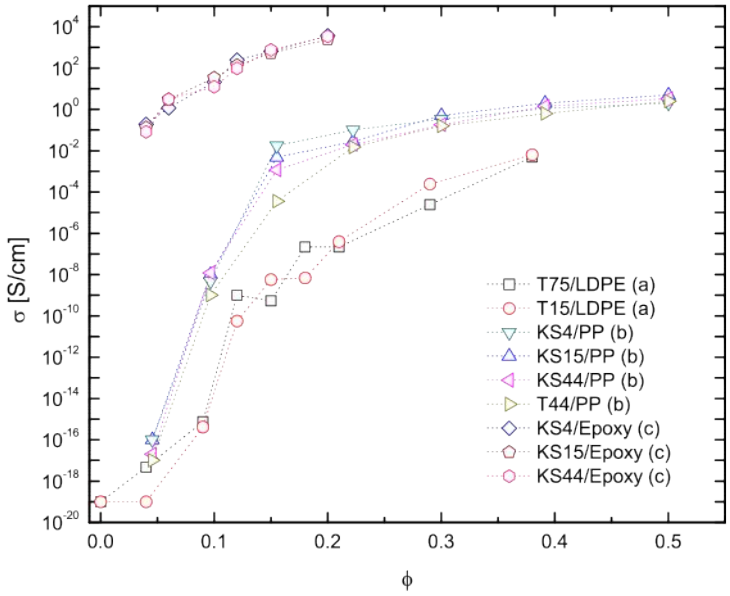

Figure 4.5: Conductivity of different graphite polymer composites as a function of the filler volume fraction in LDPE from [169, 170]pressure molding (a), PP from Timcal, extrusion compounding and injection molding (b) and our samples in EpoTEK 377 (c) [94]

The study was also performed with Martens Plus, although only KS4 and KS15 were used as fillers (Fig. 4.4b). They highlight the fact that composites made with smaller particles tend to be more conductive. If we now compare the values obtained in both epoxies, we can notice that the resistivities tend to be higher in EpoTEK 377 than in Martens Plus, which can be surprising considering the fact that the Martens Plus is more viscous (see supplier's data Table 3.1). We might indeed expect it to be easier to get close contacts between conductive particles in a low-viscosity matrix. This behavior might come from the difference in polymerization mechanisms (see Part 3.1.1.1), chemical affinity matrix/filler or from shrinking phenomena inside the material, i.e. if the shrinking is higher, particles will be pushed together and thus form more conductive paths.

Using the same fillers as above, other samples were produced in different matrices (in collaboration with Timcal). Conductivity of the samples in low-density polyethylene (LDPE) and polypropylene (PP) matrices were calculated. These results are reported in Fig. 4.5 from [94], together with the conductivities from our samples in EpoTEK 377. They show the same tendency as in our samples, i.e. little effect of the particle size upon resistivity.

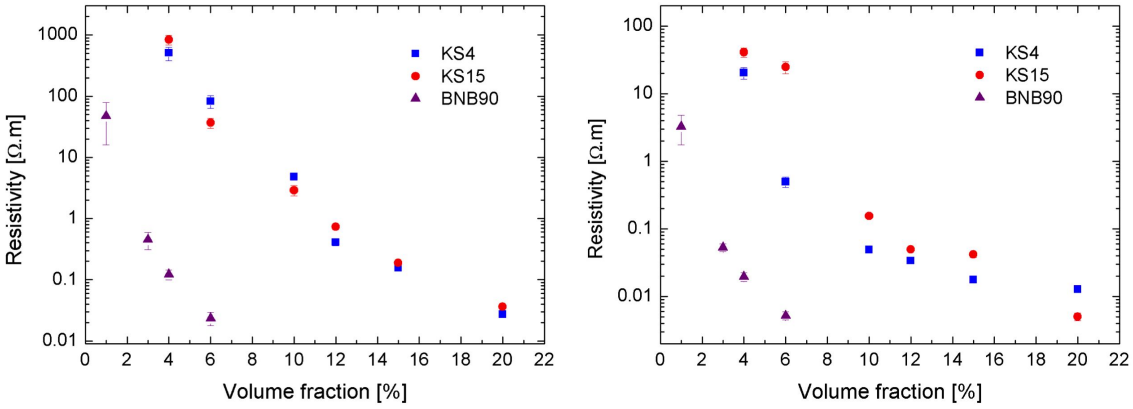

Figure 4.6: Resistivity of the composites vs graphite volume fraction of KS4, KS15 and BNB90 in EpoTEK 377 (a) and Martens Plus (b)

4.1.2.2 Influence of the filler type

We now propose to compare these two ellipsoidal shape graphite powders with BNB90, which has a worm-like shape (see Fig. 3.14a). Due to the high specific surface area of BNB90 and its high value of oil absorption (see Table 3.3), it was not possible to load the sample higher than 6% (vol.), the workability of the composite being also strongly impaired by the filler's shape. Fig. 4.6 presents the resistivities for KS4 and KS15 compared to BNB90 in both epoxies. The first observation is that the expanded graphite exhibits an extremely low percolation threshold. Indeed, due to its particular shape, giving it a high excluded volume, and high specific surface area, this material is able to form conductive paths more easily. In both epoxies, BNB90 tends to show the same behavior: the percolation curve is similar, but shifted to smaller volume fractions. We can notice that the value obtained for 6% of BNB90 basically corresponds to 20% of KS4/KS15. This means that highly conductive thick-films can be manufactured with low loadings of BNB90, which might be interesting for mechanical purposes.

The same type of experiments were performed for carbon black, i.e. Ensaco 250P. Carbon black should present a low percolation threshold but its usefulness is limited by its low intrinsic conductivity. From an experimental point of view, it was not possible to mix more than 10% (vol.) of carbon black to the epoxy, which is in agreement with the oil absorption values from Table 3.3. Fig. 4.7 presents the resulting resistivity curve for Ensaco 250P compared to ellipsoidal graphite (KS series) and BNB90. As the values for the KS series are relatively independent of particle size, only the results for KS4 are shown. As a reference, commercial resistive pastes from Electra

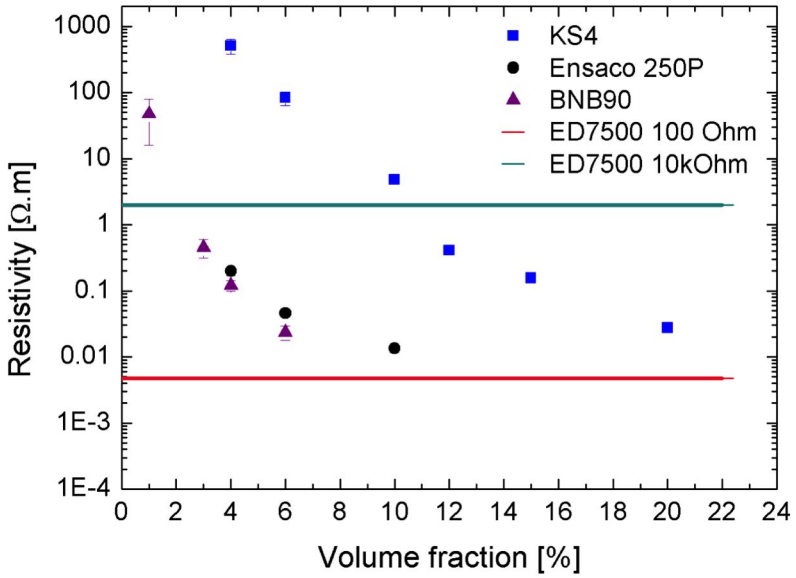

Figure 4.7: Resistivity of the composites vs. volume fraction of KS4 and Ensaco 250P in EpoTEK 377

Polymers (www.electrapolymers.com) were also tested: ED7500-100 Ω and ED7500-10 kΩ. The results can also be found here.

We can observe that, as expected the percolation threshold of the carbon black is lower than for KS graphite. It presents also a higher structure and specific surface area (see Table 3.2), which is the reason why the resistivity values are shifted to smaller volume fractions. However, it may not be possible to obtain higher conductivity with this filler, workability of the paste being already largely impaired at 10% (vol.). As far as the commercial pastes are concerned, we can see that the 10 kΩ could roughly correspond to a graphite paste loaded at 11% vol., whereas the 100 Ω paste displays a value below the ones obtained for both graphite and carbon black. This result tends to confirm that this paste is made from a mix of filler (see microstructure observations in Part 3.2.3).

4.1.2.3 Temperature effect: influence of the T_g

The two first parts were mainly dedicated to the fillers even if tests were performed in two different epoxies. In this part, we would like to investigate the effect of the matrix, and more specifically of the glass transition temperature, on the properties of the composite. We have previously explained that T_g has a tremendous effect on the resulting properties of the composite, which is the reason why two epoxies with very different T_g were chosen. Thermal stability was therefore investigated and was qualified by performing three full thermal

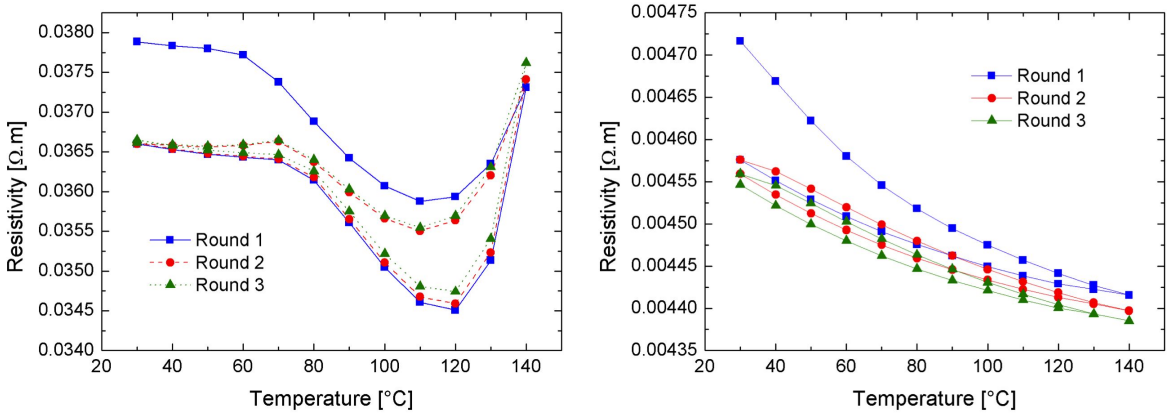

Figure 4.8: Three thermal cycles for 20% KS15 in EpoTEK 377 (a) and Martens Plus (b)

cycles between 30 and 140°C on the test resistors, with the resistivity measured each 10°C. With the aim to achieve a low drift of the resistivity up to 140°C, two compositions were prepared: one with the standard EpoTEK 377 resin and the other with Martens Plus resin. In both cases, we added KS15 graphite, to give 20% volume in the final resin, and ca. 10% mass diglyme solvent to lower the resin viscosity [70]. The results are shown in Fig. 4.8. In the curves corresponding to the EpoTEK 377 (Fig. 4.8a), we can see appreciable amounts of hysteresis, with the first cycle leading to a large permanent change in resistivity. A transition is clearly observed at 60–80°C, roughly corresponding to the T_g of the matrix. Above T_g, several effects are in competition: thermal expansion, mobility (charge carriers, bonds between cross-links) and lower elastic modulus with higher Poisson coefficient. The resistivity of the composite is therefore unstable. The use of Martens Plus (Fig. 4.8b), which has a higher T_g, shifts this undesired effect to higher temperatures. Thermal cycling between 30 and 140°C of test resistors demonstrated that the latter composite is more stable with temperature, although a significant change is still observed in the first cycle. This difference between the first cycle and the other two may come from water loss. Indeed due to the chemical structure of epoxy, it presents an affinity for water and has therefore the tendency to catch water molecules contained in the air.

4.1.2.4 Influence of the substrate

Above T_g, the free thermal expansion of the material increases. In our working temperatures (from 30°C to 140°C), alumina has a stable and low Coefficient of Thermal Expansion (CTE, see Section 4.3), hence allowing the dilatation

of the composite only in the z direction. If we use as substrate a material with a higher CTE, it would follow the dilatation of the composite more closely. Aluminum and phenolic resin were chosen as alternatives to alumina in order to evaluate the effect of the substrate's CTE. Their properties are summarized in Table 4.1. The thermal expansion of the substrates, shown in Fig. 4.9, was measured from 25 to 140°C at a 10°C/min heating rate, using an optical dilatometer Misura ODLT 1200-30, from Expert System Solutions. As the slope corresponds to the CTE of the material, we were therefore able to calculate its value for the temperature range mentioned above. We found that alumina has a CTE of 6.9 x 10^{-6}/°C, aluminum of 25.8 x 10^{-6}/°C and the phenolic resin of 32 x 10^{-6}/°C. These experiments are in good agreement with the expected CTE for these materials. For comparative purposes, thermal expansions of composites loaded at 12% KS4 in both matrices are also reported on this graph. We can see that the use of aluminum and even more the phenolic resin, yet not perfect, should less restrain the matrix in its expansion.

Table 4.1: Main properties of alumina, aluminum and substrates (suppliers data)

Type	Reference	Supplier	Young's modulus [MPa]	CTE [10^{-6}/°C]	CTE_{exp} [10^{-6}/°C]
Alumina	A-476 (96% pure alumina)	Kyocera, Japan	315'000	7	6.9
Aluminum	AW-6082, rolled	Metallica, Switzerland	69'000	23	25.8
Phenolic resin (laminated cotton)	HGW 2082	Maagtechnic, Switzerland	NA	NA	32

In order to study the effect of the CTE mismatch between the substrate and the matrix, we propose to use mainly the EpoTEK 377 matrix as it has a T_g in our classical measurement range (i.e. 30°C-140°C). For tests on aluminum, the substrate being electrically conductive, a dielectric made with EpoTEK 377 (resp. Martens Plus) loaded with silica was beforehand deposited on the substrate. Tests were performed with KS4, KS15 and BNB90 on each substrate. The corresponding resistivity vs. volume fractions of each case is reported in Fig. 4.10. For comparative purposes, KS4 composites in Martens Plus matrix were also manufactured on aluminum. Fig. 4.10d displays the obtained resistivity. In general, EpoTEK composites on other substrates than alumina tend to give slightly higher resistivity values, no matter what the filler

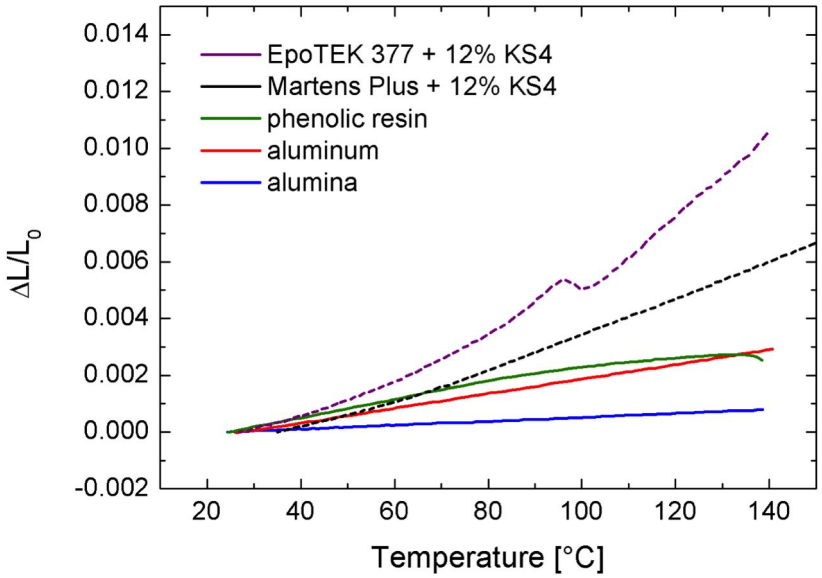

Figure 4.9: Thermal expansion of the substrates (compared to 12%KS4 composites in EpoTEK 377 and Martens Plus)

is. Indeed, the resistivity is calculated in a range of temperature that includes the T_g of EpoTEK 377 (30°C to 100°C), therefore the composites are able to expand more on the other substrates than on alumina. We can consider that the expansion of the graphite particles is very low compared to that of the matrix in the temperature range mentioned above (ca. 7.8 x 10^{-6}/°C [171]), so locally the spaces between the particles slightly "increase", leading to a higher resistivity of the composite. If we now look at the results for Martens Plus, we can see that the values are almost independent of the substrate, as there is little matrix dilatation, T_g being around 200°C. However, if we look more closely on the values found for EpoTEK 377 and KS4 composites, we can see that the values found on aluminum are significantly smaller than the ones on alumina and the phenolic resin. This can be explained by potential interactions between the dielectric and the thick-film. Indeed as described by Cognard [172], monomers from the thick-film layer, when put in temperature, can react with the dielectric, molecules diffusing inside the dielectric. Therefore, the volume of the resistor is effectively smaller than the expected one, hence a smaller resistivity value.

4.1.2.5 Comparison and discussion with percolation theory

Epoxy-graphite composites are known to form percolative materials. Theoretical background regarding percolation theory was given previously in Part 2.2.1. The conductivity should follow the curve described by the law [99]:

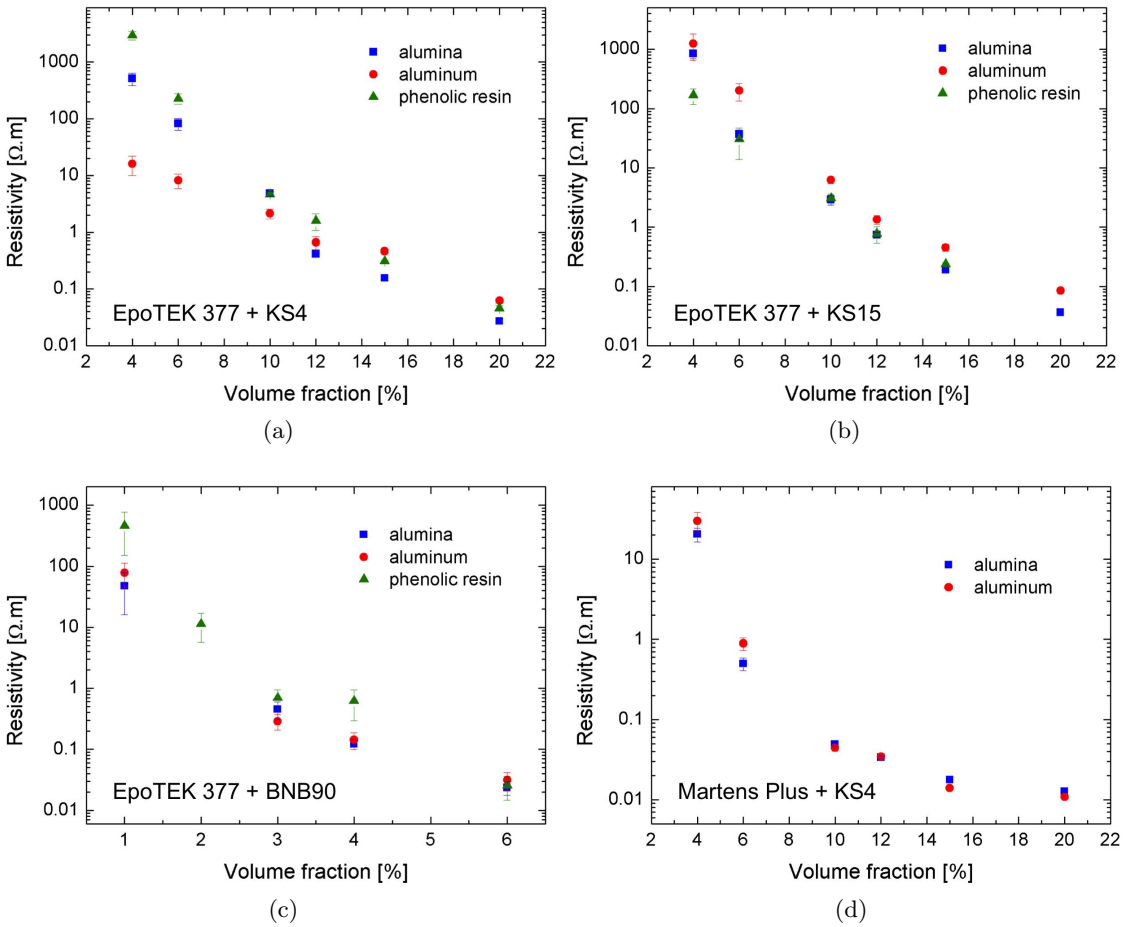

Figure 4.10: Resistivity vs. volume fraction of KS4 (a), KS15 (b) and BNB90 (c) composites with EpoTEK 377 matrix on alumina, aluminum and phenolic resin and resistivity vs. volume fraction of KS4 composites with Martens Plus matrix on alumina and aluminum (d)

$$\sigma \simeq \sigma_0 exp\left(-\frac{2\delta_c\left(\phi, a, b\right)}{\xi}\right)$$

where σ_0 is a constant, Φ the volume fraction, ξ is the characteristic tunneling length, a/b defines the aspect ratio of the particle and δ_c the "geometrical" critical distance, it corresponds to the minimum value between two connected particles.

Depending on the shape of the particle (i.e. oblate, prolate or sphere), different estimates for δ_c can be found, which will determine the final form and domain of validity of this equation. Considering the fact that the expanded graphite BNB90 and the carbon black Ensaco 250P have ill-defined shapes, we will restrict this study on the regular synthetic graphite KS series. Table 4.2 reports the values of aspect ratios a/b (with a and b respectively the spheroid polar and equatorial semi-axes) of our particles. As seen in this table, we are in the case of prolate spheroids.

Table 4.2: Aspect ratio of KS graphite from [94]

Name	KS4	KS15	KS44
Aspect ratio a/b	2.6	3.7	5.7

In this case, the equation becomes:

$$\sigma \simeq \sigma_0 exp\left[-\frac{2D}{\xi}\frac{\gamma\left(b/a\right)^2}{\phi}\right] \tag{4.1}$$

where D is the diameter of the particle and γ a constant (γ=0.4 for spheroids and γ=0.6 for spherocylinders). To apply the formula, the following condition must be fulfilled: $(b/a)^2 \leq \phi \leq 0.03$. This is not the case here, $(b/a)^2$ being always higher than 0.03.

We therefore propose to consider that we have almost spherical particles, in which case the equation becomes:

$$\sigma \simeq \sigma_0 exp\left[-\frac{2D}{\xi}\frac{1.65\left(1-\phi\right)^3}{12\phi\left(2-\phi\right)}\right] \tag{4.2}$$

The condition of validity of this approximation is $\phi \geq 0.1$, which is not always met, our volume fractions ranging from 0.04 to 0.2. However, we found that this approximation gives better results. Fig. 4.11 reports the fitting of the conductivity on KS series with EpoTEK 377 and Martens Plus matrices. The value of D is kept fixed and set to the average of the polar and equatorial semi-axes, so that the only fitting parameter are ξ and σ_0. Table 4.3 shows the values obtained for ξ from these fits. As far as the EpoTEK 377 is concerned,

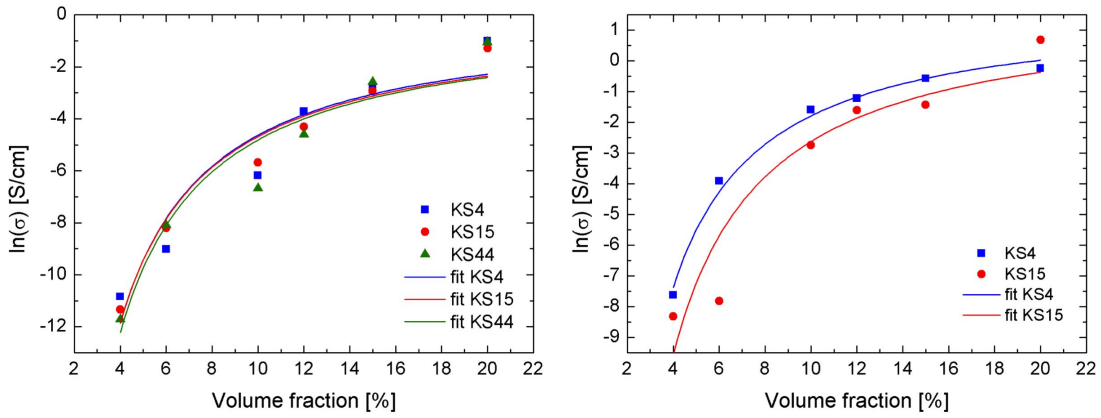

(a) (b)

Figure 4.11: Fitted curves of ln(σ) for KS series in EpoTEK 377 (a) and Martens Plus (b)

the corresponding results do not match perfectly the calculated fit. On the contrary, the curves obtained for Martens Plus nicely reflect the experimental data. However, the values of the characteristic tunneling length, obtained from this fitting procedure, are far too large. Indeed values of the order of the micrometer instead of the nanometer were found. We can therefore conclude that this model is not compatible with our results. This can be explained by the structure of our composite. In Section 3.2 we have observed that the size distribution of the particles is not homogeneous, showing smaller particles dispersed in the matrix. The above-mentioned theory considers that the system is composed of monosize conductive particles homogeneously dispersed in a perfect insulator matrix. In our composites, the matrix contains very small particles, which make it partly conductive. This is in agreement with the *"debris model"* proposed by Ambrosetti [94], i.e. the conductivity inside such composites is ruled by these small debris that enhance the conductive paths.

Table 4.3: Characteristic tunneling length ξ calculated by fitting the conductivity in EpoTEK 377 (a) and Martens Plus (b)

Particle	ξ [nm]
KS4	878 +/- 140
KS15	2431 +/- 250
KS44	6439 +/- 977

(a) EpoTEK 377

Particle	ξ [nm]
KS4	1136 +/- 50
KS15	2508 +/- 439

(b) Martens Plus

4.1.3 Measurements of the temperature coefficients of resistance

The temperature coefficients of resistance (TCR) are interesting to know for any potential applications as they characterize the resistive behavior of the composite with temperature. Extended explanations can be found in Part 2.2.3. TCR values were calculated between 30°C and 50°C for composites with KS4, KS15, KS44, BNB90 and Ensaco 250P in EpoTEK 377 and from 30°C to 100°C with KS4, KS15 and BNB90 in Martens Plus. These temperatures were chosen in order to avoid the T_g range. These measurements are shown in Fig. 4.12 as a function of the filler volume fraction. The graph where the results with EpoTEK 377 are reported also contains the results for both commercial pastes, i.e. ED7500-100 Ω and ED7500-10 kΩ. In this very figure, we can see that TCR values are positive and rather far from 0, which means that the resistivity of the composites will increase with temperature. Unlike our composites, both commercial pastes present negative TCR values that are also quite far from 0. However, composites with high loadings seem more stable with temperature, their TCR values getting closer to 0. They thus seem more suitable for any potential applications.

Let us now look at the TCR of Martens Plus composites. Overall, TCRs are smaller than for EpoTEK 377, this was predictable and is linked to the matrix's stability with temperature. However the curves show an increase and a decrease of TCR values, which means that, contrary to EpoTEK 377, the value closest to 0 is not obtained for the highest volume fraction. Nevertheless, Martens Plus composites vary less in their TCR than the EpoTEK ones, which confirm the results that were found in Part 4.1.2.3. The existence of both positive and negative TCRs at all loadings shows that selection of suitable combination of resin, fillers and processing conditions in principle allows fabrication of composites with TCR ≈ 0.

We propose now to study the influence of the substrate on TCR. Fig. 4.13 reports the results for KS4, KS15 and BNB90 in EpoTEK 377 matrix composites on alumina, aluminum and phenolic resin and for KS4 in Martens Plus matrix composites on alumina and aluminum. If we first have a look at the TCR of composites with ellipsoidal graphite particles, we can see that higher dilatation of the substrate tends to give higher values of TCR. Indeed, the more the substrate dilates, the more the resistor thick-film is able to dilate in the plane. The resistivity increases due to a larger volume for the same amount of particles, leading to an effective decrease in filler volume fraction and a concurrent increase in resistivity, hence higher TCR values for higher substrate dilatation. If we look at the results for Martens Plus, the TCR values for the smallest volume fractions are even shifted to positive values on aluminum. As for the results with BNB90, no real trend can be drawn from the graphs (high errors, lack of data). However, for a same substrate, the values are rather close, which can be explained by the shape of the filler.

Taken together, these results show some interesting features that can be, at

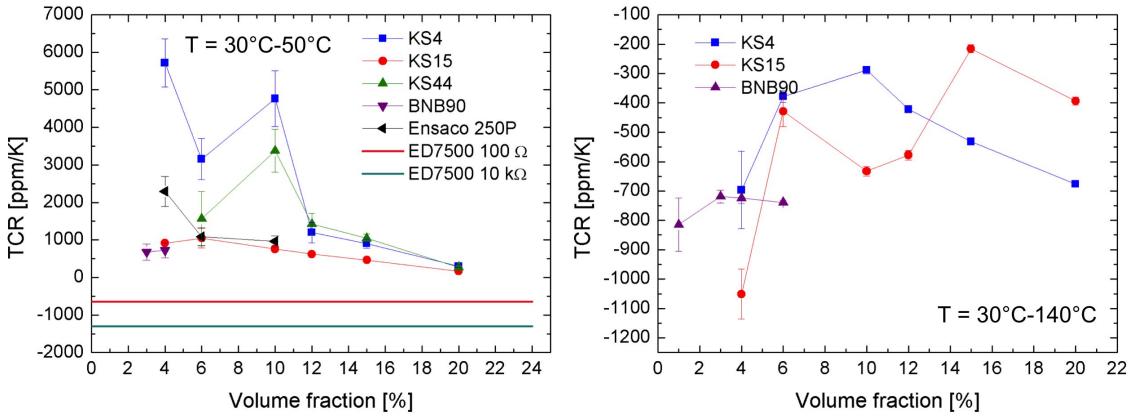

(a) (b)

Figure 4.12: Temperature coefficients of resistance for composites with KS4, KS15, KS44, BNB90 and Ensaco 250P in EpoTEK 377 (a), and with KS4, KS15 and BNB90 in Martens Plus (b)

least partially, understood by considering the network of conducting particles in the composites. Several effects add up or compete to give rise to the TCR, which is the reason for its complicated dependency on the different composite parameters. Let us first recall that the thick-film resistor is constrained in the xy plane by its adherence to the substrate, whereas it can freely deform in the z direction. The resistance is measured between two points in the xy plane of the composite. At low filler volume fractions, there are fewer interparticle contacts and the current has few alternative paths through the composite, forcing the current through poor and deformation sensitive interparticle resistances. Therefore, the path that the current will take to cross the composite will be very tortuous, and so very sensitive to the matrix deformation in the z direction. At high filler concentrations, the path will be direct and will flow on many parallel routes in the direction of the applied potential gradient. It becomes therefore almost insensitive to the matrix deformation. If we change the substrate, we can assume that at high loadings, the deformation of the substrate dominates the TCR, with substrates with higher CTE leading to higher TCRs (see for instance Fig. 4.13a).

If we now look at the TCR values for the Martens Plus matrix, we can notice that they are negative (see Fig. 4.12b). However, when the measurement is performed on aluminum (Fig. 4.13d), at low volume fraction, the matrix is able to deform more easily, the effective volume fraction decreases, which is why the TCR becomes positive. Why, depending on the matrix, the TCR is either positive (case of EpoTEK 377) or negative (case of Marten Plus) is hard to understand, but may be explained by the fact that the chemistry involved is different. Indeed, Martens Plus and EpoTEK 377 have neither the

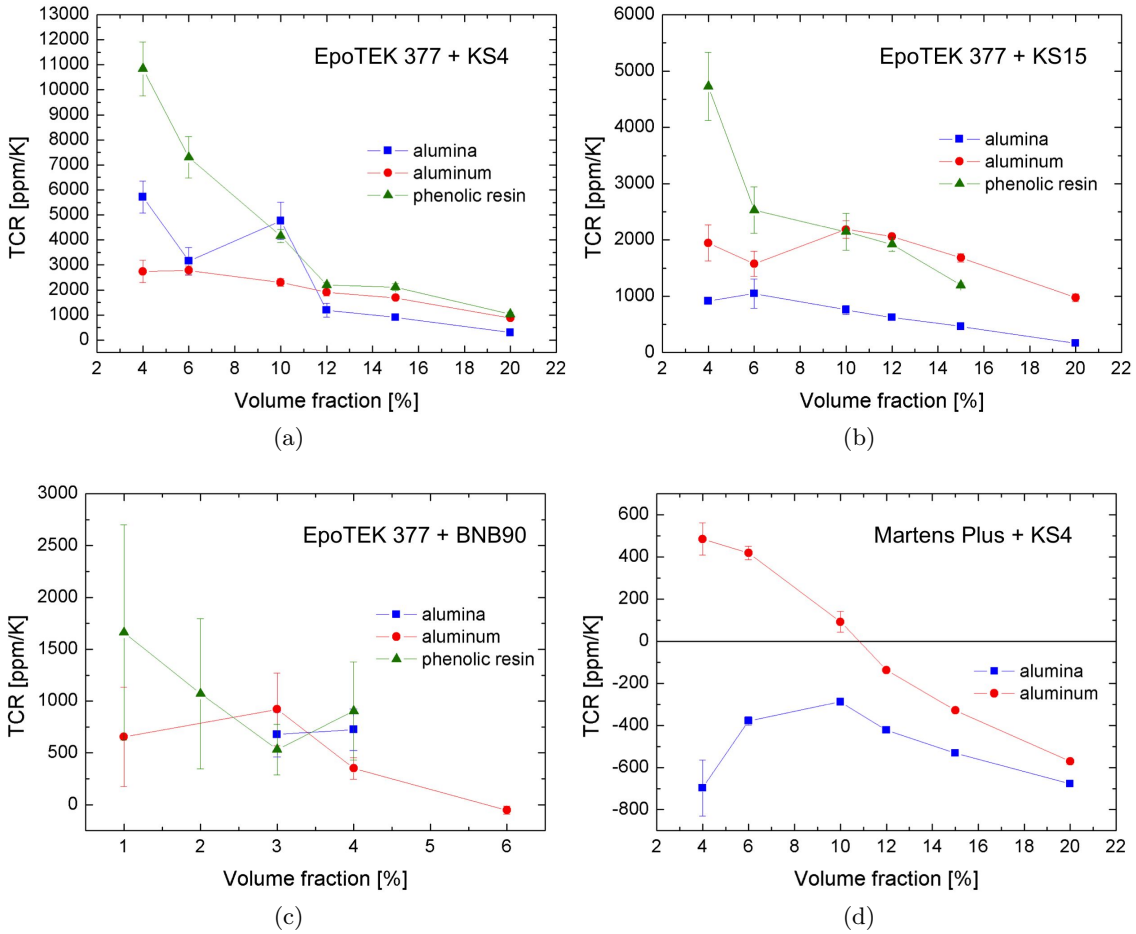

Figure 4.13: Temperature coefficients of resistance vs. volume fraction of KS4 (a), KS15 (b) and BNB90 (c) composites with EpoTEK 377 matrix on alumina, aluminum and phenolic resin and temperature coefficients of resistance vs. volume fraction of KS4 composites with Martens Plus matrix on alumina and aluminum (d)

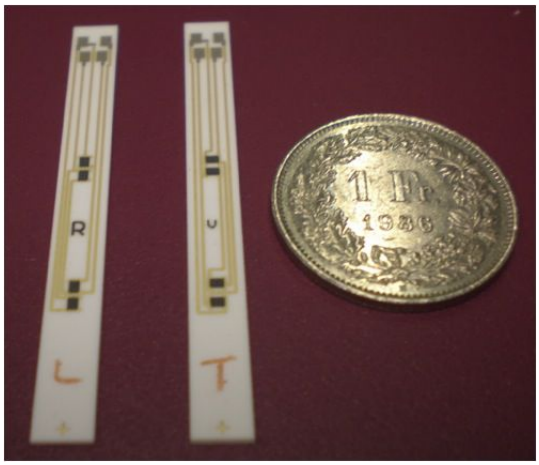

Figure 4.14: Beams for longitudinal (left) and transverse (right) gauge factors

same viscosity nor the same hardener type. This has probably an impact upon the dispersion of the graphite particles inside the matrix, hence the result. What we observe here is a quite common result in TFRs, where TCRs can be modulated to positive or negative values by changing slightly the chemistry of the material (for instance with an additive).

4.1.4 Piezoresistive response

Longitudinal and transverse beams with a Wheatstone bridge (Fig. 4.14) were manufactured using the layout in Fig. 4.1. For small volume fractions in EpoTEK 377, the same dam and fill process imagined to produce the test resistors was also used. In Part 2.2.2, we have defined the longitudinal and transverse gauge factors, GF_L and GF_T which are the values determined by the experiments. A beam is clamped at one end, a weight is then applied on the free tip of the beam and the resulting electrical signal response is recorded, leading, after calculation, to both gauge factors. GF_L is measure in the case where the current flows along the length of the beam (i.e. the current is parallel to the applied strain) and GF_T when the current flows along the width of the beam (i.e. current perpendicular to the applied strain). Both factors were determined in our experiments. However only the GF_L will be presented and discussed here, the effect being the same for GF_T but the relative error is higher due to a lower response. As done for the resistivity, several effects will be investigated: filler (particle size, shape and type), matrix and finally the substrate.

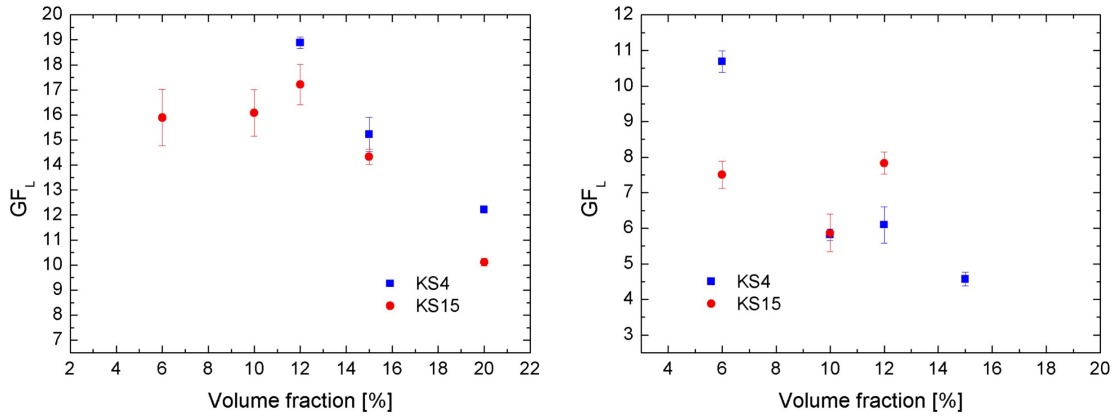

(a) (b)

Figure 4.15: GF_L vs. volume fractions of KS4 and KS15 in EpoTEK 377 (a) and Martens Plus (b)

4.1.4.1 Influence of the filler

We propose to first investigate the particle size of the filler: various volume fractions of KS4 and KS15 were used in our epoxies. GF_L and GF_T were calculated at 25°C and are presented in Fig. 4.15 as a function of the volume fractions of filler. In the curves related to the EpoTEK 377, we can see that smaller particles seem to lead to higher GF_L. In theory, at the same volume fraction, smaller particles should create more tunnel junctions, hence smaller resistivity and gauge factor. As far as the Martens Plus is concerned, an increase in the volume fraction of KS4 leads to a decrease in the GF_L which was predictable. However, KS15 composites do not seem to present a very well-defined piezoresistive response.

Theoretically, we expect to see the piezoresistivity increase linearly with the logarithm of the resistivity, we therefore replot these results as a function of the resistivity on a logarithmic scale in Fig. 4.16. This is verified for both series, KS4 and KS15, in the lower resistivity range. Continuum tunneling-percolation theory also predicts that, close enough to the percolation threshold, the piezoresistivity will eventually become independent of the filler's volume fraction (hence constant) [173]. This crossover between the increasing and constant behaviors might be what is observed here for the KS15 series in EpoTEK 377 and only the constant behavior seems to be observed in the other matrix.

In this representation of the piezoresistivity as a function of the resistivity, we would expect the two fillers to display identical values of the gauge factor, with the smaller filler eventually transitioning to a constant value at lower resistivity values than KS15. Here, although the values are indeed similar, we

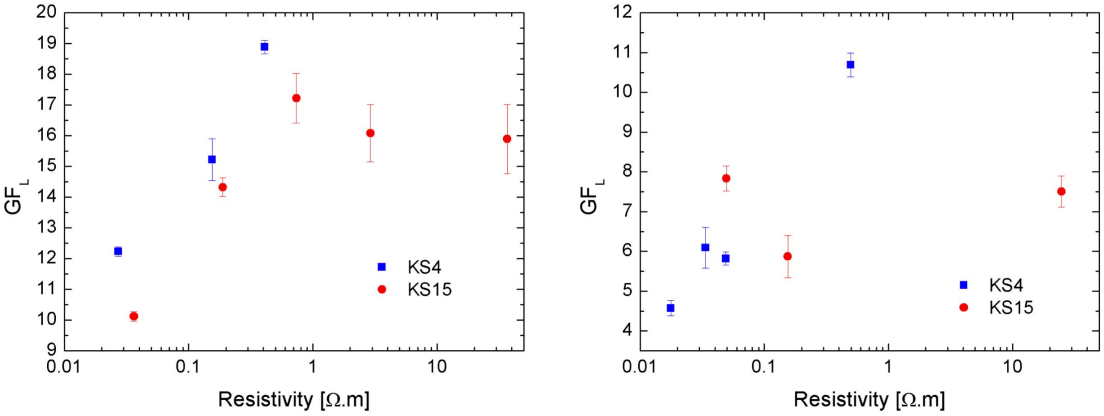

Figure 4.16: GF_L vs. resistivity of KS4 and KS15 composites in EpoTEK 377 (a) and Martens Plus (b)

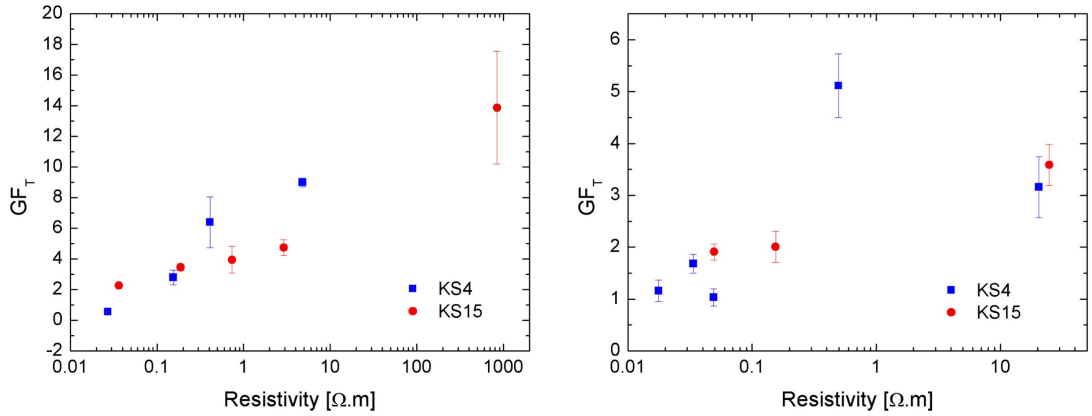

Figure 4.17: GF_T vs. resistivity of KS4 and KS15 composites in EpoTEK 377 (a) and Martens Plus (b)

observe the opposite behavior. This can be explained by several aspects. First, both fillers are very close in size. Moreover, the theory mainly applies for spherical particles, which is not our case here. Indeed, in Ref. [94], the aspect ratio of these particles was calculated and an aspect ratio of 2.6 was obtained for KS4 and 3.7 for KS15 (see Table 4.2). Higher aspect ratios are supposed to lead to smaller gauge factors, which is what is observed experimentally here. As complementary results, the values obtained for GF_T can be found in Fig. 4.17. As for GF_L, higher resistivity, leads to higher gauge factor.

Let us now look at the shape effect of the particle on the gauge factors.

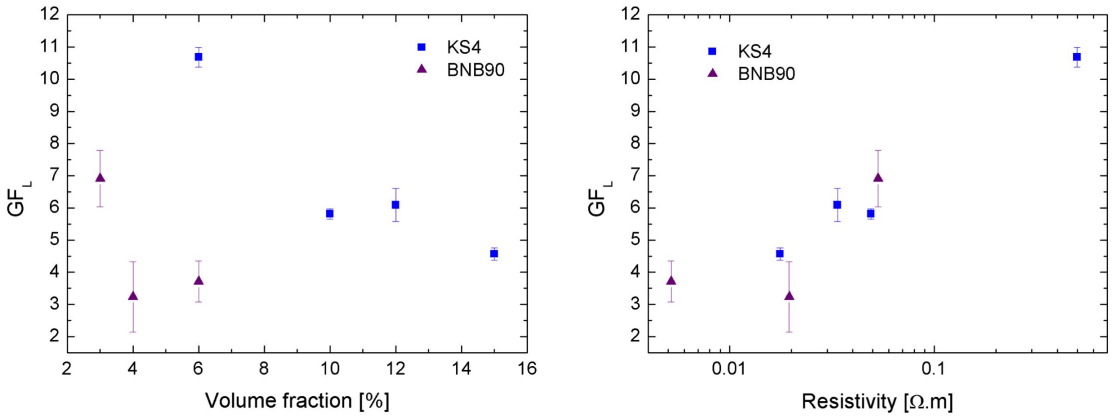

(a) (b)

Figure 4.18: GF_L of BNB90 composites in Martens Plus vs. volume fraction (a) and resistivity (b)

Measurements were performed using BNB90 as a filler and are reported in Fig. 4.18. We can see that the piezoresistive response with BNB90 shows high errors. This is quite understandable. Indeed, due to its shape, BNB90 will form conductive paths at very low volume fractions and include a high number of debris [94]. However, the classical trends suggested by theory are preserved, i.e. higher resistivity leads to higher GF_L in Fig. 4.18b.

4.1.4.2 Influence of the matrix: temperature and creep effects

We first propose here to see the influence of temperature upon piezoresistivity. Measurements were done at 65°C and 100°C. The results are reported in Fig. 4.19, where measurements at room temperature are shown as well, for comparison purposes. If we first study the effect in EpoTEK 377, we can observe that the gauge factor increases with temperature. Indeed we are in the range of the T_g of the polymer, which means that the closer we get to this temperature, the more the matrix stiffness drops. Due to high differences in the Young's modulus between matrix and graphite, most of the mechanical strain is taken up by the matrix, this strain amplification leading to an increase of the gauge factor [104]. On the contrary, the values calculated for Martens Plus are quite similar. This is due to the measurement range (30-100°C) being too far below T_g, hence stability of the matrix properties and similar gauge factors.

Let us now study the stability in time. The creep was observed for various temperatures for one complete cycle (unloaded/loaded/unloaded). Fig. 4.20 presents the results that were observed at 25°C, 50°C and 80°C for both matrices with 12% vol. KS15 loading. Firstly, regardless of the temperature,

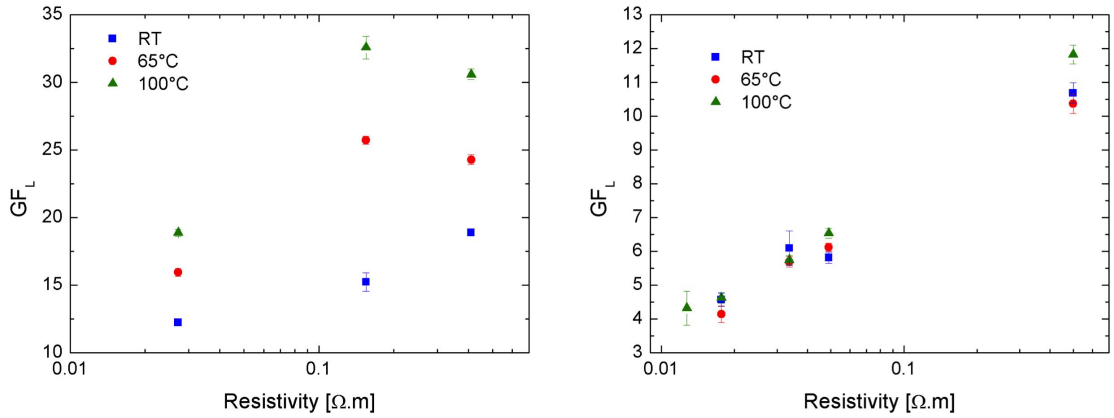

(a) (b)

Figure 4.19: GF_L vs. resistivity of KS4 composites in EpoTEK 377 (a) and Martens Plus (b) at room temperature, 65°C and 100°C

the matrix or the loading, we can notice that each curve shows variations of the signal in time. This probably comes from the relaxation of inner stresses inside the composite. Another possibility might be the adhesion problems between matrix and filler, leading to instabilities. This effect is less pronounced in the Martens Plus matrix. When the temperature is raised close to the T_g of the EpoTEK 377, the material is disturbed due to higher dilatation of the matrix and relaxation effects, leading to strong instabilities (drifts) of the signal (compare Fig. 4.20a and Fig. 4.20c). On the other hand, we can observe that the Martens Plus, while not perfect, expectedly exhibits a better stability regarding the creep.

4.1.4.3 Influence of the substrate

To complete the piezoresistive effect study, we varied the substrate and studied its effect on the gauge factors. Samples were made using alumina and aluminum. Composites investigated had an EpoTEK 377 matrix with different volume fractions of either KS4 or KS15. We can see in Fig. 4.21, that the values of GF_L are close. If we look back at Part 2.2.2, we can see that the deformation along the y axis is $\varepsilon_y = -\nu\varepsilon$, ν being the Poisson's ratio. As this ratio is higher in the case of aluminum (0.34 vs. 0.23 in the case of alumina), so will the deformation. We would therefore expect to have higher values of GF on aluminum. The little difference between values observed here can come from interactions between matrix and the dielectric (see discussion on the subject in Part 4.1.2.4). For completeness, we report the corresponding GF_T on aluminum of the composites KS4 and KS15 in EpoTEK 377 in Fig. 4.22.

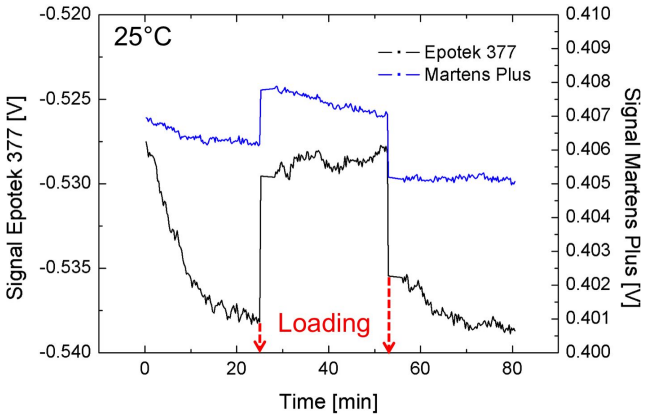

(a)

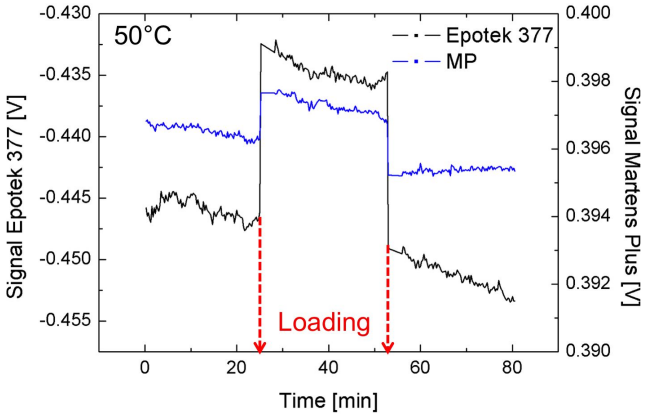

(b)

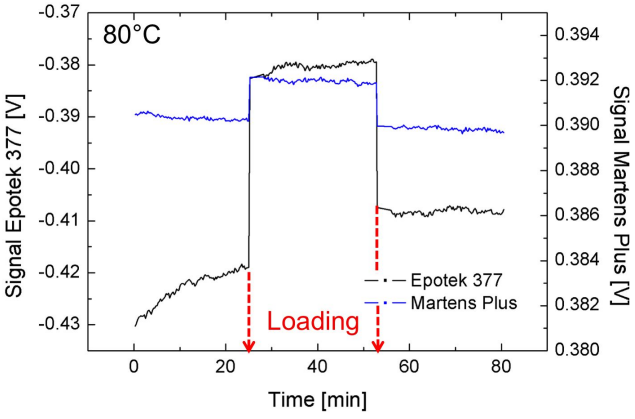

(c)

Figure 4.20: Signal vs. time for 12% vol. KS15 in EpoTEK 377 and Martens Plus at 25°C (a), 50°C (b) and 80°C (c)

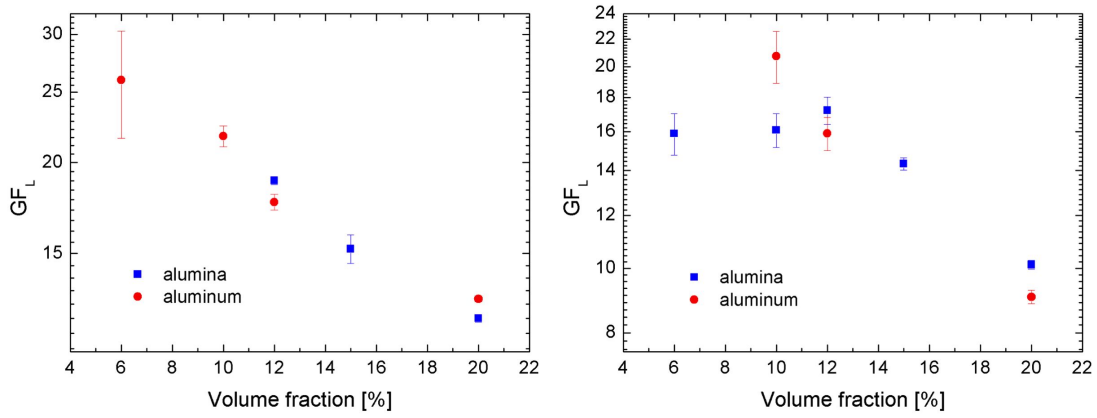

(a) (b)

Figure 4.21: GF_L vs. volume fraction of KS4 (a) and KS15 (b) composites in EpoTEK 377 on alumina and aluminum substrate

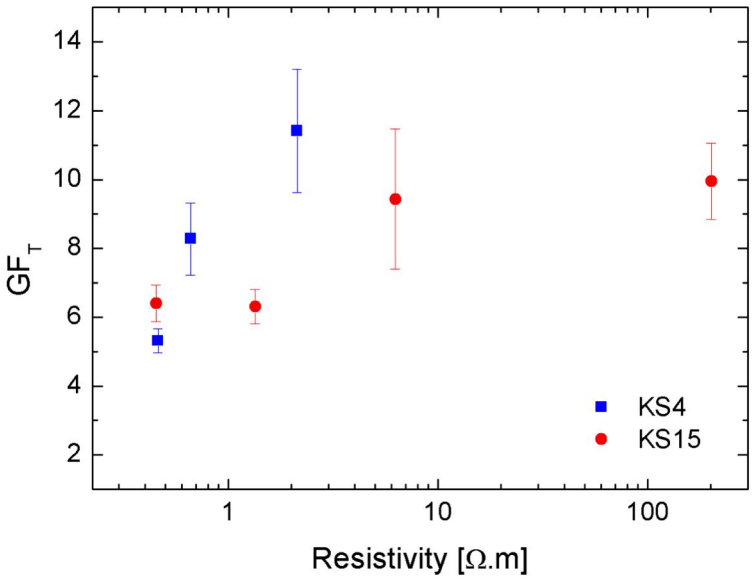

Figure 4.22: GF_T vs. resistivity of KS4 and KS15 composites in EpoTEK 377 on aluminum substrate

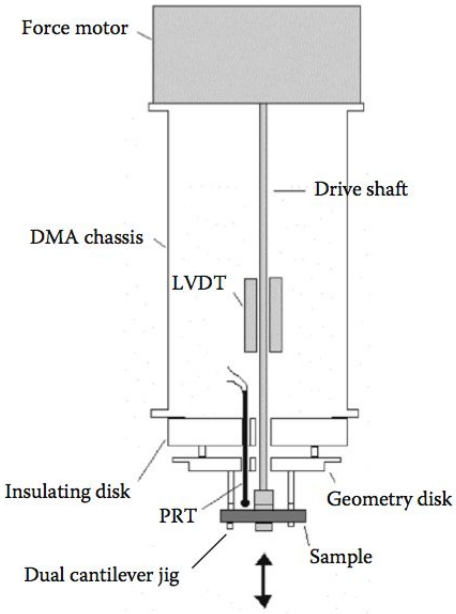

Figure 4.23: Schematic of a PerkinElmer DMA from [92]

4.2 Mechanical properties

In the previous section, we have studied the influence of the filler size and shape upon resistivity. For comparison purposes, samples with carbon black as well as commercial pastes were also manufactured. We have highlighted the importance of the specific surface of the filler on conductive properties. We also proved the particular role of T_g through thermal cycle experiments and substrates changes. Temperature coefficients of resistance were then calculated. Finally, the piezoresistive response of the composites was studied.

In this section, we will investigate the mechanical properties of the composites. Measurements were performed through Dynamic Mechanical Analysis (DMA). After explaining how a DMA works and what information it gives, we will study the results obtained for our materials.

4.2.1 What is Dynamic Mechanical Analysis?

DMA is a characterization method of materials. An oscillating force is applied to a sample, the material's response to this force is then recorded and analyzed. This technique is particularly useful to study the viscoelastic properties of polymers, a way of seeing is that we study the relaxation of the polymer chains [92]. Fig. 4.23 shows a schematic DMA.

Let us go more into detail in order to better understand the principle of the device. The theoretical background largely comes from [92]. A stress is

applied to a sample, which is subjected to a sinusoidal oscillation. It will therefore deform sinusoidally. For any point of the curve, the stress applied can be defined as:

$$\sigma = \sigma_0 sin\,(\omega t)$$

where σ is the stress applied at time t, σ_0 the maximum stress and ω the frequency. The response of the material, i.e. the strain, presents two limit cases: either it is perfectly elastic, which means that there is no phase lag, or it is purely viscous, which will give an out-of-phase response (phase lag $\delta = 90°$). Polymers are viscoelastic materials, therefore they lie in between. If the material were perfectly elastic, E being the modulus, the strain ϵ at time t would be expressed as, :

$$\varepsilon\,(t) = E\sigma_0 sin\,(\omega t)$$

Using Hooke's law, this equation becomes:

$$\varepsilon\,(t) = \varepsilon_0 sin\,(\omega t)$$

with ϵ_0 the strain at the maximum stress.

In the case of polymers, there is a phase shift between the applied stress and the resultant strain: an angle δ. The response of the material can be described as:

$$\varepsilon\,(t) = \varepsilon_0 sin\,(\omega t + \delta) \tag{4.3}$$

Eq. 4.3 can be separated into the in-phase and out-of-phase strains:

$$\varepsilon' = \varepsilon_0 sin\,(\delta) \tag{4.4}$$

$$\varepsilon'' = \varepsilon_0 cos\,(\delta) \tag{4.5}$$

The combination of these equations gives the complex strain of the sample:

$$\varepsilon^* = \varepsilon' + i\varepsilon'' \tag{4.6}$$

We can therefore define the complex modulus E^*, which has a geometrical representation in Fig. 4.24:

$$E^* = E' + iE'' \tag{4.7}$$

This approach allows us to have, from a single modulus, two terms:

- *E'* is related to the storage of energy and will show us how elastic the polymer is. It is called the storage modulus or elastic modulus. Ideally, it is equivalent to the Young's modulus.

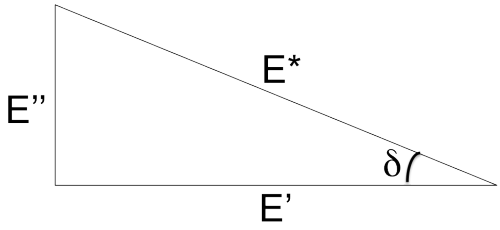

Figure 4.24: Geometrical representation of the relationship between, the complex modulus and the phase angle

- *E”* is related to the loss of energy and will show us the viscous behavior of the material. It is called the loss modulus or the viscous or imaginary modulus.

A DMA will give us the storage and loss moduli, as well as *tan* δ, *tan* δ being defined as $tan\,\delta = E''/E'$. Two main parameters have to be clearly specified when using this device: the temperature and the frequency of the oscillations, as it will affect the properties. DMA allows observing the transitions that occur, and in particular the glass transition. These thermal transitions can be described in terms of free volume changes or relaxation times. Fig. 4.25 shows an ideal scan of *E’* vs. temperature of a polymer with all the potential transitions. The transitions that happen below T_g are associated with the properties of the material in the glassy state. Above T_g, we arrive to the rubbery plateau whose length and viscosity depends on the molecular weight between entanglements or cross-links, the relative modulus of this region giving information about the cross-links or changes in the molecular weight between entanglements. In semi-crystalline polymers, the rubbery plateau is also related to the degree of crystallinity. Finally, for thermoplastics, the melting point T_m is reached.

As far as T_g is concerned, it is possible to determine it in five different ways with DMA (Fig. 4.26): the peak or onset of the *tan* δ curve, the onset of the *E’* drop or the onset or peak of *E”*. This is the reason why when determining T_g with a DMA, one has to specify the method. As far as we are concerned, the method of the peak of *tan* δ curve is chosen to determine the glass transition of our composites.

4.2.2 Sample manufacturing and measurements

Pastes were first prepared using the same process as to make screen-printable pastes. They were then cast into a poly(tetrafluoroethylene) (PTFE, Teflon®) mould in order to obtain small bars. The DMA requires having flat and regular samples. Moreover, the thinner the sample, the more accurate the measurement [174]. To meet these requirements, the bars were then cut, giving samples with fixed dimensions of 50x8x3 (mm). The tested compositions are

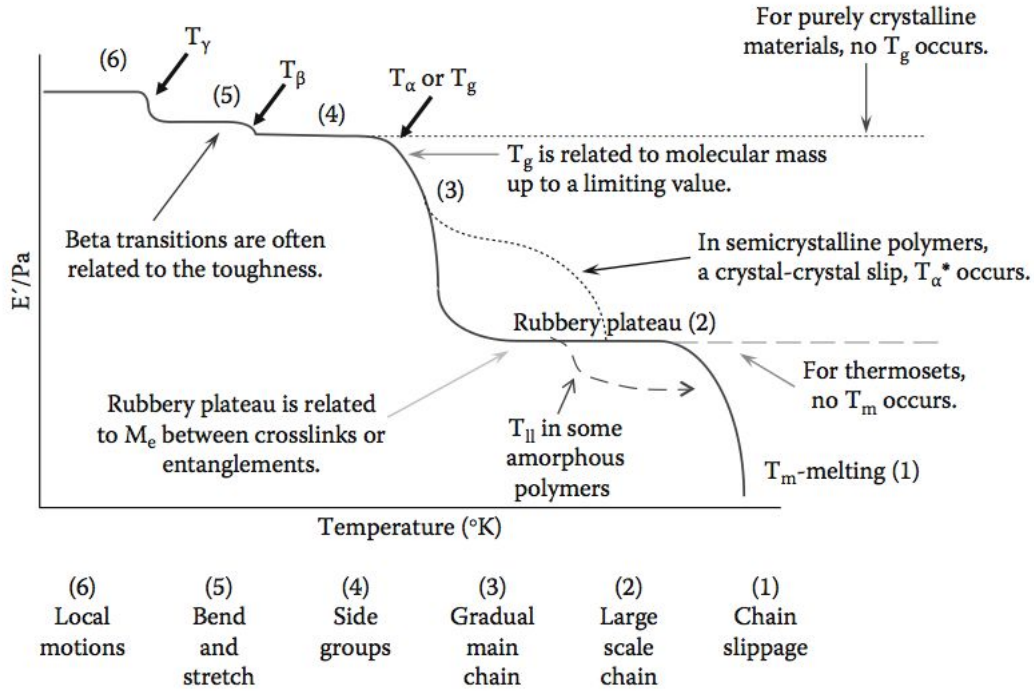

Figure 4.25: Idealized temperature scan of a polymer from [92]

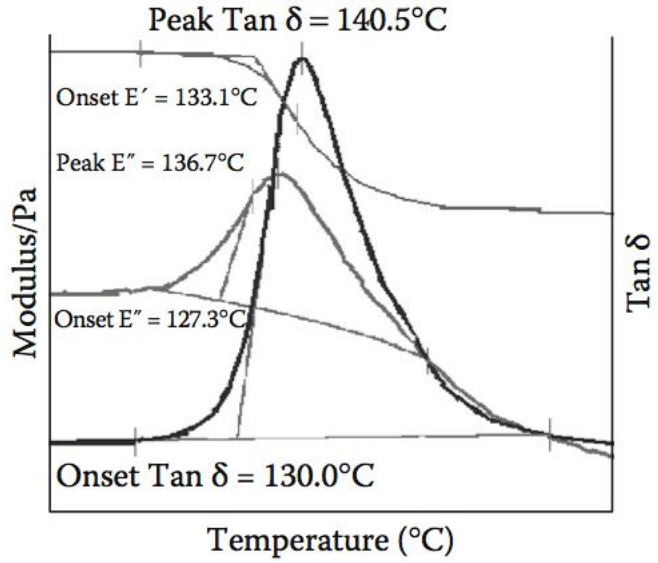

Figure 4.26: Methods of determining T_g with a DMA [92]

reported in Table 4.4. Particles size and shape as well as the matrix effect were investigated. Samples containing oxidized graphite were also tested in order to evaluate the impact of this process on the mechanical properties. Pure samples of both epoxies were measured as well.

Table 4.4: Samples manufactured and studied with the DMA with EpoTEK 377 (a) and Martens Plus (b) matrix

Volume fraction [%]	Filler type
1	BNB90
3	BNB90
4	KS4/ KS15/ BNB90/ oxidized KS4 2h
6	KS4/ KS15/ BNB90/ oxidized KS4 2h
10	KS4/ KS15/ oxidized KS4 2h
12	KS15
15	KS4/ KS15

(a)

Volume fraction [%]	Filler type
6	KS4
10	KS4
12	KS4
15	KS4

(b)

Measurements were done with a Pyris Diamond Dynamic Mechanical Analyzer, from PerkinElmer at Laboratoire de Céramiques at EPFL. A flexural test was performed on each sample using a dual cantilever. The sample is clamped at each end and in the middle. Care must be taken while setting the bar in place to clamp with similar forces in order to prevent the introduction of a distortion or twisting. Once the clamping is done, the set-up is put in the oven and test is run. Temperature scans were performed at 1 Hz, the temperature profile being as follow:

- for EpoTEK 377 samples: from 25°C to 150°C at 2°C/min
- for Martens Plus samples: from 25°C to 280°C at 3°C/min

4.2.3 Investigation on the T_g and the transitions of the composites

4.2.3.1 DMA of pure epoxy

A pure epoxy bar of EpoTEK 377 was run into the DMA with a temperature scan. Fig. 4.27 shows a typical graph that directly comes from the DMA. Several information can be drawn from this figure. We will first study the elastic modulus *E'* curve as it is the most interesting one regarding transitions. No β transition is observed, indeed, these transitions usually happen below 0°C,

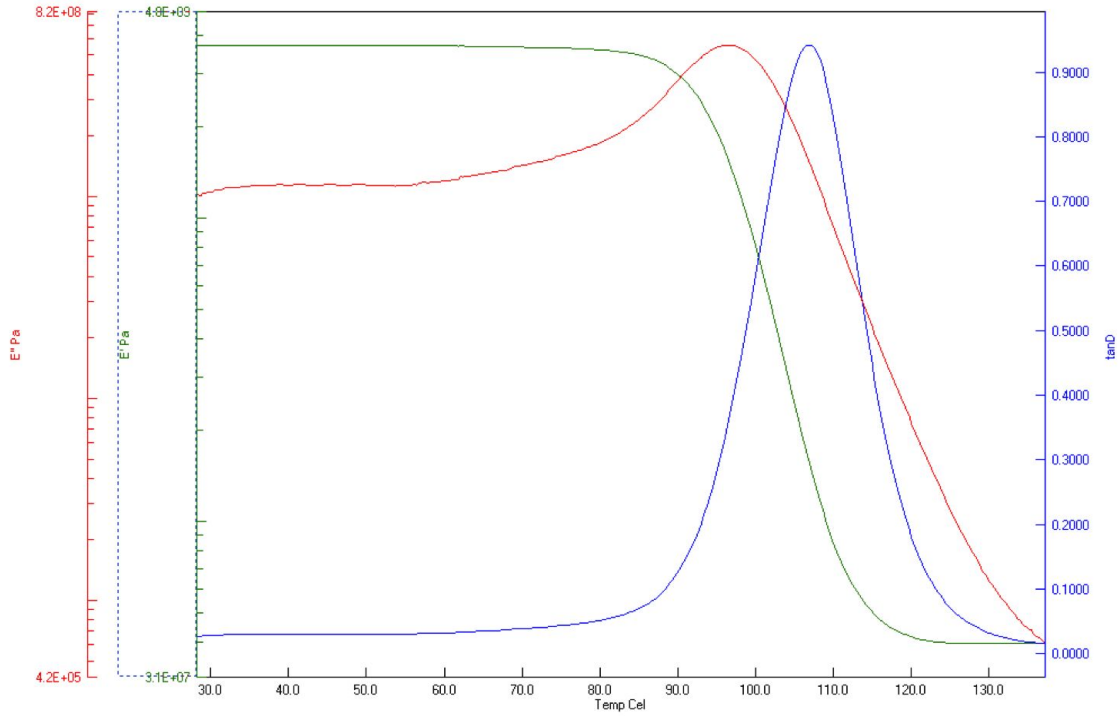

Figure 4.27: Curves obtained from the DMA showing the storage and loss moduli as well as the tan δ for pure EpoTEK 377

in most cases in the range between -80°C and -50°C [92]. As the γ transitions lie even below the β ones, they cannot be seen either. The first transition appears at 90°C where the *E'* drops: it corresponds to the α transition, i.e. T_g. This is followed by the rubbery plateau at 120°C to the end of the measurement. T_m is not present here as we have a thermoset resin: it would therefore decompose and not melt. However, due to potential damage to the DMA, we cannot go up to the decomposition of our epoxy. It is also possible to determine the Young's modulus at room temperature, which would be equal to 3.7 GPa. This value has to be taken cautiously. Indeed, the Young's modulus is defined as the slope of the stress-strain curve and is obtained by stretching of the sample, whereas in our case it is a point obtained by oscillation. However, the value is realistic and in the range of the values found for epoxies. The *E"* curve shows the loss modulus: as energy is lost when the polymer reaches T_g, the modulus increases and decreases after that (no more energy needed). Finally we can now determine the T_g of this epoxy. We have previously decided to use the peak of *tan δ* curve as a determination method. We found therefore 106.8°C.

The same experiment was performed on a Martens Plus bar. Fig. 4.28 shows the graphs of the DMA. Overall, the observed transition is broader than for EpoTEK 377. The β and γ transitions cannot be seen on the *E'* curve for

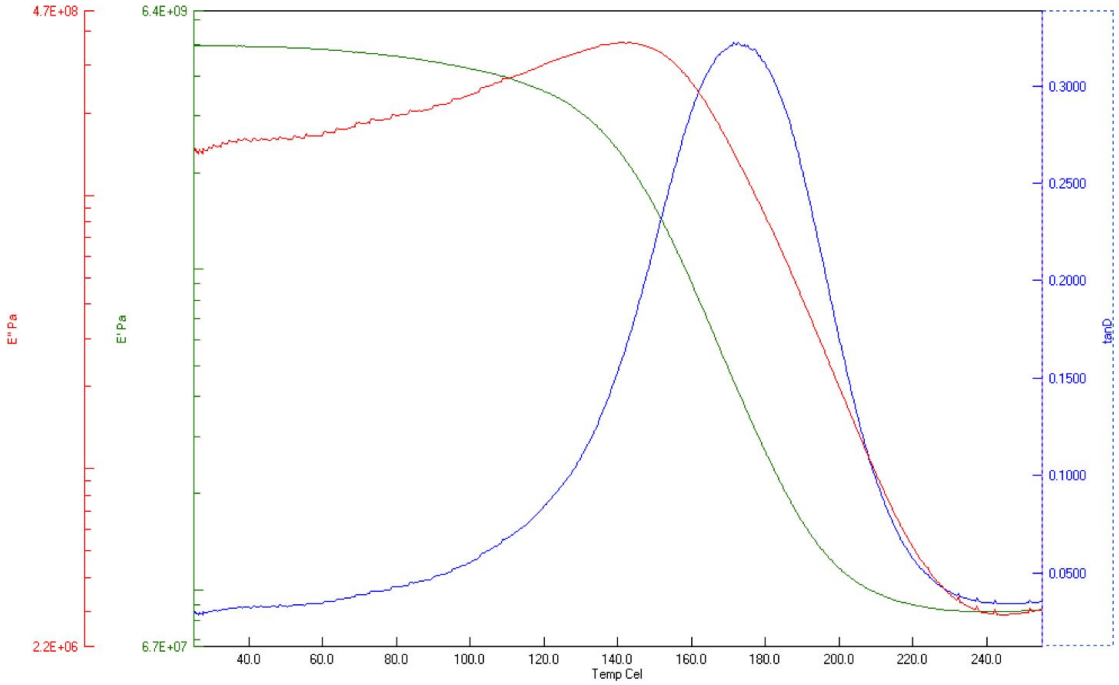

Figure 4.28: Curves obtained from the DMA showing the storage and loss moduli as well as the tan δ for pure Martens Plus

the same reasons explained previously. Still on this curve, the transition starts at 120°C and the rubbery plateau is reached at 220°C. "Young's modulus" can also be determined: it is found to be equal to 4.96 GPa at room temperature. The *tan δ* method gives a value of 177.3°C for the T_g.

To complete the study, a second run was performed on the same pure EpoTEK 377 bar. Fig. 4.29 shows superposition of *E'* and *tan δ* of the two runs. The storage modulus curve shows a "hook" in the second run and the starting value is smaller than in the first run. The T_g value is slightly shifted to a higher value (106.8°C to 108.9°C). This shows that the epoxy is essentially fully cured, as the shift is very low [92].

Finally an additional temperature run was done at the same time at various frequencies on a pure EpoTEK 377 sample, in order to ascertain the frequency dependence of properties. Frequencies used for the test were: 0.1 Hz, 0.5 Hz and 5 Hz. The storage modulus and tan δ are reported on Fig. 4.30. We can see that the storage modulus and the T_g increase with increasing frequency. Indeed, polymers are viscoelastic materials, which means that they are time-dependent. As frequency is defined as: $f = 1/t$, the viscoelastic response will therefore depend on it as well, high frequencies corresponding to short times and low frequencies to long times. At T_g, the molecules relax, but as this is a kinetic transition, it depends on time and frequency. With increasing frequency, time

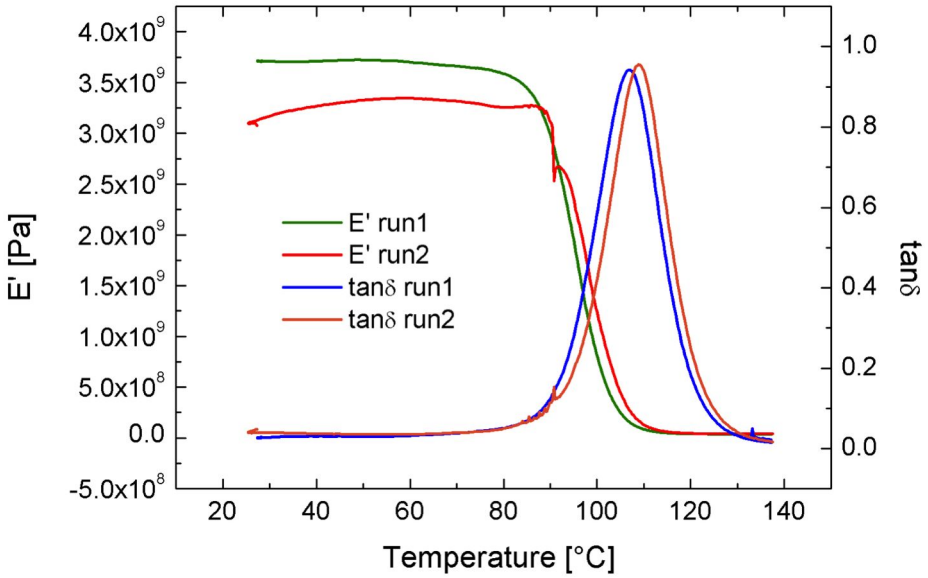

Figure 4.29: Storage modulus and tan δ of run 1 and 2 of pure EpoTEK 377

for relaxation is shortened, which must be compensated by faster kinetics, hence a shift to higher temperatures of the measured T_g. This proves that it is of high importance to give the frequency at which measurements were performed.

4.2.3.2 DMA of epoxy-graphite composites

Since we have studied the DMA of both epoxies, we can now look at the results for the composites. Volume fraction, particle size and shape will be investigated. The effect of oxidation will be also determined.

Effect of the volume fraction Tests on samples loaded with KS4 in an EpoTEK matrix were firstly performed. Fig. 4.31 reports the results for the *E'* and *tan δ* curves. An increase in the volume fraction of filler leads to an increase of the storage modulus, which was predictable, the addition of filler resulting in a stiffer material. A shift of the curve to the smaller temperature can also be noticed. T_g were determined from *tan δ* curves. For a better understanding, evolution of this value with the volume fraction can be found in Fig. 4.32. We can see that addition of filler leads to a decrease in T_g. We can therefore confirm the results that were obtained with DSC (see Fig. 3.21).

The same experiment was performed with a Martens Plus matrix (see Fig. 4.33). The first observation is that the curves are less defined and broader than the ones we obtained with EpoTEK 377. This broadening effect becomes even more pronounced at high filler volume fractions. The storage modulus

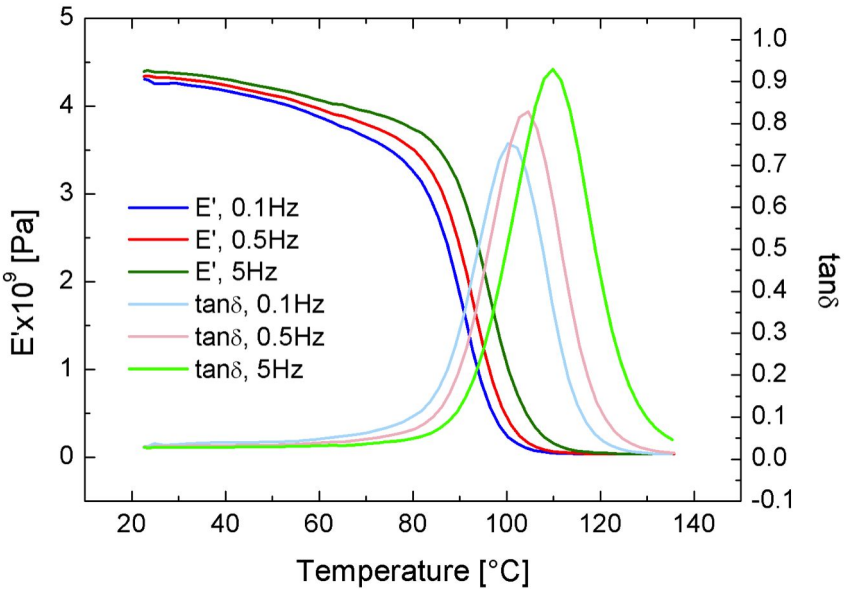

Figure 4.30: Storage modulus and tan δ at 0.1 Hz, 0.5 Hz and 5 Hz of pure EpoTEK 377

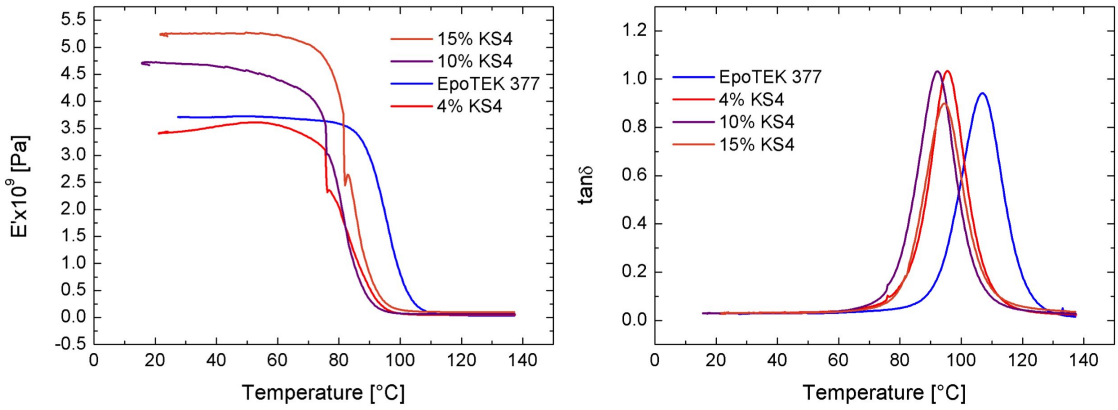

(a) (b)

Figure 4.31: Temperature scan of the storage modulus (a) and tan δ (b) for EpoTEK 377-KS4 composites

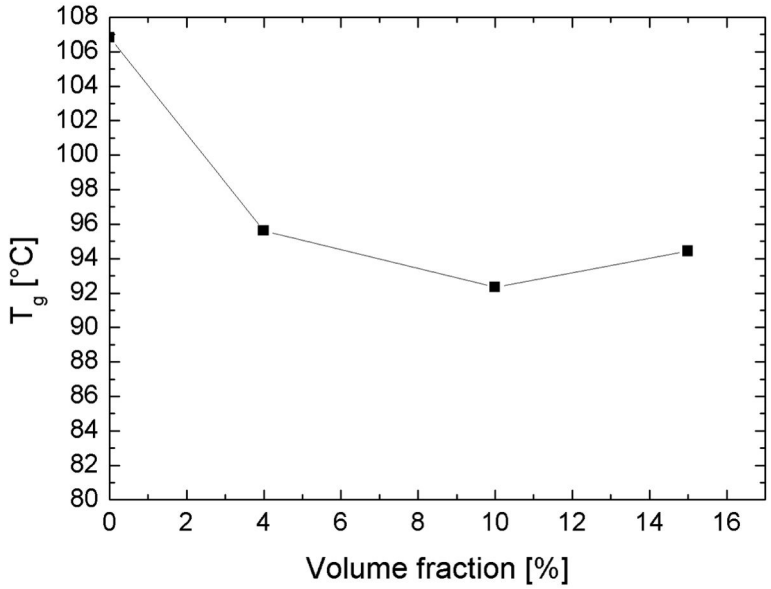

Figure 4.32: Evolution of the T_g with the volume fraction of KS4 in EpoTEK 377

curves show that the material becomes stiffer with an increase of the volume fraction, however we can notice that the 12% and 15% vol. samples behave strangely: their modulus becomes first higher, then it decreases to reach the rubbery plateau. We can see that the more loaded the samples, the more the curves are shifted to higher temperatures: is therefore not possible to see the rubbery plateau for the highest concentrations. Finally, if we look at the value calculated for T_g from the *tan* δ curves (Fig. 4.34), we can see that unlike the other epoxy, this one shows increasing values with increasing volume fraction. We find therefore the same results as with the DSC (Fig. 3.21). This particular effect explains what we obtained for the storage modulus. Indeed, we have exposed that the length of the rubbery plateau depends on the molecular weight between entanglements or cross-links (see Part 4.2.1). Therefore, an increasing T_g value and increasing storage modulus above T_g indicate an increase in the density of cross-links, which also agrees with the high elastic modulus [92].

Effect of the particle size and shape Particle size and shape were then investigated in the EpoTEK 377 matrix with KS15 and BNB90. The results are respectively reported in Fig. 4.35. In both case, we obtain the same results as with KS4: increase of the storage modulus with increasing volume fraction and shifting of the curve to the lower temperatures. The evolution of T_g is also the same, i.e. decreasing of the value with the addition of fillers (see Fig. 4.36).

We propose to compare the fillers in more detail. The storage modulus at room temperature was collected for each volume fraction and filler and reported in function of the volume fraction. Fig. 4.37 shows the corresponding

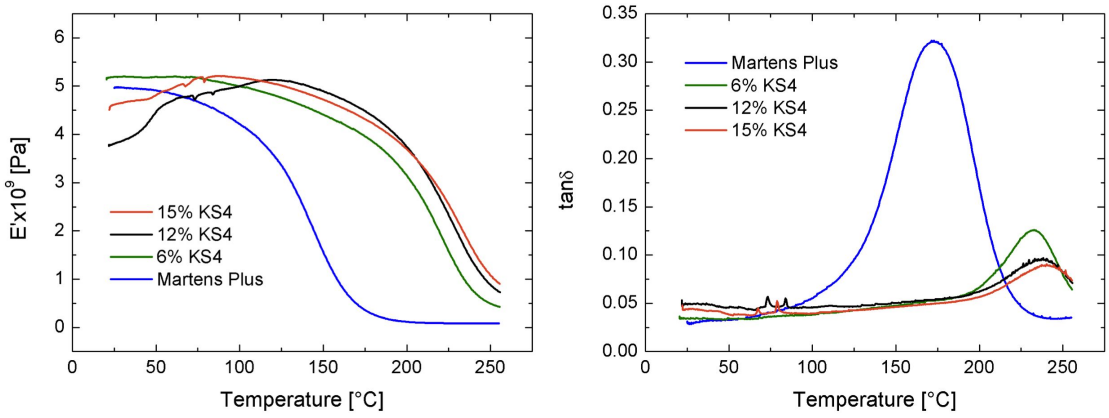

(a) (b)

Figure 4.33: Temperature scan of the storage modulus (a) and tan δ (b) for Martens Plus-KS4 composites

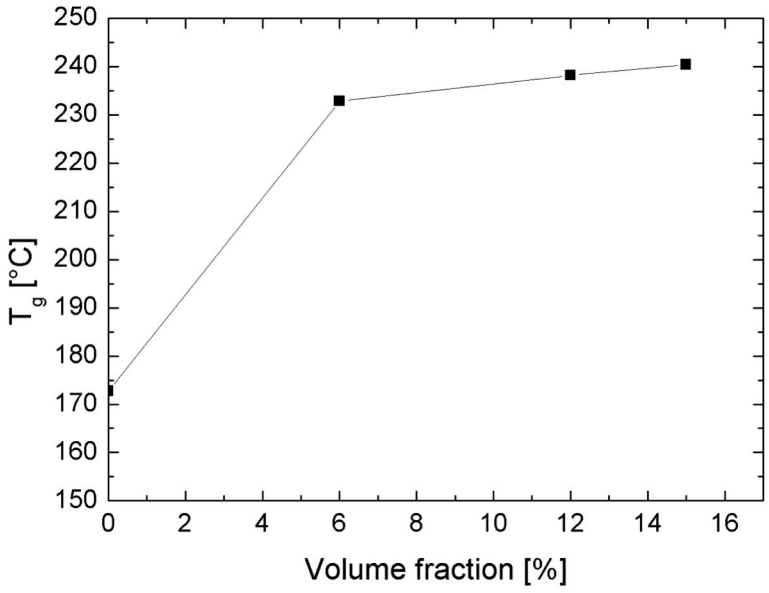

Figure 4.34: Evolution of the T_g with the volume fraction of KS4 in Martens Plus

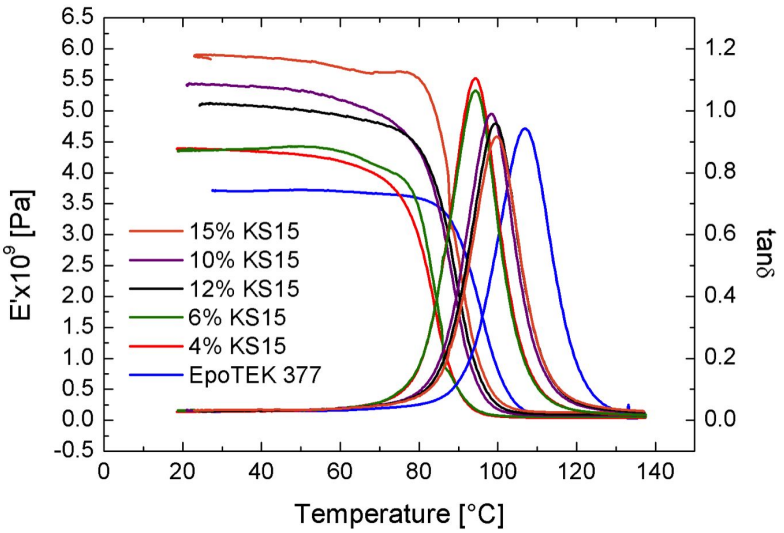

(a)

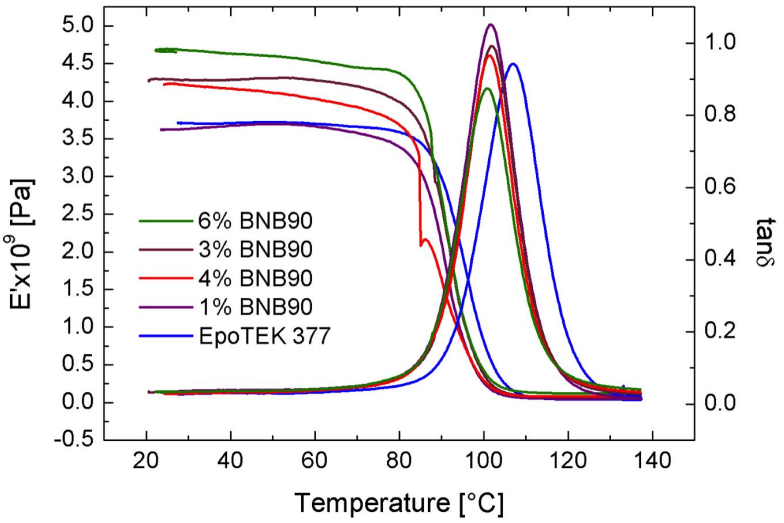

(b)

Figure 4.35: Temperature scan of the storage modulus and tan δ for EpoTEK 377-KS15 (a) and EpoTEK 377-BNB90 (b) composites

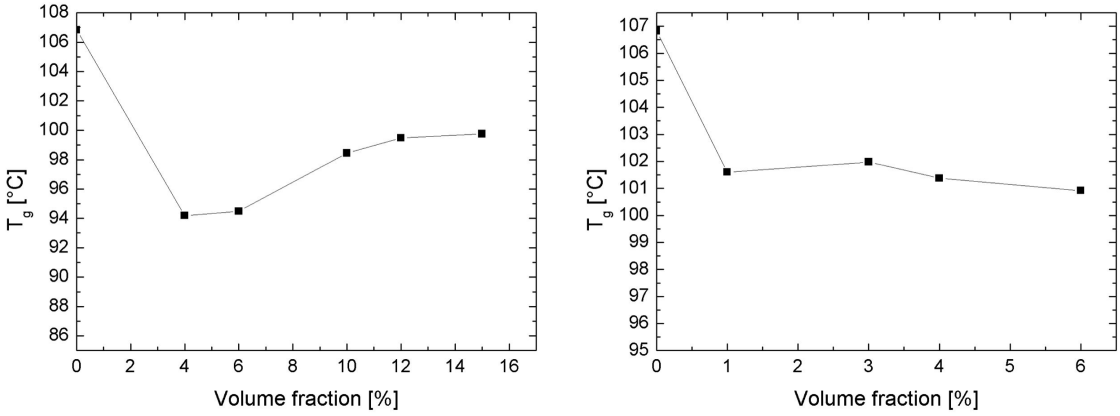

(a) (b)

Figure 4.36: Evolution of the T_g with the volume fraction of KS15 (a) and BNB90 (b) in EpoTEK 377

results. By comparing KS4 and KS15, we can see that the larger particles give stiffer material. Indeed the volume "strictly" occupied by the graphite particles is slightly higher with larger particles. As the epoxy is more compliant than the graphite, the more the epoxy in the composite, the more ductile the material, hence a lower storage modulus. This result is in agreement of what can be found in the literature [175]. As far as the shape effect is concerned, it seems that the flake composites tend to have a higher storage modulus. Indeed like in fiber-reinforced composites, the strain distribution is all along the flakes, hence a stiffer material [176].

Effect of oxidation Finally samples containing oxidized graphite were run into the DMA and analyzed. Fig. 4.38 presents the storage modulus of 4%, 10% and 15% with a 2-hour oxidation and without any. If we look at the results that were obtained for the storage modulus, we can see that the oxidation tends to give stiffer materials (increase of the value of the storage modulus). This shows that the active groups at the surface of the graphite (-OH, =CO, -COOH) have formed bonds with the matrix. The better adhesion matrix-particles results in a stiffer composite. This increase is about 30% for composites at 4% and 10% volume fraction and 45% for the composite at 15% vol., which is significant. As far as the effect on T_g is considered, it is low: Fig. 4.39 presents the curves for *tan* δ and the corresponding evolution of the T_g. The better adhesion matrix-particles may also result in a better dispersion of the particles inside the epoxy matrix. Indeed, due to their poor chemical affinity with epoxy, graphite particles usually tend to agglomerate [177]. The creation of bonds between the matrix and the filler will inhibit this effect.

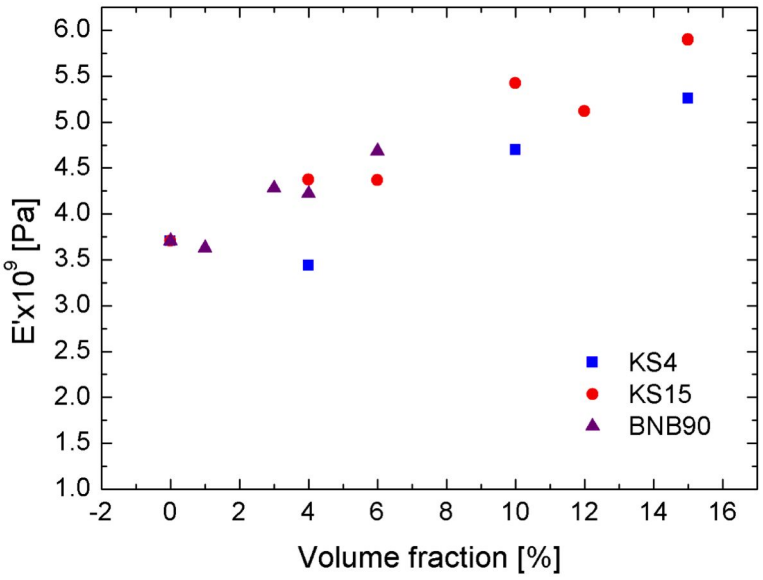

Figure 4.37: Comparison of the storage modulus at room temperature for KS4, KS15 and BNB90 composites in EpoTEK 377 matrix

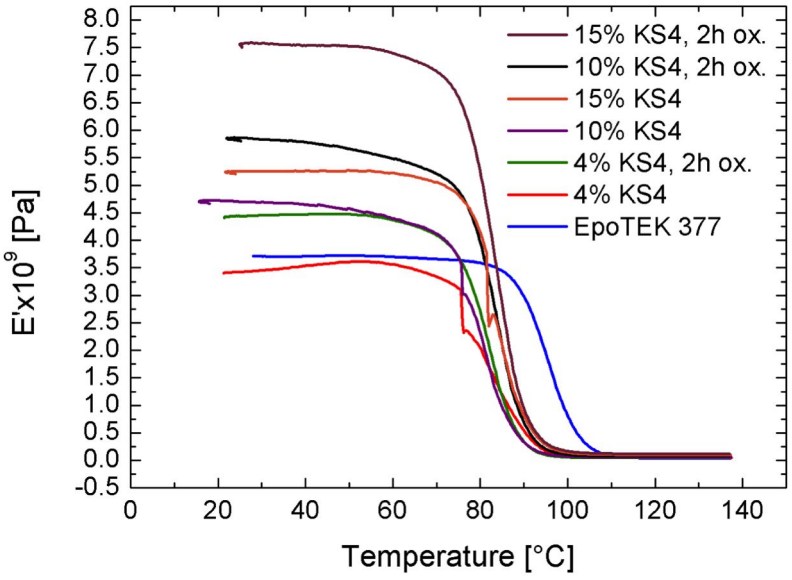

Figure 4.38: Temperature scan of the storage modulus for EpoTEK 377-KS4 composites: influence of the oxidation of graphite

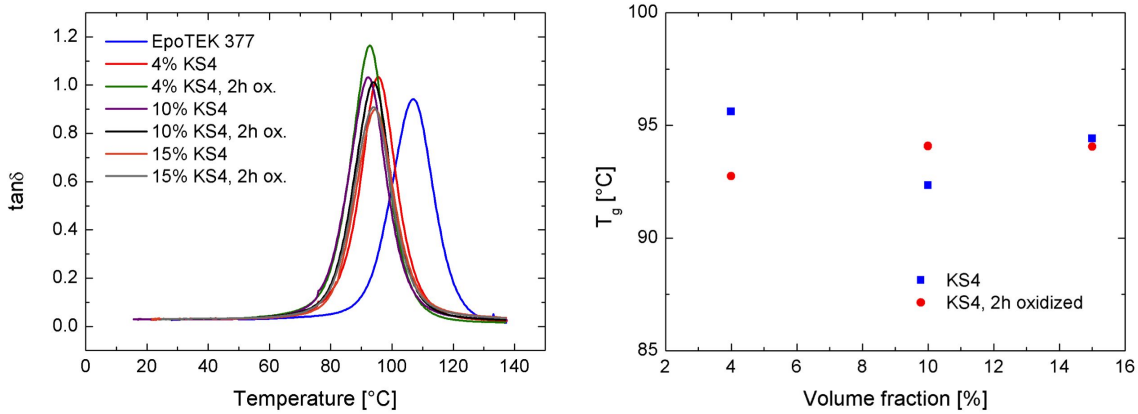

(a) (b)

Figure 4.39: Temperature scan of the tanδ (a) and corresponding evolution of T_g (b) for EpoTEK 377-KS4 composites: influence of the oxidation of graphite

4.3 Thermo-mechanical properties

Now that we have investigated the electrical and mechanical properties of our composites, we propose to study the thermo-mechanical properties. Indeed we have already demonstrated that the polymer dilates and that it even expanses drastically above the T_g range, affecting the electrical properties and their stability with temperature. After explaining how the measurements are performed with an optical dilatometer and how the samples are manufactured, we will study the thermal expansion of the composites in order to try to answer open questions.

4.3.1 Principle of an optical dilatometer and sample fabrication

An optical dilatometer is a non-contact analysis device. A sample is placed on an alumina substrate and put in temperature. A laser illuminates the sample: light is partly reflected by the sample and interfere with the incoming light, creating interference fringes. When the sample dilates (resp. contracts), the interferences move proportionally, which can be measured by the video cameras and shows how the material behaves with temperature. An optical dilatometer Misura ODLT 1200-30, from Expert System Solutions was used for the experiments and will allow us the study of the variations in thermal expansion, hence the determination of the coefficient of thermal expansion (CTE). T_g can also be determined with an optical dilatometer. Fig. 4.40 shows how the device looks like and how the sample is set inside the oven.

Samples were prepared in the same way as the DMA samples, except that they were not cut. Small bars of 50x10x5 (mm) were obtained at the end of the

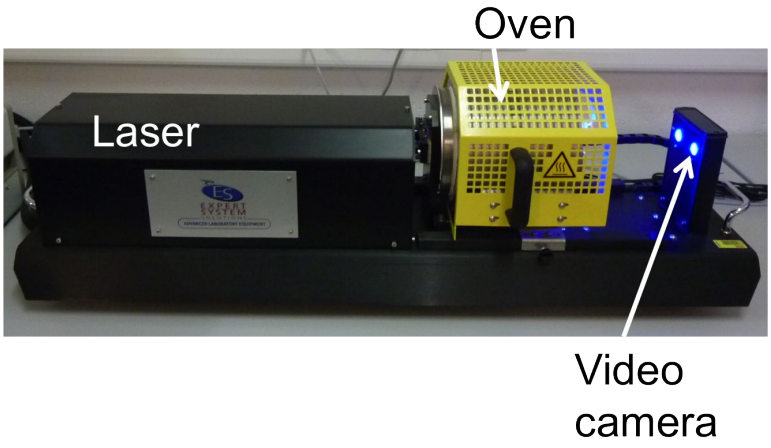

(a)

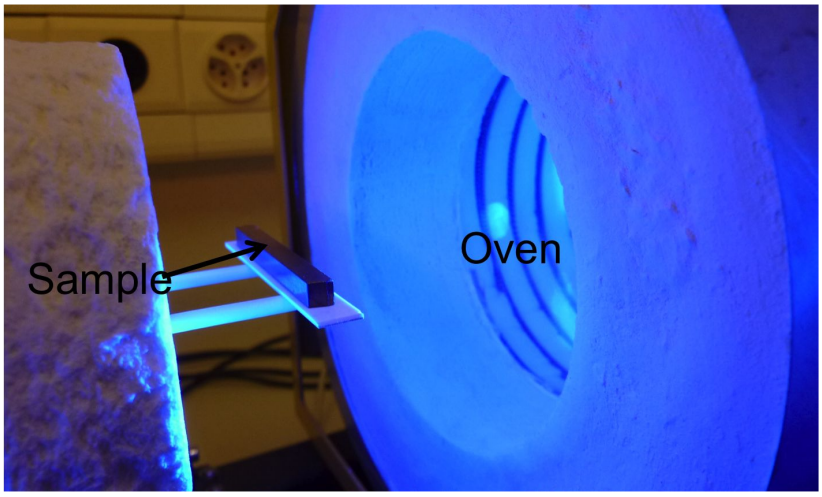

(b)

Figure 4.40: Optical dilatometer: device (a) and position of a sample (b)

process and each end was polished with sandpaper in order to have clear edges, important parameter as the acquisition is done with video cameras. Table 4.5 summarizes the formulations that were studied. Pure epoxies samples of both EpoTEK 377 and Martens Plus were also fabricated and analyzed. For each sample, two cycles were performed. Depending on the matrix, the temperature profile will be different because the transitions will not happen at the same temperatures:

- EpoTEK 377, first cycle: from 30°C to 140°C at 10°C/min; second cycle: from 30°C to 140°C at 2°C/min
- Martens Plus, first cycle: from 30°C to 280°C at 15°C/min; second cycle: from 30°C to 280°C at 5°C/min

Table 4.5: Samples manufactured and studied for the variations in thermal expansion with EpoTEK 377 (a) and Martens Plus (b) matrix

Volume fraction [%]	Filler type
1	BNB90
3	BNB90
4	KS4/KS15/ BNB90
6	KS4/KS15/ BNB90
10	KS4/KS15
12	KS4/KS15
15	KS4/KS15

(a)

Volume fraction [%]	Filler type
4	KS4
6	KS4
10	KS4
12	KS4
15	KS4

(b)

4.3.2 Study of the thermal expansion of epoxy-graphite composites

4.3.2.1 Expansion of pure epoxy

Let us first start with the basics: the thermal expansion of the matrix of our composites, namely epoxy. A first run was performed on a pure EpoTEK 377 sample at 10°C/min. This particular value was chosen in order to better see transitions, the purpose of the second run being to analyze more into detail. Fig. 4.41a reports the thermal expansion of EpoTEK 377. A shrinkage in the thermal expansion can be observed at 90-105°C. This effect has been previously reported by Tognana et al. [178], who have attributed it to the relaxation of the residual stress-strain of the polymer around the T_g. Indeed, the samples were cured in a closed mould, which induces stresses. When the dilatometry

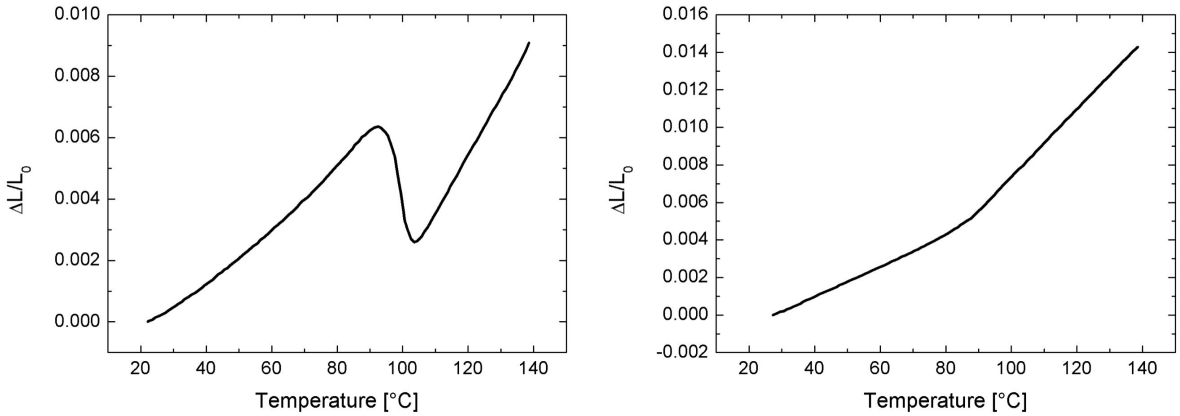

(a) (b)

Figure 4.41: Thermal expansion of EpoTEK 377 run 1 (a) and run 2 (b)

is first performed, these stresses relaxe in the rubbery state (i.e. around T_g). Coefficients of thermal expansion correspond to the slope of the curve $\Delta L/L$ vs. T and were determined before and after the glass transition temperature range. They were found to be respectively 96.3 x 10^{-6}/°C (30°C to 90°C) and 189.7 x 10^{-6}/°C (105°C to 140°C). The CTE increases drastically after T_g as the material becomes plastic. The second run of the EpoTEK 377 is shown in Fig. 4.41b. No shrinkage of the sample is observed this time, only the slope changes, and therefore the CTE at T_g. This second curve allows us to determine T_g more precisely. It also highlights the fact that the epoxy presents a sort of "cycling effect". Indeed, the shrinkage can only be observed in the first run, whereas all subsequent ones would only show the change of slope. CTE was found to be 83.2 x 10^{-6}/°C below T_g (86°C) and 181.0 x 10^{-6}/°C above. We can notice that these values are slightly smaller than the ones found in the first run.

The thermal expansion of pure Martens Plus was studied afterwards and results are reported in Fig. 4.42. First of all, no shrinkage is observed in this case. Both runs are basically the same and show only change of slope at the glass transition temperature at ca. 170°C. This can be explained by the curing mode in two steps of the Martens Plus, which may reduce the residual stress-strain inside the material, giving at the end a matrix more stable with temperature. CTE before and after T_g gives respectively in the first run 79.0 x 10^{-6}/°C (30°C to 170°C) and 164.0 x 10^{-6}/°C (170°C to 280°C), and in the second run, 80.1 x 10^{-6}/°C (30°C to 134°C) and 157.5 x 10^{-6}/°C (134°C to 280°C).

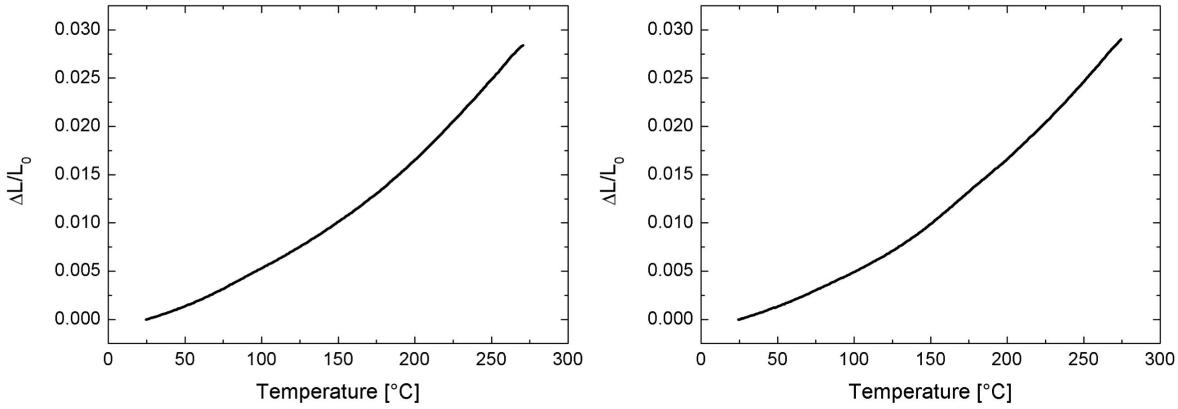

Figure 4.42: Thermal expansion of Martens Plus run 1 (a) and run 2 (b)

4.3.2.2 Thermal expansions of composites: a theoretical review

Before delving into the results we found for our composites, we will have a look at the theoretical behavior in thermal expansion of a composite. Several theories regarding a two-phase material can be found in the literature [178–180] and will be briefly reviewed here.

Hashin-Shtrikman equation This theory considers a material composed of two isotropic phases. The coefficient of thermal expansion of the composite can be expressed as:

$$CTE = CTE_M + \frac{CTE_F - CTE_M}{1/K_F - 1/K_M}\left(\frac{1}{K_C} - \frac{1}{K_M}\right) \tag{4.8}$$

where CTE_M and CTE_F are resp. the coefficient of thermal expansion of the matrix and the filler, K_M, K_F and K_C are resp. the bulk modulus of the matrix, the filler and the composite.

The K_C modulus is calculated by using the Hashin-Shtrikman model which considers the composite as isotropic aggregates, the variation of elasticity allows the determination of a lower and upper bounds: K_C (up) and K_C (low):

$$K_C\,(up) = K_F + \frac{1-\phi}{1/\left(K_M - K_F\right) + 3\phi\left(3K_F + 4G_F\right)} \tag{4.9}$$

$$K_C\,(low) = K_M + \frac{\phi}{1/\left(K_F - K_M\right) + 3\left(1-\phi\right)/\left(3K_M + 4G_M\right)} \tag{4.10}$$

where G_M and G_F are resp. the shear modulus of the matrix and the epoxy and Φ the volume fraction.

Turner equation The Turner theory is a general equation, no matter the filler type. This equation is based on the fact that "each component in the mixture is constrained to change dimensions with temperature changes at the same rate as the aggregate (composite), and that shear deformation is negligible" [179]. The coefficient of thermal expansion is defined as:

$$CTE = \frac{(1-\phi)\, K_M CTE_M + \phi K_F CTE_F}{(1-\phi)\, K_M + \phi K_F} \tag{4.11}$$

Mixture law The mixture law is the simplest equation that only depends on the variation of the volume fraction of the filler. It is expressed as follow:

$$CTE = (1-\phi)\, CTE_M + \phi CTE_F \tag{4.12}$$

Thomas equation The Thomas equation is an empirical equation based on the mixture law. Thomas defines the coefficient of thermal expansion of the composite as:

$$(CTE)^a = (1-\phi)\,.\,(CTE_M)^a + \phi\,(CTE_F)^a \tag{4.13}$$

The exponent a is a constant, whose value is between -1 and 1. For $a = 1$, we recover the mixture law and for $a =$ -1, it is the inverse mixture law. In our case, we will take $a = 0.5$ and $a = 0.1$

Wang and Kwei equation This equation supposes that the filler is a sphere. This is not totally our case, however, this equation will be calculated for comparative purposes. Wang and Kwei theory considers that each particle of filler is surrounded by a shell of polymer. This forms tiny spherical composites, which combine together are the "real" composite. The resulting equation is:

$$CTE = CTE_M - \phi\theta\,(CTE_M - CTE_F) \tag{4.14}$$

where

$$\theta = \frac{\phi\,(3E_F/E_M)}{(E_F/E_M)\,.\,(2\phi\,(1-2\nu_M) + (1+\nu_M)) + 2\,(1-\phi)\,.\,(1-2\nu_F)} \tag{4.15}$$

where E_M and E_F are resp. the Young's modulus of the matrix and the filler and ν_M and ν_F are resp. the Poisson's ratio of the matrix and the filler.

All of these models take different parameters into account and will probably not be applicable to our samples due to the hypothesis (such as isotropic phases for Hashin-Shtrikman model or spherical particles for Wang and Kwei equation). Nevertheless they will be investigated.

4.3.2.3 Expansion of epoxy-graphite composites

Effect of the volume fraction As we have determined the thermal expansion of both matrices, we now propose to study it in the composites. The effect of the volume fraction will be first investigated. Let us take the samples loaded with KS4 in EpoTEK 377. As for the matrix, two runs were also performed on the composites bars (Fig. 4.43). In the first run, a shrinkage was also observed during the first run, indicating relaxation of the residual stress-strain. The shrinkage is however smaller than in the case of pure epoxy as the graphite particles block the dilatation. We can see that the gap decreases with an increase in the volume fraction, the 15% composite showing no real shrinkage (see Table 4.6). The second run shows only the change of slope corresponding to T_g. A cycling effect is therefore observed as well as in the loaded samples. This could be correlated to the stability with temperature that was studied in Part 4.1.2.3. Indeed when a three thermal cycle was performed on thick-film sample, hysteris of the curves was observed (see Fig. 4.8a). However the first cycle differs from the second and third ones as the values before T_g are different depending on the way up or down of the curve, showing that something happens inside the material. This can be explained by the cycling effect and the relaxation of the residual stress-strain of the materials.

Table 4.6: Observed shrinkage in the dilatometric curve vs. volume fraction of KS4

Volume fraction [%]	Shrinkage [%]
0	0.53
4	0.31
6	0.30
10	0.16
12	0.05
15	-0.03

Martens Plus composites were also studied. The two runs performed on the composites can be seen in Fig. 4.44. Both runs are also very similar to each other, showing, like the pure Martens Plus, no shrinkage. This result can also be correlated to the stability with temperature of Part 4.1.2.3.

CTE of these samples were also calculated by fitting the slope before the T_g (run 1) and compared to the theoretical equations described in Part 4.3.2.2. The values needed for the calculation of the different equations are summarizes in Table 4.7[1]. The bulk modulus K and the shear modulus G can be also expressed with the Young's modulus and the Poisson's coefficient as:

[1] K and E were calculated in each case using Eq. 4.16 and 4.17, * means that the values were measured (E by DMA, and CTE by the optical dilatometer)

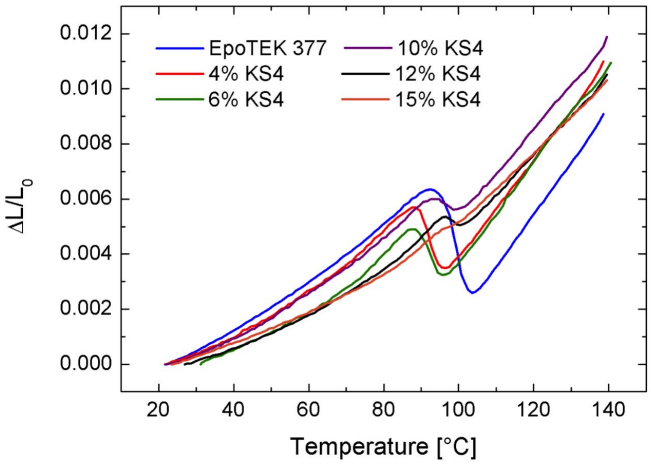

(a)

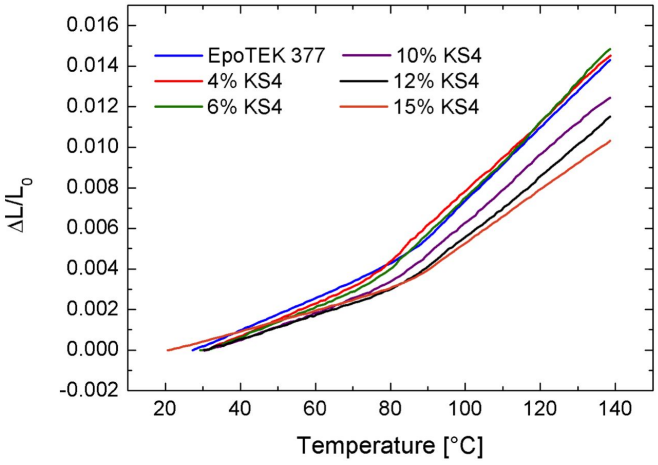

(b)

Figure 4.43: Thermal expansion of EpoTEK 377-KS4 composites: run 1 (a) and run 2 (b)

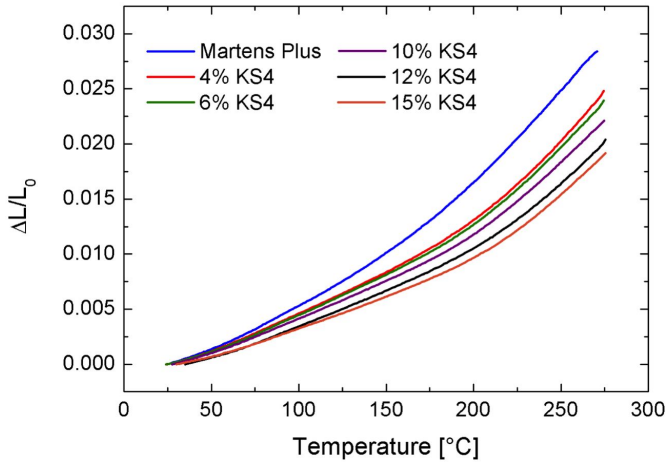

(a)

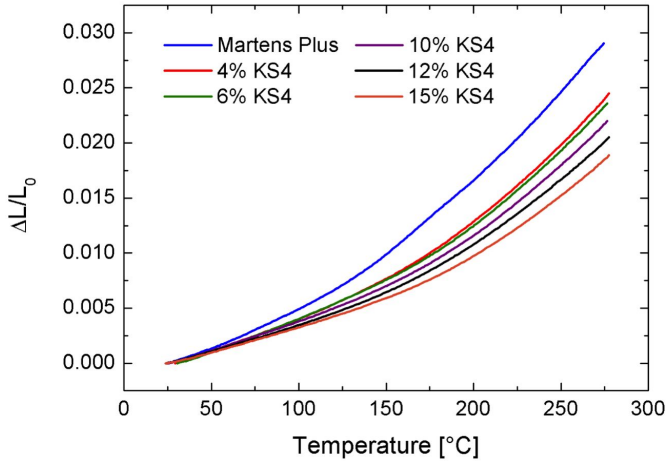

(b)

Figure 4.44: Thermal expansion of Martens Plus-KS4 composites: run 1 (a) and run 2 (b)

$$K = \frac{E}{3\,(1-2\upsilon)} \tag{4.16}$$

$$G = \frac{E}{2\,(1+\upsilon)} \tag{4.17}$$

These equations were used to calculate the missing data. The results are reported in Fig. 4.45 for EpoTEK 377. If we look at these results, we can see that the value obtained for 10% vol. seems incorrect: it should be smaller than the 6% vol. one. There must have been a problem during the measurement. Otherwise, the results quite fit the Thomas equation, which appears to be the best model for our results.

The Martens Plus values can be found in Fig. 4.46. We can see that they fit the Thomas equation (with a = -0.1) as well, showing that it is the valid model for our composites. Indeed Hashin-Shtrikman model assumes that both phases are isotropic, which is not our case, graphite being anisotropic. The Wang and Kwei model was designed for spherical particles, which was once again not exactly the shape of ours. The Turner equation may have been useful, but the weakness is that it doesn't take into account the shape or the size of the particles and only depends of the volume fraction of the filler. It was shown that this equation applies at least to two ceramic systems: Al/SiO_2 and W/MgO [179]. Therefore, the Thomas equation appears to be the best one. Indeed this equation is empirical and based on the mixture law, it must therefore fit for most of the composites, as it can be modulated with the a factor.

Table 4.7: Properties of epoxies and graphite used for simulation of the CTE vs. filler volume fraction

Properties	EpoTEK 377	Martens Plus	Graphite
CTE [x10^{-6}/°C]	96.3*	79.0*	7.8 (overall) [171]
K [GPa]	18.5	24.8	333
G [GPa]	1.3	1.8	111
E [GPa]	3.70*	4.96*	300 [181]
υ	0.4 [182]	0.4 [182]	0.35 [181]

Effect of the particle size and shape Samples using KS15 were also manufactured and measured in order to determine the impact of the particle size. The corresponding results can be found in Fig. 4.47. We can see that we recover the shrinkage we observed on the pure epoxy sample and with the loaded samples. However, the use of a larger particle tends to reduce this shrinkage, hence giving more stable materials (see Table 4.8). The second run

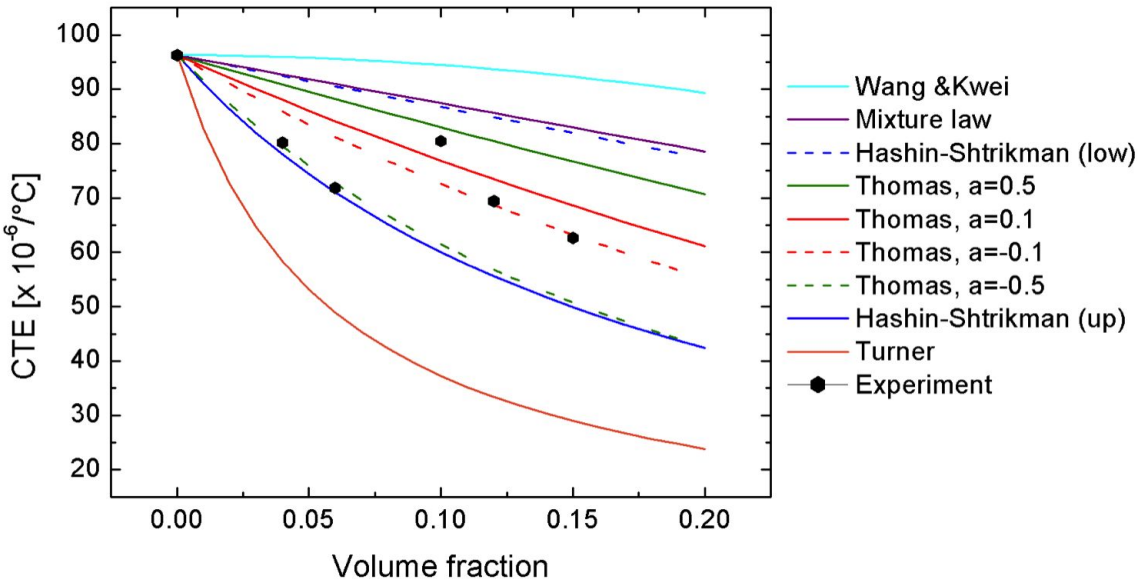

Figure 4.45: CTE (from 30°C to 80°C) of EpoTEK 377- KS4 composites: comparison between theoretical results and experiment

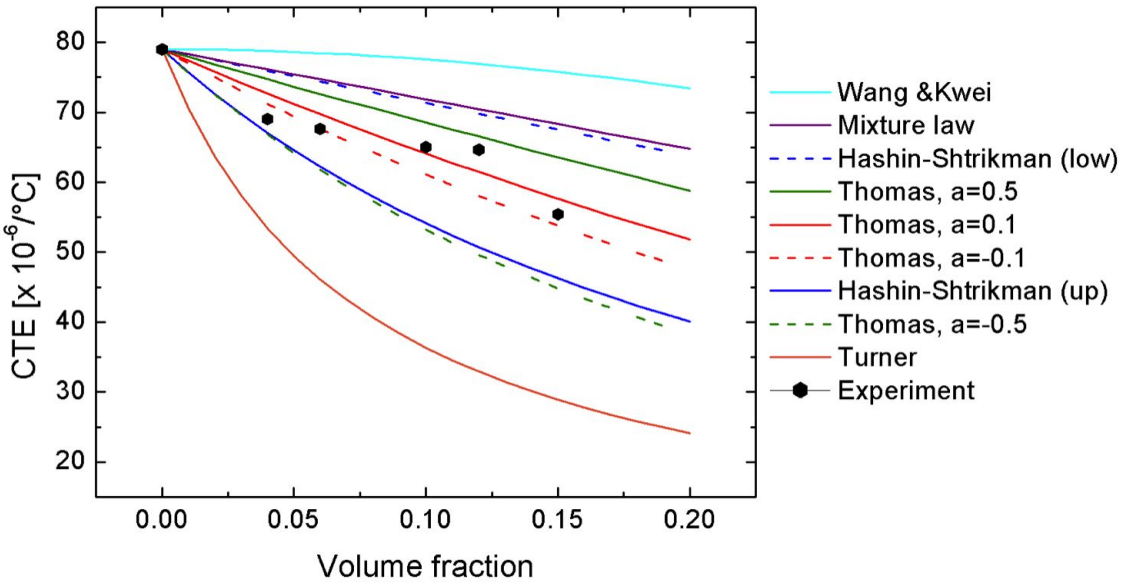

Figure 4.46: CTE (from 30°C to 170°C) of Martens Plus- KS4 composites: comparison between theoretical results and experiment

shows no shrinkage, confirming the "cycling effect" of the composites with EpoTEK 377 matrix.

Table 4.8: Observed shrinkage in the dilatometric curve vs. volume fraction of KS15

Volume fraction [%]	Shrinkage [%]
0	0.53
4	0.35
6	0.37
12	- 0.16
15	- 0.11

The particle shape effect was then investigated: samples using BNB90 were therefore prepared. Fig. 4.48 reports the corresponding results. The first run doesn't show any shrinkage. This probably comes from the particle shape. Due to its worm-like aspect, it more efficiently prevents the matrix from expanding. The second run is similar to the one obtained for KS4 and KS15, however the 1% composite shows somehow slightly higher dilatation than the pure sample.

The coefficients of thermal expansion were determined for these two fillers using the same method than for KS4 composites. Fig. 4.49 shows the obtained results. Since we have determined previously that our composites follow the Thomas equations, only these are reported here. The mixture law appears also in the graph but it is a particular case of Thomas equation (i.e. a = 1). The KS15 values do not really match any of the Thomas equation: up to 6% vol. they follow the mixture law, then the CTE drops drastically and becomes more close to the a=-0.1 equation. It seems that there is a "critical concentration".

The BNB90 composites show surprising values at 3% and 6% volume fraction, the 3% being too small and the 6% one too high. The results cannot reasonably be fitted using the Thomas equations discussed above. This may be explained by the shape of the expanded graphite, whose flakes fill the available volume more than the small ellipsoidal graphite particles. This efficiently restricts the expansion of the matrix, which is also the reason why the CTE values are close.

4.4 Consistency between different characterization methods and composite properties

In order to see whether there is consistency between our results, we propose, in this Section, to compare the T_g values obtained from various methods (dilatometry, DMA and DSC) on the one hand, and to assess the compatibility of our measurements of the TCR with those of the gauge factors. To perform the latter comparison, we will establish a theoretical link between the piezore-

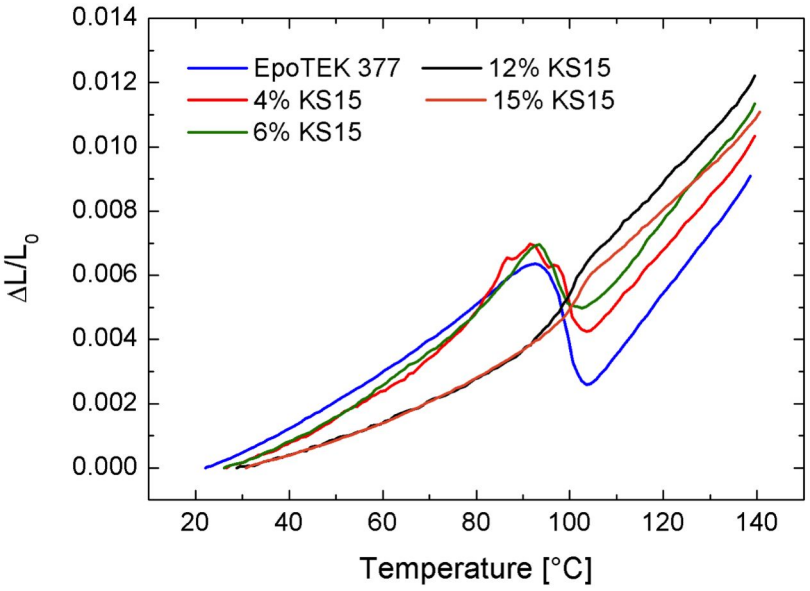

(a)

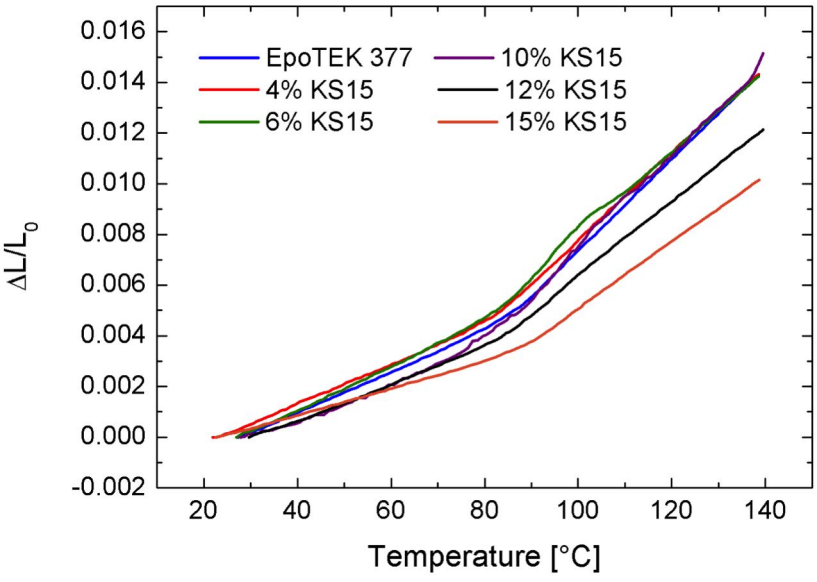

(b)

Figure 4.47: Thermal expansion of EpoTEK 377-KS15 composites: run 1 (a) and run 2 (b)

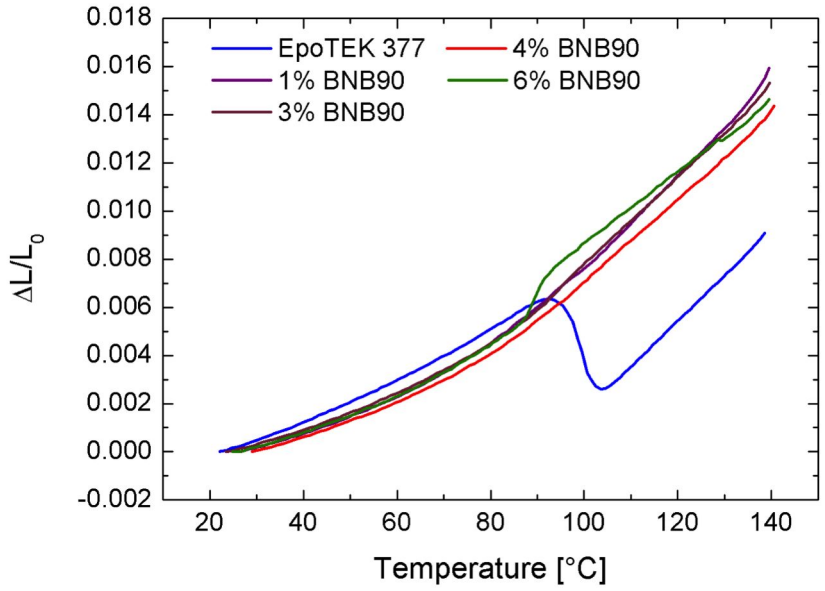

(a)

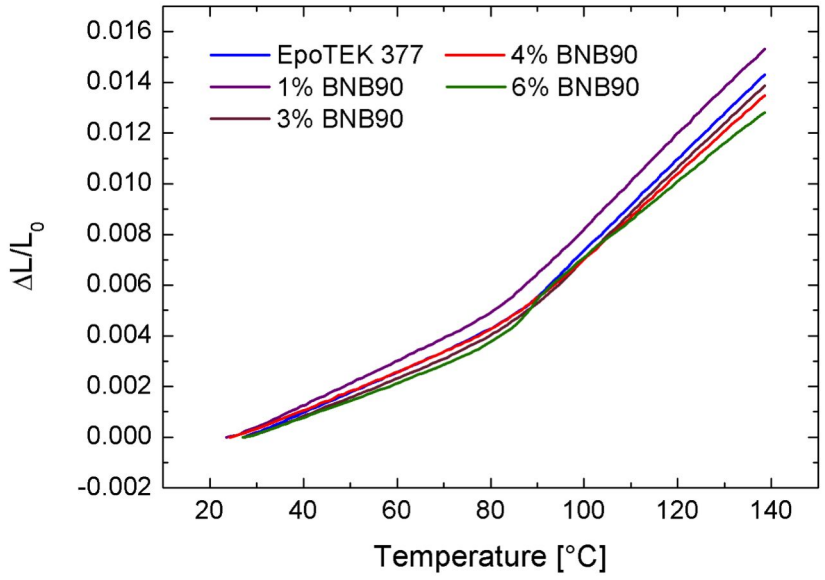

(b)

Figure 4.48: Thermal expansion of EpoTEK 377-BNB90 composites: run 1 (a) and run 2 (b)

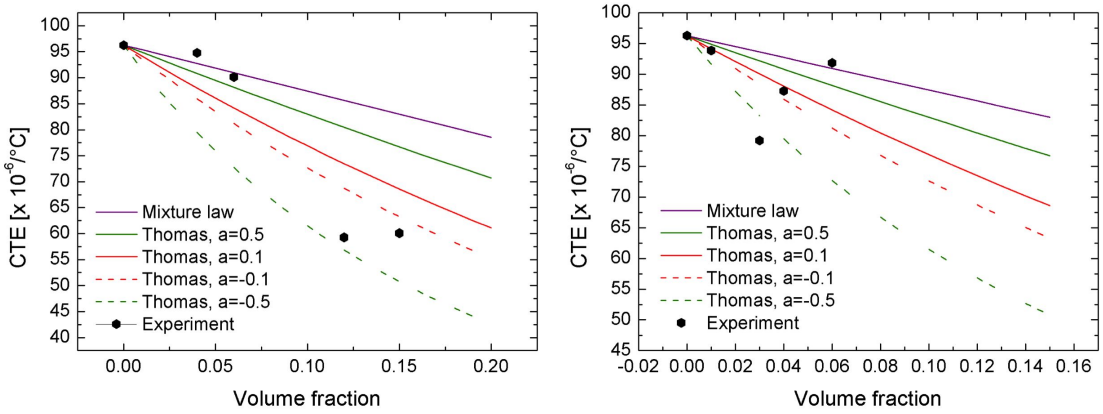

Figure 4.49: CTE (from 30°C to 80°C) of EpoTEK 377- KS15 (a) and EpoTEK 377-BNB90 (b) composites: comparison between theoretical results and experiment

sistivity and the TCR, allowing us to estimate one from the measurement of the other.

4.4.1 Relation between piezoresistivity and TCR

We will now derive an estimate value of the TCR from the piezoresistive response. Let us first consider the expression of the TCR:

$$TCR = \frac{\Delta R}{R \Delta T} \tag{4.18}$$

We know that the resistance can be expressed as:

$$R = \frac{\rho L_x}{L_y L_z}$$

with ρ the resistivity and L_x, L_y and L_z the length of the resistor. As $ln(R) = ln(\rho) + ln(L_x) - ln(L_y) - ln(L_z)$ we obtain:

$$\frac{\Delta R}{R} = \Delta ln(R) = \frac{\Delta \rho}{\rho} + \frac{\Delta L_x}{L_x} - \frac{\Delta L_y}{L_y} - \frac{\Delta L_z}{L_z} = \frac{\Delta \rho}{\rho} + \varepsilon_x - \varepsilon_y - \varepsilon_z - \alpha_R \Delta T \tag{4.19}$$

where $\Delta\rho$ and ΔL are the changes in resistivity and resistor length induced by the change in temperature (hence the additional term $-\alpha_R \Delta T$, with a_R the coefficient of thermal expansion of the resistor) . The change in conductivity is due to the strains and temperature and can be expressed in terms of the piezoresistive factors (see Part 2.2.2), with γ a constant:

$$\frac{\Delta\rho}{\rho} = \Gamma_L \varepsilon_x + \Gamma_T \left(\varepsilon_y + \varepsilon_z\right) + \gamma \Delta T \tag{4.20}$$

Finally, the deformations in the resistor due to thermal expansion conflict with the substrate can be defined in function of the CTE of the composite and substrate. We consider that the deformations are compared with the initial state (not equal to 0). In the z direction, the composite deforms and also undergoes resulting deformations from the x and y ones, whereas its deformation is constrained by the substrate in the two other directions, as in Part. 2.2.2, we can write [183]:

$$\varepsilon_x = \varepsilon_y = (\alpha_S - \alpha_R)\Delta T$$

$$\varepsilon_z = -\frac{2\nu_R}{1-\nu_R}(\alpha_S - \alpha_R)\Delta T$$

where ν_R is the resistor Poisson's ratio and α_S and α_R are respectively the linear CTE of the substrate and the resistor defined, in the absence of strain, as:

$$\alpha = \frac{\Delta L}{L \Delta T}$$

Combining Eq. 4.18, 4.19 and 4.20 and using the expression of the strains given above, we obtain the TCR as a function of the piezoresistive factors:

$$TCR = \left(\Gamma_L + \Gamma_T\right)\left(\alpha_S - \alpha_R\right) - \frac{2\nu_R}{1-\nu_R}\left(\Gamma_T - 1\right)\left(\alpha_S - \alpha_R\right) + \gamma - \alpha_R \tag{4.21}$$

We can notice that the term formed by $\gamma - \alpha_R$ is the intrinsic TCR of the strain-free resistor material. This equation can be easily transformed as follows:

$$TCR = \left(\alpha_S - \alpha_R\right)\left[\left(\Gamma_L + 1\right) + \left(\Gamma_T - 1\right)\frac{1-3\nu_R}{1-\nu_R}\right] + \gamma - \alpha_R \tag{4.22}$$

From Part 2.2.2, we have the following equations of the gauge factors as a function of the piezoresistive factors:

$$GF_L = \left(1 + \Gamma_L\right) + \left(1 - \Gamma_T\right)\left(\nu + \nu'\right) \tag{4.23}$$

$$GF_T = -\left(1 + \Gamma_L\right)\nu - \left(1 - \Gamma_T\right)\left(1 - \nu'\right) \tag{4.24}$$

where ν and ν' are respectively the Poisson's ratios of the substrate and of the "effective"resistor.

By adding Eq. 4.23 and 4.24 and using the formula of the "effective" Poisson's ratio of the resistor (see Part. 2.2.2), we obtain:

$$\frac{GF_L + GF_T}{1-\nu} = (1+\Gamma_L) + (\Gamma_T - 1)\frac{1-3\nu_R}{1-\nu_R} \tag{4.25}$$

By combining Eq. 4.22 and 4.25, we can express the TCR as a function of the gauge factors:

$$TCR = (\alpha_S - \alpha_R)\frac{GF_L + GF_T}{1-\nu} + \gamma - \alpha_R \tag{4.26}$$

Therefore, we can calculate a difference of TCR depending on the substrate. Let us first look at the term formed by $(GF_L + GF_T)/(1-\nu)$. We can see from Eq. 4.25 that, in contrast to the gauge factors, this term is nominally independent of the substrate properties. Therefore, we can consider that if we print the same resistor material on two substrates, designated 1 and 2 with their corresponding Poisson's ratio and resulting gauge factors, we can write, assuming no chemical reactions take place:

$$\frac{GF_L^1 + GF_T^1}{1-\nu_1} \simeq \frac{GF_L^2 + GF_T^2}{1-\nu_2} \tag{4.27}$$

By using Eq. 4.27, the difference in TCR between the values calculated on substrate 2 and on substrate 1, becomes therefore,

$$\Delta TCR = (\alpha_{S2} - \alpha_{S1})\frac{GF_L - GF_T}{1-\nu} \tag{4.28}$$

where α_{S1} and α_{S2} are the CTE of resp. substrate 1 and 2. GFL and GFT can be taken on substrate 1 (resp. substrate 2) with the Poisson's ratio of substrate 1 (resp. substrate 2).

This expression can now be used to estimate the difference between the TCR values on aluminum and alumina, from our measurements of the gauge factors, using the available values for the CTE of the substrate and the Poisson coefficients of the substrates. We will then compare them to the difference in the values of TCR we found experimentally between both substrates. Table 4.9 summarizes the values taken for calculation. We choose to take the values of gauge factors on alumina substrate, as we have more data.

Fig. 4.50 presents the comparison between the difference in TCRs on aluminum and alumina calculated from our resistors and the estimated one from the obtained GF on alumina. Firstly, we can see that the estimations at high filler volume fractions are quite realistic, especially with the KS4 (in EpoTEK 377, Fig. 4.50a and Martens Plus, Fig. 4.50c). At low volume fillers, matrix stresses are higher (dilatation vs. adhesion to the substrate), leading to higher TCR values (with higher errors as well). The estimation is therefore more difficult. We can notice the behavior of the Martens Plus, which presents a good estimation all over the range of volume fraction. Indeed, as the matrix

is more stable mechanically and in temperature, calculated values of TCR and gauge factors are more accurate. Differences can also come from the diffusion of the resistor resin monomers inside the dielectric (see discussion on the topic in Part. 4.1.2.4), which changes the value on aluminum substrate. Nevertheless, we can conclude to good qualitative agreement between our estimates and the measurements, i.e. the use of a substrate with a high thermal expansion causes a significant corresponding shift in TCR. Besides possible chemical reaction with the dielectric on aluminum, another possible contribution to the TCR shift lies in the temperature dependence of the gauge factor, coupled with the built-in strain the resistor film stemming from the fabrication process [184], a term that was discounted in our mathematical mode.

Table 4.9: Poisson's ratios and CTE of the substrates

Name	Value
$\nu_{alumina}$	0.23
$\nu_{aluminum}$	0.34
$CTE_{alumina}$	6.9 x 10^{-6}/°C
$CTE_{aluminum}$	25.8 x 10^{-6}/°C

4.4.2 Comparison of T_g values between dilatometry, DMA and DSC

In the previous parts, we have determined the glass transition temperature T_g using dilatometry, DMA and DSC. Let us compare them. Fig. 4.51 presents the results for KS4, KS15 and BNB90 in EpoTEK 377 composites and KS4 in Martens Plus composites. We can see that no matter the method, the tendencies are the same. We can see that DMA gives the highest values in all four systems, whereas the lowest T_g values were obtained with dilatometry. A comparison between T_g values from DSC and DMA measurements has already been done by O'Neal et al. [167] and the same tendency was found. These differences are quite normal due to the fact that T_g is not obtained nor calculated in the same manner.

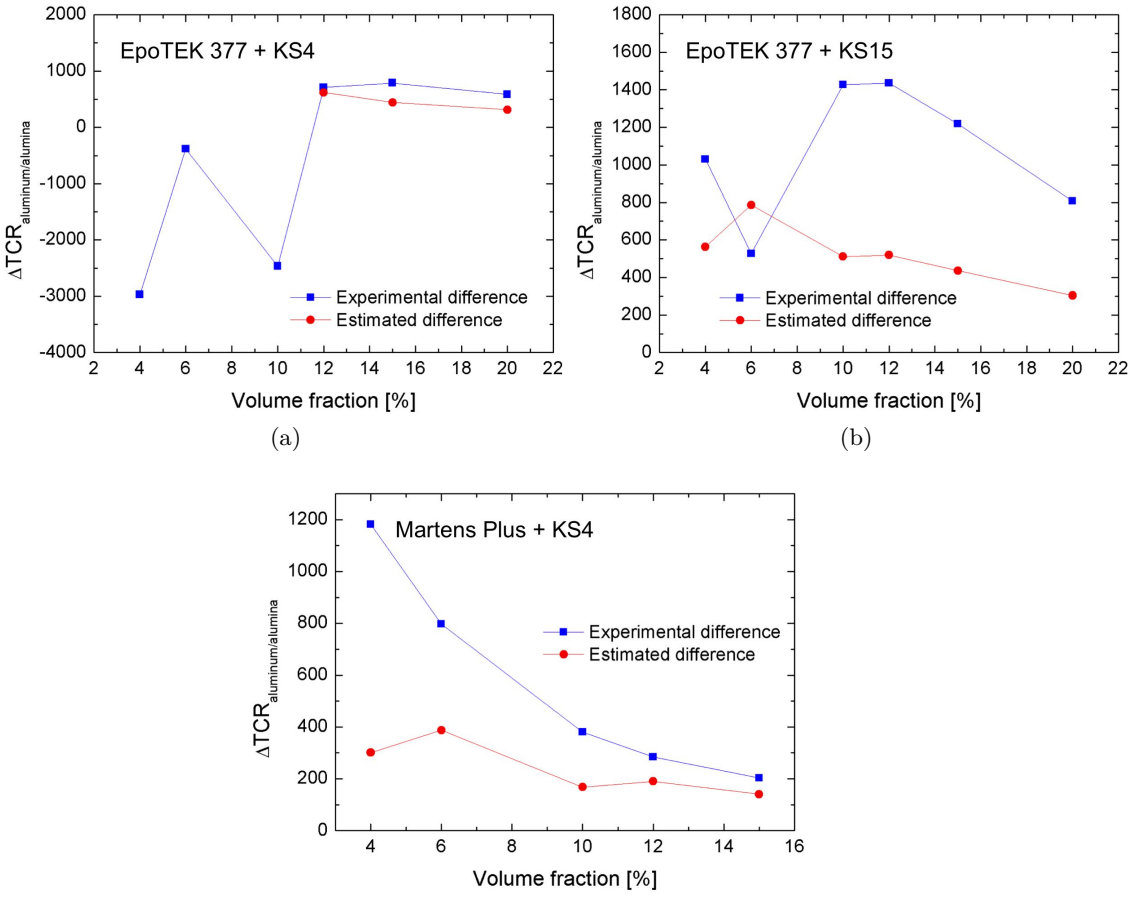

Figure 4.50: Estimated TCR of KS4 (a), KS15 (b) composites in EpoTEK 377 matrix and of KS4 (c) composites in Martens Plus matrix on alumina substrate

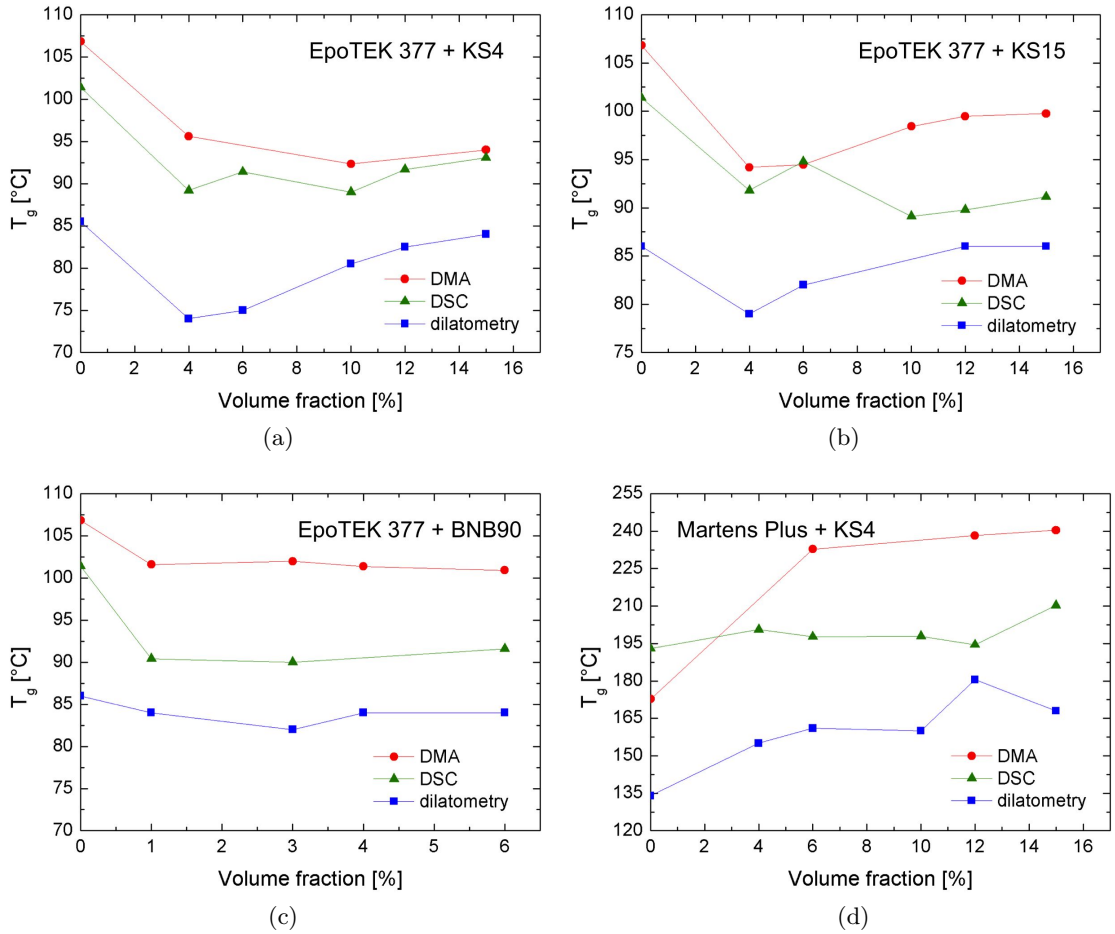

Figure 4.51: Comparison of T_g values obtained from dilatometry, DMA and DSC for KS4 (a), KS15 (b), BNB90 (c) in EpoTEK 377 matrix composites and KS4 in Martens Plus matrix composites (d)

4.5 Summary

This chapter was dedicated to the functional characterization of the epoxy-graphite composites. Both epoxies were tested with various fillers in different volume fractions. Electrical resistivity was first determined. It was found that the specific surface has a tremendous effect upon resistivity, contrary to the particle size, which was shown to have little noticeable effect. Stability with temperature through thermal cycles highlighted the importance of T_g when designing a composite, this value influencing highly the behavior of the composite resistivity with temperature. Samples were also prepared on different substrates (i.e. alumina, aluminum and phenolic resin). The values were found to be higher than on alumina (reference substrate), due to dilatation effect (increase of the volume for the same number of conductive particles). The comparison of our experimental results to percolation theory showed that the conductivity inside our composites is ruled by the "debris model". On a second step, piezoresistivity was investigated. In our experiments, we found that the largest particles lead to a smaller gauge factor. This has to be linked to the aspect ratio of the particles (higher in the case of the KS15 particles). Like in the case of resistivity, temperature effect was investigated, showing the same tendency as in the resistivity measurements. Substrate effect was also investigated: aluminum beams were prepared and gave higher gauge factors than alumina ones.

Mechanical properties were then studied using a Dynamic Mechanical Analyzer. DMA allows in particular the calculation of the storage modulus (which ideally corresponds to the Young's modulus of the material) and of T_g. The storage modulus increases with the volume fraction as the material becomes stiffer. Largest particles tend to give higher modulus. Indeed as the volume occupied by the matrix is smaller, there is more graphite, hence stiffness of the composite. The flake-shaped filler (i.e. expanded graphite) gives also higher modulus value: like fiber-reinforced composites, the strains are distributed all along the flake. Oxidation effect was also investigated. It was proved that composites using oxidized particles present higher storage modulus: bonds were therefore formed between the matrix and the functionalized particles.

In the third Section, the thermo-mechanical properties were determined with an optical dilatometer. The epoxy EpoTEK 377 showed a shrinkage when first run into the dilatometer. This is explained by the relaxation of the residual stress-strain around T_g. This effect is inhibited by increasing the filler volume fraction, the particle size and the use of flake-shaped filler. It also explains the "cycling" effect that was found in the measurement in temperature of resistivity. The shrinkage was not found for the Martens Plus matrix, which may be explained by the curing mode of the epoxy and the type of hardener. Coefficients of thermal expansion were calculated. Results were found to follow the equation of Thomas.

Finally, the results were compared: TCR was estimated using the measured

piezoresistive response, and values of T_g obtained by dilatometry, DMA and DSC were compared. In both cases, good coherence between the experimental results was observed, in general demonstrating the validity of our characterization. However, the effect of substrate thermal expansion on TCR still requires further work to achieve better quantitative agreement. Having completed the extensive characterization of the composites, we will detail in the next chapter, in preparation for applications such as microfluidics, the concept of sacrificial layers and their compatibility with our composites.

Chapter 5

Formulation of organic and sublimable sacrificial layers

The previous chapters dealt exclusively with epoxy-graphite composites. A review of both constituents was first exposed in Chapter 2, then we investigated the formulation of screen-printable pastes based on these components. Following this, the electrical (resistive and piezoresistive), mechanical and thermo-mechanical properties of the resulting composites were investigated, yielding more detailed knowledge of their behavior. Thick-film resistors were mainly fabricated on ceramic substrates, so as to obtain well-defined conditions, i.e. no interdiffusion. In order to explore other possibilities, we propose to investigate the potential manufacturing of 3D microstructures, such as fluidic microchannels or cantilevers, using sacrificial layers as a convenient and straightforward route. In this chapter, we will first explain what a sacrificial layer is, then we will detail the formulation of adequate sacrificial materials. Finally, their compatibility with our composites as well as their elimination will be characterized.

5.1 What is a sacrificial layer?

Before going more into chemical formulation, let us first explain what a sacrificial layer is. As the name suggests, this layer is not permanent and is eventually eliminated near the end of the manufacturing process, through various methods that will be described later. The point of having a sacrificial layer is either to help in the fabrication of an empty space below another layer or to protect the layer underneath, during the manufacturing process. This is particularly useful for suspended structures such as bridges or cantilevers.

So, how does it work? For instance, in the case of manufacturing a cantilever

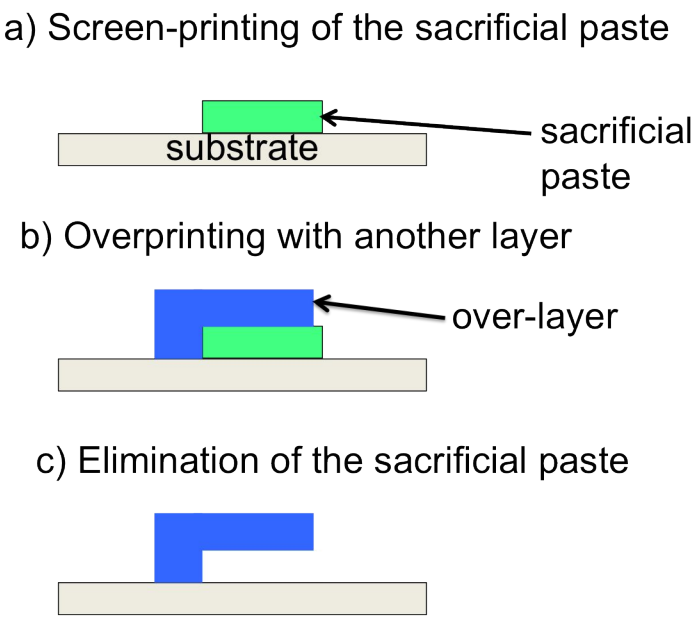

Figure 5.1: Fabrication of a cantilever using a sacrificial layer: concept

through a screen-printing process, a sacrificial layer is first deposited on a substrate and dried. On a second step, it is overprinted with the cantilever structural layer, which is also dried. Finally, the sacrificial layer is eliminated, freeing the cantilever (Fig. 5.1).

5.1.1 Types of paste

Sacrificial layers, like thick-film pastes, can be of two kinds: mineral or organic.

Mineral sacrificial pastes are usually formulated in a similar way than the "permanent" ones [185, 186] and typically contain:

- an inorganic sacrificial material (such as graphite or magnesium oxide/hydrated calcium borate)
- a binder (such as ethyl-cellulose)
- a solvent (such as terpineol, butylene glycol)
- a dispersant or temporary solvent to help initial mixing (such as acetyl acetone, this component not being mandatory)

A mineral sacrificial paste can be produced as follows. The binder is first dissolved in the solvent by applying temperature and agitation. The sacrificial material, with optionally some dispersant, is then added to the mixture. Finally, the paste is mixed together three times with a three-roll mill. After deposition, it is first dried in order to evaporate the solvent, following application of

the over-layer by screen-printing of paste or lamination of tapes. Various processes then allow the elimination of the sacrificial layer and will be detailed in Part 5.1.2. Further information about mineral pastes can be found in the doctoral theses of Birol and Fournier [139, 187].

In the case of an organic sacrificial paste, the sacrificial material is also preferentially organic, otherwise the process is the same. This is the type we are interested in here; the formulation of such organic sacrificial pastes will be discussed in detail in Section 5.2.

5.1.2 Elimination processes

Depending on the paste, different elimination processes can be envisaged, the main thing to care about being to not damage the final structure.

Layers can be removed through a chemical process: *etching*. Etching consists in dissolving the sacrificial layer with an appropriate chemical component (such as an acid). The choice of the chemical component is of high importance, as it must remove the sacrificial layer, yet not interact with other materials in order to avoid damaging the final structure, i.e. the process must have a high selectivity. For instance, for manufacturing membranes with Low-Temperature Cofired Ceramic (LTCC), the sacrificial material can be based on alkaline earth oxides or carbonates. The sacrificial layer undergoes the firing process of the ceramic, providing a temporary support to the structure and being afterwards removed by chemicals such as a weak acid [186]. The main issues of this process are access to internal structures by etchants and potential incompatibilities with the LTCC shrinkage by sintering during firing.

These membranes can also be manufactured with sacrificial layers based on graphite. In this case, the sacrificial layer has to undergo the firing process without sagging, and is removed afterwards by oxidation of graphite. One of the issues of these sacrificial layers is the sagging (i.e., graphite must not oxidize prematurely during the sintering process of LTCC) [185, 188, 189]. This leads us therefore to another possibility to remove the sacrificial layer*: heating*. The sacrificial material therefore evaporates/sublimates/decomposes. In this case, the over-layer should have sufficient high-temperature stability in order to prevent any destruction of the final structure. This process has the advantage to allow the fabrication of closed structures, such as microchannels or cavities. The sacrificial material decomposition products can escape by diffusion through the resulting structure. Microstructures based on organic sacrificial layers, such as the combination of polypropylene carbonate (sacrificial material) and SU-8, a common epoxy-based negative photoresist (over-layer) have already been reported in the literature [190].

5.2 Formulation of low-temperature sublimable organic sacrificial layers

Nowadays, a move towards polymers is observed as their properties such as low cost, transparency and good biocompatibility make them particularly suitable for disposable biomedical applications. Metz et al. have already reported the use of polypropylene carbonate as sacrificial material [190]. However, the polypropylene carbonate decomposes up to ca. 300°C, which remains too high for most polymer applications. Therefore, we propose to introduce materials with significantly lower sacrificial layer removal temperatures, thereby considerably extending the application field of this process. Moreover, the materials employed are also chosen for their sublimation ability. This particular property has the advantage to allow closed structures such as microchannels, cavities and membranes as the compounds sublimate cleanly through the overlayer, without collapse due to surface tension, and do not require any etching process. Polyols were chosen to formulate the sacrificial pastes [191,192]. Their properties will be described in the following parts.

5.2.1 Choice of the materials

The purpose is to formulate sublimable organic sacrificial pastes with moderate sublimation temperatures. It was chosen to use mixes of non-polymeric polyol-type organic materials, so-called plastic crystals. Polyols are widely used in industry for paints and coatings formulation, due to the viscosity and fast drying properties they give to the final paste. Some polyols have also attracted considerable attention due to their solid–solid order–disorder phase transitions, which make them interesting for thermal energy storage [193]. For our process, these materials are advantageous, as they have low toxicity and are biodegradable.

Four polyols were investigated for the formulation of sacrificial layers: trimethylolethane (TME), trimethylolpropane (TMP), neopentyl glycol (NPG) and 2,5-dimethyl-2,5-hexanediol (DMHD). Fig. 5.2 shows their chemical formula whereas Table 5.1 gives the relevant properties of these compounds as well as the properties of the solvents that were used for formulation. TME, NPG, TMP and DMHD are all solid at room temperature and sublimate / evaporate well below 200°C (Fig. 5.3, data from [156,194]), based on their vapor pressure. One will notice the almost perfect overlap between cyclohexanol and hexanol, and TME and TMP. Sublimation is preferable to evaporation, as it obviates surface tension effects. Therefore, NPG and TME, which have appreciable vapor pressures (ca. 5 kPa) at their melting point, are particularly attractive.

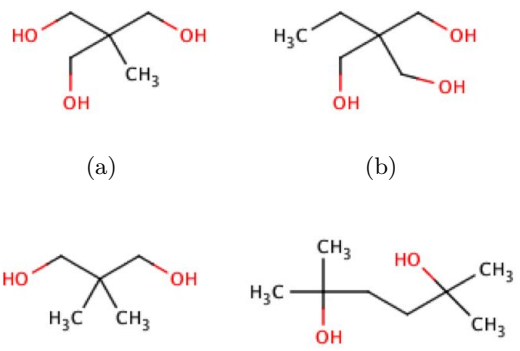

Figure 5.2: Chemical formula of TME (a), TMP (b), NPG (c) and DMHD (d)

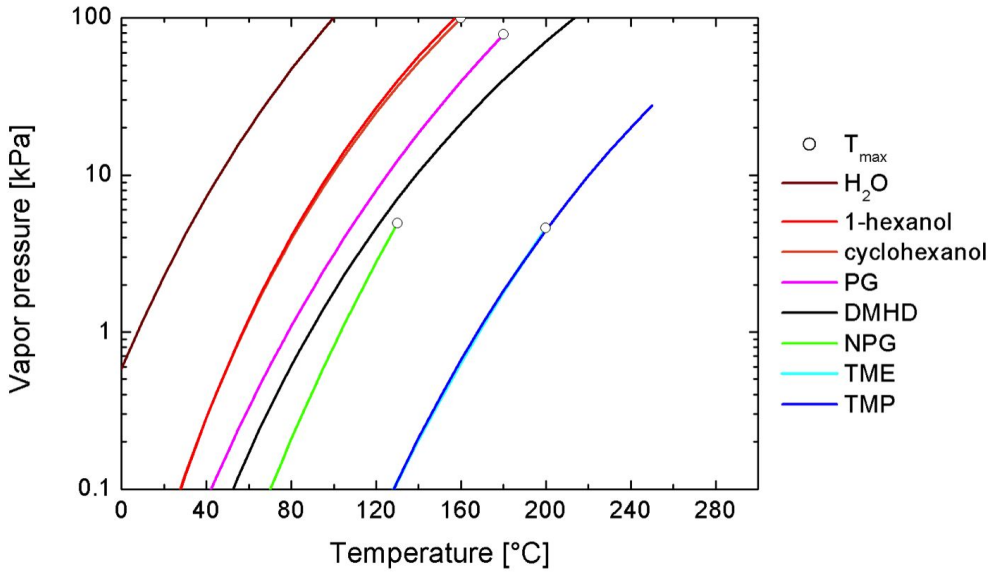

Figure 5.3: Vapor pressure vs. temperature of the compounds used to formulate sacrificial layers (almost perfect overlap between cyclohexanol and hexanol, and TME and TMP)

Table 5.1: Main properties of the polyols, with T_m/T_b.: melting/boiling point (supplier data)

Name	CAS	Supplier	T_m [°C]	T_b [°C]	P_{T_m} [kPa]
NPG	126-30-7	Sigma Aldrich	130	207	4.92
TME	77-85-0	Sigma Aldrich	200	293	4.59
TMP	77-99-6	Sigma Aldrich	58	295	114.93
2,5-dimethyl-2,5-hexanediol (DMHD)	110-03-2	Sigma Aldrich	86	214	117.38
Cyclohexanol	108-93-0	Sigma Aldrich	24	160	-
1-hexanol	111-27-30	Sigma Aldrich	-52	157	-
Propylene glycol	57-55-6	Sigma Aldrich	-60	187	-
Water	-	-	0	100	-

5.2.2 Requirements of the paste and provided solutions

Firstly, we want to formulate a screen-printable paste, which will obviously induce restrictions regarding the viscosity. The paste should ideally be thixotropic and present a consistency similar to honey. Formulation of low-molecular-weight sacrificial materials as screen-printable pastes is significantly more difficult than with polymeric materials, as there is no polymer to impart high viscosity to the solution, and the solvent thus tends to separate out of the solid material. To mitigate this issue, the solvents mixes were based on cyclohexanol, one of the rare easily evaporable solvents having a high viscosity. Its melting point is 24°C, but can be depressed easily well below room temperature by only a small amount of additions such as water, 1-hexanol, propylene glycol or even dissolved TMP. Indeed, this yields high-viscosity mixtures, with cyclohexanol having a moderate evaporation temperature, which is still high enough to be acceptable for screen-printing.

The second point deals with the processability of the paste. In order to obtain a proper sacrificial layer, the paste must be homogenous. First tests of preparing the paste by mixing plastic crystal powders were not successful, giving too coarse pastes that tended to separate out. All pastes were therefore prepared with the method giving the most homogeneous materials, which involved dissolving the plastic crystals in a 100 mL beaker into the solvents in temperature (ca. 100°C) and under stirring. Once the polyols were totally dissolved, a clear solution with very little viscosity was obtained. This solution was then reprecipitated under agitation (with a spatula) and cooling by immersing the beaker into cold water, yielding fine-grained suspensions, hence macroscopically homogeneous pastes (Fig. 5.4).

Finally, as well-defined structures are of course desired, the paste should therefore dry properly. The drying has to be done at moderate temperatures,

Figure 5.4: Sacrificial paste with an appreciable creamy consistency (system based on DMHD/TME, the blue color coming from food-grade dye)

i.e. <100°C to prevent any premature sublimation of the sacrificial materials. This is controlled by choosing adapted solvents mixtures.

5.2.3 Formulation of the sacrificial paste

Using the dissolution/precipitation process, three systems were investigated:

- TMP/TME
- NPG/TME
- DMHD/TME

It should be noticed that instead of using pure compounds, we only used mixtures, which may combine the following advantages: limit grain growth during precipitation but also introducing a kind of binder between the different parts composing the paste. Moreover, in each case, solvents based on cyclohexanol with water and optionally propylene glycol were adapted in order to get the required viscosity. This solvent mix is not trivial and each component has one/several role(s). The choice of cyclohexanol as main solvent was already described above. As far as the presence of propylene glycol, it is used to keep the cyclohexanol liquid and to retard evaporation. Regarding the fact that water can do the same, it is not mandatory, the only problem of water is that it evaporates more easily than propylene glycol. However, a formulation requiring too much water will prematurely dry. Water has also a very important function in the system. Indeed, it reacts with TME to form a trihydrate. Yamazaki et al. [195] studied the system formed by water and TME and were able to

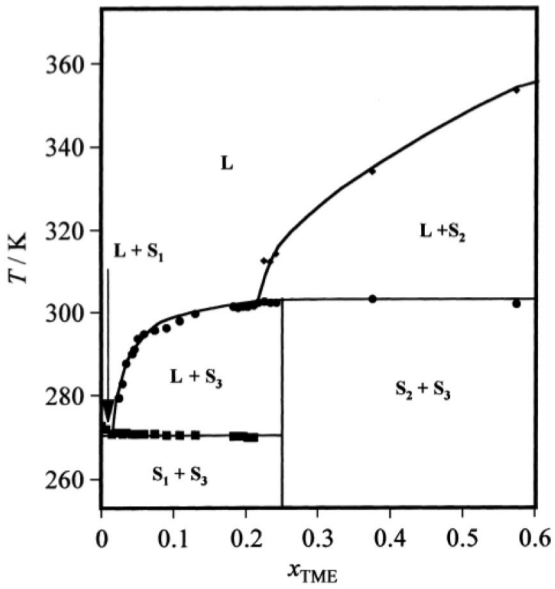

Figure 5.5: Phase diagram of TME and water, from [195]

propose a phase diagram (Fig. 5.5[1]). From this, we can see that a stable hydrate should form at room temperature. We can also assume that TME will have the tendency to catch the humidity contained in the air, giving a certain hygroscopy to the paste.

We propose now to study these systems separately in the following parts.

5.2.3.1 TMP/TME

Let us first focus on the system formed by TMP and TME. By looking at the physical properties of these two polyols (Table 5.1), TME appears as the main sacrificial material, i.e. the ultimately sublimating compound. It will be in suspension in the solution. However, TME alone essentially yields a powdery substance unsuitable for overprinting. TMP acts therefore as a "waxy" binder in the system. The other part in the paste is the solvent mix: cyclohexanol, water and propylene glycol. Nevertheless, the final system is slightly more complex. Indeed it was shown by Castaňeda et al. that TMP, water and cyclohexanol form a ternary liquid-liquid equilibrium at room temperature [196]. The consequence of this is the obtention of a stable paste at room temperature.

A screen-printable paste was obtained (see Table 5.2). We can notice that solutes represent a higher percentage in the paste than the solvents, which is quite understandable as the purpose is the obtention of a sublimable paste.

[1] with L = liquid, S1 = ice, S2 = TME, S3 = TME trihydrate

Table 5.2: Formulation of a sacrificial paste based on TMP/TME

Material	TME	TMP	cyclohexanol	H_2O	propylene glycol
Mass [%]	46	18	30	3	3

Drying tests were then performed in order to see if the paste could be used. It was determined that the paste could be dried at 80°C for 10 min., giving a soft solid yet consistent enough for further screen-printing. This first system showed very promising results, however, once the paste was screen-printed onto the substrate, it could not be left in the air as it would crumble and dry.

5.2.3.2 NPG/TME

If we now look at the system NPG/TME, we can see that they react together and form a solid solution at high temperatures. Fig. 5.6a shows the phase diagram formed by this system [2]. Once again, the system is not that simple. Indeed, recently, Singh et al [197] reported that cyclohexanol is miscible in a solid solution with NPG. The corresponding phase diagram can be found in Fig. 5.6b. Therefore, the system must be considered as ternary, TME/NPG/cyclohexanol, instead of binary. From that, we can also deduce that cyclohexanol is a co-solvent and can't be used alone, as its mixture with NPG (and probably TME) would form a solid solution. A screen-printable paste was formulated based on this system (Table 5.3). Propylene glycol was not used this time, cyclohexanol being kept liquid with water. Indeed, as propylene glycol and NPG present close vapor pressure values, it would became impossible to eliminate the solvent without eliminating all the NPG as well. Water presents the advantage to be somewhat in equilibrium with the ambient air humidity, cyclohexanol and the polyols being quite hygroscopic.

Table 5.3: Formulation of a sacrificial paste based on NPG/TME

Material	NPG	TME	cyclohexanol	H_2O
Mass [%]	32	34	31	4

Similarly to the paste based on TMP/TME, drying tests were performed prior to use them in any microstructure. The most convenient and successful drying was obtained at 100°C for 10 min. in the oven. It results in a waxy solid. It also appears to be relatively hygroscopic, which is probably due to the presence of TME in equilibrium with water. This effect was not observed in the case of the TMP/TME system. Indeed, in this case, there is no formation of a compound between TME and TMP, which presupposes that TMP surrounds

[2] M, O and Q corresponds resp. to the monoclinic, orthorhombic and tetragonal phases, whereas C_F refers to the orientationally disordered face centered cubic phase.

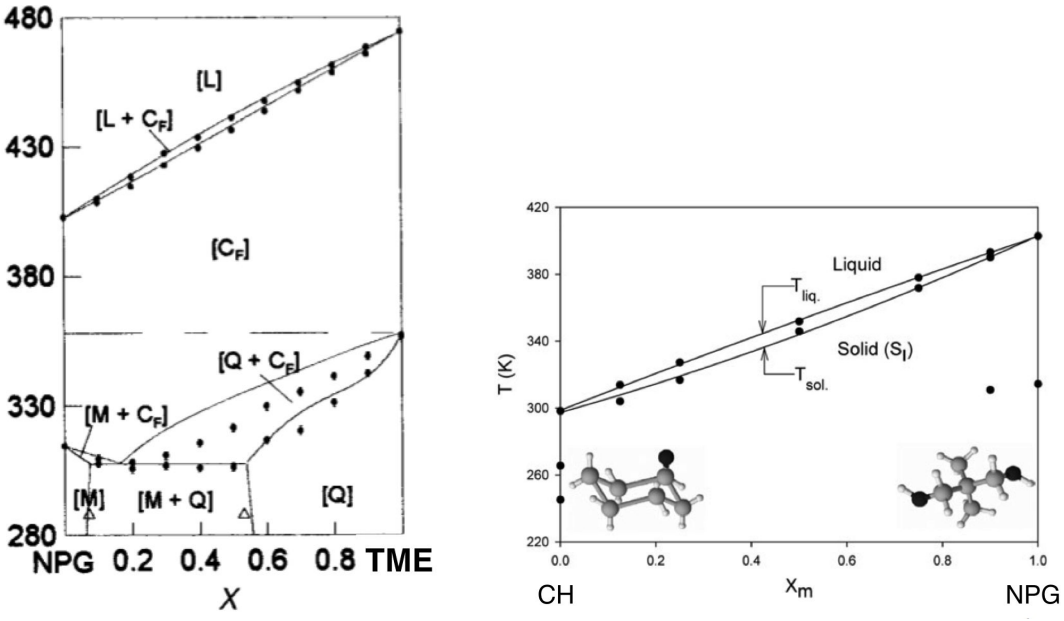

(a) (b)

Figure 5.6: Phase diagram of NPG-TME [198] (a) and NPG-cyclohexanol [197] (b)

TME particles (waxy binder), TMP being more hygroscopic. Hygroscopy is not necessarily an undesired effect as long as the dried layers are not deliquescent. In fact, it allows easier storage of the compositions, as it prevents the layers from drying prematurely (i.e. lose all the NPG). However, in case the layers are already dried, we also observed that it is possible to regenerate them by putting them in an atmosphere composed of NPG/cyclohexanol at moderate temperatures. The already dried pastes can equilibrate with the atmosphere filled with NPG and cyclohexanol. The key point is therefore to find a balance between deliquescent and powdery layers.

5.2.3.3 DMHD/TME

Finally, the system DMHD/TME was investigated. To our knowledge, no formation of a compound between them was reported in the literature. Therefore, like TMP, DMHD will act *a priori* as waxy binder for TME particles and bind them. No propylene glycol was used either (see vapor pressure). A potential composition was formulated and can be found in Table 5.4. An interesting comment that can be drawn from this last table is that when the co-solute of the TME is DMHD, it does not interact with the TME. Therefore, a larger amount of TME can be added to the paste without becoming too brittle. Drying tests were optimal at 120°C for 10 min. The paste was found to be stable in time, its only drawback being that it melts at high temperatures,

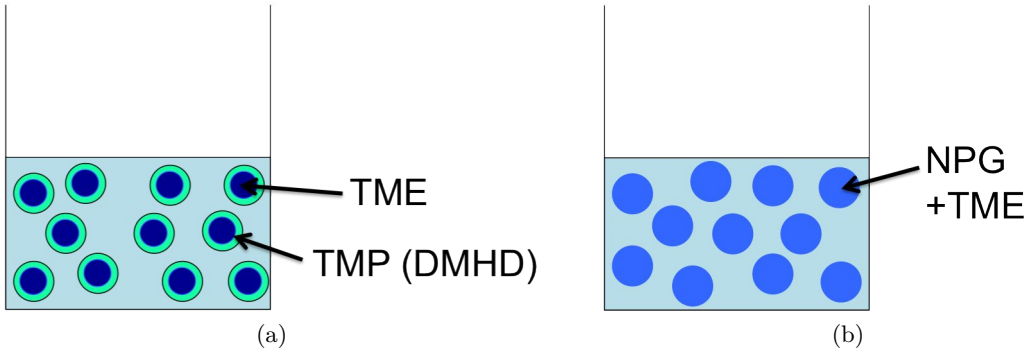

Figure 5.7: Comparison between the two possible cases of reaction mechanisms of our sacrificial layers (systems based on TME with TMP or NPG or DMHD): waxy binder (a) or formation of a new compound (b)

which indicates that DMHD depresses the melting point of TME. To confirm this hypothesis, the phase diagram of the system DMHD-TME should be established and studied.

Table 5.4: Formulation of a sacrificial paste based on DMHD/TME

Material	DMHD	TME	cyclohexanol	H_2O
Mass [%]	11	56	29	4

5.3 Characterization of the microstructures based on organic sacrificial layers

In the section above, we have studied three systems: TMP/TME, NPG/TME and DMHD/TME. We showed the different mechanisms of reaction: waxy binder or formation of a new compound (see Fig. 5.7). In this section, we will characterize these pastes in order to determine in what extent it is possible to use them for microstructures fabrication. The interactions between the polymer over-layer and the sacrificial material will be first investigated, then we will explain how the samples were fabricated and finally experiments on the obtained structures will be performed.

5.3.1 Investigation upon the interactions with the over-layer

The final purpose is to obtain all-polymeric microstructures: channels, cantilevers, membranes... Due to the process of fabrication (see Fig. 5.1), potential interactions between the sacrificial layer and the over-layer may occur. As too

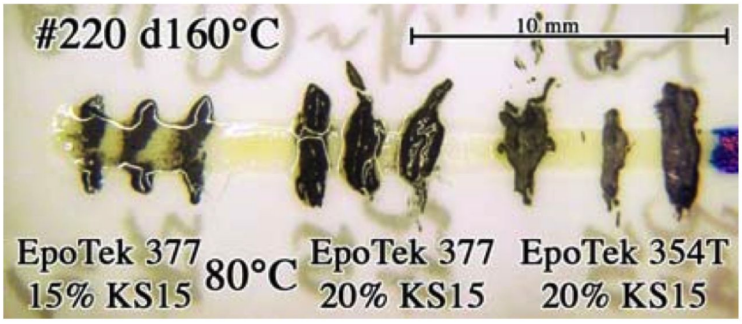

Figure 5.8: TME-TMP sacrificial layer coated with epoxy resin-graphite composite, showing strong reaction, especially with EpoTEK 377

many interactions may result in the collapse of the final structure, the polymer used for the over-layer must be carefully chosen.

5.3.1.1 Choice of the polymer used as over-layer

Depending on the structure (for instance cantilevers), a conductive layer may be desired as over-layer. As we have fully characterized our epoxy-graphite composites, it was decided to firstly use them as potential over-layer. Preliminary evaporation tests consisting in dispensing bridges of conductive paste above a sacrificial layer strip were first performed to check compatibility of sacrificial paste-polymer combinations. EpoTEK 377 was used as resin with graphite KS4 as conductive particles. The addition of graphite particles allows to impart electrical conductivity and also additional mechanical stiffness. However, interactions between the sacrificial layer and the polymer coating occur: indeed the epoxy can react with the -OH groups of the polyols contained in the sacrificial paste, disturbing polymerization by unbalancing the composition. Additionally, the resin may thus go inside the sacrificial layer preventing it from evaporating (Fig. 5.8).

Therefore other materials were tested out to replace the epoxy-graphite composite. Ethylcellulose and silicone would not *a priori* interact with the polyols, which make them potential candidates. Their main characteristics can be found in Table 5.5. As ethylcellulose needs to be dissolved in solvents, amyl acetate and triacetin were chosen to fulfill this role. KS4 graphite was finally added to both polymers.

The same tests as for epoxy were performed in order to determine the compatibility of sacrificial paste-polymer. This was verified for ethylcellulose polymer and silicone resin. Fig. 5.9 shows an example of ethylcellulose bridges after evaporation. Appreciable clean structures can be observed. From these results, we decided to forgo epoxy and focus on silicone and ethylcellulose [191].

Table 5.5: Main characteristics of the components used as over-layer

Name	CAS	Supplier	T_m [°C]	T_b [°C]
Ethylcellulose, 46 cps grade, 48% ethoxyl content	9004-57-3	Sigma Aldrich	170	
Silicone Q5-8401, two-component resin		Dow Corning		
Amyl acetate	628-63-7	Sigma Aldrich	-71	149
Triacetin	102-76-1	Sigma Aldrich	3	258

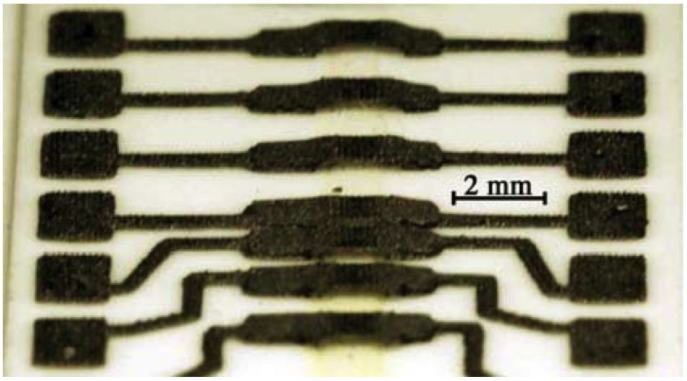

Figure 5.9: Ethylcellulose-graphite bridges after evaporation of the underlying TME-TMP sacrificial layer (yellow color is remaining colorant)

5.3.1.2 Influence of the solvent

Depending on the structure, it might be needed to have a soft over-layer (typically for a membrane) in order to allow movement of the structure. In this case, silicone will be preferred over ethylcellulose, which is a quite rigid material. As high graphite loadings tend to yield an excessive paste viscosity, the introduction of suitable high-boiling solvents was studied to allow convenient tuning of the paste rheology. As for the epoxy (see Part. 3.1.2.1), a study on solvents was performed. Solvents must be carefully chosen: they should be miscible with the resin, yet remain inert without chemical reaction with it or dissolving the sacrificial layer. Their main properties can be found in Table 5.6. One would notice that our list includes also polar solvents (octanol and tetraglyme), which are not a priori suitable solvents for silicones. However, our sacrificial material having polar groups, it might be interesting to have also a certain percentage of a polar solvent in the over-layer to promote wetting and adhesion between the layers. Therefore, knowing the behavior of these

solvents with silicones would be of great use. In order to prove their efficiency and validate their use for paste formulation, mass loss tests were performed for 10% and 20% in volume of graphite. A second "qualitative" test consisting in rheological measurements was done at 10% vol. of graphite in order to classify the "solvative" nature of the materials. Finally, fabricated structures were tested and compared [192].

Table 5.6: Main properties of tested solvents with T_b= boiling point, M = molar mass, d = density

Name	CAS-n°	T_b [°C]	M [g/mol]	d [kg/m^3]	Symbol
Dodecane	112-40-3	215	170.33	750	A/B1
Octanol	123-96-6	196	130.23	827	A/B2
(R)-(+) limonene	5989-27-5	175	136.24	840	A/B3
Tetraglyme	143-24-8	275	222.28	1009	A/B4

A first series of mass loss experiments was performed in order to determine whether solvents evaporate completely during the curing process (see Fig. 5.10). A mass loss profile was made for 10 vol.% and 20 vol.% graphite by measuring the composite mass after 30, 60 and 120 min at 150°C. A/B0 samples correspond to the reference measurement, i.e. without solvent. Whatever the solvent or the graphite loading, essentially all the mass loss occurs in the first thirty minutes, which is noticeably faster than with epoxies and agrees with the higher permeability of silicones. The somewhat slower removal of tetraglyme stems from its very high boiling point. Finally, the small mass loss seen in the reference sample probably corresponds to water.

A second series of experiments consisted in rheological measurements. The dynamic viscosity was measured with a rotary viscosimeter, Rheomat RM180 from Mettler. No measurement was possible for the reference sample, the viscosity being too high for our device. Fig. 5.11 reports the data for the four solvents. First, we can see that the pastes present a typical shape of a thixotropic / shear thinning behavior, which is satisfactory for screen-printing [134]. We can see that theoretical suppositions are confirmed, i.e. dodecane and limonene have a higher solvating power compared to the other two. Octanol and tetraglyme first form a gel but nevertheless may be incorporated into the resin under shear, yielding a strong thixotropic behavior. This can be explained by their rather low polarity. Likewise, the long alkane chain of octanol is expected to facilitate its observed easier incorporation into the resin than tetraglyme. Octanol is therefore expected to be particularly useful as a wetting agent for silicone (affinity with alkane chain) on polyol (hydroxyl head) layers. In practice, an acceptable combination of wetting and solution stability must be found, which can be done by combining octanol with dodecane or limonene.

Single microchannels using silicone as over-layer were fabricated, with the

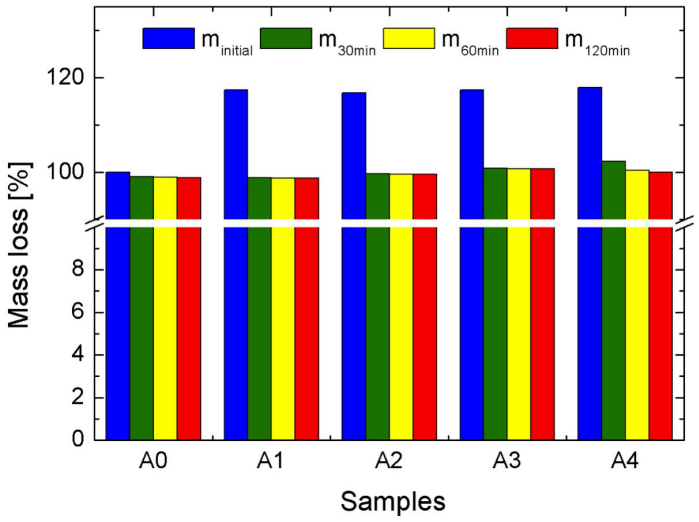

(a)

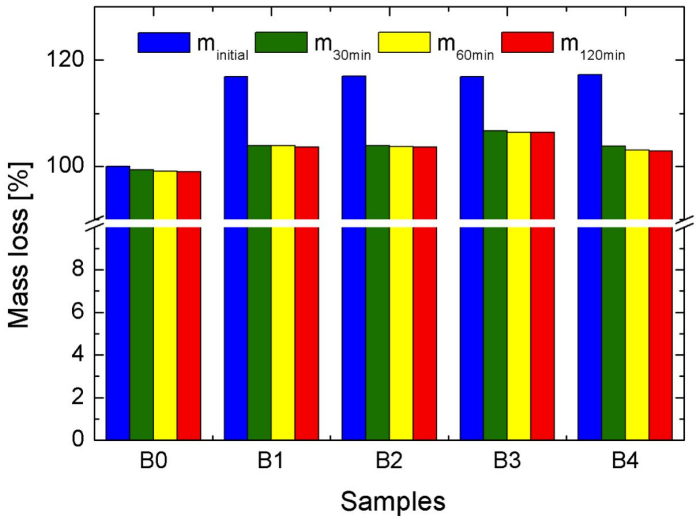

(b)

Figure 5.10: Mass loss profile of composite loaded with graphite at 10% (a) and 20% (b) volume fraction (see symbols in Table 5.6)

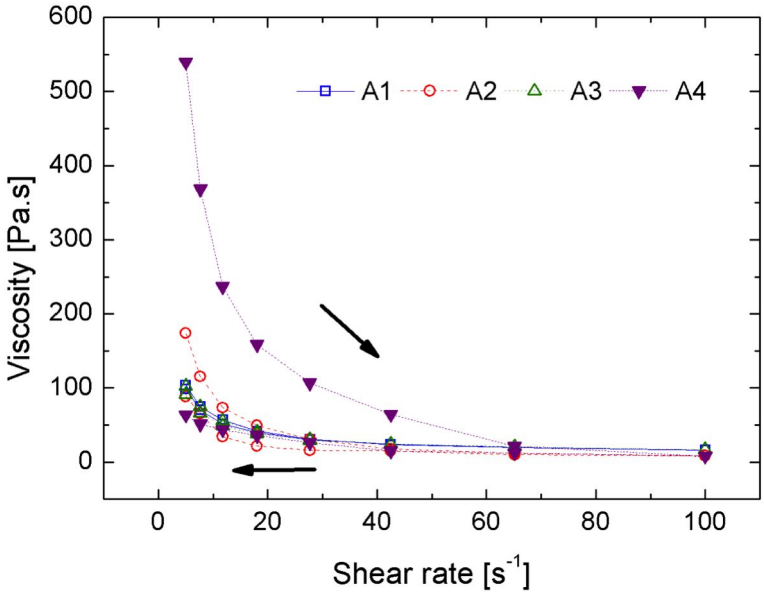

Figure 5.11: Viscosity measurement for the different solvents

aim of studying the influence of a polar solvent on the good functionality of the structures. Silicone/graphite pastes were prepared using first only dodecane as solvent, than mixes of dodecane : octanol (2:1 and 1:1). Test structures were dipped in water in order to check for leaks, air ($\approx$ 6 bar) was blown through the channel, and the maximum flow was determined in each case. The results (Table 5.7) show that without octanol, the structures tend to tear away from the substrate. On the other hand, an equal mix of dodecane and octanol gives the best results in terms of reproducible channel geometry. However, a too large amount of octanol may lead to an unstable solution, another possible problem being dissolution of the sacrificial layer by octanol during the curing of the silicone resin.

Table 5.7: Influence of solvent formulation on the maximum air flow

Dodecane : octanol ratio	Air flow [l N/min]
1:0	unreliable
2:1	1.7
1:1	2.8

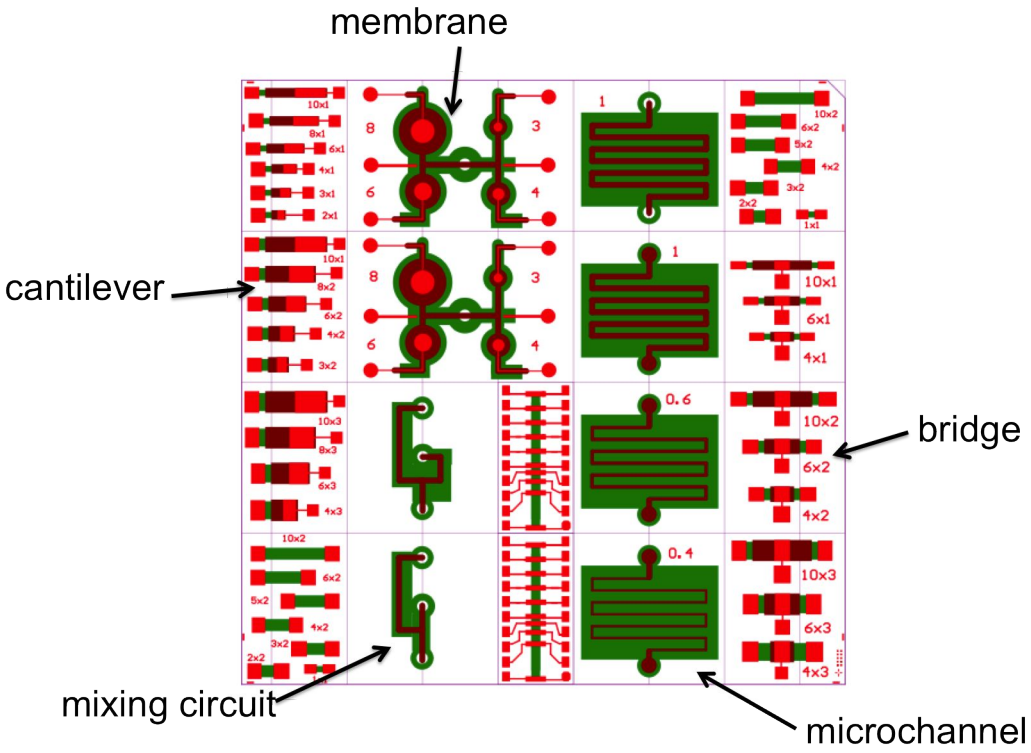

Figure 5.12: Layout of the structure with silver contact in red, sacrificial material in brown and polymer in green

5.3.2 Fabrication of samples

Different structures were then tested in order to see how the sacrificial materials evaporate and behave depending on the geometry: channels, bridges, cantilevers and membranes. For each type, several sizes were tested with different sacrificial layers. Fig. 5.12 shows the used layout, which presents the advantage of allowing simultaneous fabrication of all the different structures.

Structures were therefore screen-printed in the sacrificial materials and then covered with an over-layer in ethylcellulose and/or silicone. After the 150°C cycle, complete removal of the sacrificial layer can be observed on the substrate, leaving clean and relatively well preserved structures. Fig. 5.13 shows the total removal of the sacrificial paste covered with ethylcellulose, whereas structures in silicone-graphite can be observed in Fig. 5.14.

5.3.3 Experiments

In the previous parts we developed a valid process for the fabrication of well-defined structures. We will now test them in order to show their good functionality.

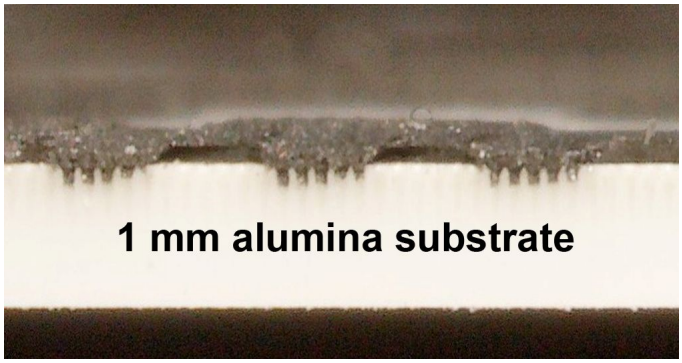

Figure 5.13: Cross-section of a microchannel after sublimation of the sacrificial paste (black stripes where the over-layer was directly printed on the substrate due to filling of the cavities created by prior laser scoring)

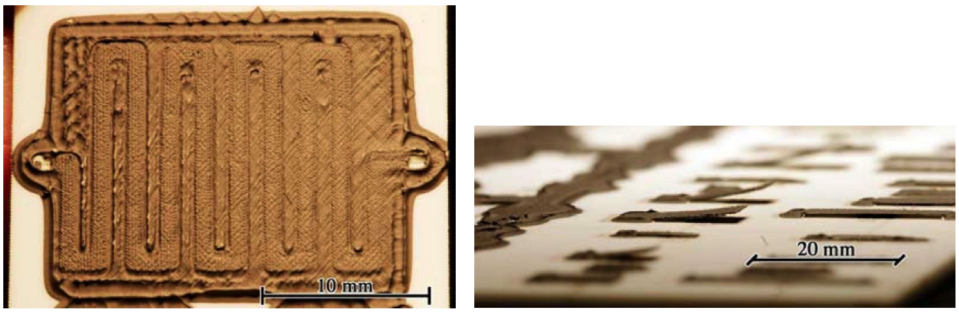

(a) (b)

Figure 5.14: Microstructures in silicone-graphite: microchannels (a) and cantilever and bridge (b)

5.3.3.1 Microfluidics

Microfluidic mixing circuits were first tested. A flowmeter was plugged to the circuit, which was dipped into water to check for leaks and see if air was able to come out of the structure (see Fig. 5.15). The flow was controlled and registered by computer.

Fig. 5.16 shows the device with air circulating through it, proving the good functionality of the structure. The flow inside the structure was also measured by the computer and can be found in Fig. 5.17. We can see a little difference between the flow set-point and the actual flow that circulates inside the structure, which may indicate leaks. Small delays can also be observed between the two curves: this is due to exit valve regulator of the flow controller. We have therefore demonstrated the suitability of our process for facile fabrication of printed fluidic structures.

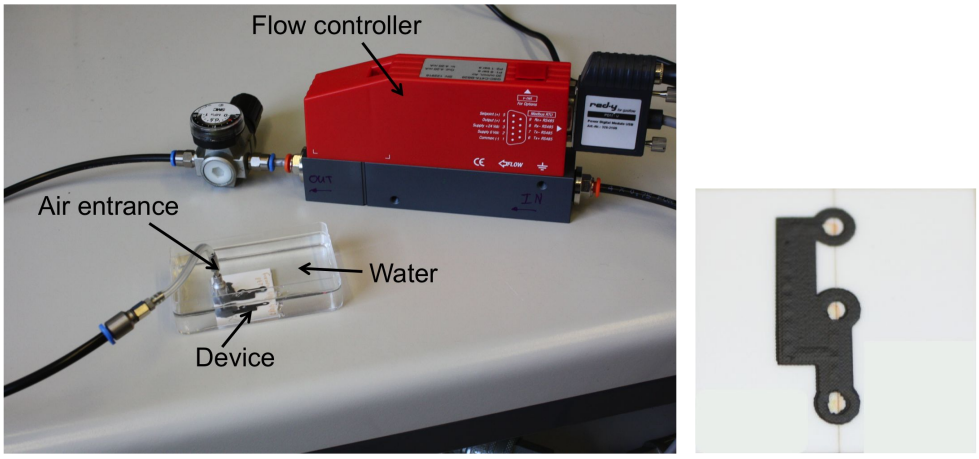

(a) (b)

Figure 5.15: Microfluidics testing: set-up (a) and screen-printed mixing circuit (b)

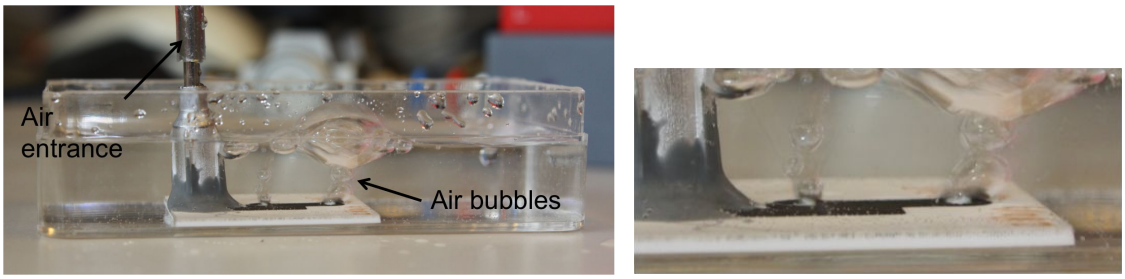

(a) (b)

Figure 5.16: Air circulates through the device: air bubbling (a) and zoom (b)

5.3.3.2 Position/force-sensing cantilevers

Fabrication of cantilevers was also investigated using this process. The elastomeric silicone resin alone being too soft for cantilever structures, a graphite-filled ethylcellulose–silicone bilayer structure was used, the idea being to combine the thermal stability of the cross-linked silicone resin during sublimation of the sacrificial layer with the rigidity of ethylcellulose at room temperature. The distance between the cantilever and the base was sensed capacitively. The top electrode was the cantilever itself (both ethylcellulose and silicone filled with 15% vol. KS4 graphite, which gives a resistivity of ca. 1 Ω.m), and the bottom electrode consisted in an Ag thick-film paste, previously screen-printed and fired onto the alumina substrate (see Fig. 5.18a). Capacitance of the cantilevers was measured through an Analog Devices AD7746/7745 integrated circuit that allows differential capacitance measurements between − 4 and + 4 pF, with a resolution of ± 4 fF [199]. Different loads were then applied on the cantilever tip using weights ranging from 0 to 0.31 g and a supporting jig, both made of

Figure 5.17: Screenshot showing the recording of the flow inside the mixing circuit, blue: flow set-point, red: actual flow, green: valve opening

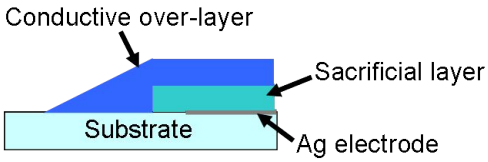

(a)

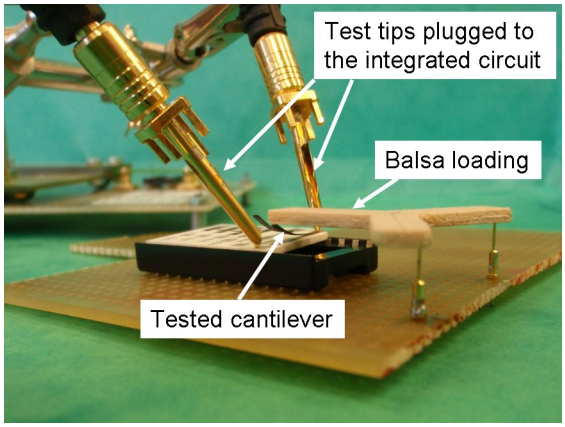

(b)

Figure 5.18: Cantilever: schema (a) and set-up of the capacitance measurement (b)

balsa wood (see Fig. 5.18b). The applied load changes the distance between the electrodes, which translates into a capacitance change. Assuming parallel electrodes, this capacitance can be calculated with the following equation:

$$C = \frac{\varepsilon_0 \varepsilon_r A}{d} \tag{5.1}$$

where C is the capacitance, ε_0 the electric constant, ε_r the relative permittivity, A the electrodes area and d the distance between the electrodes.

Cantilevers with a length of 10, 8 and 6 mm and a width of 1, 2 and 3 mm were fabricated. The theoretical capacitance without any loading was calculated using Eq. 5.1 and is reported in Table 5.8. However, due to the difference of thermal expansion coefficient between the two over-layers, leading to a stress during the cooling, some cantilevers were initially highly bent. Therefore, the two electrodes are no longer parallel and the area changes in each case, following the cantilever bending. This is the reason why the theoretical capacitance is so different from the experimental one. Indeed, the combined effects of different possible sources of error (area not equal, inhomogeneity of the charge along the cantilever leading to changes in the electrical field. . .), yield large errors in the calculations.

Table 5.8: Comparison of the theoretical C_{th} and experimental C_{exp} capacitance

Cantilever	C_{th} [pF]	C_{exp} [pF]	Ratio
10 x 1	0.0210	0.256	13
10 x 2	0.0397	0.307	8
10 x 3	0.0418	0.384	9
8 x 1	0.0165	0.289	17
8 x 2	0.0509	0.404	8
8 x 3	0.0770	0.509	7
6 x 1	0.0176	0.276	15
6 x 2	0.0516	0.429	8
6 x 3	0.0738	0.461	6

The force response was then determined for each cantilever by loading them with small balsa wood weights. The fabricated devices were able to measure small forces (0. . .1 mN). Fig. 5.19 presents the results for each length. These graphs highlight the fact that the capacitance increases with an increasing width, i.e. an increasing area of the electrode. This can be easily understood by Eq. 5.1. In most cases, we can see that the evolution of the curves is not linear but quadratic with an increase of the applied force at the end of the cantilever. Once again, this is due to the bending of the cantilever. The parallel plate model capacitor is therefore no longer applicable as two phenomena occur: change of the distance between the electrodes and change of the electrode area [192].

5.3.3.3 Membranes

Finally, the membrane structure was tested. It features a combination between fluidics and mechanics, pressure being needed to excite the membrane, whereas the response is measured through a capacitance measurement. A connective hole in the center allows the air entrance, four exits and silver pads can also be

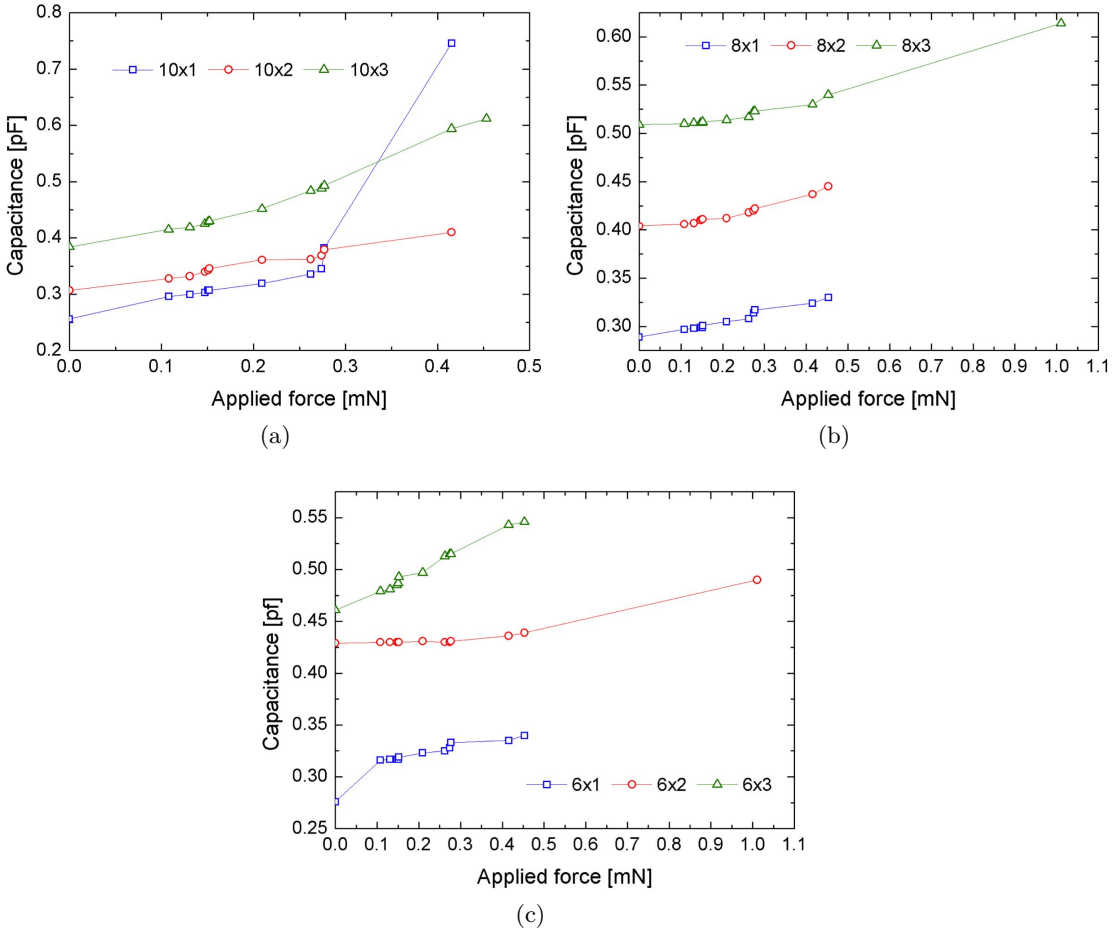

Figure 5.19: Capacitance measurements for cantilevers with a length of 10 mm (a), 8 mm (b) and 6 mm (c)

seen in the structure (Fig. 5.20). Membranes were therefore fabricated using a sacrificial material and a silicone over-layer.

The capacitance of the membrane was first measured using the Analog Devices AD7746/7745 integrated circuit. A capacitance of 1.55 pF was found. An air flow of 0.2 l N/min was then sent to the membrane using the same flow controller than for the microfluidics test. As the air goes inside the membrane, the membrane inflates and capacitance decreases (increase of the distance between the membrane and the silver pad). Fig. 5.21 presents the flow inside the membrane as well as the capacitance measurement. Like in the case of microfluidics, a delay (around 1 second) is observed between the set-point flow and the actual flow. This is also due to the exit valve regulator of the flow controller. When the air entrance is cut, the flow decreases progressively, hence a small increase of the capacitance of the membrane. Then it takes

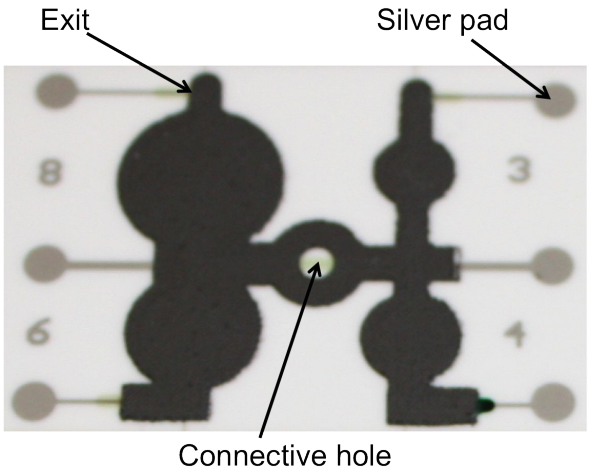

Figure 5.20: Screen-printed membrane structure

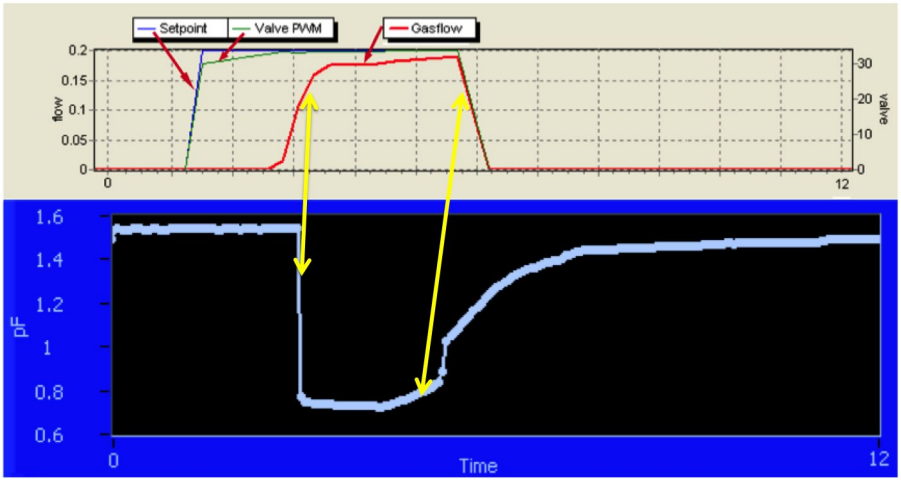

Figure 5.21: Screenshot of the recording of the flow inside the membrane (blue: flow set-point, red: actual flow, green: valve opening) vs. capacitance measurement (scales do not match exactly)

approximately 5 seconds to the membrane to recover the initial capacitance, which can be explained by the silicone layer viscoelastic relaxation [200].

5.4 Summary

In this process, we have detailed the formulation of organic sacrificial layers. Sacrificial layers are temporary layers that are eliminated during the process.

They are used either to create an empty space by allowing deposition of another layer or to protect the layer underneath, during the process. They are particularly useful to fabricate suspended structures such as bridges or cantilevers. Two types are available: mineral or organic. Here, it was chosen to formulate organic paste in order to use them with polymers. Using polyols, we were able to design a sublimable layer, which allows the fabrication of closed structures (membranes, microchannels...). These polyols are essentially non toxic, biodegradable and sublimate around 150°C, which can be of high interest for some biomedical applications. Trimethylolethane (TME) was the main sacrificial material and it was combined with trimethylolpropane (TMP), neopentyl glycol (NPG) and 2,5-dimethyl-2,5-hexanediol (DMHD). Dissolved in a mixture of solvents based on cyclohexanol, creamy screen-printable pastes were obtained by reprecipitation upon cooling.

In order to fabricate test microstructures, interactions between the sacrificial layers and the over-layer were investigated. It was determined that ethylcellulose and silicone can be envisaged as over-layer, epoxy reacting with the polyols. These two polymers were mixed with graphite KS4 to give the paste electrical conductivity and additional mechanical stability. As for the epoxy, a study on solvents compatible with the silicone was performed. A mix between octanol and dodecane was shown to be suited to our goal, the dodecane being a good solvent for the silicone, whereas the polar group of the octanol can slightly react with the polyols, resulting in a better adhesion (yet not too strong interaction) between the sacrificial layer and the over-layer.

Finally, tests structures were fabricated: microfluidic mixing circuits, cantilevers and membranes. All these structures exhibited promising functionality, in principle validating the process. Future optimization should yield further improvements in manufacturability and process control.

Chapter 6

Applications: fabrication of bulk composites

This chapter will deal with industrial application of the epoxy-graphite system. One application that emerges is in the oil industry and more specifically during the exploration step prior to the well drilling and its exploitation. We will first explain how a well drilling is performed and then how resistive materials can be surprisingly useful in this industry. Tests and results will be then presented.

6.1 The oil industry and the link with conductive composites

Nowadays, oil remains essential in our everyday life (cars, by-products of the oil, i.e. petrochemistry for instance etc), which is the reason why a lot of effort is still applied to find new oil fields. We propose to first briefly review how the research and well drilling are done, making possible the well exploitation.

6.1.1 From the soil exploration to the well drilling and exploitation

The first step is to localize where there is oil, which can be on land or in the sea. At the beginning, the search was random, wells being most of the time drilled on a hunch. Nowadays, employed techniques are more modern. Airplane or satellite pictures of large areas are taken and studied by specialists, which allows to narrow the search to smaller regions. The second step consists in seismic surveys. Indeed, as the oil is below the ground, the best way to study the area is to analyze the wave propagation. To do so, geophones are disposed all around an area where oil can potentially be found. The sound waves propagate and penetrate the rock layers. Once they reach a boundary, they

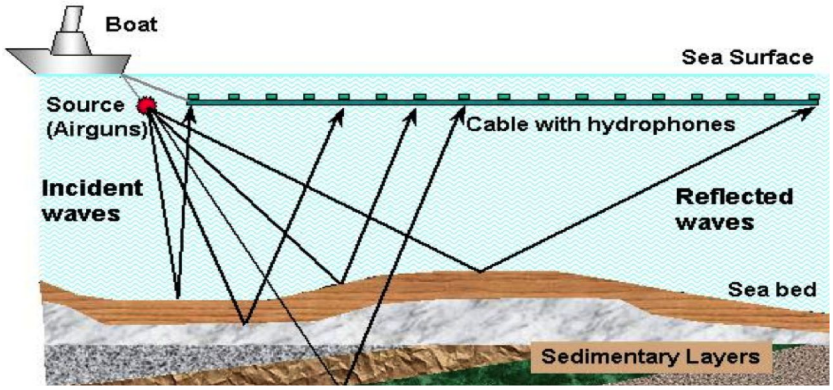

(a)

(b)

Figure 6.1: Seismic surveys: principle offshore (a) and onshore with trucks with vibrating pads in the desert (b) from [201]

are partly reflected and the rest continues downward. Geophones record the reflected sounds. Depending on how the waves propagate and are reflected, it is possible to determine the types of rock and then reconstruct how the formation looks like. The seismic study can be done either offshore (i.e. in the sea) or onshore (i.e. on land); the principle remains the same, the only difference being the way to create the vibrations, by boat and cables of hydrophones for offshore and with trucks in the case of onshore seismic studies (see Fig. 6.1).

When oil has been located, a well is built. The important thing to remember here is that this construction is executed in several steps that are repeated. Indeed, a well cannot be built in one time. As it is deep (several hundred meters), it would collapse. The well is first drilled using different kinds of bits.

Then logging, i.e physical measurements are performed: pressure, resistivity and density. This information is of high importance as it helps to determine the nature of the traversed rocks. For instance, if the resistivity is high, there is a possibility that it is oil, which has to be confirmed with density and pressure measurements. After the logging, the casing is done: a metallic tube is inserted into the hole. This will prevent the well from collapsing and isolate it from the rock formations. Finally the cementing is performed. The formulation of the slurry is adapted so as to obtain a cement with a density matched to that of the formation, i.e. there is one cement formulation per rock type in the formation. These steps (drilling, logging, casing and cementing) are repeated until oil is reached. The deeper the well goes, the smaller the well becomes. Fig. 6.2 illustrates these different steps. Oil can be now pumped up and then transported through pipelines [201].

6.1.2 Need for composite resistive materials

Knowing the different steps that conduct to oil exploitation, the question that arises now is: how can composite resistive materials be useful in this industry?

If we look closer, during the logging, we have seen that resistivity measurements of the rock formations are performed. The principle is as follows: a signal (usually a current) is sent inside the formation, sensors placed on pads of the tool measure the resulting signal (usually a voltage). Therefore the spatial resistivity distribution of the formation can be calculated, which gives, after acquisition and processing, a picture of how the formation looks like.

When designing a tool, the manufacturer obviously wants to qualify it in order to attest the validity of further measurements on the field. At the moment, only the electronics of the sensors disposed on the pad can be verified, thanks to the use of discrete components (commercially available resistors). However, by no means, this is representative of real conditions (i.e. rock formation) as the global resistivity cannot be measured precisely. The idea would be therefore to produce a dummy rock with a well-defined resistivity (see Fig. 6.3). We therefore propose to use in bulk form the resistive composites that were developed to recreate this dummy rock. Our formulations present the additional advantage to be flexible, as different models can be fabricated with a wide range of resistivity.

6.2 Formulation of conductive composites adapted to oil industry

In this part we will describe the tests that were performed to formulate the conductive pastes to recreate the dummy rock. In order to espouse the morphology of the tool pads, a soft material would be a desired option. To fulfill

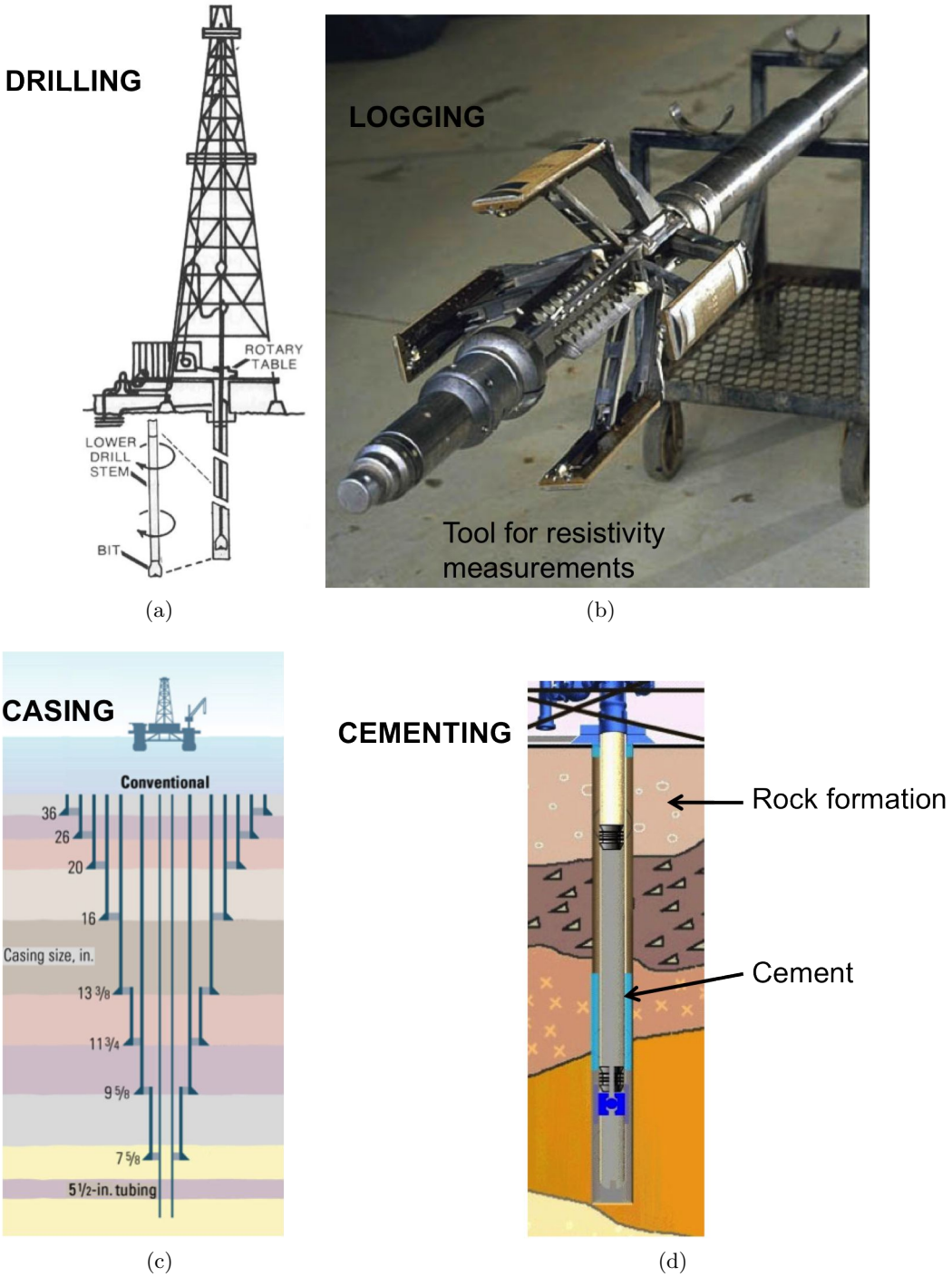

Figure 6.2: Steps of a well construction: rotary drilling rig (a), logging with analyzing tools (b), casing (c) and cementing (d) from [201]

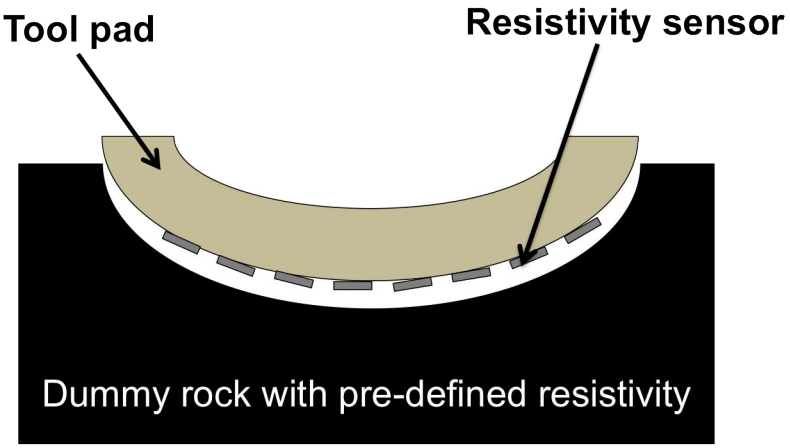

Figure 6.3: Dummy rock concept: the tool pad with its resistivity sensors is pressed against the dummy rock (i.e. resistive composite)

this requirement, we will make also tests using flexibilizer in our formulation (see 3.1.2.2).

6.2.1 Investigation on test resistors

Regarding the fact that we change the sample size, we want to be sure to obtain the same electrical properties. As the samples are in bulk instead of thick-film form, they might have a different dependence on processing and environmental conditions. Therefore, influence of the curing conditions (in particular atmosphere) and the polymerization time will be tested out first on thick-film resistors.

The first hypothesis concerns the environment. Indeed, we know from its chemical structure that epoxy has a tendency to interact with water molecules. Therefore we decided to test how the paste polymerizes under different conditions. To do so, an oven with a controlled atmosphere was used. Table 6.1 summarizes the investigated profiles. The ordered temperature was nominally 150°C, however, due to vacuum, it was measured to be between 132°C and 155°C. Test resistors were first screen-printed and polymerized in the above-mentioned oven. EpoTEK 377 was chosen as matrix with 7.5% vol. carbon black Ensaco 250P as filler. For comparative purposes, reference samples polymerized 2h at 150°C in a regular oven were also fabricated, and the P1 profile (confined air, i.e. air already present inside the oven) was made to recreate (in the controlled atmosphere oven) similar conditions as in the regular one. P2 polymerization will enable us to see the influence of the aging of the polymer upon properties, with the test resistors being screen-printed and left in the air for 24 hours at room temperature and then polymerized. Finally, P3 and P4 highlight the importance of water, as the vacuum will accelerate the

Table 6.1: Investigated profiles in the oven with a controlled atmosphere (samples = TFRs)

Curing time [hour]	Curing temperature [°C]	Profile	Symbol
2	150	confined air	P1
24h @ RT + 2h	150	confined air	P2
2	150	vacuum (15min) + N_2	P3
2	150	vacuum for 15min + no gas	P4

water evaporation.

Fig. 6.4 reports the resistivity values of the test resistors for each profile. The P2 profile (i.e. 24 hours at room temperature followed by a polymerization of 2 hours at 150°C in confined air) shows the highest value, which is quite understandable. Indeed the pot life of EpoTEK 377 was indicated to be 24 hours; therefore, by curing the epoxy after 24 hours, the material was saturated with the humidity of the air. It has already been altered and started to react, hence a higher resistivity value. The P1 profile (confined air) and the reference sample in a regular oven yield similar values, the conditions being equivalent. Finally, P3 and P4 profiles prove that water has a high influence during polymerization, as, by performing a vacuum, the water is evacuated more rapidly from the composite. The addition of N_2 has little effect, which might suggest that it is really the water and not the oxygen that causes problems during the polymerization. This hypothesis has to be confirmed with tests in the controlled atmosphere oven with air flow.

The second hypothesis concerned the polymerization time. The above-mentioned samples were taken and placed into a regular oven for additional polymerization first for 2 hours (intermediate polymerization time of 4 hours) and then for 6 hours (final polymerization time of 10 hours). Fig. 6.5 presents the evolution of resistivity with the polymerization time. The distribution is the same as in Fig. 6.4, showing three distinct blocks. We can also notice that all resistors present decreasing values of resistivity, especially in the intermediate polymerization time (4 hours). This confirms the cycling effect that was observed during temperature stability and dilatometry measurements (see Parts 4.1.2.3 and 4.3.2.3). We can notice that samples that were polymerized with vacuum and possibly under N_2 show a smaller cycling effect. Indeed, in these samples, except the one coming from the mixing of the paste (three-roll mill) and from the screen-printing, there was no additional introduction of water. Two effects occur. On the one hand, as less water was able to penetrate and react with the epoxy, the matrix is less altered. On the other hand, the amount of water to evaporate is smaller, due to the vacuum. All this leads

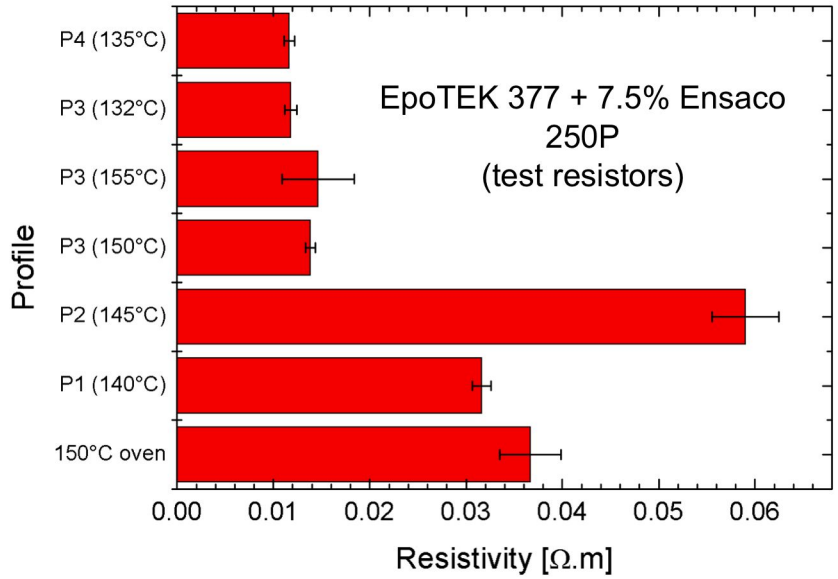

Figure 6.4: Resistivity of EpoTEK 377 + 7.5% Ensaco 250P thick-film resistors for different atmosphere profiles

to a better stability of the values of resistivity. Moreover, at the end, we can see that all profiles do not give the same resistivity, indicating that "moist" polymerization conditions permanently and irreversibly alter the resin, the final resistivity with P2 still being roughly 5 times the ones in vacuum. The matrix may have been so altered with the reactions with the water molecules that this has changed its properties. Another possibility is that the graphite particles may have reacted and oxidized with the humidity, leading to a higher resistivity. This oxidation process of the graphite with the air is supposed to be very slow, but might have an influence here.

These tests have highlighted the importance of water and its potential interactions with epoxy as well as that of the polymerization time. As the effects are already pronounced on a thick-film (50 μm thickness) we can easily imagine that they would be amplified on a bulk bar.

6.2.2 Extension to bars

Tests were performed in order to quantify these parameters upon bulk samples (i.e. bars of 50 x 10 x 5 mm). In each case, test resistors were also fabricated in parallel to compare the values. Likewise the previous test, a composite formed by 7.5% vol. Ensaco 250P in EpoTEK 377 was chosen. Table 6.2 summarizes the different conditions that were compared[1]. Curing temperature was always

[1]Tests were also performed in the controlled atmosphere oven with N_2. However, due to problems during the curing the results were inconsistent, which is the reason why they are

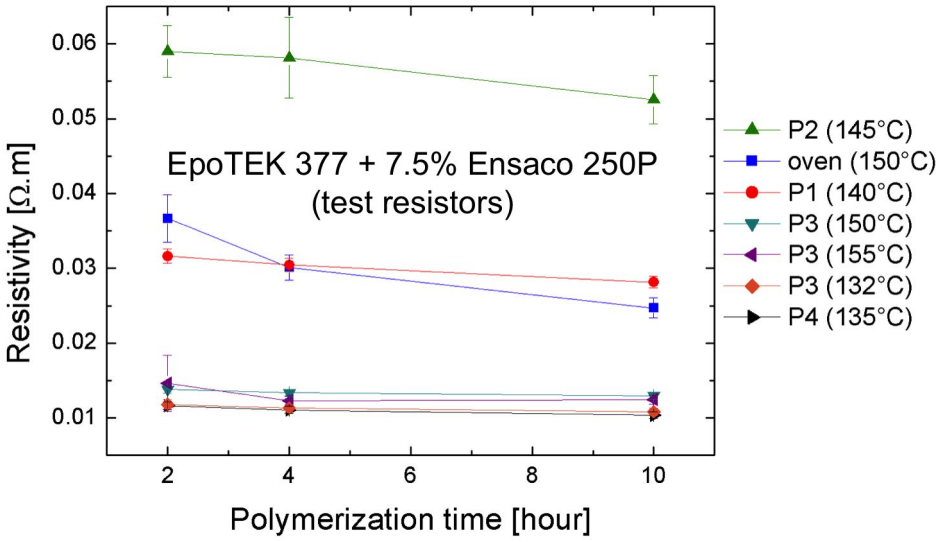

Figure 6.5: Resistivity of EpoTEK 377 + 7.5% Ensaco 250P vs. polymerization time

Table 6.2: Investigated conditions for curing of massive samples

Curing time [hour]	Type of oven	Profile	Profile symbol
2	regular	-	P'1
2	controlled atmosphere	vacuum + air	P'2
10	regular	-	P'1
10	controlled atmosphere	vacuum + air	P'2

set to 150°C.

Fig. 6.6 reports the resistivity values vs. curing profiles for bars and test resistors. Table 6.3 presents the ratios on the one hand, between the values of resistivity of bars and test resistors cured for two hours in the same conditions and on the other hand, between the values of resistivity of test resistors and test resistors cured for two hours (when not specified the oven that was used is a regular one). Indeed, as the ideal case would be to be able to "predict" from standard data (i.e. for a standard curing of 2 hours), the resistivity of a bulk composite, the first ratio is of high importance. The other one is also interesting as it gives information about the evolution of the resistivity in thick-films with polymerization time.

First, we can notice that a decrease of the resistivity with the polymerization time is observed in both bars and test resistors measurements. If we look at the ratios reported in Table 6.3, we can notice that the polymerization time seems

not reported here.

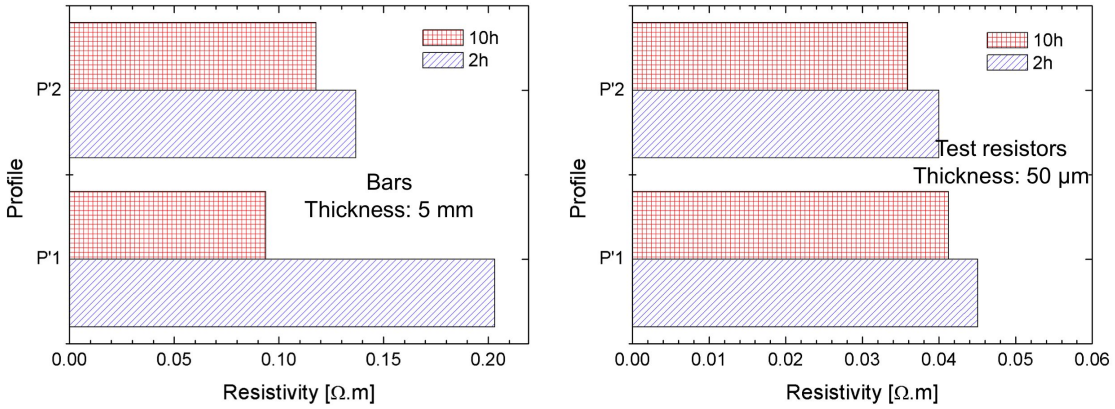

(a) (b)

Figure 6.6: Resistivity of EpoTEK 377 + 7.5% Ensaco 250P for different curing profiles: influence of the polymerization time on bars (a) and test resistors (b)

Table 6.3: Calculated resistivity ratios between bars and 2h-test resistors, and test resistors and 2h-test resistors

Curing profile	Ratios bars / test resistors (2h)	Ratios test resistors / test resistors (2h)
2h@150°C	5	1
2h@150°C, vacuum + air	4	1
10h@150°C	2	0.92
10h@150°C, vacuum + air	3	0.90

to have less effect upon the differences in resistivity between test resistors and bars (ratio of 4 to 3 in air). However, the effect is more noticeable when the samples are cured in a regular oven. Indeed, due to the layer thickness, a more significant amount of time is needed to evacuate the water contained in the polymer in the case of bars. By lengthening the polymerization time, the difference in resistivity diminished (ratio of 5 to 2).

The importance of the environment during the polymerization process was demonstrated. Indeed, for a 2-hour curing, the values of resistivity are quite similar (see Fig. 6.6b). Let us now look at the ratios of the resistivity values between test resistors vs. test resistors cured for 2h. By lengthening the polymerization time, we can see a small decrease in the resistivity.

Finally, tests using flexibilizer at 10%, 30% and 50% were made, as a flexible material is desired for the application. A curing of 10h at 150°C in a regular oven was chosen. We know that best results were not obtained in a regular oven. However, it is not always possible to use a controlled atmosphere oven,

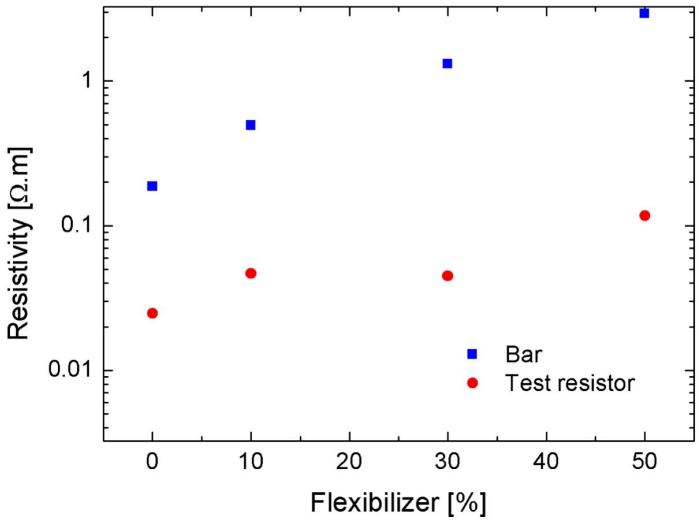

Figure 6.7: Resistivity of EpoTEK 377 + 7.5% Ensaco 250P: comparison between test resistors and bars and influence of the addition of flexibilizer

as we are limited in the size for the mould. Therefore, we preferred to perform this study in "normal" conditions. Fig. 6.7 presents the resistivity values that were obtained compared to the reference measurement (i.e. without flexibilizer) and Table 6.4 presents the ratios between resistivity values of test resistors and bars. We can see that the flexibilizer has a high influence upon resistivity. This is quite understandable as the matrix is modified by this addition, long chains being inserted into the epoxy. Ratios between the resistivity value of the test resistors and corresponding bars are high. Also, due to the flexibility of this new material, a strong piezoresistive effect is observed, which is unwanted here, as it precludes a well-defined resistivity value, casting doubt on the use of flexibilizer. An interesting effect can also be noticed. Indeed, flexibilizer seems to have a higher effect on bars than test resistors. This may be explained by the fact that, in the case of bars, the mechanical properties have a larger impact: the matrix can deform differently, the polymers chains are bigger, changing the arrangement of conducting particles inside the composite.

Table 6.4: Calculated ratios between the resistivity of test resistors and bars, influence of flexibilizer

Flexibilizer [%]	Ratios
0	8
10	11
30	29
50	25

6.3 Summary

In this chapter, we investigate the possible use of our resistive pastes for a specific application: fabrication of massive resistive objects allowing the control of resistivity of tools used for oil industry. These tools are of high importance during the construction of an oil well, as the resistivity measurements help in the determination of the rock nature and the presence of oil.

The different steps of a well fabrication were first reviewed in order to justify the need of our pastes. The main advantages are: large array of available resistivities, easiness of the process and transportable set-up.

Before fabricating massive objects, tests were carried out to determine the influence of the curing process and the polymerization time. Regular oven and controlled atmosphere oven were therefore used. The importance of the affinity of epoxy for water was once more highlighted. This has of course repercussions upon electrical properties. The better option would be to use a controlled atmosphere oven, which strongly enhances evacuation of water from the composite. Otherwise, to evacuate this residual water, it can be envisaged to leave the sample to polymerize for a longer time: the thicker the sample, the more time will be needed. We were therefore able to manufacture bulk objects with a quite low resistivity, albeit not as low as that attained with films, the systems being not as simple as it seemed. A good balance between polymerization time and heating speed must therefore be found.

The second part of the investigation was focused on having flexible samples in order to espouse the shape of the tool. Flexibilizer was mixed with the matrix at different percentages to fulfill this requirement. It was shown that this additive leads to an increase of the resistivity of the test resistors as well as the bars. This is quite understandable as the long chains are incorporated to the matrix, hence changing partly its chemistry and also possibly the arrangement of the conducting particles. Moreover, a significant piezoresistive effect was experimentally observed, which is undesirable for this application. We propose therefore to use a massive resistive block without any flexibilizer, contact being made with other materials such as conductive mud as in the field, or an artificial substitute thereof, such as gelified electrolyte.

Chapter 7

Conclusion

7.1 Conclusions

In a world where we tend to maximize integration of components in order to develop more and more efficient technological devices, percolative materials are of great interest. The aim of this work was to study systems formed by carbon-based fillers dispersed in a polymer matrix, and more specifically, epoxy-graphite composites. The use of polymer/graphite composites is very promising as they are easy to produce (only two components, a polymer matrix and a conductive filler) and to handle (ease of the process of fabrication). They also offer the advantage of being quite low cost compared to some others composites, such as those based on carbon nanotubes. The aim of this work was to characterize them, allowing a better understanding of these complex systems, and to propose adequate formulations of the final material in order to control and optimize the electrical and mechanical properties for the target applications.

The first step was to choose how to fabricate samples. As the starting material is a paste, screen-printing process appears as the most convenient and flexible way of deposition. A desired pattern can be applied on various substrates (alumina, aluminum...), the so-called thick-film resistors (TFRs) that result from this deposition can then be tested and characterized.

The use of screen-printing, although easy, engenders specific requirements regarding the paste's properties, especially its viscosity. The paste must have a thixotropic behavior, so that it can be pushed through the holes formed by the pattern on the screen by the squeegee pressure, and yet not spread out once on the substrate and keep a defined shape. The formulation of these composites was therefore investigated. Two epoxies having different *glass transition temperatures* T_{g} were chosen as matrices: EpoTEK 377 (low T_g) and Martens Plus (high T_g). Synthetic graphites from Timcal, Switzerland, with an

ellipsoidal shape and different particle sizes (4 µm, 15 µm and 44 µm) were used as fillers. For comparative purposes, expanded graphite (BNB90) and carbon black (Ensaco 250P) were also tested. At low graphite loadings, the paste may be too liquid to be screen-printed. The provided solution consisted in a dam and fill process: a dam in highly viscous epoxy was deposited, forming a cavity that could then be filled with the composite paste. At high filler loadings, the opposite effect may occur (too viscous paste). To control viscosity, we needed to find solvents that would be miscible with the resin, but remain inert, to avoid undesired chemical reactions. We used Hansen solubility parameter theory to predict the miscibility of different solvents in order to select a set of solvents for further testing. Controlled measurements on weight loss, resistivity and rheology were performed to attest the validity of our choices. This study highlighted the importance of water traces upon resistivity measurements, the epoxy having a high tendency to absorb water molecules contained in the air. We demonstrated that these solvents could be successfully used to tune the rheological properties of our composites, effectively allowing us to screen-print pastes with a much higher filler contents than otherwise possible. To complete our study, a structural characterization was done. Optical microscopy allowed us to ensure that our fabrication process led to composite that appeared homogeneous. We also noticed that, in between the large graphite particles, there are many small-size debris particles, which can promote conductivity. The structure of expanded graphite, and to a lesser extent carbon black, particles showed large irregularities: worm-like shape for the former and a mixture of aggregates and fine particles for the latter. The high specific surface area of these fillers is expected to lead to increased conductivities at low volume fractions of filler.

Finally, T_{g} of both epoxies and composites were determined with Differential Scanning Calorimetry (DSC). Results showed different behaviors depending on the epoxy: addition of filler decreases the T_{g} in the case of EpoTEK 377, whereas it increases the T_g in Martens Plus composites. This may be linked to their hardener type (resp. amine and acid anhydride), hence different polymerization mechanisms.

After having formulated and structurally characterized our composites, we focused on their functional characterization: electrical, mechanical and thermo-mechanical properties were investigated. The conductivity, as well as the piezoresistive response of our TFRs, was determined for various volume fractions, particle sizes, filler shapes and types and on different substrates. As expected, large specific surface area of the filler particles was shown to lead to higher conductivity for small volume fractions (case of expanded graphite and carbon black). Regarding thermal stability, we found that our materials displayed a cycling effect, their resistivity being permanently modified during thermal cycles. The importance of T_g was clear from these results as composites with higher T_g displayed better thermal stability. As far as piezoresistivity is concerned, it was found that the largest particles lead to a smaller gauge factor.

We think that this is linked to their higher aspect ratio. In order to prove the consistency of these different measurements, we derived a theoretical estimate of the difference in the Temperature Coefficient of Resistance (TCR) on different substrate as a function of the gauge factors, which was then compared to the one calculated from our resistivity measurements. Results were found to be coherent, which validates our measurements. Using a Dynamic Mechanical Analyzer (DMA) we were able to determine the storage modulus and the *glass transition temperature* of our composites. Addition of filler to the matrix and use of larger particles showed an increase of the stiffness of the material (higher storage modulus). We also showed that it was possible to enhance the mechanical properties of our composites by chemically altering the surface properties of our fillers and creating favorable interactions between the filler and the epoxy matrix. This was achieved through an oxidation process, used to create -OH, -COOH and =CO groups on the surface of the graphite particles that could potentially react with the epoxy. This oxidation was carried out in concentrated nitric acid, and was confirmed by XPS analysis to lead to the apparition of oxygen atoms at the surface of the graphite. A better adhesion matrix/particles was demonstrated with the achievement of a higher storage modulus. Finally, thermal expansion of the composites was measured with an optical dilatometer. A particular and very interesting effect was observed with the EpoTEK 377 matrix: a one-time shrinkage around T_{g}. This effect is explained by the relaxation of the residual stress-strain around T_g, enabled by the softening of the matrix, and is decreased with increased the filler volume fraction, the particle size and the use of flake-shaped filler. It also confirmed the "cycling effect" that was found in the measurements of thermal stability of resistivity. The values of T_{g} determined by three different methods, namely DSC, DMA and dilatometry were compared and found to be coherent.

In the two last chapters, we investigated potential applications of our composites. The first challenge was to show they could be used to fabricate low-cost microdevices, such as cantilevers, membranes or microfluidic circuits. Sacrificial layers are quite commonly used, in mineral thick-film technology, for the fabrication of such devices, but none of the existing ones were suitable for our purpose, as they involve high temperatures during the evaporation/sublimation process. As our over-layers (i.e. our composites) are polymers with a low degradation temperature, we needed to develop entirely new sacrificial layers that would function without damaging them. In order to be able to fabricate completely closed structures, we decided to focus on sublimable compounds, so that our sacrificial layer could sublimate and diffuse through the over-layer. Using systems based on polyols, organic sublimable sacrificial pastes that can be dried, over-printed and evaporated at temperatures as low as 150°C were successfully formulated. Trimethylolethane (TME) was the main sacrificial material and it was combined with trimethylolpropane (TMP), neopentyl glycol (NPG) and 2,5-dimethyl-2,5-hexanediol (DMHD). Dissolved in a mixture of solvents based on cyclohexanol, creamy screen-printable pastes were obtained.

Interactions due to molecular affinity were demonstrated between these systems and epoxies, making difficult the use of our regular composites. Over-layers in silicone and ethylcellulose, both loaded with graphite, were developed and allowed us to fabricate usable microstructures. As the microdevices created by this process are only composed of organic and non-toxic materials, this process presents a very high potential for applications requiring biocompatibility.

The second application consists in recreating a dummy and yet representative rock to help in the quality control of measuring tools used in the oil industry. Indeed, when drilling a well, resistivity measurements are performed to determine the type of rock and the presence/absence of oil in the formation. The use of composites based on polymer and carbon-based filler presents several advantages: large array of available resistivities, easiness of the process and transportable set-up. Test resistors were first made in order to test the influence, of the curing profile on the one hand and of the polymerization time on the other. It was shown that conductivity was increased when the polymerization occurred in a controlled atmosphere. It indeed prevents the reaction between epoxy and water molecules by speeding up the removal of the latter. The cycling effect was once more confirmed with the polymerization time, a longer one leading to a smaller resistivity value (elimination of residual water). Finally, bulk objects were manufactured with a quite low resistivity, albeit not as low as that attained with films, the systems being not as simple as it seemed. A good balance between polymerization time and heating speed must be found.

Overall, this thesis allowed us to get a better understanding of the systems formed by epoxy and graphite. From that perspective, we were able to:

- formulate and in particular tune these materials with solvents, which can be of high importance for different applications
- measure the electrical, mechanical and thermo-mechanical properties of these composites, which allowed us to link the different observations and propose explanations about the behavior of these particular materials
- fabricate bulk resistive objects while controlling their resistivity (better understanding of the polymerization process) and microdevices based on organic sublimable sacrificial layers

Although much remains to be done, the extensive formulation and characterization work accomplished during this thesis, have given us the fundamental tools and knowledge that will hopefully lead to many commercial applications of these materials in the future.

7.2 Outlook: open questions induced by this work

As expected, some questions have also arisen in the course of this thesis and remain open at this time. We will detail them hereafter.

7.2.1 Compatibility of sacrificial layers?

Chapter 5 was dedicated to the formulation of organic sacrificial layers. Polyols were therefore chosen for their ability to sublimate at relatively low temperature (150°C). However, due to their high polarity, we also highlighted the fact that these materials tend to react with the epoxy, leading to the collapse of the structures. Consequently, we proposed to use silicone and/or ethylcellulose as over-layers, instead of epoxy-graphite composites. Depending on the application, a more rigid material may be desired, for instance for the manufacturing of cantilevers. Our solution was to use ethylcellulose loaded with graphite, but this polymer is quite sensitive to temperature and requires lower application temperatures than epoxy or silicone.

The use of secondary, or even tertiary alcohols or polyols, instead of primary ones such as NPG, TME and TMP, may diminish the reactivity of the sacrificial paste with the over-layer (hydroxyl groups being otherwise desirable to impart suitable viscosity to the paste). One idea could be for instance to change the proportions of DMHD (tertiary diol) in the system TME/DMHD and study the affinity with the epoxy. Due to the high potential of these all-polymeric and biocompatible structures, we think that it is of great interest to continue the research on these compounds.

7.2.2 Interactions with the substrate?

The first question concerns the interactions with the substrate. Indeed, when working on alumina, no interaction is possible between the two materials, alumina being quite inert. However, one of the advantages of thick-film resistors based on polymer matrix is the curing temperature. As it is significantly lower than that of mineral TFRs, other materials can be envisaged as substrate, such as PCBs. Therefore, the question of the compatibility between substrates and thick-film layers must be investigated.

In this study we have performed tests on alumina, aluminum and phenolic resin (see 4.1.2.4). On aluminum substrate, interactions between the epoxy-based dielectric and the thick-film resistors were observed, the monomers of the resistor resin diffusing inside the dielectric. Indeed as the T_g of both resin and dielectric are exceeded, the materials become rubbery and can diffuse extensively and react between each other. This reasoning may be extended to a PCB substrate. PCB is an epoxy resin pre-preg (i.e. with fibers) and has of course also a glass transition temperature, which varies but is generally above 120°C. Depending on the over-layer (for instance a high T_g epoxy such as Martens Plus), this temperature can be exceeded. Based on different studies (in particular Cognard [172]) interactions can occur, which will modify the behavior of the final composite. Indeed the diffusion of monomers at the bottom of the resistor into the substrate will raise the volume fraction of conductive particles there, resulting into a higher conductivity.

The opposite effect can be envisaged. For some applications, it may be desired to coat the thick-film resistor with also an epoxy resin, for instance, or another polymer. As the composite has already polymerized, the monomers from the coating can diffuse inside the thick-film and form chains, in this case decreasing the conductive material volume fraction at the top of the resistor, resulting into a smaller conductivity.

These effects remain at the moment neither well quantified nor defined and few studies can be found. For a better understanding and with the purpose of expanding the potential applications field, investigation should be made.

7.2.3 Model of the conductivity inside these composites?

In Part 4.1.2.5, we have calculated the estimated values of the conductivity from the equations developed by Ambrosetti. We have highlighted the fact that our composites follow the "debris model", i.e. the conductivity is driven by the small conductive debris of the particles dispersed in the insulating matrix. Ambrosetti proposed a model for his debris model, where he has expressed the debris number density as [94]:

$$d_d = \lambda \frac{\phi}{1-\phi} \tag{7.1}$$

where λ is a proportionality constant and Φ the volume fraction. This allowed him to express the conductivity of the matrix with debris dispersed in it as:

$$\sigma \simeq \sigma_0 exp\left(-\frac{3.5\, d_d^{-1/3}}{\xi}\right) \tag{7.2}$$

However, when trying to fit our results using these two equations, we were not able to do proper simulation. This leads us to assume that the debris number density should be refined. Likewise, at the moment, we are not able to propose a correct expression of the conductivity in composites with expanded graphite, the peculiar particle shape, making any potential simulation quite difficult.

7.2.4 Influence of the external conditions during the polymerization?

In Chapter 6, we have highlighted the fact that, depending on the external conditions during the polymerization, resistive properties of the final composite can be altered. It was shown that, due to its chemistry, epoxy has a tendency to catch the water contained in the air. This effect becomes more important when manufacturing massive objects.

When looking more deeply into the chemical components, it has been proven that it is the amine (i.e. the hardener for some epoxies) that tends to

catch water molecules, as well as the CO_2. It is actually a known industrial problem, referred as "amine blush" or "sweating" [202–205]. Manufacturers try to minimize the amine blush by using for instance amine adducts which pre-react with epoxide groups.

However, the water may still disturb the system. In our case, we got round the problem by lengthening the polymerization time in order for the water molecules to diffuse from the composite. Other options could be investigated, such as the addition of drying agent inside the resin, or put the hardener in the vacuum prior to make the paste. More detailed investigations need therefore to be carried out.

7.2.5 Interactions of the matrix with the filler?

In Chapter 3, we have detailed the functionalization process through oxidation in nitric acid of the graphite particles. The purpose of this functionalization was the creation of -OH, -COOH and =CO groups on the surface that can react afterwards with the polar groups of the epoxy. The validity of this process was demonstrated in Chapter 4. We mechanically tested composites formulated with oxidized graphite particles. We obtained a higher Young's modulus for this composites compared to the ones with standard graphite. From literature [129, 130], we can deduce that bonds were formed between graphite and epoxy, resulting in a stiffer material. However, due to its poor chemical affinity with epoxy, graphite tends to agglomerate [177]. The oxidation may also have the effect to provide a better dispersion of the particles inside the matrix, hence the higher modulus. This is probably a combination of both effects, but it is of high interest to understand the reactions that occur inside the composite, for instance with SEM (Scanning Electron Microscopy). If oxidized graphite provides indeed a better dispersion, this may result in the achievement of a more stable material, which is of high interest for industrial applications (sensors for instance).

Nevertheless, due to the wide range of potential applications offered by these materials, we think that it worth continuing the theoretical effort that should lead to a better understanding of these materials.

Bibliography

[1] C.M. Williams, M.A. Nash, and L.A. Poole-Warren. Electrically conductive polyurethanes for biomedical applications. volume 5651, pages 329–335, Sydney, NSW, 2005. Conference of Biomedical Applications of Micro- and Nanoengineering II; Conference Date: 13 December 2004 through 15 December 2004. 1

[2] E. Fortunati, F. D'Angelo, S. Martino, A. Orlacchio, J.M. Kenny, and I. Armentano. Carbon nanotubes and silver nanoparticles for multifunctional conductive biopolymer composites. *Carbon*, 49(7):2370–2379, 2011. 1

[3] J.D. Stenger-Smith. Intrinsically electrically conducting polymers. synthesis, characterization, and their applications. *Progress in Polymer Science (Oxford)*, 23(1):57–79, 1998. 2

[4] A. Kokil. *Conjugated polymer networks: synthesis and properties*. PhD thesis, Case Western Reserve University, 2005. 2

[5] A.O. Patil, Y. Ikenoue, N. Basescu, N. Colaneri, J. Chen, F. Wudl, and A.J. Heeger. Self-doped conducting polymers. *Synthetic Metals*, 20(2):151–159, 1987. 2

[6] H-C. Kim, J-C. Kim, S. Baek, and M. Ree. Functional polythiophene bearing hydroxyethyl groups and their derivatives. *Macromolecular Research*, 14:173–178, 2006. 2

[7] P.F. Carcia, A. Suna, and W.D. Childers. Electrical conduction and strain sensitivity in ruo2 thick film resistors. *Journal of Applied Physics*, 54(10):6002–6008, 1983. 2

[8] S. Vionnet-Menot, C. Grimaldi, T. Maeder, P. Ryser, and S. Straessler. Study of electrical properties of piezoresistive pastes and determination of the electrical transport. *Journal of the European Ceramic Society*, 25(12 SPEC. ISS.):2129–2132, 2005. 2, 16

[9] T. Maeder, C. Jacq, C. Grimaldi, and P. Ryser. Lead-free low-firing thick-film resistor based on bismuth glasses and ruthenium oxide. In

Proceedings, XXXIII International Conference IMAPS Poland Chapter, pages 222–229, Gliwice, 2009. 2

[10] L.-M. Huang, T.-C. Wen, and A. Gopalan. Electrochemical and spectroelectrochemical monitoring of supercapacitance and electrochromic properties of hydrous ruthenium oxide embedded poly(3,4-ethylenedioxythiophene)-poly(styrene sulfonic acid) composite. *Electrochimica Acta*, 51(17):3469–3476, 2006. 2

[11] W. Caseri. Color switching in nanocomposites comprising inorganic nanoparticles dispersed in a polymer matrix. *Journal of Materials Chemistry*, 20(27):5582–5592, 2010. 2

[12] A. Bjorneklett, L. Halbo, and H. Kristiansen. Thermal conductivity of epoxy adhesives filled with silver particles. *International Journal of Adhesion and Adhesives*, 12(2):99–104, 1992. 3

[13] I. Krupa, G. Miková, I. Novák, I. Janigová, Z. Nógellová, F. Lednický, and J. Prokes. Electrically conductive composites of polyethylene filled with polyamide particles coated with silver. *European Polymer Journal*, 43:2401–2413, 2007. 3

[14] M. Azizi, W. Schneider, and W. Plieth. Electrolytic co-deposition of silicate and mica particles with zinc. *Journal of Solid State Electrochemistry*, 9(6):429–437, 2005. 3

[15] J. Wieczorek and J. Sleziona. Sliver matrix composites reinforced with galvanically silvered particles. *Archives of Materials Science and Engineering*, 28:475–478, 2007. 3

[16] ICBA. Carbon black user's guide- safety, health and environmental information, June 2004. 5

[17] C. Jaeger, T. Henning, R. Schloegl, and O. Spillecke. Spectral properties of carbon black. *Journal of Non-Crystalline Solids*, 258(1):161–179, 1999. 5

[18] W. Zhu, D.E. Miser, W.G. Chan, and M.R. Hajaligol. Hrtem investigation of some commercially available furnace carbon blacks. *Carbon*, 42(8-9):1841–1845, 2004. 5

[19] T. Jawhari, A. Roid, and J. Casado. Raman spectroscopic characterization of some commercially available carbon black materials. *Carbon*, 33(11):1561–1565, 1995. 6

[20] R.E. Franklin. The interpretation of diffuse x-ray diagrams of carbon. *Acta Crystallographica*, 3:107–121, 1950. 6

[21] Timcal. Timrex graphite and ensaco carbon black- carbon additives for polymer compounds. Technical report, Timcal. 6

[22] O.A. Al-Hartomy, F. Al-Solamy, A. Al-Ghamdi, N. Dishovsky, M. Ivanov, M. Mihaylov, and F. El-Tantawy. Influence of carbon black structure and specific surface area on the mechanical and dielectric properties of filled rubber composites. *International Journal of Polymer Science*, 2011. 6

[23] M. Kozlowski and A. Kozlowska. Comparison of electrically conductive fillers in polymer systems. *Macromolecular Symposia*, 108:261–268, 1996. 6

[24] N.C. Das, D. Khastgir, T.K. Chaki, and A. Chakraborty. Electromagnetic interference shielding effectiveness of carbon black and carbon fibre filled eva and nr based composites. *Composites Part A: Applied Science and Manufacturing*, 31(10):1069–1081, 2000. 6

[25] Avrom I. Medalia. Electrical conduction in carbon black composites. *Rubber Chemistry and Technology*, 59(3):432–454, 1986. 6

[26] R.A. Antunes, M.C.L. De Oliveira, G. Ett, and V. Ett. Carbon materials in composite bipolar plates for polymer electrolyte membrane fuel cells: A review of the main challenges to improve electrical performance. *Journal of Power Sources*, 196(6):2945–2961, 2011. 6

[27] D.M. Bigg and D.E. Stutz. Plastic composites for electromagnetic interference shielding applications. *Polymer Composites*, 4(1):40–46, 1983. 6

[28] A.L. Dicks. The role of carbon in fuel cells. *Journal of Power Sources*, 156(2):128–141, 2006. 6

[29] J.B. Donnet. Structure and reactivity of carbons: from carbon black to carbon composites. *Carbon*, 20:267–282, 1982. 6

[30] V. Lavrentiev, J. Vacik, and H. Naramoto. Structural phenomena in glassy carbon induced by cobalt ion implantation. *Applied Physics A: Materials Science and Processing*, 92(3):673–680, 2008. 6

[31] I.W. Chiang, B.E. Brinson, R.E. Smalley, J.L. Margrave, and R.H. Hauge. Purification and characterization of single-wall carbon nanotubes. *Journal of Physical Chemistry B*, 105(6):1157–1161, 2001. xi, 7

[32] C. Gommes, S. Blacher, K. Masenelli-Varlot, Ch. Bossuot, E. McRae, A. Fonseca, J.-B. Nagy, and J.-P. Pirard. Image analysis characterization of multi-walled carbon nanotubes. *Carbon*, 41(13):2561–2572, 2003. xi, 7

[33] T.W. Ebbesen and P.M. Ajayan. Large-scale synthesis of carbon nanotubes. *Nature*, 358(6383):220–222, 1992. 7

[34] T. Guo, P. Nikolaev, A.G. Rinzler, D. Tománek, D.T. Colbert, and R.E. Smalley. Self-assembly of tubular fullerenes. *Journal of Physical Chemistry*, 99(27):10694–10697, 1995. 7

[35] T. Guo, P. Nikolaev, A. Thess, D.T. Colbert, and R.E. Smalley. Catalytic growth of single-walled manotubes by laser vaporization. *Chemical Physics Letters*, 243(1-2):49–54, 1995. 7

[36] A. Peigney, P. Coquay, E. Flahaut, R.E. Vandenberghe, E. De Grave, and C. Laurent. A study of the formation of single- and double-walled carbon nanotubes by a cvd method. *Journal of Physical Chemistry B*, 105(40):9699–9710, 2001. 7

[37] E.T. Thostenson, Z. Ren, and T.-W. Chou. Advances in the science and technology of carbon nanotubes and their composites: A review. *Composites Science and Technology*, 61(13):1899–1912, 2001. 7

[38] K. Kim, K. Shin, J.-H. Han, K.-R. Lee, W.-H. Kim, K.-B. Park, B.-K. Ju, and J.J. Pak. Deformable single wall carbon nanotube electrode for transparent tactile touch screen. *Electronics Letters*, 47(2):118–120, 2011. 7

[39] M. Jakubowska, M. Lukasik, A. Mlozniak, and M. Sloma. Contact resistance of polymer thick-films filled with carbon nanotubes. In *XXXII International Conference of IMAPS-CPMT IEEE Poland, Pultusk*, 2008. 7

[40] S. Iijima. Helical microtubules of graphitic carbon. *Nature*, 354(6348):56–58, 1991. 8

[41] M. Monthioux and V.L. Kuznetsov. Who should be given the credit for the discovery of carbon nanotubes? *Carbon*, 44(9):1621–1623, 2006. 8

[42] S. Iijima and T. Ichihashi. Single-shell carbon nanotubes of 1-nm diameter. *Nature*, 363(6430):603–605, 1993. 8

[43] D.S. Bethune, C.H. Kiang, M.S. De Vries, G. Gorman, R. Savoy, J. Vazquez, and R. Beyers. Cobalt-catalysed growth of carbon nanotubes with single-atomic-layer walls. *Nature*, 363(6430):605–607, 1993. 8

[44] L.V. Radushkevich and V.M. Lukyanovich. O strukture ugleroda, obrazujucegosja pri termiceskom razlozenii okisi ugleroda na zeleznom kontakte. *Zh. Fiz. Khim.*, 26(1):88–95, 1952. 8

[45] M. Hillert and N. Lange. The structure of graphite filaments. *Z. Krist.*, 111:24–34, 1958. 8

[46] R.T.K. Baker, P.S. Harris, R.B. Thomas, and R.J. Waite. Formation of filamentous carbon from iron, cobalt and chromium catalyzed decomposition of acetylene. *Journal of Catalysis*, 30(1):86–95, 1973. 8

[47] A.K. Geim and K.S. Novoselov. The rise of graphene. *Nature Materials*, 6(3):183–191, 2007. xi, 8, 9

[48] A.K. Geim. Graphene: Status and prospects. *Science*, 324(5934):1530–1534, 2009. 8

[49] K.S. Novoselov, A.K. Geim, S.V. Morozov, D. Jiang, Y. Zhang, S.V. Dubonos, I.V. Grigorieva, and A.A. Firsov. Electric field in atomically thin carbon films. *Science*, 306(5696):666–669, 2004. 8

[50] W.A. de Heer, C. Berger, X. Wu, P.N. First, E.H. Conrad, X. Li, T. Li, M. Sprinkle, J. Hass, M.L. Sadowski, M. Potemski, and G. Martinez. Epitaxial graphene. *Solid State Communications*, 143(1-2):92–100, 2007. 8

[51] C. Lee, X. Wei, J.W. Kysar, and J. Hone. Measurement of the elastic properties and intrinsic strength of monolayer graphene. *Science*, 321(5887):385–388, 2008. 8, 11, 23

[52] J.D. Fowler, M.J. Allen, V.C. Tung, Y. Yang, R.B. Kaner, and B.H. Weiller. Practical chemical sensors from chemically derived graphene. *ACS Nano*, 3(2):301–306, 2009. 8

[53] J.T. Robinson, F.K. Perkins, E.S. Snow, Z. Wei, and P.E. Sheehan. Reduced graphene oxide molecular sensors. *Nano Letters*, 8(10):3137–3140, 2008. 8

[54] F. Schedin, A.K. Geim, S.V. Morozov, E.W. Hill, P. Blake, M.I. Katsnelson, and K.S. Novoselov. Detection of individual gas molecules adsorbed on graphene. *Nature Materials*, 6(9):652–655, 2007. 8

[55] M.C. Lemme, T.J. Echtermeyer, M. Baus, and H. Kurz. A graphene field-effect device. *IEEE Electron Device Letters*, 28(4):282–284, 2007. 9

[56] M.C. Lemme. Current status of graphene transistors. *Diffusion and Defect Data Pt.B: Solid State Phenomena*, 156-158:499–509, 2009. Conference of 13th International Autumn Meeting - Gettering and Defect Engineering in Semiconductor Technology, GADEST 2009; Conference Date: 26 September 2009 through 2 October 2009; Conference Code: 79253. 9

[57] X. Wang, L. Zhi, and K. Muellen. Transparent, conductive graphene electrodes for dye-sensitized solar cells. *Nano Letters*, 8(1):323–327, 2008. 9

[58] J. Wu, H.A. Becerril, Z. Bao, Z. Liu, Y. Chen, and P. Peumans. Organic solar cells with solution-processed graphene transparent electrodes. *Applied Physics Letters*, 92(26), 2008. 9

[59] N. Mohanty and V. Berry. Graphene-based single-bacterium resolution biodevice and dna transistor: Interfacing graphene derivatives with nanoscale and microscale biocomponents. *Nano Letters*, 8(12):4469–4476, 2008. 9

[60] B. Song, D. Li, W. Qi, M. Elstner, C. Fan, and H. Fang. Graphene on au(111): A highly conductive material with excellent adsorption properties for high-resolution bio/nanodetection and identification. *ChemPhysChem*, 11(3):585–589, 2010. 9

[61] L.I. Aksel'rod, D.E. Denisov, Yu.V. Materikin, N.G. Khudyakov, A.A. Evstigneeva, N.A. Mashkovtseva, and G.M. Kharitonov. Production of refractories from graphite metallurgical waste products. *Refractories*, 28(1-2):40–43, 1987. 10

[62] I.G. Fuks, E.B. Ivankina, A.P. Kozlovtsev, and A. Luksa. Lubricating oils with ultrafine molybdenum disulfide or graphite as an additive (review). *Chemistry and Technology of Fuels and Oils*, 11(7-8):652–656, 1975. 10

[63] G. Juri, H-A Wihlhelm, and J. L'Heureux. High-purity graphite powders for high performance. Technical report, Timcal. 10

[64] I. Novák and I. Krupa. Electro-conductive resins filled with graphite for casting applications. *European Polymer Journal*, 40:1417–1422, 2004. 10

[65] J.-F. Zou, Z.-Z. Yu, Y.-X. Pan, X.-P. Fang, and Y.-C. Ou. Conductive mechanism of polymer/graphite conducting composites with low percolation threshold. *Journal of Polymer Science- Part B: Polymer Physics*, 40:954–963, 2002. 10

[66] J. Cho, J.J. Luo, and I.M. Daniel. Mechanical characterization of graphite/epoxy nanocomposites by multi-scale analysis. *Composites Science and Technology*, 67:2399–2407, 2007. 10, 24

[67] K. Nagata, H. Iwabuki, and H. Nigo. Effect of particle size of graphites on electrical conductivity of graphite/polymer composite. *Composite Interfaces*, 6:483–495, 1999. 10

[68] I. Krupa, I. Novák, and I. Chodák. Electrically and thermally conductive polyethylene/graphite composites and their mechanical properties. *Synthetic Metals*, 145(2-3):245–252, 2004. 10, 24

[69] L. Du and S.C. Jana. Highly conductive epoxy/graphite composites for bipolar plates in proton exchange membrane fuel cells. *Journal of Power Sources*, 172:734–741, 2007. 10

[70] N. Serra, T. Maeder, P. Lemaire, and P. Ryser. Formulation of composite resistive pastes for fabrication of micro-heaters. *Sensors and Actuators, A: Physical*, 162:367–372, 2010. 10, 41, 68

[71] A. Yasmin, J.-J. Luo, and I.M. Daniel. Processing of expanded graphite reinforced polymer nanocomposites. *Composites Science and Technology*, 66:1182–1189, 2006. xi, 10, 11

[72] A. Celzard, E. McRae, J.F. Marêché, G. Furdin, M. Dufort, and C. Deleuze. Composites based on micron-sized exfoliated graphite particles: electrical conduction, critical exponents and anisotropy. *J. Phys. Chem. Solids*, 57:715–718, 1996. 10

[73] I.M. Afanasov, D.V. Savchenko, S.G. Ionov, D.A. Rusakov, A.N. Seleznev, and V.V. Avdeev. Thermal conductivity and mechanical properties of expanded graphite. *Inorganic Materials*, 45(5):486–490, 2009. 10

[74] A. Celzard, M. Krzesinska, D. Bégin, J.F. Marêché, S. Puricelli, and G. Furdin. Preparation, electrical and elastic properties of new anisotropic expanded graphite-based composites. *Carbon*, 40:557–566, 2002. 10

[75] K. Kalaitzidou, H. Fukushima, and L.T. Drzal. Mechanical properties and morphological characterization of exfoliated graphite-polypropylene nanocomposites. *Composites Part A: applied science and manufacturing*, 38:1675–1682, 2007. 10, 24

[76] L.N. Song, M. Xiao, and Y.Z. Meng. Electrically conductive nanocomposites of aromatic polydisulfide/expanded graphite. *Composites Science and Technology*, 66:2156–2162, 2006. 10

[77] C. Ciadella, T.M. Gruenberger, E. Grivei, and N. Probst. Expanded graphite offers new opportunities. *Plastics Additives & Compounding*, pages 40–41, 2008. xi, 11

[78] P.E. Khizhnyak, A.V. Chechetkin, and A.P. Glybin. Thermal conductivity of carbon black. *Journal of Engineering Physics*, 37(3):1073–1075, 1980. 11

[79] D.G. Fink and Beaty H.W. *Standard handbook for electrical engineers*. McGraw-Hill, 1978. 11

[80] E. Dervishi, Z. Li, Y. Xu, V. Saini, A.R. Biris, D. Lupu, and A.S. Biris. Carbon nanotubes: Synthesis, properties, and applications. *Particulate Science and Technology*, 27(2):107–125, 2009. 11, 23

[81] P. Kim, L. Shi, A. Majumdar, and P.L. McEuen. Thermal transport measurements of individual multiwalled nanotubes. *Physical Review Letters*, 87(21):2155021–2155024, 2001. 11

[82] E. Pop, D. Mann, Q. Wang, K. Goodson, and H. Dai. Thermal conductance of an individual single-wall carbon nanotube above room temperature. *Nano Letters*, 6(1):96–100, 2006. 11

[83] Q. Li, Y. Li, X. Zhang, S.B. Chikkannanavar, Y. Zhao, A.M. Dangelewicz, L. Zheng, S.K. Doorn, Q. Jia, D.E. Peterson, P.N. Arendt, and Y. Zhu. Structure-dependent electrical properties of carbon nanotube fibers. *Advanced Materials*, 19(20):3358–3363, 2007. 11

[84] A.A. Balandin, S. Ghosh, W. Bao, I. Calizo, D. Teweldebrhan, F. Miao, and C.N. Lau. Superior thermal conductivity of single-layer graphene. *Nano Letters*, 8(3):902–907, 2008. 11

[85] J.-H. Chen, C. Jang, S. Xiao, M. Ishigami, and M.S. Fuhrer. Intrinsic and extrinsic performance limits of graphene devices on sio 2. *Nature Nanotechnology*, 3(4):206–209, 2008. 11

[86] A. Yasmin and I.M. Daniel. Mechanical and thermal properties of graphite platelet/epoxy composites. *Polymer*, 45(24):8211–8219, 2004. 11, 23, 24

[87] R.L. Powell and G.E. Childs. *American Institute of Physics Handbook*. McGraw-Hill, 1972. 11

[88] C.A. Poland, R. Duffin, I. Kinloch, A. Maynard, W.A.H. Wallace, A. Seaton, V. Stone, S. Brown, W. MacNee, and K. Donaldson. Carbon nanotubes introduced into the abdominal cavity of mice show asbestos-like pathogenicity in a pilot study. *Nature Nanotechnology*, 3(7):423–428, 2008. 12

[89] O. Akhavan and E. Ghaderi. Toxicity of graphene and graphene oxide nanowalls against bacteria. *ACS Nano*, 4(10):5731–5736, 2010. 12

[90] M. Endo. Carbon nanotubes: State-of-the-art technology and safety for success. *Indian Journal of Engineering and Materials Sciences*, 17(5):317–320, 2010. 12

[91] C.L. Geraci and V. Castranova. Challenges in assessing nanomaterial toxicology: A personal perspective. *Wiley Interdisciplinary Reviews: Nanomedicine and Nanobiotechnology*, 2(6):569–577, 2010. 12

[92] K.P. Menard. *Dynamic mechanical analysis- a pratical introduction*. Taylor & Francis Group, LLC, 2008. xiii, 14, 84, 87, 89, 90, 93

[93] T. Kuilla, S. Bhadra, D. Yao, N.H. Kim, S. Bose, and J.H. Lee. Recent advances in graphene based polymer composites. *Progress in Polymer Science (Oxford)*, 35(11):1350–1375, 2010. 14

[94] G. Ambrosetti. *On the insulator-conductor transition in polymer nanocomposites*. PhD thesis, Ecole Polytechnique Fédérale de Lausanne, 2010. xii, 15, 65, 72, 73, 79, 80, 162

[95] N. Johner. *On the origin of transport non-universality and piezoresistivity in segregated conductor-insulator composites and application to thick-film resistos*. PhD thesis, Ecole Polytechnique Fédérale de Lausanne, 2009. 15, 16

[96] S. Kirkpatrick. Percolation and conduction. *Reviews of Modern Physics*, 45(4):574–588, 1973. 15

[97] D.B. Gingold and C.J. Lobb. Percolative conduction in three dimensions. *Physical Review B*, 42(13):8220–8224, 1990. 16

[98] I. Balberg. Tunneling and nonuniversal conductivity in composite materials. *Physical Review Letters*, 59, 1987. 16

[99] G. Ambrosetti, C. Grimaldi, I. Balberg, T. Maeder, A. Danani, and P. Ryser. Solution of the tunneling-percolation problem in the nanocomposite regime. *Physical Review B - Condensed Matter and Materials Physics*, 81(15), 2010. 16, 70

[100] S. Vionnet-Menot. *Low firing temperature thick-film piezoresistive composites- Properties and conduction mechanism*. PhD thesis, Ecole Polytechnique Fédérale de Lausanne, 2005. xi, 16, 26, 27, 38

[101] S. Vionnet-Menot, C. Grimaldi, T. Maeder, S. Straessler, and P. Ryser. Tunneling-percolation origin of nonuniversality: theory and experiments. *Physical Review B*, 71, 2005. 17

[102] C. Canali, D. Malavasi, B. Morten, M. Prudenziati, and A. Taroni. Piezoresistive effects in thick-film resistors. *Journal of Applied Physics*, 51(6):3282–3288, 1980. 18

[103] M. Hrovat, D. Belavic, Z. Samardzija, and J. Holc. A characterisation of thick film resistors for strain gauge applications. *Journal of Materials Science*, 36(11):2679–2689, 2001. 18

[104] C. Grimaldi, P. Ryser, and S. Straessler. Gauge factor enhancement driven by heterogeneity in thick-film resistors. *Journal of Applied Physics*, 90(1):322–327, 2001. 18, 80

[105] C. Grimaldi, P. Ryser, and S. Straessler. Anisotropic random resistor networks: A model for piezoresistive response of thick-film resistors. *Journal of Applied Physics*, 92(4):1981, 2002. 18, 20

[106] C.R. Pichard, C.R. Tellier, and A.J. Tosser. Three-dimensional analytical expressions of strain gauge coefficients of infinitely thick polycrystalline metal films. *Journal of Materials Science*, 15(12):2991–2994, 1980. 18

[107] D.G. Bellow, G. Ford, and J.S. Kennedy. Anticlastic behavior of flat plates - the mode of transverse distortion in a rectangular plate subjected to large longitudinal curvatures depends on the dimensionless parameter b2/rt. using a numerical technique, experimental results are shown to agree with theory for b2/rt values up to 50. *Experimental Mechanics*, 5(7):227–232, 1965. 19

[108] H.D. Conway and W.E. Nickola. Anticlastic action of flat sheets in bending - analytical expressions for the stresses in bent elastic strips are obtained and found to agree very well with experimental results. *Experimental Mechanics*, 5(4):115–119, 1965. xi, 19

[109] W.D. Ryden, A.W. Lawson, and C.C. Sartain. Electrical transport properties of iro2 and ruo2. *Physical Review B*, 1(4):1494–1500, 1970. 20

[110] S. Achmatowicz, M. Bartholomew, M. Coleman, D. Dean, A. Hobby, M. Jakubowska, K. Pitt, and Q. Reynolds. *Handbook of thick-film technology*. Electrochemical Publications, 2005. xi, 20, 27, 28

[111] S.J. Record. *The mechanical properties of wood*. John Wiley & Sons, 1914. 21

[112] J. Li, B.Y. Zong, Y.M. Wang, and W.B. Zhuang. Experiment and modeling of mechanical properties on iron matrix composites reinforced by different types of ceramic particles. *Materials Science and Engineering: A*, 527:7545–7551, 2010. 23

[113] N. Mourik, Y.C. Chen, and K. Salama. Nondestructive determination of the elastic anisotropy in aluminum-sic and -al2o3 metal-matrix composites. *Research in Nondestructive Evaluation*, 11(1):1–13, 1999. 23

[114] K.C. Yung, B.L. Zhu, T.M. Yue, and C.S. Xie. Preparation and properties of hollow glass microsphere-filled epoxy-matrix composites. *Composites Science and Technology*, 69(2):260–264, 2009. 23

[115] W. Zhou. Effect of coupling agents on the thermal conductivity of aluminum particle/epoxy resin composites. *Journal of Materials Science*, 46(11):3883–3889, 2011. 23

[116] L.G.B. Manhani, L.C. Pardini, and F.L. Neto. Assessement of tensile strength of graphites by the iosipescu coupon test. *Materials Research*, 10(3):233–239, 2007. 23

[117] L.-F. Wang and Q.-S. Zheng. Extreme anisotropy of graphite and single-walled carbon nanotube bundles. *Applied Physics Letters*, 90(15), 2007. 23

[118] S. Bhadra, P.P. De, N. Mondal, R. Mukhapadhyaya, and S. Das Gupta. Regeneration of carbon black from waste automobile tires. *Journal of Applied Polymer Science*, 89(2):465–473, 2003. 23

[119] M. Kojima, M. Tosaka, Y. Ikeda, and S. Kohjiya. Devulcanization of carbon black filled natural rubber using supercritical carbon dioxide. *Journal of Applied Polymer Science*, 95(1):137–143, 2005. 23

[120] N. Abdel-Aal, F. El-Tantawy, A. Al-Hajry, and M. Bououdina. Epoxy resin/plasticized carbon black composites. part ii. correlation among network structure and mechanical properties. *Polymer Composites*, 29(7):804–808, 2008. 23

[121] R.S. Ruoff, D. Qian, and W.K. Liu. Mechanical properties of carbon nanotubes: Theoretical predictions and experimental measurements. *Comptes Rendus Physique*, 4(9):993–1008, 2003. 24

[122] J.-P. Salvetat, J.-M. Bonard, N.B. Thomson, A.J. Kulik, L. Forro, W. Benoit, and L. Zuppiroli. Mechanical properties of carbon nanotubes. *Applied Physics A: Materials Science and Processing*, 69(3):255–260, 1999. 24

[123] M. Smalc, G. Chen, G. Shives, S. Guggari, J. Norley, and R. Andy Reynolds III. Thermal performance of natural graphite heat spreaders. volume PART A, pages 79–90, San Francisco, CA, 2005. cited By (since 1996) 0; Conference of ASME/Pacific Rim Technical Conference and Exhibition on Integration and Packaging of MEMS, NEMS, and Electronic Systems: Advances in Electronic Packaging 2005; Conference Date: 17 July 2005 through 22 July 2005; Conference Code: 66620. 24

[124] Z. Wu and C.U. Pittman Jr. Nitric acid oxidation of carbon fibers and the effects of subsequent treatment in refluxing aqueous naoh. *Carbon*, 33:597–605, 1995. xi, 24, 25

[125] A. Fukunaga, S. Ueda, and M. Nagumo. Air-oxidation and anodization of pitch-based carbon fibers. *Carbon*, 37:1081–1085, 1999. 24

[126] V.J. Mimeault. Carbon fiber composites: effects of fiber oxidation on composite behavior. *Fibre Science and Technology*, 3:273–283, 1971. 24, 52

[127] J.B. Donnet and G. Guilpain. Surface treatments and properties of carbon fibers. *Carbon*, 27:749–757, 1989. 24

[128] P. Magne and X. Duval. Existence de quatre types de sites réactionnels dans l'oxydation du graphite. *Carbon*, 11:475–484, 1973. 24

[129] S. Yumitori and Y. Nakanishi. Effect of anodic oxidation of coal tar pitch-based carbon fibre on adhesion in epoxy matrix: Part 1. comparison between h2so4 and naoh solutions. *Composites Part A*, 27A:1051–1058, 1996. 24, 163

[130] S. Yumitori and Y. Nakanishi. Effect of anodic oxidation of coal tar pitch-based carbon fibre on adhesion in epoxy matrix: Part 2. comparative study of three alkaline solutions. *Composites Part A*, 27A:1059–1066, 1996. 24, 163

[131] A. Fukunaga and S. Ueda. Anodic surface oxidation for pitch-based carbon fibers and the interfacial bond strength in epoxy matrices. *Composites Science and Technology*, 60:249–254, 2000. 24

[132] S.-K. Ryu, B.-J. Park, and S.-J. Park. Xps analysis of carbon fiber surfaces- anodized and interfacial effects in fiber-epoxy composites. *Journal of Colloid and Interface Science*, 215:167–169, 1999. 24, 53

[133] H. Altenburg, J. Plewa, G. Plesch, and O. Shpotyuk. Thick films of ceramic, superconducting, and electro-ceramic materials. *Pure and Applied Chemistry*, 74(11):2083–2096, 2002. 26

[134] Hugues Baudry and Francoise Franconville. Screen printing inks for high resolution. rheology and printing. [encres serigraphiables pour haute definition. rheologie et impression.]. *Acta Electron*, 21(4):283–295, 1978. 27, 134

[135] C. Jacq, T. Maeder, and P. Ryser. Load sensing surgical instruments. *Journal of Materials Science: Materials in Medicine*, 20(SUPPL. 1):S223–S227, 2009. 28

[136] C. Jacq, B. Luethi, T. Maeder, O. Lambercy, R. Gassert, and P. Ryser. Thick-film multi-dof force/torque sensor for wrist rehabilitation. *Sensors and Actuators, A: Physical*, 162(2):361–366, 2010. 28

[137] T. Maeder, C. Jacq, and P. Ryser. Low-firing thick-film piezoresistive sensors for medical instruments. *Sensors and Actuators, A: Physical*. Article in Press. 28

[138] Y. Fournier, T. Maeder, G. Boutinard-Rouelle, A. Barras, N. Craquelin, and P. Ryser. Integrated ltcc pressure/flow/temperature multisensor for compressed air diagnostics. *Sensors*, 10(12):11156–11173, 2010. 28

[139] Y. Fournier. *3D structuration techniques of LTCC for microsystems applications*. PhD thesis, Ecole Polytechnique Fédérale de Lausanne, 2010. 28, 61, 123

[140] F.C. Krebs, M. Jorgensen, K. Norrman, O. Hagemann, J. Alstrup, T.D. Nielsen, J. Fyenbo, K. Larsen, and J. Kristensen. A complete process for production of flexible large area polymer solar cells entirely using screen printing-first public demonstration. *Solar Energy Materials and Solar Cells*, 93(4):422–441, 2009. 29

[141] M. Singh, H.M. Haverinen, P. Dhagat, and G.E. Jabbour. Inkjet printing-process and its applications. *Advanced Materials*, 22(6):673–685, 2010. 29

[142] Mori N.a Nam S.-M.a b Kakemoto H.a Wada S.a Tsurumi T.a Akedo J.a b Momotani, M.a. Fabrication of microstrip band pass filters in ghz region by aerosol deposition process. *Key Engineering Materials*, 301:117–120, 2006. 29

[143] Suchicital C. Priya S. Folgar, C.E. Solution-based aerosol deposition process for synthesis of multilayer structures. *Materials Letters*, 65(9):1302–1307, 2011. 29

[144] R.V. Williamson. Relation of oil absorption to consistency of pigment-oil pastes. *Industrial and Engineering Chemistry*, 21:1196–1198, 1929. 37

[145] A synopsis of analytical procedures. Technical report, Timcal. 37

[146] C.M. Hansen. The three dimensional solubility parameters-key to paint component affinities: I- solvents, plasticizers, polymers, and resins. *Journal of Paint Technology*, 39:104–117, 1967. 39, 40

[147] C.M. Hansen. The three dimensional solubility parameters-key to paint component affinities: Ii and iii- dyes, emulsifiers, mutual solubility and compatibility, and pigments. *Journal of Paint Technology*, 39:505–510, 1967. 39

[148] W.L. Archer. Using the hansen solubility parameter theory in reformulating solvent-based coatings. *American Paint & Coatings Journal*, pages 38–46, 1992. 39

[149] J Burke. Solubility parameters: theory and application. In *The Book and Paper Group*, volume 3. The American Institute for Conservation, 1984. 40

[150] Huntsman. Huntsman miscibility predictor. Technical report, Huntsman, 2008. 40

[151] C.M. Hansen. Polymer additives and solubility parameters. *Progress in Organic Coatings*, 51(2):109–112, 2004. 40

[152] B.D. Hardin. Reproductive toxicity of the glycol ethers. *Toxicology*, 27(2):91–102, 1983. 41

[153] B.D. Hardin, R.L. Schuler, and J.R. Burg. Evaluation of 60 chemicals in a preliminary developmental toxicity test. *Teratogenesis Carcinogenesis and Mutagenesis*, 7(1):29–48, 1987. 41

[154] P. De Ketttenis. The historic and current use of glycol ethers: A picture of change. *Toxicology Letters*, 156:5–11, 2005. 41

[155] A.S. Tatavarti, D. Dollimore, and K.S. Alexander. A thermogravimetric analysis of non-polymeric pharmaceutical plasticizers: Kinetic analysis, method validation, and thermal stability evaluation. *AAPS Journal*, 4(4), 2002. xi, 42

[156] J. Dykyj, J. Svoboda, R.C. Wilhoit, M. Frenkel, and K.R Hall. *Landolt-Boernstein: Index of organic compounds -Vapor pressure of chemicals*, volume IV. Springer-Verlag GmbH & Company KG, Berlin, Germany, 1999. xi, 42, 124

[157] Dow Chemical. Dipropylene glycol dimethyl ether data, report "epa-hq-oppt-2006-0046.2". Technical report, USA Environmental Protection Agency (EPA), 2009. xi, 42

[158] S. Horstmann, H. Gardeler, K. Fischer, F. Koester, and J. Gmehling. Vapor pressure, vapor-liquid equilibrium, and excess enthalpy data for compounds and binary subsystems of the chlorohydrin process for propylene oxide production. *Journal of Chemical and Engineering Data*, 46(2):337–345, 2001. xi, 42

[159] T. Treszczanowicz and B.C.-Y. Lu. Isothermal vapour-liquid equilibria for 11 examples of (an ether + a hydrocarbon). *The Journal of Chemical Thermodynamics*, 18(3):213–220, 1986. xi, 42

[160] J. Mewis. Thixotropy - a general review. *Journal of Non-Newtonian Fluid Mechanics*, 6(1):1–20, 1979. 42

[161] H.A. Barnes. Rheology of emulsions - a review. *Colloids and Surfaces A: Physicochemical and Engineering Aspects*, 91(C):89–95, 1994. 44

[162] J.Q. Li and R. Salovey. Model filled polymers: The effect of particle size on the rheology of filled poly(methyl methacrylate) composites. *Polymer Engineering and Science*, 44(3):452–462, 2004. 44

[163] P.M.A. Sherwood. Surface analysis of carbon fibers for composites. *Journal of Electron Spectroscopy and Related Phenomena*, 81:319–342, 1996. 53

[164] T.A. DeVilbiss, D.J. Progar, and J.P. Wightman. Sem/xps analysis of fractured adhesively bonded graphite fibre surface resin-rich/graphite fibre composites. *Composites*, 19(1):67–71, 1988. 53

[165] S.D. Gardner, C.S.K. Singamsetty, G.L. Booth, and G.-R. He. Surface characterization of carbon fibers using angle-resolved xps and iss. *Carbon*, 33:587–595, 1995. 53

[166] D. Youxian, W. Dianxun, and S. Mujin. A study of the surface of carbon fiber by means of x-ray photoelectron spectroscopy-iii. *Composites Science and Technology*, 30:119–126, 1987. 53

[167] H.R. O'Neal, S. Welch, J. Rogers, S. Guilford, G. Curran, and K.P. Menard. Comparison of tg values for a graphite epoxy composite by differential scanning calorimetry (dsc), thermomechanical analysis (tma), and dynamic mechanical analysis (dma). *Journal of Advanced Materials*, 26(3):49–54, 1995. xii, 55, 56, 115

[168] M. Yamashita, T. Nishii, and H. Mizutani. Resistivity measurement by dual-configuration four-probe method. *Japanese Journal of Applied Physics, Part 1: Regular Papers and Short Notes and Review Papers*, 42(2 A):695–699, 2003. 63

[169] T.A. Ezquerra, M. Kulescza, C.S. Cruz, and F.J. Baltá-Calleja. Charge transport in polyethylene-graphite composite materials. *Advanced Materials*, 2:597–600, 1990. xii, 65

[170] T.A. Ezquerra, M. Kulescza, and F.J. Baltá-Calleja. Electrical tranport in polyethylene-graphite composite materials. *Synthetic Metals*, pages 915–920, 1991. xii, 65

[171] R.K. Kirby, T.A. Hahn, and B.D. Rothrock. *American Institute of Physics Handbook*. 1972. 70, 107

[172] J. Cognard. Some recent progress in adhesion technology and science. *Comptes Rendus Chimie*, 9(1 SPEC. ISS.):13–24, 2006. 70, 161

[173] N. Johner, P. Ryser, C. Grimaldi, and I. Balberg. Piezoresistivity and tunneling-percolation transport in apparently nonuniversal systems. *Physical Review B - Condensed Matter and Materials Physics*, 75(10), 2007. 78

[174] T. Provder, S. Malliprakash, S.H. Amin, A. Majid, and J. Texter. Dynamical mechanical analysis and curing analysis of fouling release coatings and components. *Macromolecular Symposia*, 242:279–289, 2006. 86

[175] S. Firmino Mendes, C.M. Costa, V. Sencadas, J. Serrado Nunes, P. Costa, R. Gregorio Jr., and S. Lanceros-Méndez. Effect of the ceramic grain size and concentration on the dynamical mechanical and dielectric behavior of poly(vinilidene fluoride)/pb(zr 0.53ti0.47)o3 composites. *Applied Physics A: Materials Science and Processing*, 96(4):899–908, 2009. 96

[176] R.L. Quirino, J. Woodford, and R.C. Larock. Soybean and linseed oil-based composites reinforced with wood flour and wood fibers. *Journal of Applied Polymer Science*. Article in Press. 96

[177] C.-N. Chen, Y.-L. Chen, and W.J. Tseng. Surfactant-assisted deagglomeration of graphite nanoparticles by wet ball mixing. *Journal of Materials Processing Technology*, 190(1-3):61–64, 2007. 96, 163

[178] S. Tognana, W. Salgueiro, A. Somoza, J.A. Pomarico, and H.F. Ranea-Sandoval. Influence of the filler content on the thermal expansion behavior of an epoxy matrix particulate composite. *Materials Science and Engineering B: Solid-State Materials for Advanced Technology*, 157(1-3):26–31, 2009. 100, 102

[179] L. Holliday and J. Robinson. Review: The thermal expansion of composites based on polymers. *Journal of Materials Science*, 8(3):301–311, 1973. 102, 103, 107

[180] Z. Hashin. Analysis of composite materials - a survey. *Journal of Applied Mechanics, Transactions ASME*, 50(3):481–505, 1983. 102

[181] G. Duvaut. *Mécanique des milieux continus*. 1998. 107

[182] S. Pandini and A. Pegoretti. Time, temperature, and strain effects on viscoelastic poisson's ratio of epoxy resins. *Polymer Engineering and Science*, 48(7):1434–1441, 2008. 107

[183] B.S. Verma and S.K. Sharma. Effect of thermal strains on the temperature coefficient of resistance. *Thin Solid Films*, 5(4):R44–R46, 1970. 113

[184] C. Jacq, T. Maeder, S. Vionnet-Menot, H. Birol, Saglini I., and P. Ryser. Integrated thick-film hybrid microelectronics applied on different material substrates. In *Proceedings of the 15th European Microelectronics and Packaging Conference (EMPC), Brugge (BE), IMAPS*, 2005. 115

[185] H. Birol, T. Maeder, and P. Ryser. Application of graphite-based sacrificial layers for fabrication of ltcc (low temperature co-fired ceramic)

membranes and micro-channels. *Journal of Micromechanics and Microengineering*, 17(1):50–60, 2007. 122, 123

[186] T. Maeder, C. Jacq, Y. Fournier, W. Hraiz, and P. Ryser. Structuration of zero-shrinkage ltcc using mineral sacrificial materials. Rimini, 2009. Conference of 2009 European Microelectronics and Packaging Conference, EMPC 2009; Conference Date: 15 June 2009 through 18 June 2009; Conference Code: 78423. 122, 123

[187] H. Birol. *Fabrication of Low-Temperature Co-fired Ceramic (LTCC)-based sensor and micro-fluidic structures*. PhD thesis, Ecole Polytechnique Fédérale de Lausanne, 2007. 123

[188] H. Birol, T. Maeder, and P. Ryser. Processing of graphite-based sacrificial layer for microfabrication of low temperature co-fired ceramics (ltcc). *Sensors and Actuators, A: Physical*, 130-131(SPEC. ISS.):560–567, 2006. 123

[189] Hansu Birol, Thomas Maeder, and Peter Ryser. Preparation and application of minerals-based sacrificial pastes for fabrication of LTCC structures. In *4th European Microelectronics and Packaging Symposium - IMAPS*, pages 57–60, 2006. 123

[190] S. Metz, S. Jiguet, A. Bertsch, and Ph. Renaud. Polyimide and su-8 microfluidic devices manufactured by heat-depolymerizable sacrificial material technique. *Lab on a Chip - Miniaturisation for Chemistry and Biology*, 4(2):114–120, 2004. 123, 124

[191] N. Serra, T. Maeder, C. Jacq, Y. Fournier, and P. Ryser. Screen-printed polymer-based microfluidic and micromechanical devices based on evaporable compounds. Rimini, 2009. Conference of 2009 European Microelectronics and Packaging Conference, EMPC 2009; Conference Date: 15 June 2009 through 18 June 2009; Conference Code: 78423. 124, 132

[192] N. Serra, T. Maeder, O. Gentsch, and P. Ryser. Fabrication of polymer-based micro devices: Formulation and study of the paste. *Sensors and Actuators, A: Physical*, 172:336–340, 2011. 124, 134, 141

[193] Hunter. *Alcohols, polyhydric*. Kirk-Othmer Encyclopedia of Chemical Technology, 1991. 124

[194] J. Font and J. Muntasell. Comparative study on solid crystalline-plastic-vapour equilibrium in plastic crystals from pentaerythritol series. *Journal of Materials Chemistry*, 5(8):1137–1140, 1995. 124

[195] M. Yamazaki, C. Sasaki, H. Kakiuchi, Y.T. Osano, and H. Suga. Thermal and structural characterization of trimethylolethane trihydrate. *Thermochimica Acta*, 387(1):39–45, 2002. xv, 127, 128

[196] J.M. Castaneda, F.J. Lozano, and S. Trejo. Ternary equilibrium for the system water/cyclohexanol/2-ethyl-2-(hydroxymethyl)-1,3-propanediol. *Journal of Chemical and Engineering Data*, 26(2):133–135, 1981. 128

[197] L.P. Singh and S.S.N. Murthy. Dielectric and calorimetric investigation of an unusual two-component plastic crystal: Cyclohexanol-neopentylglycol. *Physical Chemistry Chemical Physics*, 11(25):5110–5118, 2009. xv, 129, 130

[198] J. Salud, D.O. Lopez, M. Barrio, J.L.l. Tamarit, and H.A.J. Oonk. Two-component systems of isomorphous orientationally disordered crystals. part 2: Thermodynamic analysis. *Journal of Materials Chemistry*, 9(4):917–921, 1999. xv, 130

[199] Ad7746 evaluation board eval-ad7746eb, analog devices, 2005. 139

[200] O. Gentsch. Micro-fluidique imprimé. Semester project, Laboratoire de Production Microtechnique, EPFL, 2009. 143

[201] Schlumberger. Technical report, Schlumberger. xv, 146, 147, 148

[202] S.G. Croll. Atmospheric gases and the hardening of an amine-cured epoxy coating. *Journal of Coatings Technology*, 52:65–69, 1980. 163

[203] P.A. Lucas, P.A. Clark, R.J. Haney, and M.R. Kittek. Investigation of water spot and blush resistance of epoxy industrial floors. *Journal of Protective Coatings and Linings*, 15(8):20–27, 1998. 163

[204] B.L. Burton. Amine-blushing problems? no sweat! Technical report, Huntsman Corporation, Epoxy resin formulators' meeting of the Society of the Plastics Industry, 2001. 163

[205] D.J. Weinmann, K. Dangayach, and C. Smith. Amine-funtcional curatives for low temperature cure epoxy coatings. Technical report, Resolution Performance Products, 2001. 163

Nathalie SERRA

Rue Mathurin-Cordier 1
CH-1005 Lausanne
+41 (0)79 849 13 49
nathalie.serra@a3.epfl.ch

French, single, 04.02.1984

Education

01.2008-2012 **Ph.D. student in chemistry at the Ecole Polytechnique Fédérale de Lausanne (EPFL).** Specialization in composite materials

2004-09.2007 **M.Sc. in Chemistry at Ecole Nationale Supérieure de Chimie de Lille (ENSCL, part of the « Grandes Ecoles » network).** Orientation towards formulation and material science.

2002-2004 **Intensive university level preparation course** for the nationwide competitive entrance exam to French graduate schools of Chemistry and Physics

1999-2002 High school at Lycée La Bruyère, Versailles (France) and obtention of **"Baccalauréat série S, option mathématiques"** in 2002

Professional experience

01.2008-2012 **Research assistant at the Laboratoire de Production Microtechnique (LPM)** at the EPFL. Experimental study of epoxy/graphite composite materials and their use as thick-film resistors. Main emphasis on formulation composites based on epoxy and graphite, formulation and electrical and mechanical characterization

03-08.2007 **6-month internship at the university RWTH,** Aachen, Germany in the Gesteinhüttenkunde Institute. Study of glass etching surfaces with hydrofluoric acid by chemical analyses.

07-09 2006 **3-month internship at Schlumberger, SRPC** in Clamart, France. Research on the effects of silicates upon cements used in the oil industry, optimization of the slurry's formulation.

07-08 2005 **2-month internship at Schlumberger, SRPC** in Clamart, France. Assessment of the effects of silicates and use of UV for characterization purposes.

Languages

French **Mother tongue**
English **Fluent,** scored 597 on TOEFL (2005) and 875 on TOEIC (2006)
German **Good,** Zertifikat Deutsch (Befriedifigend), studied one year in Germany

Informatics

Origin Pro, MS office, LyX, Photoshop

List of publications and conference papers

2011

N. Serra, T. Maeder, O. Gentsch, P. Ryser, **"**Fabrication of polymer-based micro devices: Formulation and study of the paste **"***Sensors and Actuators, A: Physical,* 172: 336-340, 2011

N. Serra, T. Maeder, P. Ryser, "Piezoresistive effect in epoxy-graphite composites", *Procedia Engineering*, 25:235-238, 2011

2010

N. Serra, T, Maeder, P. Lemaire, P. Ryser, **"**Formulation of composite résistive pastes for micro-heater manufacturing**"**, *Sensors and Actuators A : Physical* 162(2):367-372, 2010

N. Serra, T. Maeder, O. Gentsch, P. Ryser, **"**Fabrication of polymer-based micro devices: Formulation and study of the paste **"** *Procedia Engineering* 5:874-877, 2010

2009

N. Serra, T. Maeder, C. Jacq, Y. Fournier, P. Ryser, **"**Screen-printed polymer-based microfluidic and micromechanical devices based on evaporable compounds**"**, *European Microelectronics and Packaging Conference, EMPC 2009*

N. Serra, T, Maeder, P. Lemaire, P. Ryser, **"**Formulation of composite résistive pastes for micro-heater manufacturing**"**, *Procedia Chemistry*, 1(1):48-51, September 2009

Conferences

2011

Eurosensors XXV, Athens, Greece: poster presentation

2010

Eurosensors XXIV, Linz, Austria: poster presentation

Macro2010, 43rd IUPAC World Polymer Congress, Glasgow, Scotland: talk

2009

Eurosensors XXIII, Lausanne, Switzerland: poster presentation

European Microelectronics and Packaging Conference (EMPC), Rimini, Italy: talk

Hobbies

Music (organ player for 9 years), dance (modern-jazz), movies, literature